ISSN 1913-1844 (Print)
ISSN 1913-1852 (Online)

MODERN APPLIED SCIENCE

Vol. 5, No. 1
February 2011

CCSE

Canadian Center of Science and Education®

Editorial Board

Contents

Contents

 ISSN 1913-1844 E-ISSN 1913-1852

Behavior of Dissolved Organic Matter in Coral Reef Waters in Relation with Biological Processes

Mohamed Farook Mohamed Fairoz (Corresponding author), Beatriz E. Casareto & Yoshimi Suzuki

Department of Environment and Energy Systems

Graduate School of Science and Technology, Shizuoka University

836, Oya Suruga ku, Shizuoka 422-8529, Japan

Tel/Fax: 81(0)54-2384-799 E-mail: fairoz.mfm@gmail.com

Shizuoka University Japan was acknowledged for financial support

Abstract

Behavior of dissolved organic carbon (DOC) and dissolved organic nitrogen (DON) in coral reef waters in relation with biological processes was studied with incubation experiments and field observations in May 2008 and 2009 at the fringing reef of Sesoko Island, Okinawa, Japan. Reef sea water (RSW) and coral mucus added RSW collected from *Acropora digitifera* (AcrRSW) and *Montipora digitata* (MonRSW) were incubated for one day *in situ* and then for 77 days in the laboratory under dark condition. The results indicated that the behavior of DON was different compared to that of DOC in RSW and mucus added (AcrRSW and MonRSW) during dark incubation. Concentration of DON increased from 8.3 μM to 11.8 μM for AcrRSW and 4.0 μM to 15.4 μM for MonRSW during dark incubation period. The increasing rates for DON in AcrSRW and MonRSW were 0.05 μM day^{-1} and 0.1 μM day^{-1} respectively. On the other hand DOC concentration decreased from 129.0 μM to 75.0 μM for AcrRSW and 75.1 μM to 64.7 μM for MonRSW, with decreasing rates of 0.7 μM day^{-1} and 0.1 μM day^{-1} respectively. We assume that the increase of DON may be determined by difference between rates of inputs of organic matter mainly from mucus and rate of degradation of dissolved organic matter in the water column. These results suggest that recycling of DON is slow than that of DOC in coral reef ecosystem.

Keywords: DON, DOC, Coral reef water, Incubation, Coral mucus

1. Introduction

Coral reefs in tropical and sub-tropical oceans are biologically diverse ecosystem with high gross primary production (Sorokin, 1995). This high productivity in oligortophic areas with very low nutrients supply might be due to the rapid recycling of organic matter to inorganic forms (Suzuki et al., 2000). In this view point dissolved organic matters as dissolved organic carbon (DOC) and dissolved organic nitrogen (DON) play an important role because it is rapidly consumed and re-mineralized by the microbial community in reef waters. Several studies suggested that dissolved organic carbon (DOC) derived from coral mucus must sustain the high production rates in coral reef waters by promoting microbial growth (van Duyl and Gast 2001, Ferrier-Pages et al., 2000). However the sources and behavior of dissolved organic nitrogen (DON) is often not well described as that of DOC in reef waters due to the limitation of available data until now. Because most of the studies described organic matter in coral reef water relation to the measurement of DOC without DON (Boyer et al., 1997, Van Duyl and Gast 2001, Hata et al., 2002, Wild et al., 2004). They thought the behavior of DON may be similar to that of DOC, therefore it is possible to calculate the concentration, flux and others from the results of DOC using DOC/DON ratio. Suzuki et al., (2000) reported that the behavior of DON was relatively different than that of DOC from the study on the molecular weight of dissolved organic matter in coral reef water. Therefore further studies are necessary to unveil much details of the behavior of DOC and DON in relation with the biological processes.

This paper reports the behavior of DOC and DON in reef sea water in relation with biological processes with incubation experiments and field observation in Sesoko reef waters.

2. Materials and Methods

2.1 Study site and water sampling

Sesoko reef is located on the west coast of Sesoko Island, Okinawa, Japan (26°38'N, 27°51'E). The reef is characterized by a shallow lagoon (0.2 – 6.5 m depth) and a well-developed reef crest, located 150–200 m from the shore. The live coral community is composed of about 44% *Goniastrea aspera*, 21% *Montipora digitata*, 7.4%

Porites sp., and 2.2% *Acropora digitifera*. Sea water samples were collected from three locations; site A (middle of lagoon), site B (located near the entrance of the lagoon) within the Sesoko reef and site C outside the reef (Fig. 1).

2.2 Sesoko reef water condition

Reef water from sites A and B at near shore, middle reef and the reef crest, were collected on 9-10 May 2008 (14:30, 17:30 and at 06:00, except for site A, reef crest at 6:00) into 5 liter Nalgene acid clean bottles and sub-samples of 40ml transfer to amber glass vials for measurement of DOC and DON. Light and temperature in reef water was also registered using *in-situ* light and temperature sensors (Alec electronics).

2.3 Incubation experiments

Incubation experiments were carried out using reef water (site. A or B), open ocean water and coral mucus. Sea water from site B and coral mucus used and from open ocean were used for incubation experiments.

All bottles (Nalgene®) and glass vials used for incubation experiments were washed and rinsed with 10% HCL and Milli-Q water before use.

Coral mucus was collected from *Acropora digitifera* (Acr) and *Montepora digitata* (Mon) coral species. Coral branches were harvested using hammer and chisel and placed the coral branches in cleaned container with 200ml of RSW to collect coral mucus for addition to RSW during incubation experiment. For pure mucus collection from *A. digitifera,* coral branches were air exposed (Dumas et al., 1982) into a bacteria free tube.

Experiment I

Reef sea water from site B (RSW) and coral mucus added RSW were used. Three experimental groups 1 liter of RSW and 950 ml of RSW plus 50ml of AcrRSW and MonRSW were prepared in triplicate. All bottles contain RSW, AcrRSW and MonRSW were arranged to submerge *in situ* at a 1m depth and incubated one day (from 9th May 2008, 15:00 to next day, 15: 00). After incubation in the field all the bottles were transported to laboratory and kept in dark under room temperature for 77 days. Samples were collected at 0, 2, 4, 15 and 78 days of incubation and concentrations of DOC, DON, DIN and microbial abundance (heterotrophic bacteria, picocyanobacteria and pico-nanoflagellaes) were measured. The change of concentrations of DOC, DON and DIN were calculated from the difference between beginning day (Day 2) and end day (Day 78) of dark incubation. The differences of concentrations between day 2 and day 78 were divided by the number of incubation days to calculate the rates of concentration change.

Experiment II

Three experimental groups contain 5 liter of reef sea water from site A, site B and open ocean water from site C (OOW) were prepared. All bottles were arranged to submerge *in situ* at about 1m depth and incubated one day (from 21st May 2009, 15:00 to next day, 15: 00) and transported to laboratory to incubate in dark for 14 days. Samples were collected at 0, 2, 4, and 15 days of incubation and concentrations of DOC, DON, DIN were measured.

During experiment II, a short degradation was carried out using pure coral mucus collected from *Acropora digitifera*. 15ml of collected coral mucus plus 5 ml of RSW in glass vial was incubated in dark for two days (from 21st May 2009). Samples for initial and after two days were collected to measure DOC and DON concentrations.

2.4 Analytical method

Samples for dissolved organic matter were transferred to 40 ml cleaned pre-combusted amber glass vials, after passing through pre-combusted 25mm GF/F filter (Whatman). The sample vials were covered with Teflon-lined caps and stored at -20°C until analysis of DOC, DON and DIN.

DOC and total dissolved nitrogen (TDN) were determined using a total organic carbon analyzer equipped with a total nitrogen unit (TOC V, Shimadzu) following the methods of Suzuki et al., 1993 and UNESCO 1994. DIN was determined with an auto analyzer (TRAACS-2000) following the methods of Hansen and Koroleff 1999. DON concentration was calculated by subtracting the total dissolved inorganic nitrogen ([NO_2 + NO_3+ NH_4]) or DIN from the concentrations of the total dissolved nitrogen (TDN).

Microbial abundance was measured after staining the sample (preserved in Glutaraldehyde) using DAPI (4', 6-diamino-2-phenylindole) under epi-florescence microscope (Nikon- Eclipse) following the method of Porter and Feig 1980.

Nitrogen and carbon biomass of heterotrophic bacteria, Pico-cyano bacteria and heterotrophic nano flagellates

were calculated according to Casareto et al., 2000 and Houlbreque et al., 2004.

3. Results

3.1 Sesoko reef water condition

Temporal variations of DOC and DON in Sesoko during the sampling period are shown in Fig. 2. The maximum light intensity at day time was 2024 μM $cm^{-2}s^{-1}$. The average temperature recorded during the sampling period was 25.5°C with a diurnal variation of ±2 °C. Concentrations of DOC and DON varied from 68.9 to 77.8 μM and 3.1 to 4.7 μM respectively. The temporal change of DOC: DON ratio (C/N) was from 15 to 18 (Fig. 2).

3.2 Incubation experiments

Experiment I

Temporal changes of DOC, DON, DOC: DON ratio, DIN concentrations and microbial abundance of experiment are shown in Fig. 3 and Fig. 4 respectively.

During 77 days dark period concentration of DOC in RSW decreased from 70.2 μM to 67.3 μM with a rate of 0.04 μM C day^{-1}. In AcrRSW and MonRSW DOC decreased from 129 μM to 75 μM and 75.1 μM to 64.67 μM respectively. The decrease rates for DOC in AcrSRW and MonRSW were 0.7 μM day^{-1} and 0.1 μM day^{-1} respectively.

During 77 days dark period the concentration of DON showed slight increase for all treatments. DON concentration in RSW increased from 2.9 μM to 4.3 μM with rate of 0.02 μM day^{-1}. DON concentrations in AcrRSW and MonRSW also increased during dark period from 8.3 μM to 11.8 μM and 4.0 μM to 15.4 μM respectively. The increase rates for DON in AcrSRW and MonRSW were 0.05 μM day^{-1} and 0.1 μM day^{-1} respectively. These results show that the DON concentration increase largely in case of reef waters enriched with coral mucus. Increase of DON concentration for coral mucus added RSW were significantly high compared to increase of DON in RSW (ANOVA, $p < 0.05$).

The DIN concentration in RSW increased from 0.9 μM to 2.1 μM with the rate of 0.02 μM day^{-1}. The increased DIN concentrations in coral mucus added RSW were more higher compared to RSW from (for AcrRSW from 2.2 μM to 4.8 μM and for MonRSW and 1.2 μM to 6.3 μM).

The concentrations of DON and DIN at day 15 for AcrRSW and MonRSW were high. The DON and DIN concentration increased for MonRSW from day 15 to day 78 and the DON and DIN concentration for AcrRSW decreased from day 15 to day 78. The increase of DON and DIN concentrations for AcrRSW, MonRSW and RSW were compared with relation to the difference between the day 2 and day 78.

The changes of concentrations of DOC and DON were shown by the DOC: DON ratio. The DOC: DON ratio was decreased in RSW from 24.2 to 15.4. The DOC: DON ratio was decreased in AcrRSW from 16.6 to 6.3 and for MonRSW 12.5 to 4.1.

Microbial abundance increased rapidly during initial 4 days period, and the microbial abundance decreased gradually until 77^{th} day for all experimental groups. Bacteria cell abundance decreased from 8.3 x 10^5 ml^{-1} to 1.2 x 10^5 ml^{-1} for RSW. The bacteria cell abundance decreased from 16 - 19 x 10^5 ml^{-1} to the range of 3 – 6 x 10^5 ml^{-1} for RSW with added mucus. Pico-cyano bacteria cells also decreased during dark period for RSW and mucus enriched RSW. HNF abundance increased as the bacteria and picocyanobacteria decrease. Contribution of organic carbon and nitrogen to RSW from microbial biomass was calculated using conversion factors (Table 1). This shows that the possibility of contribution from microbial biomass as carbon and nitrogen source were relatively low.

Experiment II

DOC and DON concentrations for reef sea water and open ocean water during 14 days degradation (incubation under dark condition) after one day *in-situ* incubation are shown in Table 2. DOC concentration decreased for site A and site B from 74.3μM to 63.9 μM and 69.0 μM to 64.1 μM respectively. DOC concentration of OOW did not remarkably change compared to the initial concentration and it was 68.3 μM to 69.7 μM during 15 days. DON concentration increased for site A and site B from 3.9μM to 4.8μM and 3.9μMN to 4.5 μMN respectively. Comparing reef sea water (site A and B) with OOW, the concentration of DON was decreased from 4.2μM to 3.7μM during 15 days showing a different pattern, however the initial value of DON concentration was high in OOW (Table 2).

Short degradation during 2 days of coral mucus added reef seawater showed that DOC and DON concentration decreased from 2846 μM to 1407 μM and 141.1 μM to 119.7 μM respectively (Table 3). The percentage for

DOC decrease showed that about 50% decreased from the initial during two days. DON concentration decrease was less than 20% from the initial.

4. Discussion

In this study, the results of Experiment (I) show that the behavior of DON in RSW, AcrRSW and MonRSW during dark incubation process was different from that of DOC (Fig.3). And also we found in Experiment (II) that the behavior of DOC and DON was different for RSW but not for OOW. This suggests that the organic matters which are dissolved in RSW are of different characteristics to that of open ocean. Mucus degradation for two days showed that the DON degradation rate was slower than DOC. Concentration of DOC was decreased about 50% from the initial but DON concentration decreased less than 20% from the initial. This is the first report on this difference of behaviors between DON and DOC in relation with biological processes. When considering previous works reported on organic matter contain in reef waters (Boyer et al., 1997, Van Duyl and Gast 2001, Hata et al., 2002, Wild et al., 2004) none of these studies mentioned the behavior of DOC and DON. In these studies dissolved organic matters were described using measurements of DOC, assuming that the behavior of DON is similar to DOC. And also most of work about the DOC was done at the field observation, not incubation (Van Duyl and Gast 2001, Hata et al., 2002, Wild et al., 2004). Among the limited works on DOC and DON, Suzuki et al., 2000 reported on the difference of flux and behavior between DON and DOC based on the molecular size in reef water and open ocean water at the field. They showed that the different behaviors between both components are due to the characteristics and sources in relation with biological process.

The DOC and DON concentrations in reef water at the field (Sesoko reef) showed that the temporal changes of DOC and DON during light hours had similar trends, indicating that C/N ratio in temporal changes is nearly constant ranging from 15 to 18 (Fig.2). This result indicated that the changes of DON and DOC concentrations between field observation and laboratory incubation experiment were different. During incubations where we isolated the seawater from the environment and cancelled the physical effects of tides and water mixing, therefore we can assess the biological processes during degradation period under dark conditions. Results showed that degradation of DOC and DON is of different speed, being more rapid in case of DOC and slow for DON.

Present study indicate that the degradation rate of DON is slow than that of DOC. However if we consider only this result, we cannot explain about increase of DON concentrations during degradation processes. We assume that the increase of DON may be determined by the difference between rates of inputs of dissolved organic matter (DOM) mainly from coral mucus and rate of degradation of dissolved organic matter in the water column. These suggest that recycling of DON is slow than that of DOC in coral reef ecosystem.

For confirmation of this assumption we need to study on the lability of the dissolved organic matter in reef waters, in particular the mucus source DOC and DON. Therefore to study the behavior of DON in relation with the biological processes, we should measure directly DON and DOC at the same time.

References

Boyer, J. N., Fourqurean, J. W., Jones, R. D. (1997). Spatial characterization of water quality in Florida Bay and Whitewater Bay by multivariate analyses: zones of similar influence. *Estuaries,* 20, 743–758.

Casareto, B.E., Suzuki, Y., Casareto, B. E., and Kurosawa, K. (2000). Particulate organic carbon budget and flux in a fringing coral reef at Miyako Island, Okinawa. *Proc. 10th Int. Coral Reef Symp.,* 1, 568-572.

Daumas R., Galois, R., Thomassin, B., (1982). Biogeochemical composition of soft and hard coral mucus on a new Caledonian lagoonal reef. *Proc. 4th Int. Coral reef Symp.,* 2, 59- 68.

Ferrier-Pages, C., Leclercq, N., Jaubert, J., and Pelegri, S. P. (2000). Enhasment of pico- and nanoplankton growth by coral exudates. *Aquat. Microb. Ecol.,* 21, 203-209.

Hansen, K., and Koroleff, F. (1999). Determination of nutrients. *In Methods of seawater analysis. (ed. By Grasshoff K, Kremling K, Ehrhardt M.)*. Wiley, Weiheim, pp.159-228.

Hata, H., Kudo, S., Yamano, H., Kurano, N., Kayanne, H. (2002). Organic Carbon flux in Shirano coral reef (Ishigaki Island, Japan). *Mar. Ecol. Prog. Ser.,* 232, 129-140.

Houlbreque, F., Tambulte, E., Richard, C., Ferrier-Pages, C. (2004). Importance of micro-diet for scleractinian corals. *Mar. Ecol. Prog. Ser.,* 282, 151-160.

Porter, K.G., and Feig, Y. S. (1980). The use of DAPI for identifying and counting aquatic microflora. *Limnol. and Oceanogr.,* 25, 943-948.

Sorokin, Y. I. (1995). *Coral reef ecology.* 2nd edition, Springer Verlag, New York, pp. 465.

Suzuki, Y., Hedeges, J., Lee, C., Wengersky, P. (1993). On the measurement of DOC and DON in sea water, *Mar Chem.,* 41**,** 287-290.

Suzuki, Y., Casareto, B. E., Kurosawa, K. (2000). Import and export fluxes of HMW-DOC and LMW- DOC on a coral reef at Miyako Island, Okinawa *Proc. 9th Int. Coral Reef Symp.,* 1,555-559.

UNESCO (1994). Protocols for the Joint Global Ocean Flux study (JGOFS) Core Measurements. IOC report Manuals and Guidelines 29. 170 p.

Van Duyl, F. C., and Gast, G. J. (2001). Linkage of small-scale spatial variations in DOC, inorganic nutrients and bacterioplankton growth with different coral reef water types. *Aquat. Microb. Ecol.,* 24, 17-24.

Wild C., Huettel M., Kuelter A., Kremb S. G., Rasheed M.Y.M., and Jorgensen B. (2004). Coral mucus function as an energy carrier and particle trap in the reef ecosystem. *Nature,* 428, 66 -70.

Table 1. Biomass of bacteria, pico cyanobacteria and pico and nano-flagellates. (a) nitrogen biomass (b) carbon biomass of initial and final for the 77days of dark period for experiment I (Mean ± standard deviation of three incubation bottles).

(a)

Organism group	Nitrogen biomass (µM)					
	RSW		AcrRSW		MonRSW	
	Initial	Final	Initial	Final	Initial	Final
Bacteria	0.37±0.1	0.05±0	0.70±0.2	0.15±0.02	0.87±0.04	0.25±0.02
Pico cyanobacteria	0.05±0	0	0.02±0	0	0.04±0.01	0
Pico and nano-flagellates	0.01±0	0	0.06±0.02	0.01±0	0.06±0.04	0

(b)

Organism group	Carbon biomass (µM)					
	RSW		AcrRSW		MonRSW	
	Initial	Final	Initial	Final	Initial	Final
Bacteria	1.6±0.6	0.23±0.01	3.10±1.2	0.66±0.09	3.81±0.19	1.09±0.07
Pico cyanobacteria	0.8±0.02	0	0.34±0.05	0.01±0	0.71±0.13	0
Pico and nano-flagellates	0.12±0.03	0.05±0.02	0.57±0.15	0.08±0.04	0.58±0.03	0.04±0

Table 2. Changes in DOC and DON during 15 day incubation with one day *in-situ* incubation and 14 day incubation in laboratory dark condition for water samples from Sesoko coral reef (site A and site B) and open ocean surface water (site C). Mean values ± standard deviations from three measurements

Location of sea water collection	Time (Days)	Concentration	
		DOC (µM)	DON(µM)
Open ocean (site C)	Initial	68.3±0.2	4.2±0.1
	2	69.2±0.1	3.9±0.1
	15	69.7±0.1	3.7±0.1
Sesoko reef site A	Initial	74.3±0.1	3.9±0.1
	2	69.2±0.1	4.3±0.1
	15	63.9±0.1	4.8±0.1
Sesoko reef site B	Initial	69.0±0.1	3.9±0.1
	2	70.3±0.2	5.6±0.4
	15	64.1±0.4	4.5±0.1

Table 3. Concentrations of DOC and DON for mucus of *A. digitifera* plus reef water during 2 days degradation. Mean values ± standard deviations from three measurements.

Time (Days)	Concentration (µM)	
	DOC	DON
Initial	2846±7	141.1±1
2	1407±7	119.7±2

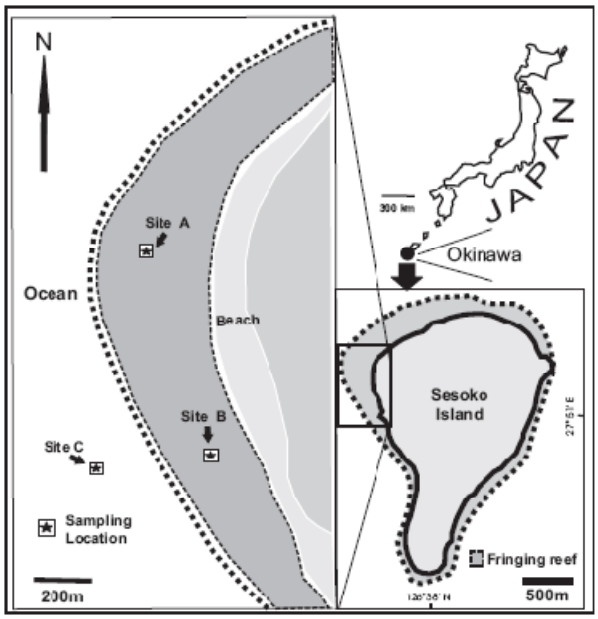

Figure 1. Map of the Sesoko Island, Okinawa, Japan indicating three sampling locations including two locations with the reef (site A and site B) and one location adjacent open ocean water (site C).

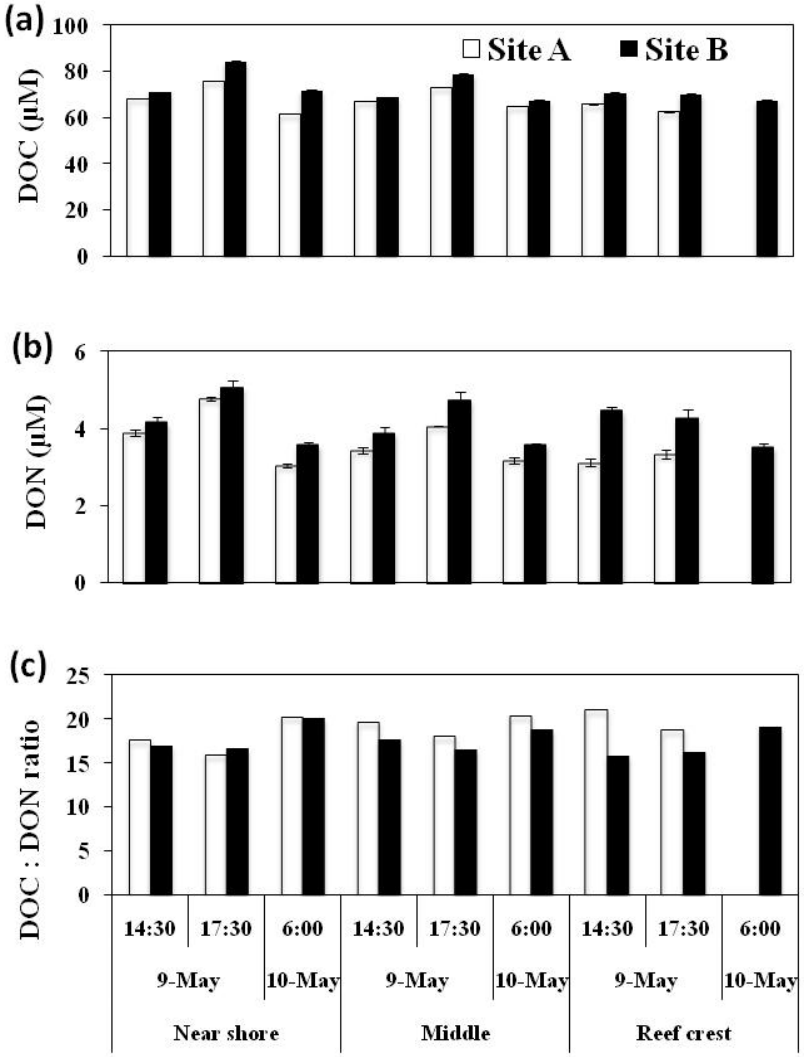

Figure 2. Variation of (a) DON, (b) DOC concentrations and (c) DOC: DON ratio measured for Sesoko coral reef water at site A and site B along three different points (near shore, middle and reef crest) during 14:00, 17:00 and following day at 06:00 (except for site A, reef crest) in May 2008. Concentrations indicated with mean values and standard errors.

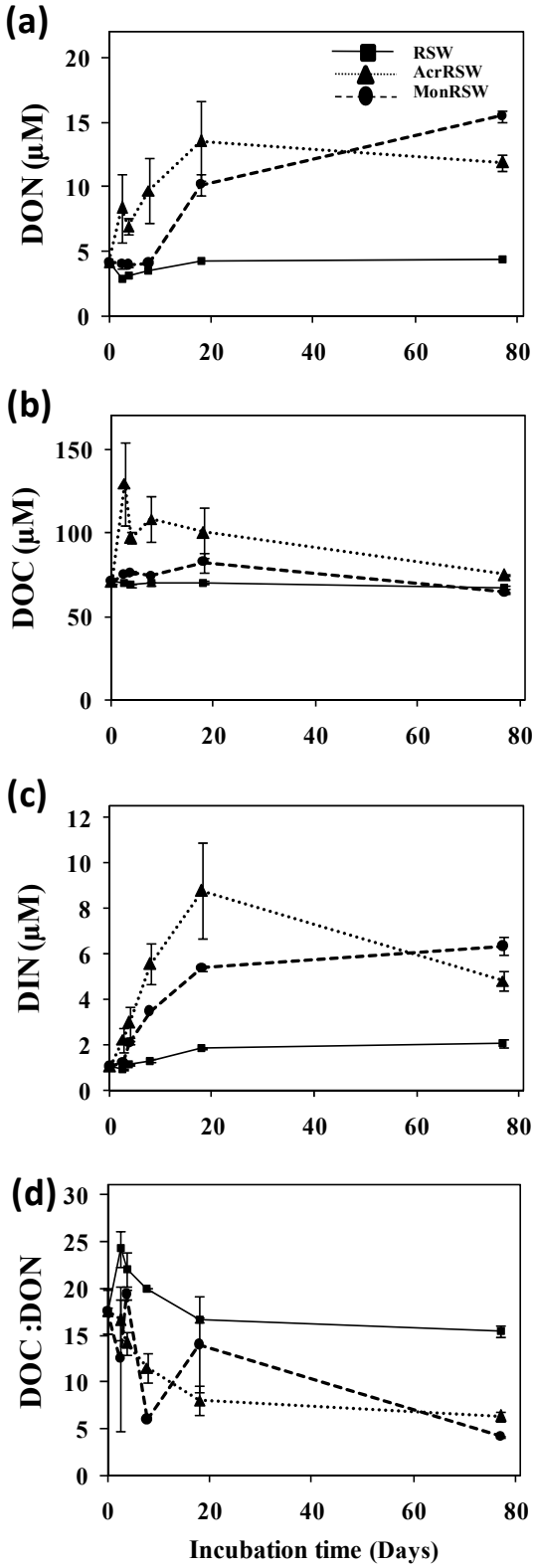

Figure 3. Changes in (a) DON, (b) DOC, (c) DIN concentrations and (d) DOC: DON ratio during 78day incubation period with one day *in-situ* incubation and 77 days in laboratory dark condition. (RSW ——■——), and enriched coral mucus from *Acropora digitifera* (AcrRSW – –●– –) and *Montepora digitata* (MonRSW ···▲···). Concentrations indicated by mean with standard error.

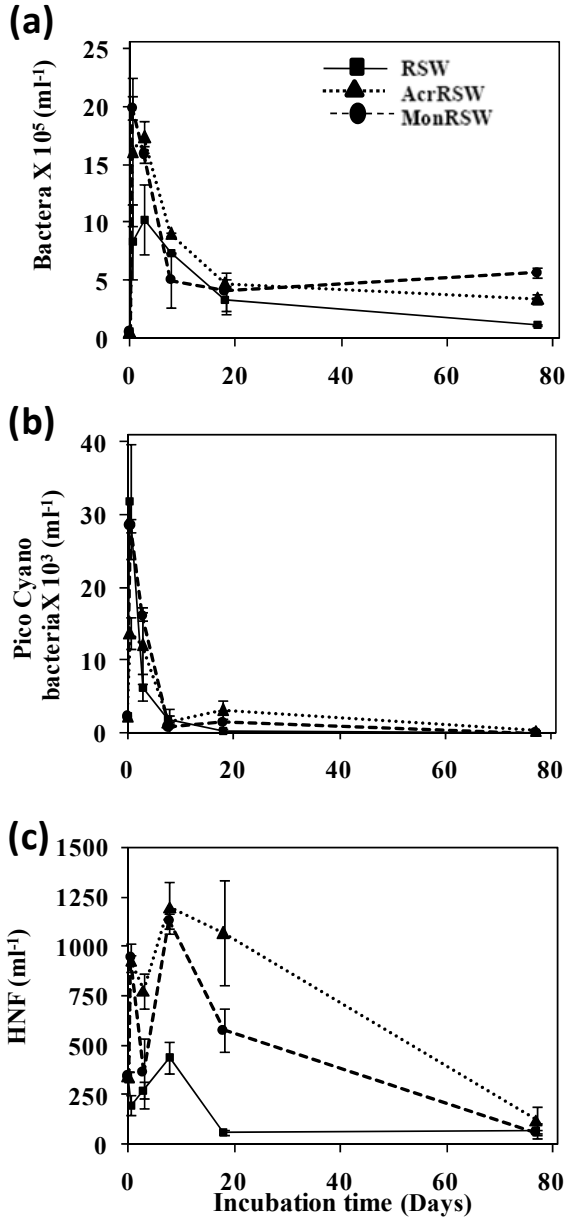

Figure 4. Changes of Heterotrophic (a) bacteria (b) pico-cyanobacteria (c) nano-flagelltes (HNF) abundance for light and dark during 78day incubation period with one day *in-situ* incubation and 77 days in laboratory dark condition. (RSW ——■——), and enriched coral mucus from *Acropora digitifera* (AcrRSW ···▲···) and *Montepora digitata* (MonRSW – – ● – –). Concentrations indicated by mean with standard error.

Enhancing Agile Methods for Multi-cultural Software Project Teams

A Sutharshan

School of Computer Science and Security Science, Edith Cowan University

2 Bradford Street, Mount Lawley, Western Australia, 6050, Australia

Tel: 61-8-9310-1164 E-mail: anu.sutharshan@transport.wa.gov.au

S P Maj

School of Computer Science and Security Science, Edith Cowan University

2 Bradford Street, Mount Lawley, Western Australia, 6050, Australia

Abstract

It is well documented that software projects are typically over schedule, over budget and often do not meet user requirements. The main problems are all associated with people related issues. In order to address this problem the Agile philosophy was introduced with an associated portfolio of Agile methods. These methods are specifically designed to improve software project team management. However it is now increasingly common for software projects to have multicultural team members. It is well documented that people from different cultures have considerably different expectations and methods of interacting in a team environment. In order to address this problem cultural specific Agile attributes were defined based on Hofstede's cultural dimensions. The result of this study gives an insight to how cultural differences may affect a software methodology implementation, specifically Agile and how these problems can be addressed. Hence it is possible to select appropriate 'culture and Agile specific attributes' when working with multicultural software project team to help software development projects with agile methods.

Keywords: Hofstede, Agile, Software project management, Multi cultural team

1. The Software Engineering Crisis

Software development is an expensive, and often a difficult process (Cerpa & Verner, 2009; Imamoglu & Gozlu, 2008). Although corporate expenditure on information technology (IT) has dropped in recent years, firms spend more than a trillion US dollars a year on IT (Love, Ghoneim, & Irani, 2004). It is well documented that the majority of software project are problematic. A survey of over 8000 projects undertaken in the year 2000 by 350 US companies revealed that one third of the projects were never completed and one half succeeded only partially, that is, with partial functionalities, major cost overruns, and significant delays (Lamsweerde, 2000). Software project management continues to be a challenging area for practitioners: more than half of all software projects experience severe difficulties and/or failure (Standish Group, 2004). The Standish Group's "CHAOS Report," (Eveleens & Verhoef, 2010; Standish Group, 2004), a widely respected survey of software projects in industry and government, estimated that, in the year 2009, only 32% of software projects in large enterprises succeeded (i.e., produced acceptable results that were delivered close to on-time and on-budget). 44% were "challenged" (significantly over budget and schedule), and 24% failed to deliver any usable result (Table 1). The projects that are in trouble have an average budget overrun of 56%. This represents a serious and chronic problem.

In order to address this on-going problem many different software development methods have been developed and introduced. There are three broad categories of methods: formal, structured and soft. Formal methods, such as Z and the Vienna Definition Method (VDM), are mathematically based allowed proof of completeness and consistency (Abernethy, Kelly, Sobel, Kiper, & Powell, 2000). However such methods are complex and beyond the scope of most system developers. Structured methods, such as Structured Systems Analysis Design Method (SSADM), provide detailed guidelines along with commonly used tools and techniques such as Data Flow Diagrams (DFDs) (Cohen & Bar-On, 1989). Soft methods such as Soft Systems Methodology (SSM), Multiview and Effective Technical and Human Implementation of Computer-Based Systems (ETHICS), were designed to accommodate the problems associated with team dynamics (Bustard & Lundy, 1995). It is now recognized that human factors are the most significant components that determine project success.

Clearly, personalities are complex and many software engineers exhibit a variety of different traits and attitudes (Bostrom & Kaiser, 1981). The importance of end user participation is also an important factor in project success (Hartwick & Barki, 1994). Thimbleby (2001) has stated that, "the lack of user centered design is the classic

reason for the failure of almost all programmed systems". There is considerable research summarizing supporting user participation and involvement in IT (Hartwick & Barki, 1994). Hartwick & Barki further stressed the importance of the IT organization and the user community working together to develop high value systems. The need for the participation and involvement of end users in IT development has been recognized (Avital & Vandenbosch, 2000). The philosophy is that products have no reason to exist without people, therefore people and their goals must be a critical part of the process and the practice (Rohn et al., 2002). Hence a range of different software development methods were developed and introduced such as Extreme Programming (XP), Lean Development, Feature Driven Development etc. In 2000 the Agile philosophy was introduced as framework of principles for software development projects. The need for the participation and involvement of users in IT development was recognized even in 70s (Lucas, 1971). Human related skills became important as a result of increased user involvement in the IS development process (Cheney, 1988). Cheney (1988) also identified the changing emphasis towards general interpersonal skills and, specifically, the ability to communicate with end users involved in the IS development process.

2. Agile Philosophy

Agile is a framework of principles that employs a range of different software methods – referred to as Agile methods. Software through people is the motto of the Agile Manifesto (Highsmith, 2002). The Agile philosophy is primarily informal with minimal documentation. Hence the emphasis is on verbal and social communication within the development team (Valencia, Olivera, & Sim, 2007). Significantly Agile based methods have been gaining widespread acceptance amongst practitioners (Valencia et al., 2007).

The Agile philosophy evolved based on four key values:

1. Individuals and interactions over processes and tools
2. Working software over comprehensive documentation
3. Customer collaboration over contract negotiation
4. Responding to change over following a plan

The principles behind this manifesto recommend that change should be welcomed at every stage of the software development cycle; that working software should be delivered frequently; and that conveying information via face-to-face conversation is more efficient than through written documentation (Valencia et al., 2007). A 2003 global survey of experience using Agile methodologies carried out by an Australian company produced the results that have been summarized below:

- 88% of organizations cited improved productivity
- 84% of organizations reported improved quality of software products
- 46% of respondents reported that development costs were unchanged using Agile methodologies, while 49% stated that costs were reduced or significantly reduced
- 83% stated that business satisfaction was higher or significantly higher
- 48% cited that the most positive feature of Agile methodologies was their ability to 'respond to change rather than follow a predefined plan' (Shine Technologies, 2003).

Results from a survey done in 2006 at Microsoft to identify what the participants thought were the top 10 benefits with Agile development are listed in table 2 (Begel & Nagappan, 2007). The top benefit was improved communication and coordination among team members. The second most cited benefit was timely and rapid software releases. For a good software project to be successful, it has been indicated that focus should be placed on the processes, technology and people in order to achieve better performance, and the people-focus is by far the component that gets the least attention (Leonard, 2002). However it is now common for projects to consist of team member from very diverse cultures – each with their own unique expectations and communication methods.

3. Multicultural Software Development Teams

Cultural factors may have an impact on the success of software development. This problem may be exacerbated when projects are multicultural. Culture is one area of social science that receives constant attention (Jones, 2007). It has been reported that until studies were done on cultural factors, there was difficulty in understanding software development problems with two projects that involved software developers from India, Japan and the United States (Chand, 2004). Cultural study and inter-cultural communication have been of interest since 1950 (Rogers, Hart, & Mike, 2002). Much interest has been placed on culture in business in the last two decades, and

it has never been as important in business terms as it is today. Culture is important for many aspects of business life especially when a business must interface with people, either as customers, employees, suppliers or stakeholders.

Cross-cultural research has had most value therefore when it has been able to provide substance to modern management practices and techniques. Differences between nations and societies make it critical to understand how institutional and cultural factors influence IT application (Martinsons & Davison, 1998). Theories tend to be developed in a specific cultural environment and expect to transfer seamlessly to a different cultural environment is naïve (Martinsons & Davison, 1998). The study of the field began in earnest with the work of Hofstede with his landmark study of IBM (Hofstede, 1980).

4. Hofsteds Cultural Dimensions

Hofstede's work on culture is the most widely cited in cultural studies (Hofstede, 1997; Jones, 2007). His results are based on an extensive study consisting of 116,000 questionnaires, from which over 60,000 people responded from over 50 countries. From the data he obtained he provided a factor analysis of 32 questions in 40 countries. From this he identified four dimensions of societal culture (Hofstede, 1980) - power distance index (PDI), Individualism (IDV), Masculinity (MAS), Uncertainty avoidance index (UAI). A subsequent study revealed a fifth dimension - Long term orientation (LTO).

According to Hofstede (1997) the most important differences between cultures can be captured by finding out to what extent members of these cultures differ with regard to five values:

- Power distance index (mainly the degree of dependence between boss and subordinates),

- Individualism (the degree in which everyone is expected to look after him or herself) versus Collectivism (integration into cohesive in-groups),

- Masculinity versus femininity (masculinity is high in societies in which social gender roles are clearly distinct and femininity is high in societies in which social gender roles overlap),

- Uncertainty avoidance index (the extent to which the members of a culture feel threatened by uncertain or unknown situations)

- Long term orientation (the importance attached to the future versus the past and present.

Figure 1 shows Hofstede's values for these cultural dimensions for Australia, India, United Kingdom and Japan and a clear picture indicating that cultures around the world have different patterns of social behaviour and interaction. From the figure it is clear that what works for one culture may or may not work for somewhere else.

5. Cross-Cultural Research in Implementing Agile

In recent years multi-cultural practices and values have become significantly conspicuous in corporate businesses (Kanungo, 2006). According to Herbsleb (2007), globally-distributed projects are rapidly becoming the norm for large software systems, even as it becomes clear that global distribution of a project seriously impairs critical coordination mechanisms. Over decades, organizations are devoting effort to address this issue. According to Rama Prasad Kanungo (2006) openness, transparency, acceptance of ideas and products, willingness to engage are all some of the shared values that will reflect interdependence between cultures. Cross cultural research has had most value when it has been able to provide substance to modern management practices and techniques (Jones, 2007).

There are and will continue to be inter-cultural factors that affect both collocated and distributed software development efforts (MacGregor, Hsieh, & Kruchten, 2005). Connections between Software Development Methodologies (SDM) and cultural issues have been discussed previously (Abrahamsson, Salo, Ronkainen, & Warsta, 2002; Yourdon, 1986). There is clear visibility of connections between SDMs and cultural related issues on the national level. It is no longer unusual for a large software project to have teams in more than one location, often in more than one continent. Many forces have conspired to bring about this situation, including concern for cost, the need to tap global pools to acquire highly skilled resources, finding an appropriate mix of expertise for a project, satisfying investment requirements imposed by governments in foreign markets, and mergers and acquisitions (Herbsleb, 2007). There is little reason to expect these factors to diminish in the future. Rather, it appears that we face increasing globalization of markets and production, increasing the pressure to distribute projects globally.

This paper emphasizes or studies culture and software methodology, specifically Agile methodology. The authors are addressing problems that arise when developers from different culture work together and also focus on problems that originate in gaps between a national culture and the culture that is inspired by a given SDM,

here Agile methodology. This research deals with connections between cultural characteristics and the willingness of software engineering teams to adopt a given SDM. As it is well known software development entails many problems including clashes in customer-developer communication, bugged software, misunderstanding among team members, requirements not being clearly understood by the team etc.

In order to address these multicultural software development concerns the authors analysed the Agile principles (defined by Agile Manifesto) for cross-cultural factors. Agile specific cultural attributes relevant to multicultural concerns were identified (Table 3). A good relationship pattern was clearly seen and all these Agile specific cultural attributes corresponded to Hofstede's cultural dimensions. Further to this, the culture and Agile specific attributes were categorized into different groups based on Hofstede's cultural dimensions (Table 4). Hofstede's previous study helped in identifying societal cultural dimensions for different nationalities. Based on these values, a set of cultural specific attributes were matched (Table 5).

For example, Power Distance Index for India is high with a value of 77, and in turn Power Distance Index (PDI) for Australia is low with a value of 36 and world average value is 55. Power Distance Index dimension looks at how much a culture does or does not value hierarchical relationships and respect for authority (Hofstede, 1998). The set of cultural specific Agile attributes that have relationship with PDI include:

- Trust people more than process
- Transparency
- Authoritative
- Quick Decision Making
- Empowered
- Proactiveness
- Management support
- Collective ownership
- Blame sharing
- Negotiation
- Conflict Resolution

A mixed team with different cultural dimensions will be highly problematic. This condition is not necessarily forced upon the population, but rather accepted by the society as their cultural heritages. Cultures with a lower power distance have employees who are not afraid of authority and the bosses are not autocratic or paternalistic. Employees from these cultures express a preference for a consultative style of decision making and participative management style. In turn cultures with a high power distance are not expected to be involved in decision making and participative. Thus an understanding of the culture specific Agile attributes will help in a better team management and a successful project team. The cultural bias can be used to build a sense of team management and in turn a better software development project. Previous research in similar fields is listed in Table 6. The findings of this research aim to make contribution to agile adoption and to societal culture research. In addition this research contributes to and extends theoretical knowledge on agile adoption process. This study is the first to research agile methodology implementation in different cultures.

6. Conclusion

It is difficult to get every team member to change how they think overnight. Rather than trying to build understanding about agile methods as a full set, this study helps select and introduce attributes that best apply to a given societal culture. Specifically, based on our research on cultural differences and issues related to software development teams, a model is presented to help understand what attributes to consider depending on the national cultural dimensions. This will help to adapt and adjust the team expectations to the realities of the cultural impacts. The outcome of this study is to provide a framework that can be used to describe, analyse, and change culture that will help to implement Agile methods. We hope that the results of our efforts will be not only tangible and utilizable set of results but also a clear path for future research.

References

Abernethy, K., Kelly, J., Sobel, A., Kiper, J. D., & Powell, J. (2000). *Technology Transfer Issues for Formal Methods of Software Specification.* Paper presented at the 13th Conference on Software Engineering Education and Training, USA.

Abrahamsson, P., Salo, O., Ronkainen, J., & Warsta, J. (2002). *Agile software development methods - Review and Analysis*: University of Oulu.

Avital, M., & Vandenbosch, B. (2000). *The relationship between psychological ownership and IT-driven value.* Paper presented at the Proceedings of the twenty first international conference on Information systems Brisbane, Queensland, Australia

Begel, A., & Nagappan, N. (2007). *Usage and Perceptions of Agile Software Development in an Industrial Context: An Exploratory Study.* Paper presented at the First International Symposium on Empirical Software Engineering and Management.

Bostrom, R. P., & Kaiser, K. M. (1981). *Personality Differences Within Systems Project Teams: Implications for Designing Solving Centres*.

Bustard, D. W., & Lundy, P. J. (1995). *Enhancing soft systems analysis with formal modelling*. Paper presented at the RE '95 Proceedings of the Second IEEE International Symposium on Requirements Engineering.

Cerpa, N., & Verner, J. M. (2009). Why did your project fail? *Communications of the ACM, 52*(12), 130 - 134.

Chand, D. (2004). Is an understanding of national cultures essential for Global IT Managers?

Cheney, P. H. (1988). *Information Systems Skills Requirements: 1980 & 1988*.

Cohen, I., & Bar-On, D. (1989). *Working with Structured Methods - a Case Study*. Paper presented at the Proceedings of fourth conference on Computer Systems and Software Engineering.

Eveleens, L., & Verhoef, C. (2010). The Rise and Fall of the Chaos Report Figures. *IEEE software*.

Hartwick, J., & Barki, H. (1994). Explaining the role of User participation in Information System use. *Management Science, 40*(4), 440 - 465.

Herbsleb, J. D. (2007). *Global Software Engineering: The Future of Socia-technical Coordination.* Paper presented at the Future of Software Engineering.

Highsmith, J. (2002). *Agile Software Development Ecosystems*. Indianapolis: Addison-Wesley.

Hofstede, G. (1980). *Culture's consequences: International differences in work-related values*. Newbury Park, CA: Sage.

Hofstede, G. (1997). *Culture and Organisations: Software of the Mind*. New York: McGraw-Hill.

Hofstede, G. (1998). Attitudes, Values and Organisational Culture: Disentangling the concepts. *Organisational studies, 19*(3), 477.

Imamoglu, O., & Gozlu, S. (2008). *The Sources of Success and Failure of Information Technology Projects: Project Manager's Perspective*. Paper presented at the PICMET 2008 Proceedings.

Jones, M. L. (2007). *Hofstede - Culturally questionable?* : University of Wollongong.

Kanungo, R. P. (2006). Cross culture and business practice: are they coterminous or cross-verging? . *Emarald, 13*(1), 23-31.

Lamsweerde, A. v. (2000). *Requirements engineering in the year 00: a research perspective*. Paper presented at the Proceedings of the 22nd international conference on Software engineering.

Leonard, A. (2002). *Enabling End Users To Be More Efficient During Systems Development.* Paper presented at the Proceedings of SAICSIT 2002.

Love, P. E. D., Ghoneim, A., & Irani, Z. (2004). Information technology evaluation: classifying indirect costs using the structured case method. *Journal of Enterprise Information Management, 17*(4), 312-325.

Lucas, H. C. (1971). *A User-Oriented Approach to Systems Design*. Paper presented at the Proceedings of the 1971 annual conference.

MacGregor, E., Hsieh, Y., & Kruchten, P. (2005). *Cultural Patterns in Software Process Mishaps: Incidents in Global Projects.* Paper presented at the Human and Social Factors of Software Engineering (HSSE), Missouri, USA.

Martinsons, M. G., & Davison, R. M. (1998). Cultural Considerations in Business Process Change.

Rogers, E. M., Hart, W. B., & Mike, Y. (2002). Edward T Hall and the history of Intercultural Communication: The United States and Japan. *Keio Communication Review, 24*.

Rohn, J. A., Spool, J., Ektare, M., Koyani, S., Muller, M. J., & Redish, J. G. (2002). *Usability in practice*

alternatives to formative evaluations - evolution and revolution. Paper presented at the Conference on human factors and computing systems.

Shine Technologies. (2003). Agile methodologies - Survey results. Retrieved 27th May 2010, 2010, from http://www.shinetech.com/attachments/104_ShineTechAgileSurvey2003-01-17.pdf

Standish Group. (2004). *2004 Third Quarter Research Report*. West Yarmouth, MA, USA: The Standish Group International.

Valencia, R. E. G., Olivera, V., & Sim, S. E. (2007). *Are Use Cases Beneficial for Developers Using Agile Requirements?* Paper presented at the Fifth International Workshop on Comparative Evaluation in Requirements Engineering.

Yourdon, E. (1986). *What ever happend to structured analysis?*

Table 1. Standish Chaos report – project benchmark over the years (Eveleens & Verhoef, 2010)

Year	**Successful (%)**	**Challenged (%)**	**Failed (%)**
1994	16	52	31
1996	27	33	40
1998	26	46	28
2000	28	49	23
2004	29	53	18
2006	35	46	19
2009	32	44	24

Table 2. Benefits to Agile development methodologies (Begel & Nagappan, 2007)

No.	**Benefits with Agile development**	**Participant number**
1.	Improved communications	121
2.	Quick releases	101
3.	Flexibility of design	86
4.	More reasonable process	65
5.	Increased quality	62
7.	Better customer focus	50
8.	Increased productivity	28
9.	Better morale	23
10.	Testing first	22

Table 3. Culture and Agile specific attributes defined based on Agile principles

Defined/Identified Culture and Agile Specific Attributes	**Agile Principles – defined by Agile Manifesto**											
	Satisfy the customer through early and continuous delivery of valuable software	Sustainable development is promoted, facilitating indefinite development	Simplicity is essential – the art of maximising the amount of work not done is essential	Welcome changing requirements, even late in development	Deliver working software frequently	Working software is the primary measure of progress	Continuous attention to technical excellence	Business people and developers must work together daily	Face-to-face communication is the best method of conveying information	The team regularly reflects on how to become more productive and efficient	The best work emerges from self-organising teams	Build projects around motivated individuals
Trust people more than process		✓			✓			✓		✓	✓	✓
Transparency	✓		✓		✓			✓	✓	✓	✓	✓
Team collaboration		✓			✓			✓		✓	✓	✓
Self-organizing team		✓			✓	✓	✓	✓		✓	✓	✓
Dedicated team		✓			✓			✓		✓	✓	✓
Risk Taking				✓							✓	
Innovation				✓						✓		
Authoritative					✓							
Quick Decision Making	✓	✓	✓	✓	✓	✓		✓		✓	✓	
Open and honest communication		✓			✓	✓			✓			
Tolerance for change	✓			✓	✓	✓						
Empowered												✓
Meeting deadlines and expectations	✓	✓		✓	✓	✓						
Proactiveness	✓	✓	✓		✓	✓						
Time keeping	✓	✓			✓							
Direct customer involvement	✓	✓		✓		✓			✓			
Management support	✓	✓			✓	✓		✓				✓
Collective ownership	✓	✓		✓				✓			✓	✓
Blame Sharing	✓			✓				✓			✓	
Negotiation	✓	✓		✓				✓		✓	✓	
Conflict Resolution	✓			✓				✓		✓	✓	

Table 4. Culture and Agile specific attributes versus Hofstede's cultural dimensions

Culture and Agile specific attribute	**Hofstede Cultural Dimension**				
	Power Distance	Individualism	Masculinity	Uncertainty Avoidance Index	Long term Orientation
Trust people more than process	✓				✓
Transparency	✓				
Team collaboration		✓			
Self-organizing team		✓			
Dedicated team		✓			
Risk Taking				✓	✓
Innovation				✓	
Authoritative	✓		✓		
Quick Decision Making	✓	✓			✓
Open and Honest Communication		✓			
Tolerance for change				✓	
Empowered	✓		✓		
Meeting deadlines and expectations				✓	✓
Proactiveness	✓	✓			
Time keeping				✓	✓
Direct customer involvement		✓			
Management support	✓				
Collective ownership	✓	✓			
Blame Sharing	✓	✓			
Negotiation	✓	✓	✓		
Conflict Resolution	✓	✓	✓	✓	

Table 5. Hofstede's Cultural dimensions and related culture and Agile specific attributes

Hofstede's Cultural Dimensions	**Culture and Agile Specific Attributes**
Power Distance Index (PDI)	Trust people more than process
	Transparency
	Authoritative
	Quick Decision making
	Empowered
	Proactiveness
	Management support
	Collective ownership
	Blame Sharing
	Negotiation
	Conflict Resolution
Individualism (IND)	Team Collaboration
	Self organising Team
	Dedicated Team
	Quick Decision making
	Open and Honest Communication
	Proactiveness
	Direct Customer Involvement
	Collective Ownership
	Blame Sharing
	Negotiation
	Conflict Resolution
Masculinity (MAS)	Authoritative
	Empowered
	Negotiation
	Conflict Resolution
Uncertainty Avoidance Index (UAI)	Risk taking
	Innovation
	Tolerance for Change
	Meeting deadlines and expectations
	Time keeping
	Conflict Resolution
Long term Orientation (LTO)	Trust people more than process
	Risk taking
	Quick Decision Making
	Meeting deadlines and expectations
	Time keeping

 ISSN 1913-1844 E-ISSN 1913-1852

Table 6. Previous research in similar fields

Previous Methodology Studies	**Previous Societal Culture Studies**
Actual use of methods in UK (Fitzgerald (1997), Hardy, Thompson and Edwards (1995), and Chatzoglou (1997)	Differences in motivation of analysts and programmers in Singapore and the U.S (Couger (1986)
Use of software systems development methods in Brunei (Rahim, Seyal and Rahman (1998)	The Effects of Culture on Performance Achieved through the use of Human Computer Interaction (Ford & Gelderblom (2003)
Use of methodologies and CASE tools in Norway (Krogstie (1995))	Evaluating the impact of Cultural Differences among software Programmers in India and in the US (Maudgalya, 2004)
Adoption of SSADM in a government agency in Australia (Sauer and Lau (1997)	Exploring the Relationships between Individualism and Collectivism and Attitudes towards Counseling among Ethnic Chinese, Australian and American University students (Snider, 2003)
	Cross-cultural leadership (Grisham, 2006)
	Culture and International Usability Testing: The effects of Culture in Interviews (Vatrapu, 2002)
	Cultural Influences and Differences in Software Process Improvement Programs (Wong & Hasan, 2008)
	An investigative study into the adoption of cross-cultural management practices in selected public and private sector organizations – A grounded theory approach (Reyes, T M, 2005)
	The Reflexivity between ICTs and Business Culture: Applying Hofstede's theory to compare Norway and the united States (Sornes, Stephens, Saetre & Browning, 2004)

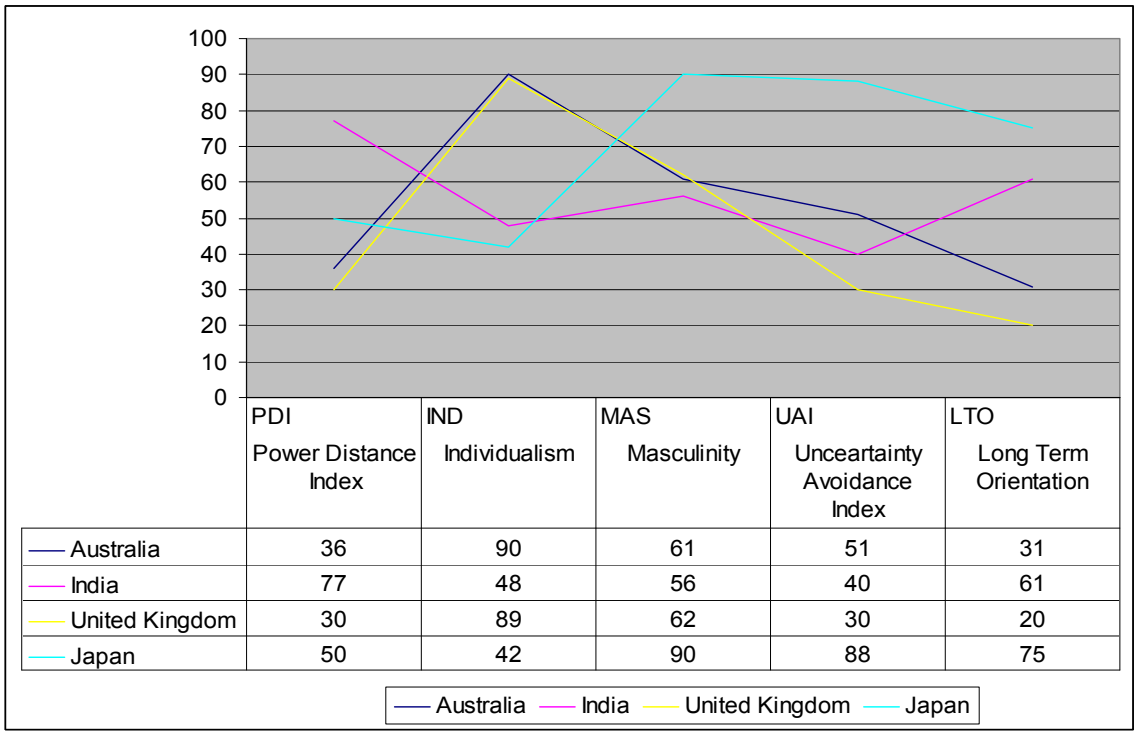

	PDI Power Distance Index	IND Individualism	MAS Masculinity	UAI Uncertainty Avoidance Index	LTO Long Term Orientation
Australia	36	90	61	51	31
India	77	48	56	40	61
United Kingdom	30	89	62	30	20
Japan	50	42	90	88	75

Figure 1. Hofstede's cultural dimensions – Australia, India, United Kingdom, and Japan

ISSN 1913-1844 E-ISSN 1913-1852

Influence of Cement Content on Recycled Aggregates Concrete Properties

Athanas KONIN (Corresponding author)
Institut National Polytechnique Félix HOUPHOUET-BOIGNY
BP 1093 Yamoussoukro, Côte d'Ivoire
Tel: 225-30-64-36-32 E-mail: kathanas@yahoo.fr

David Mangoua KOUADIO
Laboratoire du Bâtiment et des Travaux Publics
04 BP 03 Abidjan 04, Côte d'Ivoire
Tel: 225-21-21-23-35 E-mail: madok83@yahoo.fr

Abstract

This article presents the results of an experimental investigation carried out to study the influence of cement content on the properties of recycled aggregates concrete. Five concrete mixtures (containing natural aggregates or recycled ones) with different cement content (250, 300, 350, 400 and 450 kg/m^3) were studied. Tests were performed to measure porosity to water, permeability to gas and compressive strength (at 2, 7 and 28 days). The results indicated that an increase in cement content (over 300 kg/m^3) allows to reduce significantly the porosity to water and to enhance the compressive strength of recycled aggregates concrete. Correlations based on properties of these concrete are presented. That allows to apply the formulation method of natural aggregates concrete to prepare recycled aggregates concrete.

Keywords: Natural aggregates, Recycled aggregates, Porosity to water, Compressive strength, Cement content

1. Introduction

The treatment of waste becomes nowadays a priority. We can store after processing or, better, recycle them in a new product. The re-use of demolition waste has increased as recycling technologies have been developed and improved during the last years (RILEM TC, 2000; RILEM TC, 2004; SBEICO, 2009). Unfortunately, the amount of concrete demolition waste is still increasing world wide. Taking into account that concrete will continue to be the dominant construction material in the future, several research projects have been conducted on the use of recycled aggregates into concrete. The potential benefits and drawbacks of using recycled aggregate concrete have been studied (Topcu, 1995; Neville, 2000; Tu *et al*., 2006; Zega *et al*., 2010).

The use of recycled aggregate generally increases the drying shrinkage, creep and porosity to water and decreases the compressive strength of concrete compared to those of natural aggregate concrete (Sri and Tam, 1985; Hansen, 1996; Wirquin *et al*., 2000; Poon *et al*., 2002; Domingo *et al*., 2010). However, the shortcomings of using recycled aggregate can be mitigated by increasing the cement content into the concrete mixture since it is well-known that the amount of cement has an effect on concrete's compressive strength and porosity to water (Tavakoli and Sorousian, 1996; Limbachiya *et al*., 2007).

In Côte d'Ivoire, the use of recycled aggregates in the manufacture of concrete is still at artisanal stage, no rules and specifications concerning the use of these materials exist. Moreover, the natural aggregate resources are limited, recycled aggregates can be used as a supplement to natural aggregates or under certain conditions, instead of them. That can constitute an alternative to environmental preservation and satisfying the needs of sustainable development.

The purpose of this paper is to study the effect of cement content on recycled aggregates concrete properties. In the study, the influence of cement content on compressive strength, permeability to gas and porosity to water on recycled aggregate concrete were investigated.

The final objective of this work is to establish correlation between recycled aggregate concrete and natural aggregate concrete.

2. Experimental program

2.1 Materials

A Portland cement type CPA CEM II 32.5 is used in the concrete mixtures. The properties of cement are given in Table 1.

Natural and recycled aggregates were used as the coarse aggregate in the concrete mixtures. For this study, crushed granite was used as the natural aggregate and recycled aggregate sourced from demolition waste was used. The porosity to water of the aggregate was determined. Natural siliceous sand was used as fine aggregate in the concrete mixture. The physical and mechanical characteristics of the coarse aggregate are shown in Table 2.

2.2 Concrete mixtures

The concrete mixtures were formulated with five different cement contents (250, 300, 350, 400 and 450 kg/m^3). Full replacement of natural coarse aggregate by recycled aggregate was adopted, keeping constant the coarse aggregate volume. Water proportioning was adjusted to obtain concrete having a value with the slump test of 8 cm. The absolute volume method was adopted to design the mix proportions of the concrete compositions as shown in Table 3. The notations are as follows:

- NAC : Concrete made with natural coarse aggregate,
- RAC : Concrete made with recycled coarse aggregate.

2.3 Specimens casting and curing

For each composition, cylindrical specimens of 16 x 32 cm were cast. Specimens were used to determine the physical and mechanical properties of concrete. All samples were cast in steel moulds and compacted using a vibrating needle. After unmolding, the specimens for porosity to water and permeability to gas were kept in a saturated chamber for 7 days, then sawed in 4 cylindrical specimens of 5 cm height (Figure 1) which were dried at 50°C in an air forced oven during 3 days, after that, each sample was sealed with plastic and put in a chamber at the same temperature for humidity redistribution until 28 days of age when they were tested. The others specimens were cured in a water tank at 27 ± 1°C until test ages were reached.

2.4 Physical and mechanical tests

Tests for the determination of physical and mechanical properties have been carried out on the samples.

- For the physical properties, the tests carried out are:
    - Porosity to water was measured by total water satured method according to AFPC-AFREM (1997) procedure. The initial weight of the specimens were determined (M_a) and then immersed in tanks containing water. The specimens were kept immersed until they reached to a constant weight (M_w). After that, they were moved to an oven and maintained at 105°C until they reached to a constant weight (M_d).
    - A permeameter with constant load of nitrogen type CEMBUREAU was used to measure the capacity of concrete to be crossed by a gas. That supplies the apparent permeability of the material dependent on the pressure of injection. To determine the intrinsic permeability, the relation proposed by Klinkenberg (1941) was used.
- For the mechanical properties, it relates to the testing of:
    - Compressive strength was determined using a PERRIER compression machine with a loading capacity of 300 kN. The compressive strength tests were carried out at the ages of 2, 7 and 28 days.

3. Results and Discussion

3.1 Porosity to water

The results of porosity to water given on figure 2 are the average of 4 measurements on 4 specimens of the same sample. This figure shows that the porosity to water decreases with the increase of cement content for all concrete. As expected, the values of porosity of normal aggregate concrete are low than those of recycled aggregate concrete. However, for the concrete with high cement content (350 to 450 kg/m^3), the difference between mixtures with recycled and natural aggregates is less than the others. This is due to the better matrix quality. With low cement content compositions, there is a more porous matrix involving the participation of the recycled aggregates.

Indeed, in the case of natural aggregates concrete, the porosity is mainly due to the network of the capillary pores (concrete is by nature a porous material). While in the case of recycled aggregates concrete, besides this network of capillary pores, there are mechanical cracks existing in the recycled aggregates. That increases strikingly the porosity of these concretes. Figure 3 schematizes the progress of the water in these two types of concrete.

3.2 Permeability to gas

Figure 4 gives the results of the measures of permeability to gas. The results are presented as permeability coefficient obtained from the measured flux of nitrogen at different pressures through the specimen. This figure shows that the permeability coefficient decreases with the increase in cement content. The results are in the same way of those of porosity to water. For the high cement content, the difference between nitrogen permeability of recycled aggregates concrete and natural aggregate concrete is less than for low cement content. Comparing the results of mixtures with recycled aggregates to those with natural aggregate of lower cement content, it can be said that to achieve the same level of nitrogen permeability for the two concrete, it is necessary to increase the cement content. Similar results have been obtained by Kou *et al.* (2008) on recycled aggregate concrete containing fly ash.

Not withstanding the fact that natural aggregates concrete are better physical properties than those of recycled one (Domingo *et al.*, 2010), the porosity to water and gas permeability of recycled aggregate concrete tend to decrease with an increase in the cement content.

3.3 Compressive strength

Each value presented in Table 4 is the average of three measurements. For all samples tested, the compressive strength of concretes made with recycled aggregates is lower than that with natural aggregates. These results confirm the role played by the Interfacial Transition Zone (ITZ) in the resistance of concretes (Maso, 1980). Indeed, the works of Konin *et al* (1998) showed that even in the case of high-performance concretes, this interfacial zone paste-aggregate is a zone of low resistance, because of his big porosity. And as more porous is the concrete and less resistant it is, the values obtained were predictable. However, the average decrease is low for concrete with low cement content, the variations are included between 4 % and 5 % for mixtures with 250 to 300 kg/m^3 cement content, whereas the variations are over 8% for mixtures with high cement content (over 300 kg/m^3). Nevertheless, the higher strength decrease was 10% at 28 days for mixture with 450 kg/m^3 of cement.

3.4 Relation between recycled aggregate concrete and natural aggregate concrete

Figures 5 to 7 present the relations between properties of recycled aggregates concrete and those of natural aggregates concrete. On each figure, an equation and a correlation coefficient are presented.

Figure 5 presents the relation between the porosity to water of recycled aggregates concrete and that of natural aggregates concrete. The porosity to water of recycled aggregates concrete is strictly linked to that of natural aggregates concrete. The coefficient of correlation is 0.98.

Figure 6 presents the relation between the nitrogen permeability of recycled aggregates concrete and that of natural aggregates concrete. The nitrogen permeability of recycled aggregates concrete is strictly linked to that of natural aggregates concrete. The coefficient of correlation is 0.94.

Figure 7 presents the relation between the compressive strength of recycled aggregates concrete and that of natural aggregates concrete. The compressive strength of recycled aggregate concrete is strictly linked to that of natural aggregate concrete. The coefficient of correlation is 0.99, 0.98 and 0.99 respectively at 2, 7 and 28 days.

From these data, it is possible to obtain a reduction factor "r" which allows to estimate the compressive strength of recycled aggregates concrete when that of natural aggregates concrete is known for the same proportion of concrete. This coefficient can also be used to adapt the formulation method of natural aggregates concrete to recycled aggregates concrete. So, to produce a recycled aggregates concrete with compressive strength f_{cr}, it is enough to use proportion of mixture corresponding to a natural aggregates concrete with compressive strength: $f_{cm} = f_{cr} / r$.

For this study, the main value of the coefficient "r" is worth 0.92 as indicated in Table 5 below.

4. Conclusion

The presented study concerns the possibility of using recycled aggregates in the formulation of concrete as a replacement of natural aggregates. At the end of this experimental study, the following conclusions can be drawn:

- The use of recycled aggregates produces concrete with lower performances to durability related properties, mainly due to the higher porosity of recycled aggregates. Nevertheless, the use of high cement content (over 300 kg/m^3) allows improving recycled aggregate concrete properties.
- The variation between the compressive strength of recycled aggregates concrete and those of natural aggregates concrete are lower than 10 % independently to cement content.
- The correlations are presented between the properties recycled aggregates concrete and those of natural aggregates concrete.
- A reduction factor "r" is determined that allows to adapt the formulation of natural aggregates concrete to recycled aggregates concrete.

The results confirm the opportunity of a large use of recycled aggregates in the manufacturing of concretes. The use of these aggregates constitutes an undeniable ecological contribution.

References

AFPC-AFREM. (1997). *Durabilité des bétons, méthodes recommandées pour la mesure des grandeurs associées à la durabilité*, compte-rendu des journées techniques de l'AFPC-AFREM, France, 11-12 Décembre.

DOMINGO, A., LAZARO, C., GAVARRE, F. L., SERRANO, M. A. & LOPEZ-COLINA, C. (2010). Long term deformation by creep and shrinkage in recycled aggregate concrete, *Materials and Structures, Vol. 43*. PP 1147-1160.

HANSEN, J. C. (1996). *Recycling of demolished concrete and masonry*. In RILEM report 6, Ed. E & FN Spon.

KLINKENBERG, L. J (1941). *The permeability of porous media to liquids and gases*, American Petroleum Institute, Drilling and Production Practice.

KONIN, A., FRANCOIS, R. & ARLIGUIE, G. (1998). Penetration of chloride in relation to the microcracking state into reinforced ordinary and high strength concrete, *Materials and Structures, vol. 31*. PP 310-316.

KOU, S. C., POON, C. S., & CHAN, D. (2008). Influence of fly ash as a cement addition on the hardened properties of recycled aggregate concrete, *Materials and Structures, Vol. 41*. PP 1191-1201.

MASO, J. C. (1980). *La liaison entre les granulats et la pâte de ciment hydraté*. In 7ème Congrès International de Chimie des ciments, Rapport principal.

LIMBACHIYA, M. C., MARROCHINO, E., & KOULOURIS, A. (2007). Chemical-mineralogical characterization of coarse recycled concrete aggregate, *Waste Management, vol. 27*. PP 201-208.

NEVILLE, A. M. (2000). *Propriétés des bétons*, Ed. Eyrolles.

POON C. S., KOU, S. C., & LAM, L. (2002). Use of recycled aggregates in molded concrete bricks and blocks, *Construction and Building Materials, vol. 16.* PP 281-289.

RAO, A., JHA K. N., & MISRA, S. (2007). Use of aggregates from recycled construction and demolition waste in concrete, *Resource Conservation and Recycling, Vol. 50*. PP 71-81.

RILEM T.C. (2000). *Workshop on Use of recycled materials as aggregates in the construction industry,* France, 11–12 Septembre. Technical communications.

RILEM T. C. (2004). *Conference on use of the recycled materials in building and structures*, Espagne, 9-11 Novembre. Technical communications.

SBEICO (2009). *1st International conference on Sustainable Built, Environment, Infrastructures in developing Countries*, Algérie, 12-14 Octobre. Technical communications.

SRI RAVINDRARAJAH, R. & TAM, C. T. (1987). Recycling concrete as fine aggregate in concrete, *International Journal of Cement Composites and Lightweight Concrete, vol. 9.* PP 235-241.

TAVAKOLI, M. & SOROUSHIAN, P. (1996). Strength of recycled aggregate concrete made using field demolished concrete as aggregate, *ACI Materials Journal, Vol. 93*. PP 178-181.

TOPCU, I. B. & GUNCAN, N. F. (1995). Using waste concrete as aggregate, *Cement and Concrete Research, vol. 25*. PP 1385-1390.

TU, T. Y., CHEN, Y. Y. & HWANG, C. L. (2006). Properties of HPC with recycled aggregates, *Cement and Concrete Research, vol. 36*. PP 943-950.

WIRQUIN, E., ZAHARIEVA, R. H., & BUYLE-BODIN, F. (2000). Utilisation de l'absorption d'eau des bétons comme critère de leur durabilité – Application au bétons de granulats recyclés, *Materials and Structures, vol. 33*. PP 403-408.

ZEGA, C.J., VILLAGRAN-ZACCARDI, Y. A., & DI MAIO, A. A. (2010). Effect of natural coarse aggregate type on the physical and mechanical properties of recycled coarse aggregate, *Materials and Structures, vol. 43*.PP 195-202.

Table 1. Chemical, physical and mechanical properties of cement

Chemical compositions (%)	Al_2O_3	6.94
	CaO	54.50
	Fe_2O_3	3.30
	MgO	1.68
	SO_3	2.05
	SiO_2	17.49
Physical properties	Density (g/cm^3)	2.98
	Specific surface (cm^2/g)	3214
Compressive strength (MPa)	2 days	14.00
	7 days	28.80
	28 days	44.30

The table presents the properties of cement used in this study

Table 2. Aggregate properties

	Size	Density (g/cm^3)	Porosity to water	L.A coefficient
Natural sand	0/2	2.43	-	-
Natural aggregate	5/15	2.70	1.46 %	16.20
	15/25			16.00
Recycled aggregate	8/25	2.61	6.39 %	26.00

Table presents the properties of aggregates used in this study

Table 3. Mixture proportion (kg/m^3)

Materials	NAC 250	NAC 300	NAC 350	NAC 400	NAC 450	RAC 250	RAC 300	RAC 350	RAC 400	RAC 450
Cement	250	300	350	400	450	250	300	350	400	450
NA (15/25)	801	782	761	741	719	-	-	-	-	-
NA (5/15)	549	536	522	508	493	-	-	-	-	-
RA (8/25)	-	-	-	-	-	1296	1267	1218	1180	1139
Natural sand	585	572	557	542	526	582	568	546	530	511
Water (L)	176	176	178	180	183	180	181	192	196	202
Density (g/cm^3)	2.31	2.34	2.40	2.45	2.46	2.26	2.30	2.35	2.40	2.44

This table presents the different proportion of mixture

Table 4. Compressive strength of studied concrete (MPa)

Testing age	NAC 250	RAC 250	NAC 300	RAC 300	NAC 350	RAC 350	NAC 400	RAC 400	NAC 450	RAC 450
2 days	5.6	5.1	8.8	8.3	9.6	8.9	11.1	10.5	12.2	11.6
7 days	12.0	11.5	16.5	15.2	17.7	16.9	23.8	20.2	26.7	24.3
28 days	15.2	14.3	21.6	20.2	23.5	21.6	27.7	25.0	29.9	27.1

This table shows the compressive strength of concrete studied

Table 5. Recycled to natural aggregate concrete strength ratio « r »

	Testing ages		
Cement content (kg/m3)	2 days	7 days	28 days
250	0.89	0.96	0.94
300	0.94	0.92	0.94
350	0.93	0.95	0.92
400	0.95	0.85	0.90
450	0.95	0.91	0.91
Average value of r	0.93	0.92	0.92

This table shows the reduction ratio between recycled to natural aggregate concrete

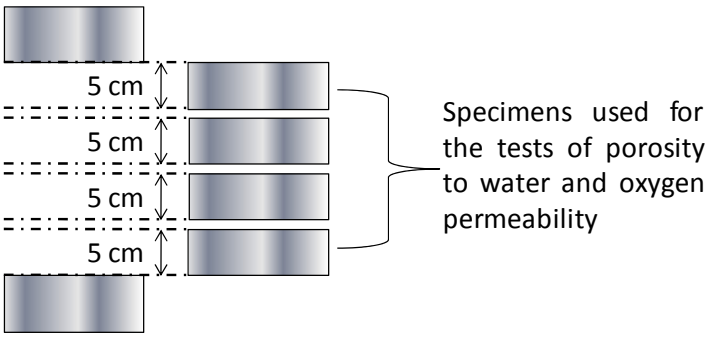

Figure 1. sawing samples used for physical tests

Presentation of the specimens used for physical tests

ISSN 1913-1844 E-ISSN 1913-1852

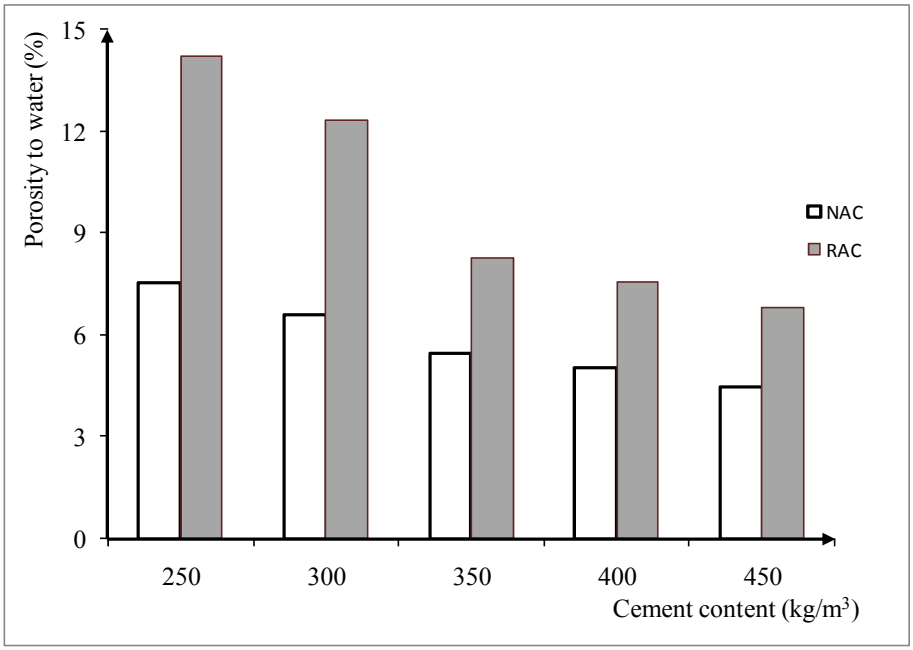

Figure 2. variation of the porosity to water of studied concretes according to the dosage in cement

Results of measurements of porosity to water of studied concrete

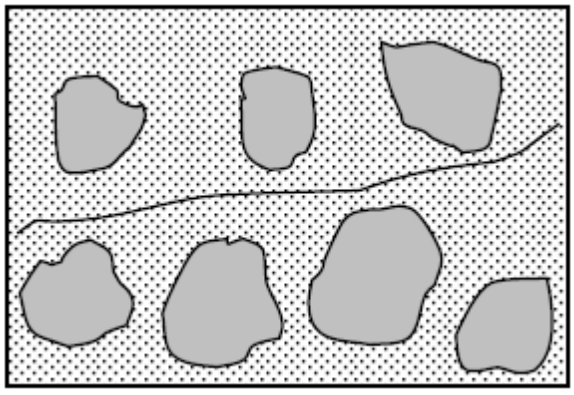

Figure 3a : Natural aggregate concrete

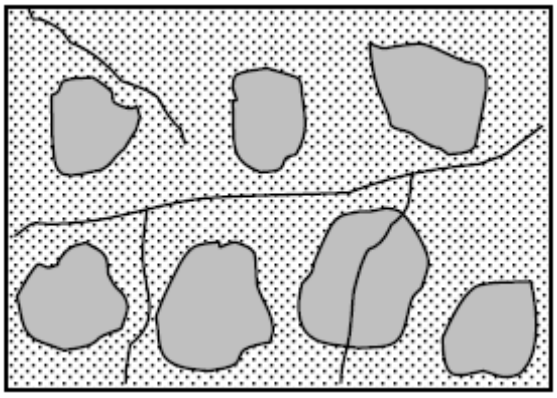

Figure 3b : Recycled aggregate concrete

Figure 3. Preferential path of water according to studied concrete

These figures show the preferential path of water into the two types of concrete

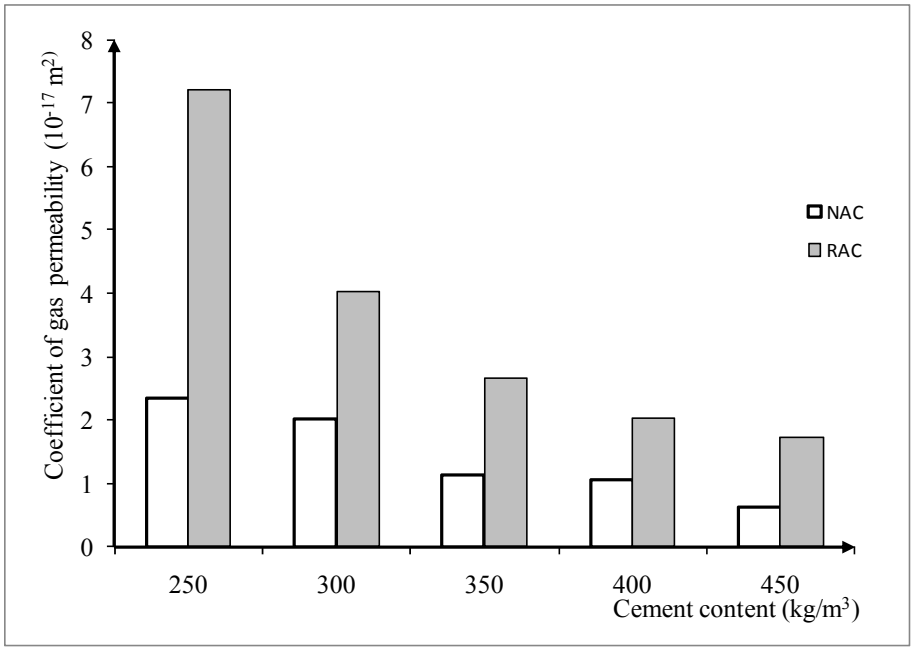

Figure 4. variation of the permeability to gas of concretes according to the dosage in cement

This figure shows the variation of gas permeability of studied concrete

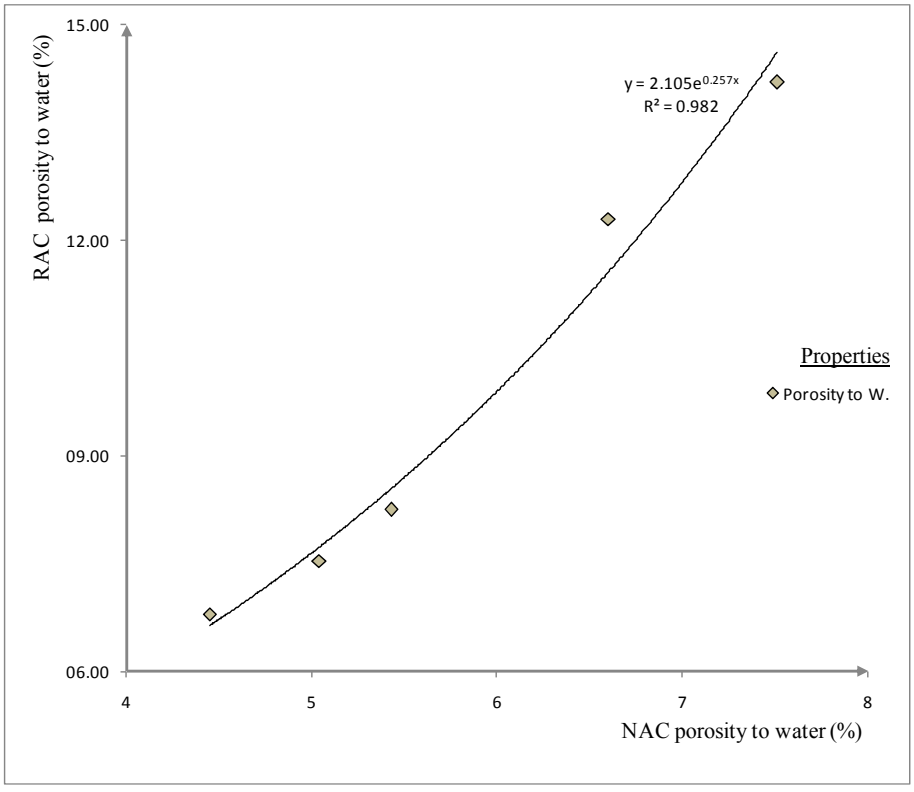

Figure 5. Correlation between recycled aggregates concrete porosity to water and that of natural aggregate concrete

This figure shows correlation between porosity to water of two types of concrete

 ISSN 1913-1844 E-ISSN 1913-1852

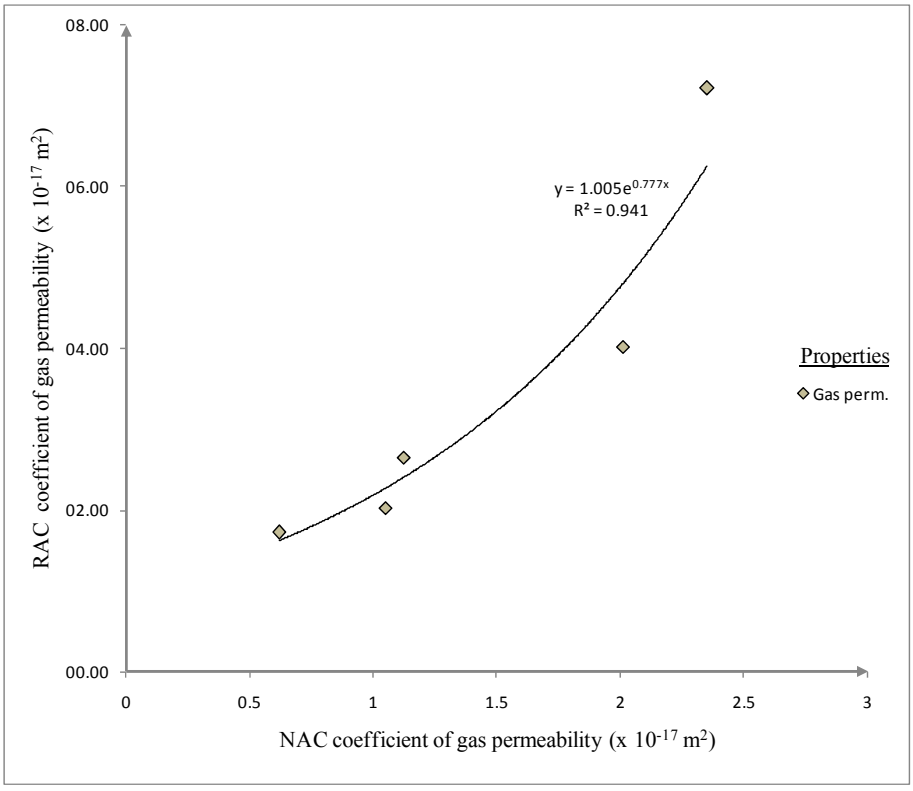

Figure 6. Correlation between recycled aggregates concrete permeability and natural aggregate concrete permeability

This figure shows correlation between gas permeability of two types of concrete

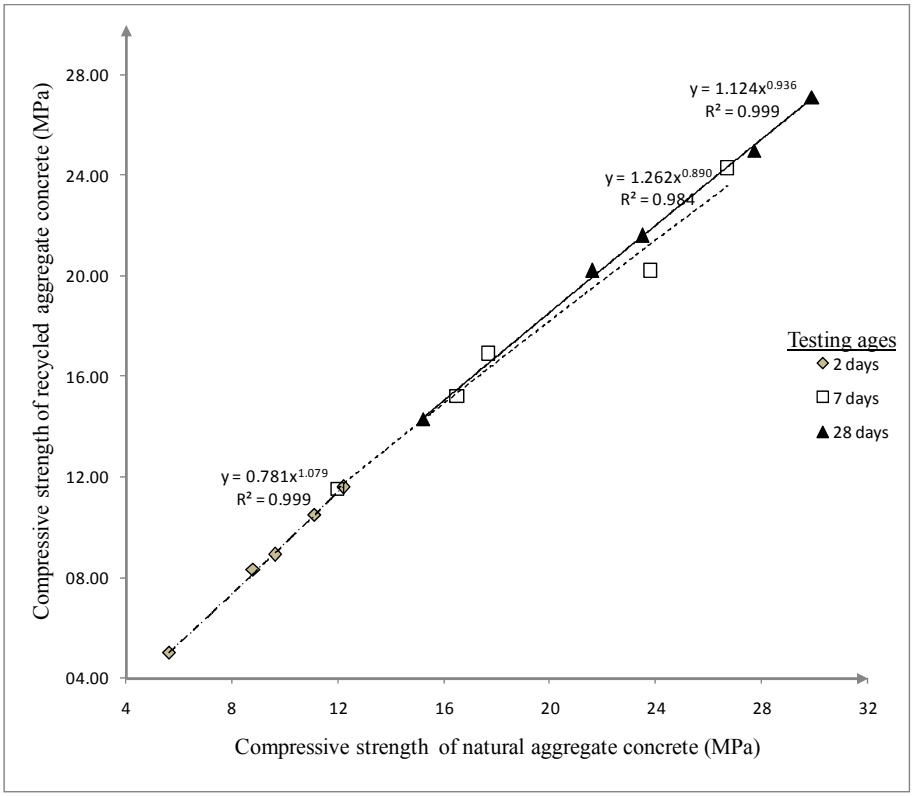

Figure 7. Correlation between recycled aggregates concrete strength and natural aggregate concrete strength

This figure shows correlation between compressive strength of two types of concrete

The Relationship between Environmental Factors and the Onsets of Avian Influenza Outbreaks in Thailand

Hirun Sawaengkaew
Environmental Science (Interdisciplinary Program)
Graduate School, Chulalongkorn University
Phyathai Road, Pathumwan, Bangkok 10330, Thailand
E-mail: hiruns@yahoo.com

Surat Baulert (Corresponding author)
Department of General Science, Faculty of Science, Chulalongkorn University
Phyathai Road, Pathumwan, Bangkok 10330, Thailand
E-mail: surat.b@chula.ac.th

Kumthorn Thirakhupt
Department of Biology, Faculty of Science, Chulalongkorn University
Phyathai Road, Pathumwan, Bangkok 10330, Thailand
E-mail: Kumthorn.T@chula.ac.th

This work was funded by The 90th Anniversary of Chulalongkorn University Fund (2008) (Ratchadaphiseksomphot Endowment Fund)

Abstract

The relationship between environmental factors and the onsets of avian influenza virus (AIV; H5N1) outbreaks in Thailand was studied. The results show that the onsets of the disease correlate with the maximum gradient of temperature and wind speed within 24 hours, density of villages in a radius of five kilometers, and distance from the last AIV outbreak area. This study also presents how meteorological conditions have an effect on the occurrence of onsets of AIV in Thailand.

Keywords: Environmental factors, Avian influenza

1. Introduction

Avian influenza virus (AIV) or bird flu is one of the avian diseases. It can be classified in the Family Orthomyxoviridae and has four types: A, B, C, and D (Thogotovirus). These four types can be further subdivided by Glycoproteins, Hemagglutinin (H) and Neuraminidase (N), which have 16 and 9 subtypes, respectively (Fouchier et al., 2005). AIV is a highly pathogenic avian influenza, which is classified as type A, H5N1. According to the first report of an AIV outbreak in 1997 on Hong Kong Island, it caused an infection in poultry and wild birds, leading to a great number of deaths, and a rapid spread to many countries consequently. Although the disease affected birds, other studies also showed that the infection had caused the death of other animals and human. At present, 262 patients have died from this disease (World Health Organization, 2009).

In Thailand, AIV was first reported in poultry and wild birds in 2004. From 2004 - 2006, the deaths of 17 patients were reported because of infection by AIV. The government established defensive measures to control or to inhibit the spread of AIV by destroying poultry in many areas (Bureau of Disease Control and Veterinary Services, 2006), but the epidemic recurred in these areas. It was thought that there might be other factors involved in the outbreak. Water bird migration, for instance, was presumed to be a factor in the outbreak because the water birds survived AIV (Webster et al., 1992). That meant that if the pandemic occurred along with the migration of water birds, they would have the infection and become carriers to other areas (Sturm-Ramirez et al., 2005; Zhou et al., 2006). However, if the pandemic does not match just the range of bird migration, environmental factors would be seen to assist in spreading the disease to other areas.

At present, scientific reports have found relationships between AIV and several limiting factors namely temperature, pH, and medicinal liquids (World Health Organization, 2009) as well as the ability of AIV to survive in water for 3 days (Songserm et al., 2005). Nevertheless, none of the literature has mentioned the relationship of environmental factors to the AIV outbreak and with the onsets of AIV outbreaks. Therefore, this paper describes the relationship between environmental factors and the onsets of the AIV outbreaks in Thailand, in order to plan disease control in the future.

2. Materials and Methods

2.1 Data preparation

2.1.1 Data about the onsets of AIV outbreaks in Thailand from 2004 to 2008 was taken from the reports by The World Organization for Animal Health (OIE: Office International des Epizooties) and the Department of Livestock Development Thailand (DLD).

2.1.2 Data of meteorology in Thailand from 2004 to 2008 was taken from the report of the Thai Meteorological Department (TMD) and Hydro and Agro Informatics Institute (HAII). The meteorological data included temperature, atmospheric pressure, specific humidity, windspeed, and rainfall. The meteorological data were taken from monitoring stations near the areas of disease outbreaks within a radius of about 100 kilometers.

2.1.3 The procedures for data preparation concerning meteorology consisted of first, the one-day meteorological record of an onset date, which was the date before the AIV outbreak was officially announced in Thailand, which corresponded to the OIE and DLD criteria since AIV was found to be a symptom of sick animals, and second, the delta (ΔX) representing the maximum gradient of meteorological parameters in 24 hours (Table 1). The following description presents the meaning of each variable in the equations below: (*1*) Xi was the maximum of the meteorological data over 24 hours, and Xj was the minimum of the meteorological data over 24 hours. The specific humidity was calculated by equation (*2*). Q was the specific humidity (g/kg), p was the total atmospheric pressure (mb), e was the vapor pressure (mb) calculated by equation (*3*), f was the relative humidity in percent, and e_m was the saturation vapor pressure (George, 1965).

$$\Delta Xi = Xi_{maximum} - Xj_{minimum} \qquad (1)$$

$$Q = \frac{622e}{p} \qquad (2)$$

$$f = \frac{e}{e_m} x100 \qquad (3)$$

2.1.4 The variance was defined on one day before the OIE and DLD officially announced the onset of AIV outbreak in Thailand, because H5N1 disease takes 24 hours for incubation in poultry.

2.1.5 The data collection of environmental factors consisted of physical data such as the distance between the surrounding villages and the onset AIV village, distance of a stream to the onset AIV village, distance of a road to the onset AIV village, distance of the last outbreak to the onset AIV village, and the density of villages in a radius of five kilometers.

2.1.6 The selection criteria for the study area were based on information about the outbreaks of H5N1 from DLD. DLD determined the circle of the epidemic, which was taken as the period from the first report on the outbreak until the surveillance ended and there was no further report on the outbreak. If there was a new report on the outbreak, the circle of epidemic would start again.

2.2 Statistic Analysis

2.2.1 The data ΔX_i was analyzed by descriptive statistics and multiple regressions.

2.2.2 The data was obtained through the process of multiple regression analysis. The variable was k (X_1, X_2, X_3,....,X_k) correlated with the dependent variable Y by the multiple regression equations. Equation (*4*) was used for checking the criteria of variables before analysis, which consisted of steps: 1) dependent variable must be quantitative whereas independent variable can be both quantitative and categorical; 2) all independent variables (X_1, X_2,., X_k) can be separated from one another; 3) average of the errors equals zero (e = 0); 4) the margin of error has normal distribution; and 5) the variance of e, σ^2, is constant for all values of X (Kalaya, 2008). If Y is high and suggests that the environment affects the limiting factors of AIV infection, this indicates that the environment is conducive to survival of the virus.

$$Y = \beta_0 + \beta_1 X_1 + \beta_2 X_2 \ldots + \beta_k X_k. \qquad (4)$$

where

Y= opportunity to become the onset of disease in Thailand

β = constants from the equation

X_k = variables

3. Results and Discussions

The phenomena of AIV onsets in Thailand happened seven times from 2004 to 2008 (Fig. 1). In 2004, AIV was found in a layer chicken farm (*a,b*); in 2005 it was found in a partridge farm (*c*); in 2006 it was found in backyard chicken in one village (*d*); in 2007 it was found in a layer duck farm and in backyard chicken (*e*) and in 2008 it was also found in backyard chicken (*f,g*). The study areas for this research covered seven provinces including Suphan Buri, Phichit, Phitsanulok, Phra Nakhon Si Ayutthaya, Sukhothai, Nakhon Sawan, and Uthai Thani (Fig. 2). These areas reported repeated outbreaks, especially in some provinces such as Suphan Buri, Phitsanulok, and Phichit, which reported outbreaks more than twice.

According to descriptive statistics, the ratio of the occurrence of AIV was 1,098,579 (± 1,097,818), Delta temperature was 8.3 (± 2.6) celsius (°C), Delta atmospheric pressure was 5.8 (± 2.8) hectopascals (hPa), Delta specific humidity was 2.5 (± 0.5) grams per kilogram (g/kg), Delta wind speed was 0.8 (± 0.2) meters per second (m/s), and average rainfall within 24 hours was 1.2 (± 3.4) millimeter (mm.). Besides the above, physical environmental factors showed that the number of villages around the onset village in a radius of five kilometers was 15.6 (± 8.36) villages/five kilometer; the density of villages in a radius of five kilometers was -0.8 (± 0.2) village/density of village in onset area; the distance between the last point of the outbreak and the onset of outbreak was 30.6 (± 17.3) kilometers (km.); the distance of water from the onset area was 2.6 (± 0.7) km; and the distance of a road from the onset area was 1.8 (± 2.5) km.

The analysis of multiple regression found that there was a relationship between the environmental factors and the onsets of AIV outbreak such as delta temperature (p-value= 0.02), delta wind speed (p-value= 0.014), the density of villages in a radius of five kilometers (p-value = 0.015), distance of the last outbreak to the onset AIV village (p-value = 0.045), and the distance of the stream to the onset AIV village (p-value = 0.051). Factors, according to the patterns of relationship, can be divided into 2 groups. Firstly, the dynamic factors such as delta temperature and delta wind speed, and secondly, the static factors such as the density of villages in a radius of five kilometers, and the distance of the last outbreak to the onset AIV village. Furthermore, the results showed that if the possibility of getting symptoms for the onset of disease (Y) increases, it will contribute to the increase in the values of four environmental factors. In the other words, if environmental factors are disappear, the possibility of getting illness will not occur.

Opportunity for the onset to occur required 4 factors. These factors influence one another, thus the onset could not happen if the composition was incomplete. For example, if the difference of daily temperature changes a great deal, the difference of wind speed would increase as well. This is because a higher temperature will cause a hot air mass, causing the phenomenon called convection. Then, the cold air mass will replace the rising hot air mass, which is called the advection. If the rising of the hot air mass happens quickly, the cold air mass will also move in quickly to replace it, and this causes the wind. Furthermore, the difference in temperature and humidity causes changes in air mass making a cold front with cold air displacing warm air, and warm front with warm air displacing cool air. From the meteorological data for Thailand in 2004-2008, it was found that there was more water vapor three days before the onset date because four to seven days before the onset date there may have been rain. This phenomenon caused changes in weather conditions, making high humidity before it rained. Therefore, once it was raining, the animals' health would be affected as they could not adjust to the changes of weather and thus their health was weakened. The environmental factors resulted in healthy animals being susceptible, rather than being an issue of distribution of the infection or pollutants in the air.

Wind speed, besides the relation with temperature, is also related to geology. In other words, the onset areas were agricultural areas such as paddy fields, which were an obstruction to the influence of wind speed. According to the principle of Surface Roughness, the wind speed in agricultural areas, for example, does not change because there is less obstruction than in the city.

The density of villages in a radius of five kilometers and the distance from the last outbreak to the onset AIV village are relevant. Where there is a higher density of villages, the community is larger. This makes it easy for extensive transmission of AIV carriers inside the community. Moreover, if the distance between the last onset and the community area is small, it is easy for the carriers, which are infected from the last onset, to incubate the disease and cause the next pandemic circle once there are appropriate meteorological factors.

References

Åkesson, S. and Hedenström, A. (2000). Wind selectivity of migratory flight departures in birds. *Behavioral Ecology and Sociobiology.* 47, 3: 140–144.

Bureau of Disease Control and Veterinary Services. (2005). Guidelines for Avian Influenza Control. Department of Livestock Development. 2nd ed. *The Agricultural Co-operative Federation of Thailand,* Ltd. Printing. Bangkok Thailand. 61 p.

Bureau of Epidemiology. (2004). Epidemiological Surveillance Annual Report 2547. http://203.157.15.4/Annual/ Annual47/ part1/16-%E4%A2% E9%CB%C7%D1%B4%B9%A1.pdf (online) 1 June 2009

Bureau of Epidemiology. (2005). *Epidemiological Surveillance Annual Report* 2548 [Online] Available: http://203.157.15.4/Annual /Annual48/Part1/16-Avian%20influenza.doc (online) 1 June 2009

Bureau of Epidemiology. (2009). *Surveillance of avian influenza in humans.* [Online] Available: http://203.157.15.4/surdata/ai/ dailyreport/y52/r280952.pdf (online) 7 October 2009

Fouchier, R.A., Munster, V., Wallensten, A., Bestebroer, T.M., Herfst, S., Smith, D., Rimmelzwaan, G.F., Olsen, B., Osterhaus, A.D. (2005). Characterization of a novel influenza A virus hemagglutinin subtype (H16) obtained from black-headed gulls. *J Virol.* 79: 2814–22.

George F. Taylor, G. F. (1965). *Elementary Meteorology.* 8th ed. New York: Prentice-Hall; Englewood Cliffs, N.J., USA. 366

Kanlaya Vanichbuncha, K. (2008). *SPSS for Windows*. 11th ed. Bangkok: Chulalongkorn University Press, Thailand. 520

Songserm, T., Sae-Heng, N., Jam-on, R., and Meemak, N. (2005). Abstracts of the OIE/FAO International Conference on Avian Influenza. In survival of highly pathogenic avian influenza H5N1 in different conditions and susceptibility to disinfectants. Page 1-7. Paris; 7-8 April 2005.

Sturm-Ramirez, K. M., and others? (2005). Are ducks contributing to the endemicity of highly pathogenic H5N1 influenza virus in Asia? *Journal of Virology.* 79, 17 (2005): 11269–11279.

Webster, R.G., Bean, W.J., Gorman, O.T., Chambers, T.M., Kawaoka, Y. (1992). Evolution and ecology of influenza A viruses. *Microbiological Reviews.* 56, 1: 152–79.

World Health Organization. (2009). Cumulative number of confirmed human cases of avian influenza A/(H5N1) reported to WHO 28th May 2009 [Online] Available: http://www.who.int/csr/disease/avian_influenza/ country/cases_table_2009_05_28/en/index.html (online 1st June 2009)

Zhou, J.Y. et al.? (2006). Characterization of a highly pathogenic H5N1 influenza virus derived from bar-headed geese in China. *Journal of General Virology.* 87:1823–1833.

Table 1. Definitions of the variables

Variable	Definition
Opportunity to become the onset of disease in Thailand (Y)	the opportunity to become the starting point of AIV outbreak in Thailand
Ratio of AIV	the number of positive AIV reports from a laboratory during each time divided by all reports in this time
Delta temperature	maximum temperature during the day minus minimum temperature during the day ($temp_{max}$-$temp_{min}$)
Delta atmospheric pressure	maximum atmospheric pressure during the day minus minimum atmospheric pressure during the day ($pres_{max}$-$pres_{min}$)
Delta specific humidity	maximum specific humidity during the day minus minimum specific humidity during the day (SpH_{max}-SpH_{min})
Delta wind speed	maximum wind speed during the day minus minimum wind speed during the day ($windS_{max}$-$windS_{min}$)
Rain24	average rainfall within 24 hours (rainfall/24 hours)
Villages	the number of villages around the onset village in a radius of five kilometers
The density of villages	the density of villages in a radius of five kilometers
The distance between the last point of outbreak and the onset outbreak	the distance between the last point of outbreak and the onset outbreak
The distance from water to the onset area	the distance from the onset point to water or reservoirs
The distance from a road to the onset area	the distance from the onset point to the main street of the village.

ISSN 1913-1844 E-ISSN 1913-1852

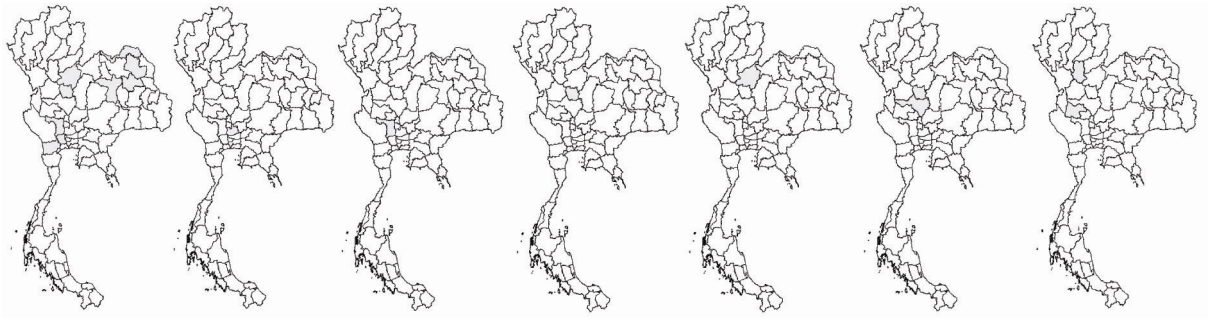

Figure 1. Kickoff areas in Thailand, 2004-2008

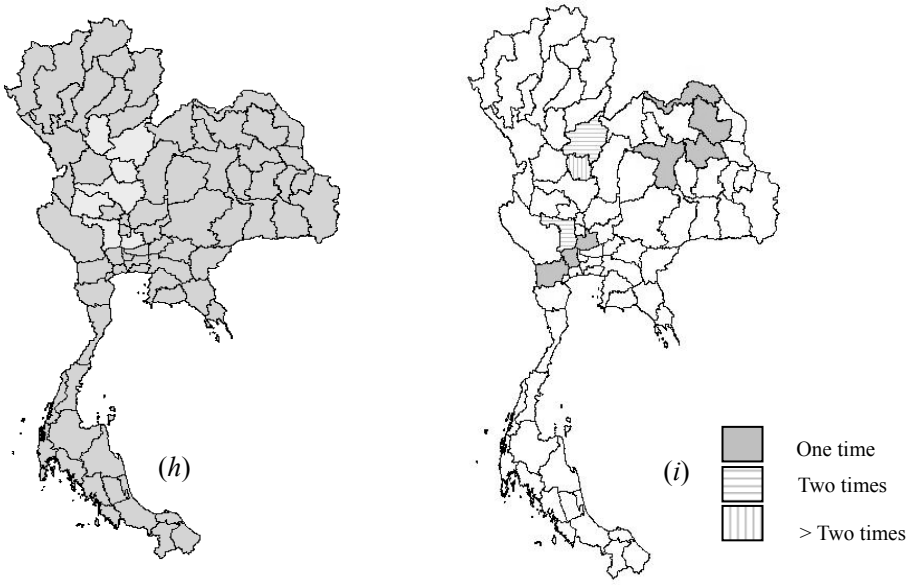

Figure 2. Gray in (*h*) represents the study areas and colors in (*i*) represent the repeated outbreak areas

Application of Water Evaluation and Planning (WEAP): A Model to Assess Future Water Demands in the Niger River (In Niger Republic)

Zakari Mahamadou Mounir (Corresponding author)
School of Environment Studies, China University of Geosciences
No. 388 Lumo Road, Wuhan 430074, Hubei Province, China
E-mail: mounir_zakari@yahoo.fr

Chuan Ming Ma
School of Environment Studies, China University of Geosciences
No. 388 Lumo Road, Wuhan 430074, Hubei Province, China
E-mail: cugmcm@hotmail.com

Issoufou Amadou
School of Food Science and Technology, Jiangnan University
No. 1800 Lihu Road, Wuxi, 214122, Jiangsu Province, China
E-mail: issoufsara@gmail.com

Abstract

Water resources management in Niger River basin is an issue of very high significance because of great socio-cultural, ecological and economic values. The basin comprises biospheres reserves, parks with a variety of wildlife, a significant livestock activity, a very fertile land for agriculture and a growing industry. In the territory of Niger, the Niger River Basin covers mostly all regions of Tillabéry (including the city of Niamey), Dosso, Tahoua and some of the regions of Maradi and Agadez. This area is composed of an active part, including the river valley and its major tributaries and some inactive area.

Water Evaluation And Planning (WEAP) provides a seamless integration of both the physical hydrology of the region and water management infrastructure that governs the allocation of available water resources to meet the different water needs. It is a priority driven software, employs priority based optimization algorithm as an alternative to hierarchal rule based logic that uses a concept of Equity Group to allocate water in time of inefficient supply. There is need for optimization of Niger River resources future need of its population.

Keywords: Water Resources, Water demand, Water supply, Niger River, Basin

Abbreviations and Acronyms

ABN: Niger Basin Authority

FAO: Food and Agriculture Organization

GUI: Graphic User Interface

HDI: Human Development Index

IWRI: International Water Management Institute

IWRM: Integrated Water Resources Management

MDGs: Millennium Development Goals

SEI: Stockholm Environment Institute

UNDP: United Nations Development Program

WEAP: Water Evaluation And Planning

WDI: World Development Indicators

1. Introduction

Water is the most essential element to life on Earth, sometimes scarce resource and fundamental for living. It is also essential for both agriculture in many regions of the world and means to achieve sustainability in production systems. Maximizing net returns with the available resources is of the utmost importance, but doing so is a complex problem, owing to the many factors that affect this process (e.g. climatic variability, irrigation system configuration, production costs, and subsidy policies). Many regions are facing formidable freshwater management challenges. Allocation of limited water resources, environmental quality and policies for sustainable water use are issues of increasing concern (Uitto, 2004; Conway *et al.,* 2009).

Niger is a landlocked Sahelian country, the largest in West Africa (1,267,000 km^2 in area), with a diffuse and mostly rural population, sandy soils, immense and largely untapped fossil aquifer supplies, and multiple surface water basins, most of which are shared with upstream and downstream riparian, receive very little precipitation and three quarters hyper-arid desert, making the country the hottest and driest in the world with little water resources (Dessouassi, 2000; Conway *et al.,* 2009). The population exceeds fifteen million in 2010 (INS, 2010) and is growing at more than 3.3 percent per annum. The overall population density of Niger is about 11.83 persons per square kilometer, and land-locked (about 1,000 km from the sea).

The nine Basin countries are among the poorest in the world. Four are among the bottom 20 countries on the World Development Indicators (WDI) scale, and seven are among the bottom 20 on the United Nations Development Programme (UNDP) Human Development Index (HDI).The need for development and investment in the region is evident, and the Niger River holds tremendous development potential. Development opportunities range from those directly related to the river, such as power, irrigation, and navigation, to those "beyond the river," such as increases in trade, communication investments, and enhanced labor flows (Dessouassi, 2000).

The radioactive and physiological effects of increased atmospheric CO_2 in the future cause a reduction in rainfall in most of West Africa (Alo *et al.,* 2010). The Niger River Basin, home to approximately 100 million people, is a vital, complex asset for West and Central Africa. It is the continent's third longest river (4,200 kilometers), traversing nine countries: Benin, Burkina Faso, Cameroon, Chad, Côte d'Ivoire, Guinea, Mali, Niger, and Nigeria. The Niger River Basin is an extraordinary asset for the nine countries that are within its watershed and for the broader West and Central Africa region. Each country within the Basin has unique geographic settings and a wide range of available resources (Andersen *et al.,* 2005).

In terms of managing and using the Niger's water resources, the nine Basin countries can be clustered as water resources producers: Guinea, Cameroon, and to a lesser extent Benin; or water resources consumers: Mali and Niger. Nigeria is both a producer and a consumer. Côte d'Ivoire, Burkina Faso, and Chad are part of the Basin but are minimally affected by the use and management of the river's water resources (ABN, 1999). The Niger River crosses Niger on a distance of 550 km with a hydro-logically active area of approximately 357,000 square kilometers occupying proportionally 23.8 percent of the Basin. This area extends through the Maradi region, which is part of the Sokoto watershed.

The Niger River embodies the livelihoods and geopolitics of the nations it crosses. This river is not simply water, but is also an origin of identity, a route for migration and commerce, a source of potential conflict, and a catalyst for cooperation (Andersen *et al.,* 2005). Each country within the Basin has unique geographic settings and a wide range of available resources that drive local and regional development. The Niger River's hydrologically active basin covers a surface area of nearly 1.5 million square kilometers shared among the nine countries according to the following approximate percentages: Benin (2.5 percent), Burkina Faso (3.9 percent), Cameroon (4.4 percent), Chad (1.0 percent), Côte d'Ivoire (1.2 percent), Guinea (4.6 percent), Mali (30.3 percent), Niger (23.8 percent), and Nigeria (28.3 percent) (Andersen *et al.,* 2005; Warren *et al.,* 2001).

The left-bank tributary network, originating in Aïr and Azaouâk Mountains, is characterized by intermittent flows that are isolated from the Niger River without any hydrologic connection to the river network. The Niger River partially irrigates large alluvial plains and lowlands of the Dallol Bosso, the Dallol Maouri, and the Maradi area. Rice production is low, but production of traditional grains of the Sahel region, although subject to climate variations, is significant (more than 2.4 million tons per year). In many places farmers preferred to cultivate black-eyed peas than groundnuts as an export crop and cotton is also no longer grown. Agricultural practices have undergone significant changes since the severe droughts of the past several decades. Niger is dependent on the navigable waterways of the Niger River through Nigeria (Sieber *et al.,* 2002; Andersen *et al.,* 2005). Modeling and analysis methods for evaluating the water distribution capabilities of reservoir/river systems are fundamental to the effective management of the highly variable water resources of a river basin. Both hydrologic

and institutional considerations are important in assessing water availability and reliability of such assessments (Sieber *et al.,* 2002).

This paper describes the use of the Water Evaluation And Planning (WEAP) model to investigate scenarios of future water resource development in the Niger River Basin in Niger Republic. Therefore, the investigation consisted on the use of water consumption for human needs, for agriculture (irrigation) and industries in the cities of Niamey and Tillabéry due to their position along the Niger basin (Figure 1).

2. Experimental Design

In WEAP the typical scenario modeling effort consists of three steps. First, a Current Accounts year is chosen to serve as the base year of the model; two a Reference scenario is established from the Current Accounts to simulate likely evolution of the system without intervention; and thirdly "what-if" scenarios created to alter the "Reference Scenario" and evaluate the effects of changes in policies and/or technologies. The data used in modeling for current accounts, is ranged for the period of (2009-2030) as it's shown in Table 1. For allocation of available resources a number of option tested by developing several scenarios and future water demands are projected.

The WEAP21 (Water Evaluation And Planning) software was used to evaluate the future water demands in the two region of the Niger River (Niamey city and Tillabéry).

3. Generalities and presentation of the WEAP model

The Water Evaluation and Planning (WEAP) model has a long history of development and use in the water planning arena. Raskin *et al.* (1992) first applied WEAP to a study on the Aral Sea, but that version of WEAP had several limitations, including an allocation scheme that treated rivers independently, gave priority to demands on upstream sites over downstream sites, and assured demand sites that preferred groundwater to surface water were last in line in getting surface water allocations. Given these deficiencies, WEAP21 introduces major advances including a modern Graphic User Interface (GUI), a robust solution algorithm to solve the water allocation problem, and the integration of hydrologic sub-modules that include a conceptual rainfall runoff, an alluvial groundwater model, and a stream water quality model (Rosenzweiga *et al.,* 2004).

The WEAP model was developed by the Stockholm Environment Institute (SEI). It operates at a monthly step on the basic principle of water balance accounting. The user represents the system in terms of its various sources of supply (e.g. rivers, groundwater, and reservoirs), withdrawals, water demands, and ecosystem requirements (SEI, 2001).

WEAP applications generally involve the following steps:

• Problem definition including time frame, spatial boundary, system components and configuration;

• Establishing the 'current accounts', which provides a snapshot of actual water demand, resources and supplies for the system;

• Building scenarios based on different sets of future trends based on policies, technological development, and other factors that affect demand, supply and hydrology;

• Evaluating the scenarios with regard to criteria such as adequacy of water resources, costs, benefits, and environmental impacts.

The scenarios can address a broad range of 'what if' questions, such as: What if population growth and economic development patterns change? What if ecosystem requirements are tightened? What if irrigation techniques and crop patterns are altered? What if various demand management strategies are implemented?

WEAP model has two primary functions (Sieber *et al.,* 2005):

- Simulation of natural hydrological processes (e.g., evapotranspiration, runoff and infiltration) to enable assessment of the availability of water within a catchment.
- Simulation of anthropogenic activities superimposed on the natural system to influence water resources and their allocation (i.e. consumptive and non-consumptive water demands) to enable evaluation of the impact of human water use.

To allow simulation of water allocation, the elements that comprise the water demand-supply system and their spatial relationship are characterized for the catchment under consideration. The system is represented in terms of its various water sources (e.g. surface water, groundwater, and desalinization and water reuse elements); withdrawal, transmission, reservoirs, and wastewater treatment facilities, and water demands (i.e. user-defined sectors but typically comprising industry, mines, irrigation, domestic supply, etc.). The data structure and level

of detail can be customized (e.g. by combining demand sites) to correspond to the requirements of a particular analysis and constraints imposed by limited data. A graphical interface facilitates visualization of the physical features of the system and their layout within the catchment (Purkey and Huber-Lee, 2006; Sieber *et al.,* 2005).

This intuitive graphical interface provides a simple yet powerful means for constructing, viewing and modifying the system and its data. The main functions - loading data, calculating and reviewing results - are handled through an interactive screen structure. WEAP also has the flexibility to accommodate the evolving needs of the user: e.g. availability of better information, changes in policy, planning requirements or local constraints and conditions.

The present application of the WEAP model forms part of ongoing research at the International Water Management Institute (IWMI) to develop, test and promote management practices and decision-support tools for effective management of water and land resources.

WEAP has been described as being ‘‘comprehensive, straight forward and easy-to-use, and attempts to assist rather than substitute for the skilled planner’’ (University of Kassel, 2002).

4. Case of study

In Republic of Niger the uncontrolled growth of population, inappropriate agricultural practices, overgrazing, soil erosion and deforestation are among the other causes of degradation of its land.

Climate change is important to water planners and managers because it may change underlying water management conditions (Barnett *et al.,* 2008) and increase the need for new water management programs and capital investments (California Urban Water Agencies, 2007). Climate change may also confound water resources planning because the local effects of climate change are so uncertain and difficult to predict (Conway *et al.,* 2009).

For the range of this study (2009-2030) period, the rate of Niger population increase with 3.3% per year. Demand for irrigation is 7367 m^3/ha and the irrigated area increased by 1.6% per year (INS, 2010). Niger industries water consumption estimated in 2009 raised in 11.5 million m^3 with and annual increase of 3%. Figure 3 shows an application for water demand of the four sites (Niamey town; Tillabéry town, industries and irrigation). Table 1 shows that water consumption for the year 2009 (Current Accounts) for the four sites which are our main target in this study. Niamey (capital city of Niger republic) is estimated to have 1 146 000 inhabitants in year 2009 (INS, 2010) with 23.1 million m^3 water consumption; whereas Tillabéry city with estimated population of 278 100 inhabitants have 2.8 million m^3 water consumption. The water demand for all the irrigated area of Niger River valley is estimated to 14 005 ha (107 million m^3) and the water consumption for the main industries located around the Niger River is evaluated to 11.5 million m^3 (Table 1). Figure 2 shows the evolution (growth) of water consumption for the four sites for the period 2009-2030. It was projected that the total water demands for the 4 sites increased from 144.4 million m^3 in year 2009 date of beginning of our study to 290.5 million m^3 for the end of the scenario (year 2030). First scenario: Higher population growth 7% and 6% respectively to Niamey town and Tillabéry Town. Water consumption for irrigation and industry remain unchanged; Figure 3 shows the annual demand for the 4 sites. It is shown that the water demand for 2030 is 618.1 million m^3. It was observed that a null value (0 m3) for 2009 to 2030 as far as the Unmet Demand is concern for the 4 sites studied (Figure 3), therefore, satisfied all the sites despite the high rate of population growth.

Second scenario: Using the Water Year Method, the previous exercise only varied demand, not supply. In this step we now want to see how natural variation in climate data (stream flow, rainfall etc.) can be taken into account in WEAP through scenario analyses. We will use the “Water Year Method” as an example. The Water Year Method is a simple means to represent variation in climate data such as streamflow, rainfall, and groundwater recharge. The method first involves defining how different climate regimes (e.g., very dry, dry, very wet) compare relative to a normal year, which is given a value of 3. Dry years have a value less than 3, very wet years have a value greater than 3.

The next step in using the “Water Year Method” is to create the sequence of climatic variation for the scenario period. Each year of the period is assigned one of the climate categories (e.g., wet). For the “Reference” scenario, we will assume the following sequence shown in Figure 4.

The inflows to the model (in our case, the headflow of the main river) vary in time, WEAP offered two strategies. If detailed forecasts are available, those that can be read using the ReadFromFile function (are referred to the Tutorial module on Format and Data for more details). Another method, which as presented in this study, is the “Water Year Method" Under which method every year in the model’s duration that can be defined as normal,

wet, very wet, dry or very dry. Different scenarios can then alter the chosen sequence of dry and wet years to assess the impact of natural variation on water resources management.

Third scenario: Generally in the Sahel region and Niger in particular the phenomenon of drought is recurrent. Several research works have shown that one of three years, there has been a drastic drop in rainfall causing poor harvest. The characteristic of Figure 5 is that, we wanted to see the case whereby a recrudescence of the dry years; without any climate "very wet year". Thus we tried to see the extreme case of the dryness on the Niger River. However, we noted that with time (in 2030), there would be cases where the Niger River will not be enough to satisfy the need for the 4 sites studied.

If scenario results from the scenario of "Reference", the demand for water is said to be completely satisfied. However, where this scenario is gotten from the scenario (high population growth) the observation periods during which the demand, for water is said to be satisfied for only 59.3% in May 2030; 90.8% in June 2030 for Niamey city and Tillabéry. Furthermore, 84% in July 2030 was observed for irrigation and drinking water for Niamey and Tillabéry, respectively. Figure 6 projects that the nonsatisfied request would be observed in the months of June, May and July; in this study, we supposed that the four sites have the same priority (Priority 1 with software WEAP). That is to say, the water delivery for all the sites should be made equitable. Moreover, the request for industries is set satisfactory. However, water demand would be nonsatisfied during 3 months (May, June, and July) for the populations of Niamey and Tillabéry. This request also would not be satisfied for the month of July for the irrigation which is practiced in Niger for 5 months in a year that is from July at November.

By observing all the scenarios and for all the sites of demand, the nonsatisfied demand is shown in Figure 7. The nonsatisfied demand is observed only on the level of the scenario Higher Population Growth and Climate Variable. In 2030, there would be a deficit of 33.7 million cubic meter of water set as follows: 9.8 million m^3 for the irrigation, 22.1 million m^3 for Niamey city and 1.8 million m^3 for Tillabéry town.

5. Conclusion

With the use of this software, we can confirm that the difficulty of water will arise with acuity in Niger as long as mechanisms of management are not in place to retain the phenomena of rapid population increase and climate change. It will be a good thing if a hydro-electric dam could be constructed on the Niger River, which will make it help to control the flows of water fall and low water levels on river. The dam will also make it possible to find adequate drinking water for two growing cities Niamey and Tillabéry. Dam provides available water for modern agriculture practice so to eradicate poverty and contribute directly to the achievement of the Millennium Development Goals (MDGs). In a country like Niger, where more than 3/4 of the population lives from agriculture products; the development of the irrigation is essential to achieve the Millennium Development Goals. The main and fundamental objective of this study is to propose a significant method to assist reduction by half the extreme poverty and the famine in Niger from now to 2015 as proclaimed by United Nations Development Program. Attention should be drown to optimize the Niger River resources use if not the scarce resources available in this River may not meet the future needs.

References

ABN. (1999). The Niger Basin Authority Three-Year Action Plan 2000-2002, *ABN, Niger*.

Alo, A., & Wang, G. (2010). Role of dynamic vegetation in regional climate predictions over western Africa Clement, *Climate Dynamics*, 35, 907–922.

Andersen, I., Dione, O., Jarosewich-Holder, M., & Olivry, J.C. (2005). The Niger River Basin: A Vision for sustainable management, foreword, *World Bank-Washington, DC*. Available on the Internet: www.worldbank.org (October 1st, 2010).

Barnett, T.P., Pierce, D.W., Hidalgo, H.G., Bonfils, C., Santer, B.D., Das, T. Bala, G., Wood, A.W., Nozawa, T., Mirin, A.A., Cayan, D.R.., & Dettinger, M.D. (2008). Human-Induced Changes in the Hydrology of the Western United States, *Science*, 319, 1080–1083.

California Urban Water Agencies. (2007). Climate Change and Urban Water Resources, 15 pp., *California Urban Water Agencies*, Sacramento, CA.

Conway, D., Persechino, A., Ardoin-Bardin, S., Hamandawana, H., Dieulin, C., & Mahé, G. (2009). Rainfall and Water Resources Variability in Sub-Saharan Africa during the Twentieth Century, *Journal of Hydrometeorology,* 10, 41–59.

Dessouassi, R. (2000). Revue des perspectives dans le Bassin du fleuve Niger, *ABN, Niger*.

Institut National de la Statistique: INS, Niamey, Niger, 2010.

Purkey, D., & Huber-Lee, A. (2006). A DSS for long-term water utility planning, *Southwest Hydrology*, 4, 18–31

Raskin, P., Hansen, E., & Zhu, Z. (1992). Simulation of water supply and demand in the Aral Sea, *Region 17*, No. 2, 55–67.

Rosenzweiga, C., Strzepekb, K.M., Major, D.C., Iglesias, A., Yates, D.N., McCluskeyb, A., & Hillel, D. (2004). Water resources for agriculture in a changing climate: international case studies, *Global Environmental Change,* 14, 345–360.

Stockholm Environment Institute, SEI. (2001). WEAP: Water evaluation and planning system –user guide. Boston, USA.

Sieber, J., Huber-Lee, A., & Raskin, P. (2002). WEAP:Water Evaluation And Planning System User Guide (for WEAP 21), Stockholm Environmental Institute—Boston, and Tellus Institute, User Guide for WEAP 21, Boston, MA.

Sieber, J., Yates, D., Huber Lee, A., & Purkey, D. (2005). WEAP a demand, priority, and preference driven water planning model: Part 1, model characteristics, *Water International*, 30(4), 487–500.

University of Kassel, (2002). ECOBAS project: meta-database for existing mathematical models in ecology. Available from http://eco.wiz.uni-kassel.de/model_db/mdb/weap.html (September 5th, 2010).

Uitto, J.I. (2004). Multi-country cooperation around shared waters: role of monitoring and evaluation, *Global Environmental Change*, 14, 5–14.

Warren, A., Batterbury, S., & Osbahr, H. (2001). Soil erosion in the West African Sahel: a review and an application of a "local political ecology" approach in South West Niger, *Global Environmental Change,* 11, 79–95.

Table 1. Water Demand for current account for year 2009 (million cubic meter)

Demand site		Niamey	Tillabéry
Water demand (million m^3)		23.1	2.8
Irrigation		107	
Industries	Aluminum	11.5	
	Brewing		
	Dairy		
	Chemical		
	Slaughter house		
	Steelworks		
	Textile		
	Thermic electricity		
Total		144.4	

Source: INS, Institut National de la Statistique, Niamey, Niger, 2010

Figure 1. The Schematic diagram of proposed study cities of Niamey and Tillabéry (Not to scale)

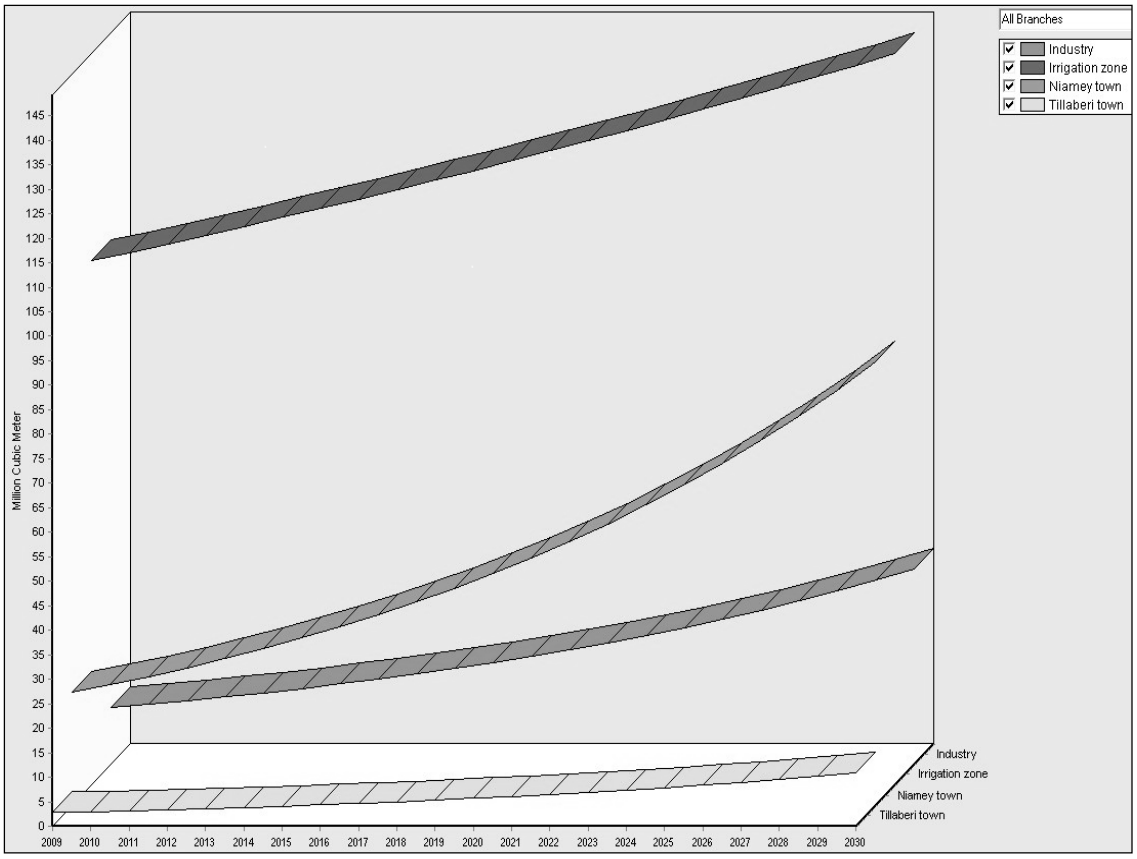

Figure 2. Water Demand (Reference Scenario)

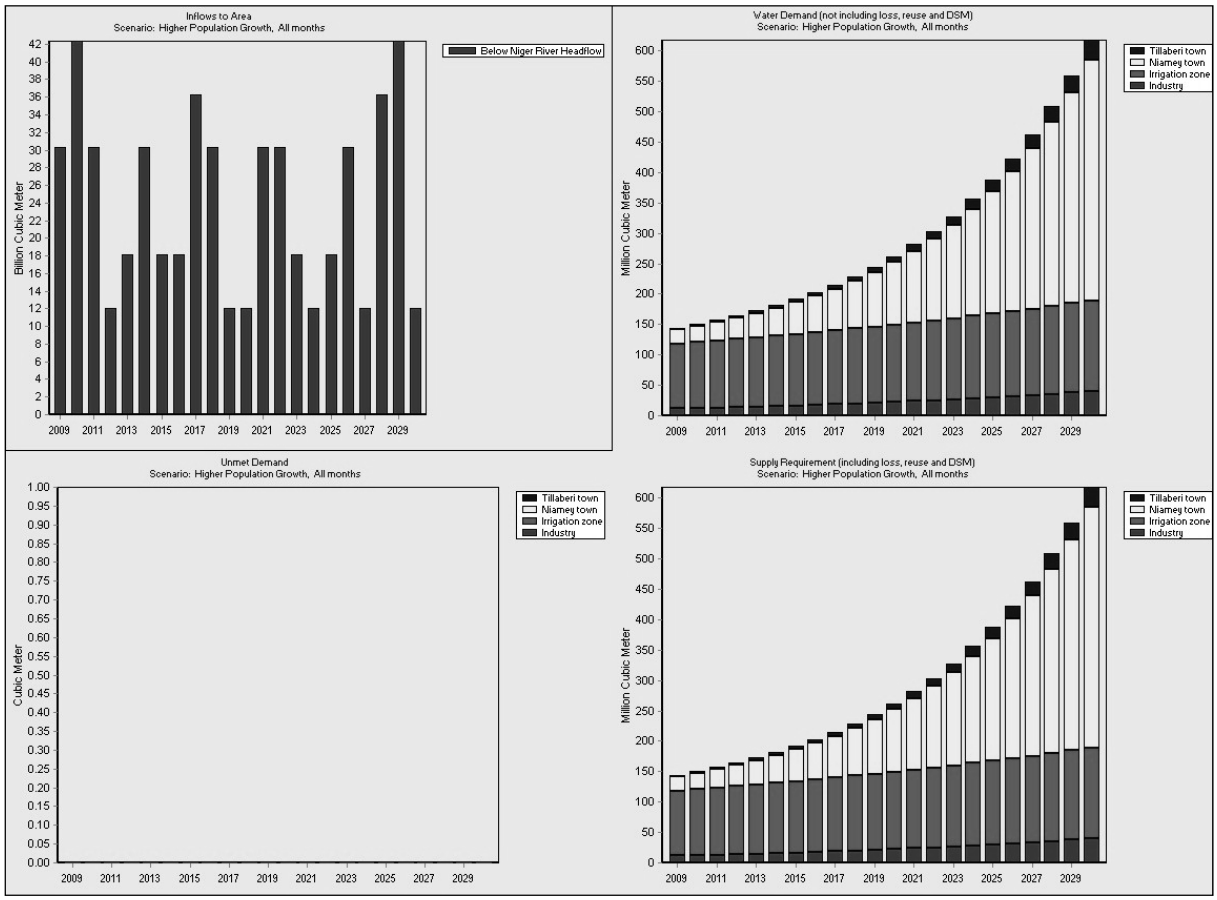

Figure 3. Overviews for Inflows to area, Water Demand, Unmet Demand and Supply Requirement for Higher population growth scenario

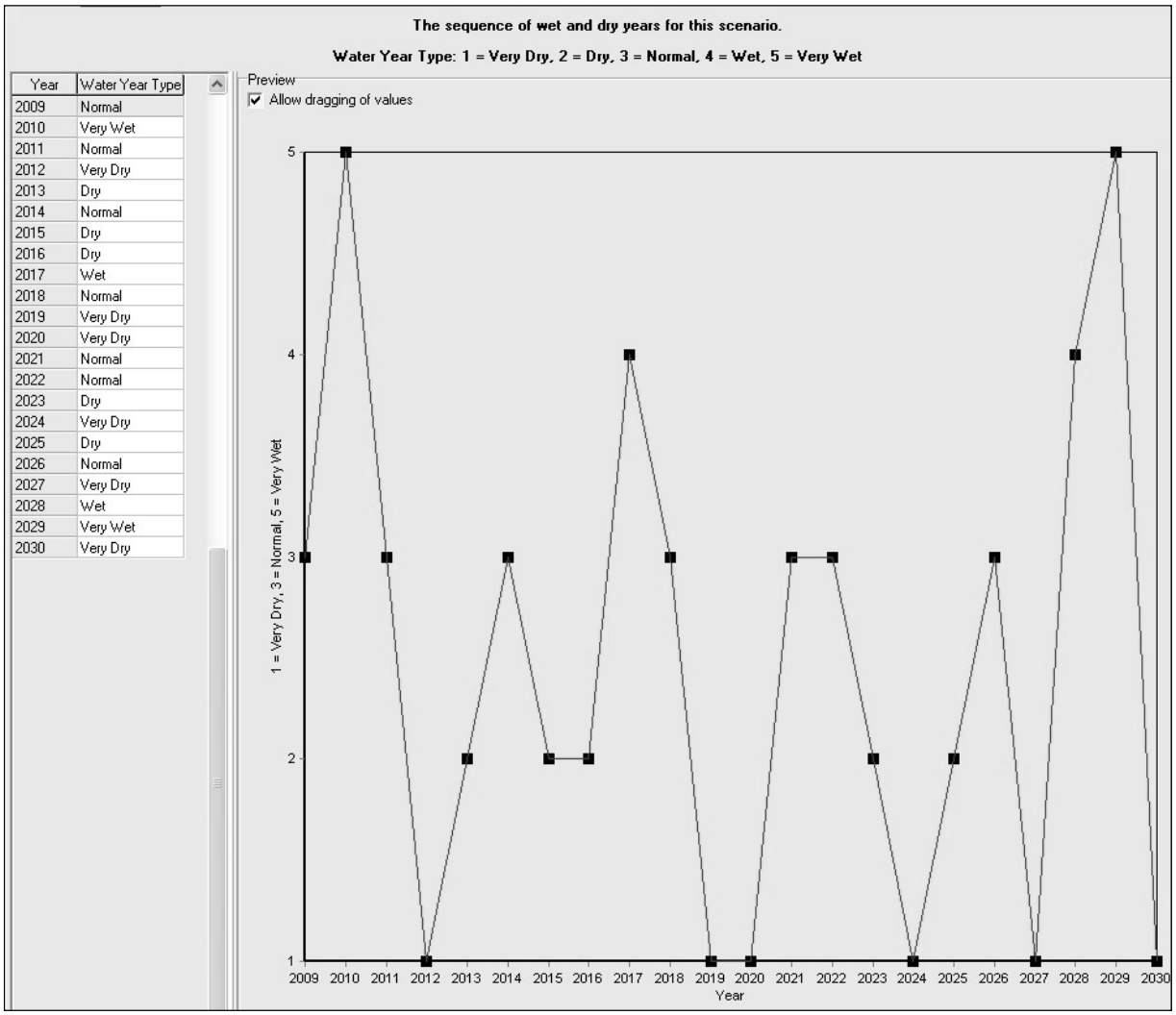

Figure 4. Climate Sequence for Reference Scenario

 ISSN 1913-1844 E-ISSN 1913-1852

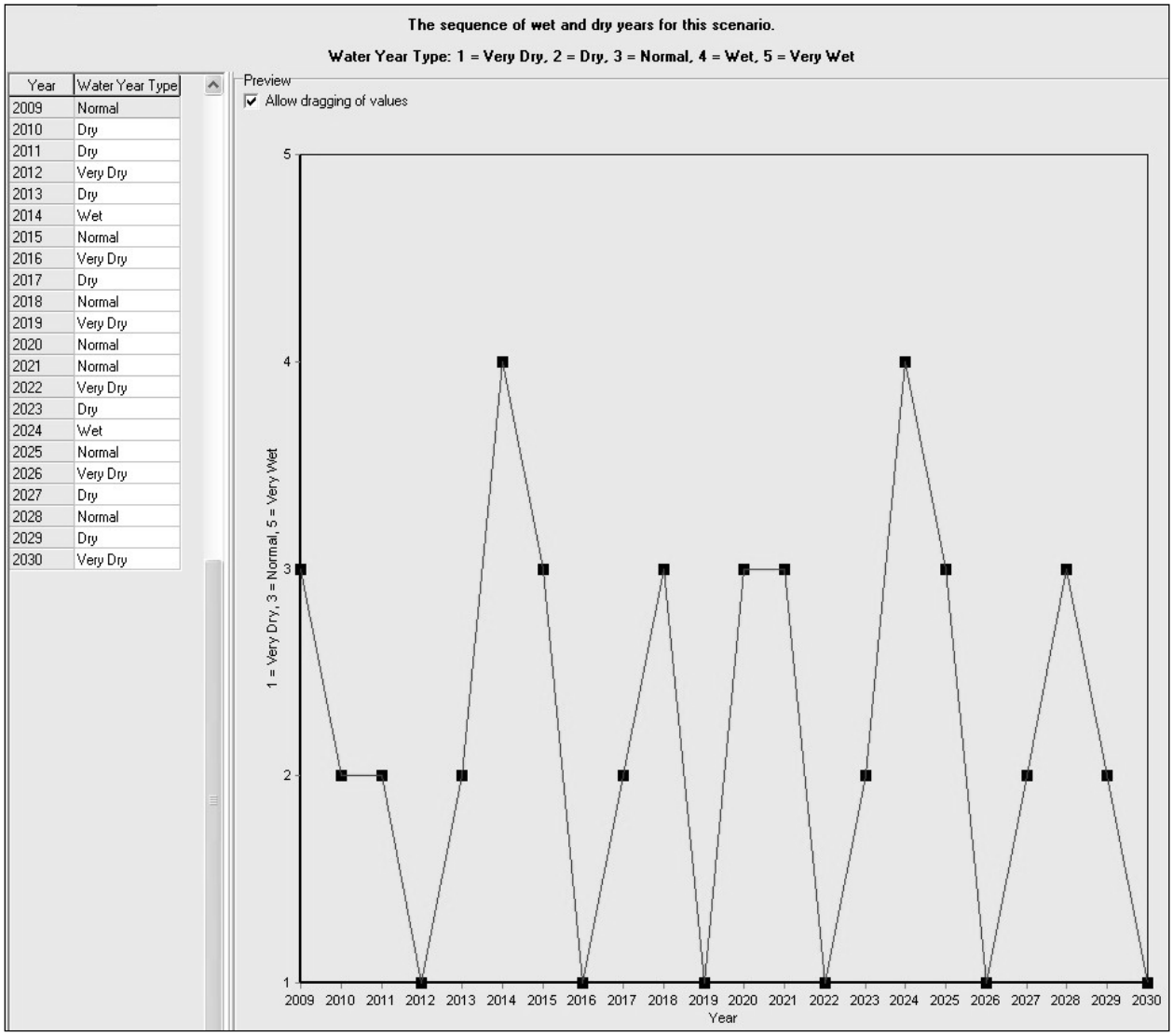

Figure 5. Climate Sequence for Extended Dry Scenario

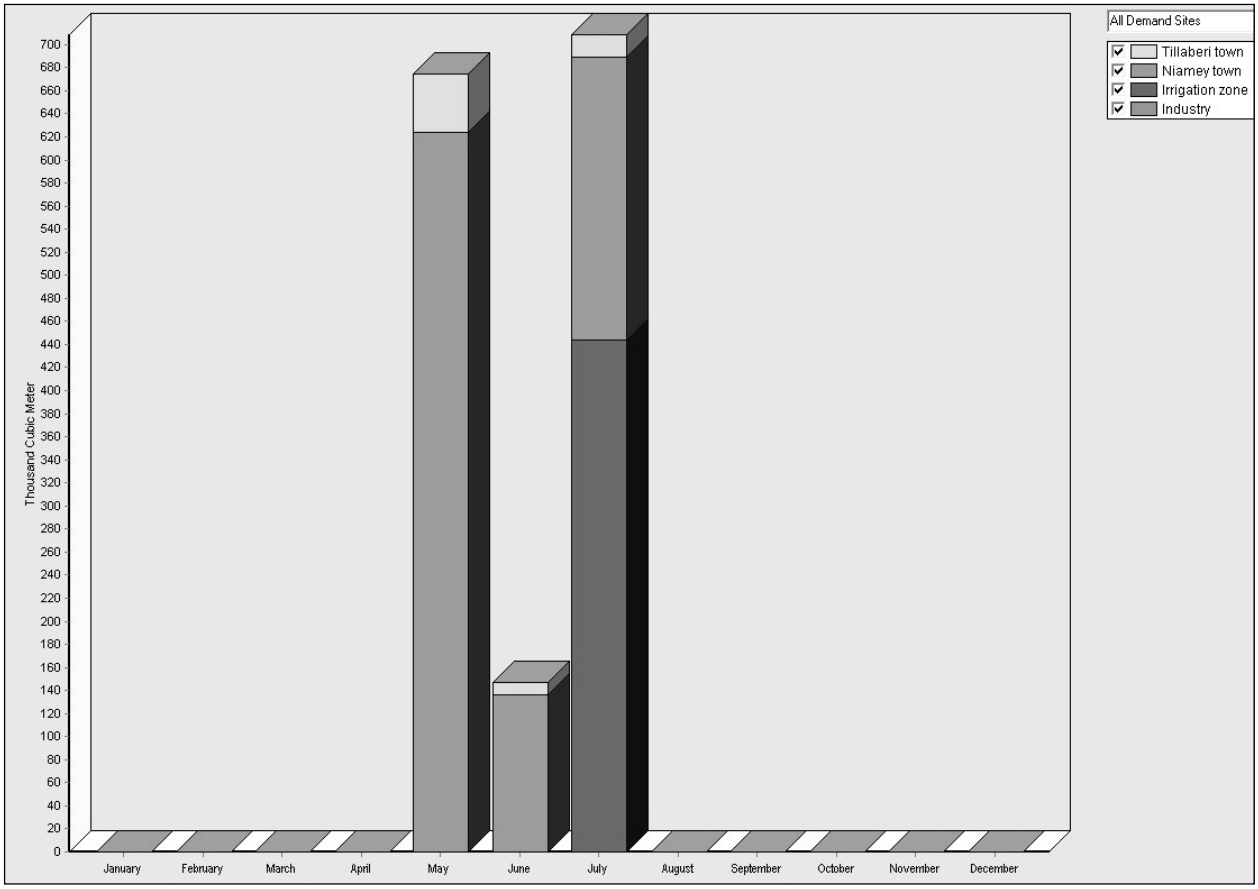

Figure 6. Unmet Demand for Higher population growth and variable climate scenario

 ISSN 1913-1844 E-ISSN 1913-1852

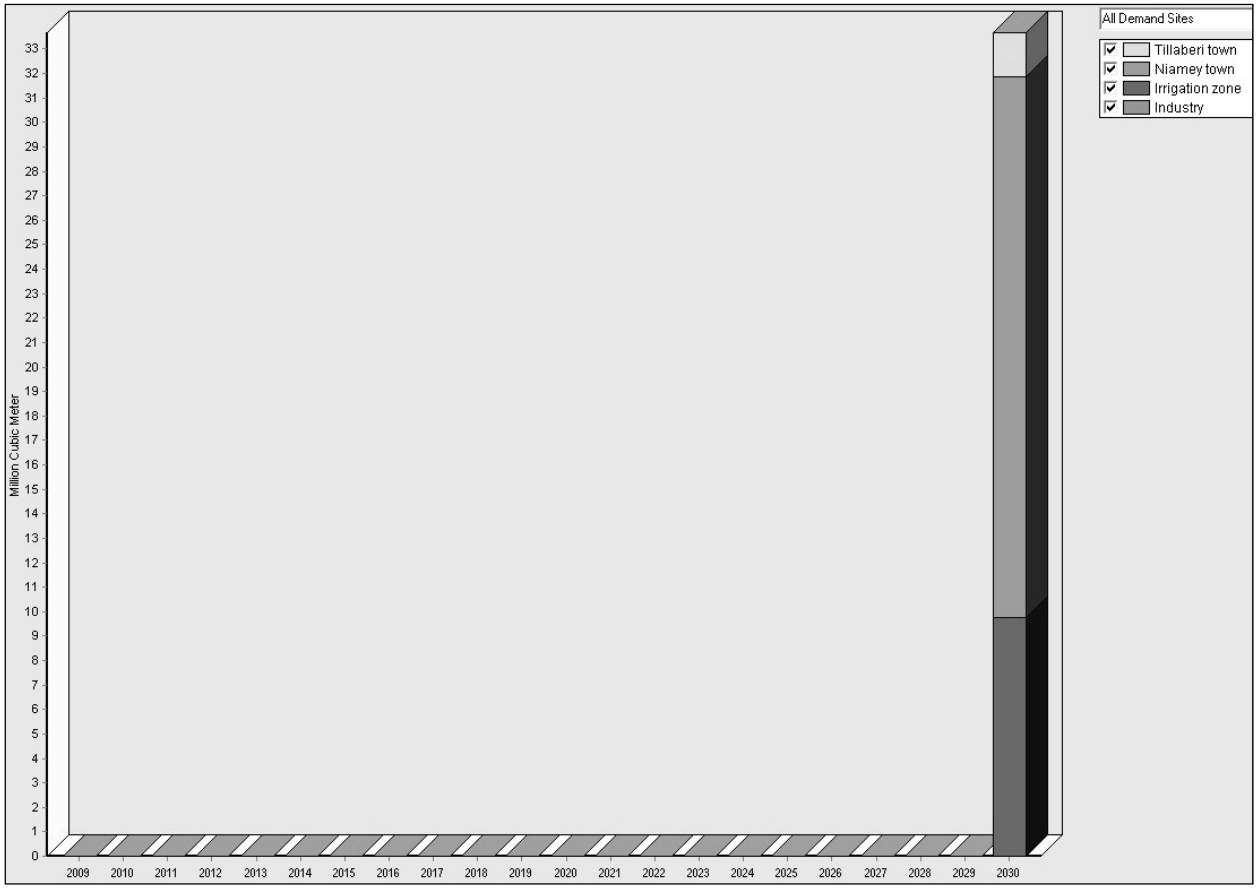

Figure 7. Unmet Demand by site

Dilution Effect during Laser Cladding of Inconel 617 with Ni-Al Powders

Ahmed Ali Moosa
Department of Production Engineering and Metallurgy
University of Technology, Baghdad, Iraq
Tel: 964-790-179-3866 E-mail:uot_vicepresident@yahoo.com

Mohammed Jasim Kadhim
Department of Production Engineering and Metallurgy
University of Technology, Baghdad, Iraq
Tel: 964-790-549-9306 E-mail: alimohammed1957@yahoo.com

Akeel Dhahir Subhi
Department of Production Engineering and Metallurgy
University of Technology, Baghdad, Iraq
Tel: 964-780-882-7048 E-mail: drengads@yahoo.com

Abstract

In this study, continuous wave CO_2 laser with 1.7 and 2 kW were used to deposit clad layers of premixed powders of either Ni-10 wt% Al or Ni-30 wt% Al onto inconel 617 substrate. Different cladding traverse speeds in the range 1 to 35 mm/s were used for premixed clad powder of Ni-10 wt% Al and 1.65 to 11.2 mm/s for premixed clad powder of Ni-30 wt% Al. Two powder feeding rates were used, 10 and 8.9 gm/min for premixed clad powders of Ni-10 wt% Al and Ni-30 wt% Al respectively. The other laser independent variables were selected to be constant. The results showed that different percentages of area dilution were found ranging from 3.7 to 78.3% for premixed clad powder of Ni-10 wt% Al and 6.9 to 41 % for premixed clad powder of Ni-30 wt% Al depending on the laser cladding independent variables used. Furthermore, dilution was affected mainly by cladding traverse speeds.

Keywords: Laser cladding, Dilution, Inconel 617, Ni-Al powders, Independent variables

1. Introduction

There has never been a period in history during which the evolution of materials and products has been faster and the range of their properties more varied than today (Nenadovć, 2002). The traditional forte of the materials scientist has been the control of the physical, chemical and mechanical properties to produce an ensemble of useful product profiles. With continually improving understanding of chemistry - structure - property relationships, incrementally improved materials steadily appear (Das and Davis, 1988). Lasers have greatly contributed to major fields of science, technology and medicine since the first success in laser applications in 1960 (Maiman, 1960). Laser surface treatments under selected variables have been proven to improve the surface properties in several ferrous and nonferrous alloys. Laser cladding is one of laser surface treatments that required overlay one metal or alloy with another, producing a sound interfacial bond with minimum dilution of the cladding metal or alloy with substrate material (Yang, 1999; Manna, Majumdar, Chandra, Nayak and Dahotre, 2006).

In industrial gas turbine engine manufacturing industry, materials used are specifically to meet the needs of the hot gas path components exposed to the most severe operating conditions; where high temperature creep, tensile strength, ductility and oxidation resistance are required to withstand the loadings imposed. Replacement of the degraded parts is a successful solution but costly. Therefore, repairing the degraded parts for example turbine blades tips is the most important process with accepted cost. Laser cladding with selected clad layers is the most important repairing process distinguished with controlled chemical composition and dimensions (Adak, Nash and Chen, 2005). Several metals and alloys are used as a clad layer material. Nickel-Aluminum clad material systems are distinguished with intermetallic compounds. The melted part of substrate that mixed with the clad material makes clad layer studies very important (Liang and Su, 2000). Thus, one must study all properties that

are related to clad layer in order to approach the optimum evaluation. Therefore, careful evaluation of clad layers may be used effectively to obtain a successful industrial applications after determination of the required clad layer properties (Steen and Courtney, 1980).

In this work, light will be thrown to illuminate the mixing that occurred between clad layer and substrate material, i.e.dilution percentage in order to control the chemical composition of clad layers of laser cladding of inconel 617 with Ni-10 wt% Al and Ni-30 wt% Al premixed powder mixtures under different conditions.

2. Experimental Work

A 2 kW, fast axial continuous wave CO_2 laser (10.6 μm wavelength) was used to clad different powder mixtures of chemical compositions of 90 wt% Ni (< 150 μm particle size) and 10 wt% Al (< 250 μm particle size) and the other was 70 wt% Ni and 30 wt% Al on the inconel 617 substrate with dimensions of 75 x 40 x 5.5 mm. The main laser beam diameter was of approximately 22 mm which delivered to the substrate by focusing through 150 mm focal length KCl lens to obtain a 5 mm laser beam diameter on the substrate. Argon gas was blown to protect the lens from contamination. The chemical composition and microstructure of inconel 617 substrate were illustrated in Table 1 and Fig.1 respectively.

The substrate samples were clamped with a suitable jig on a hydraulic powered x-y table which was moved relative to the stationary laser beam. The cladding of samples was carried under argon gas as shrouding against contamination from the atmosphere. The laser processing parameters are listed in Table 2. After laser cladding, the features of clad layers such as depth of penetration and clad height were determined from the transverse sections after grinding, polishing and etching. Area dilution as illustrated in Fig.2 can be obtained from the following equation (Bruck, 1980):

$$\%\text{Area dilution} = A_2/(A_1 + A_2) \times 100 \qquad 1$$

where A_1 is the area of region (1)

A_2 is the area of region (2)

The areas of regions 1 and 2 present in Eq.1 can be calculated using an Image programme. In this programme, standard ruler picture was used to establish measurement scale. After established scale of measurement, the microstructure of clad layers of laser cladding of inconel 617 with Ni-10 wt% Al and Ni-30 wt% Al premixed clad powders of different cladding speeds was inserted to the programme separatly and measurement was taken place. This can be accomplished by determination the region that must be measured.

3. Results and Discussion

After the substrate has been wetted with the molten of premixed clad powder, spreading of the melt pool on the substrate will be took place. Spreading can be divided into distinct stages. The first stage is the very rapid spreading under the driving force for the balance of interfacial tensions characteristic of melt pool. In the second stage, the substrate dissolve in the melt pool and forms compounds that nucleate on preferred sites at the solid-liquid interface and later grow to form the reaction product (s). Laser clad layers properties are mainly affected by dilution. Dilution determines the strength of clad layer. Generally, increasing area dilution percentage for specific limit, the bond strength between the clad layer and substrate will be increased too. Dilution is very important property especially in bond strength sensitive applications which are rquiring good wear resistance. In applications which are requiring good corrosion resistance or oxidation resistance, the clad layer composition must be approached that of clad mixture composition. Therefore, theoretically the best quality of clad layer is produced when the clad layer conserve as possible its chemical composition with minimum dilution. Figure. 3 shows the relationship between dilution percentage (D) and cladding traverse speed (V) in which the dilution increases at low and intermediate cladding traverse speeds. At high cladding traverse speed, dilution is decreased as compared with intermediate cladding traverse speed especially for premixed clad powder of Ni-30 wt% Al. While for premixed clad powder of Ni-10 wt%Al, dilution continues in increasing rate at high cladding traverse speeds. This can be explained on the basis that at low cladding traverse speeds, melt penetration is high but because of the large thickness of clad layer, minimum melting in the substrate will take place. This means that minimum mixing between premixed clad powder and substrate material occurred. At intermediate cladding traverse speeds, melt penetration is less than that in the low cladding traverse speed, but because the clad height is small, therefore, large melting in the substrate surface will occured. This means that large mixing is taken place and therefore dilution is high. At high cladding traverse speeds, lower melt penetration will take place. The melt penetration, specially for premixed clad powder of Ni-30 wt% Al, does not allow high mixing between clad layer and substrate material to occur, but when compared with mixing at low cladding speeds, it will be high. In preplaced powder laser cladding, the dilution was found to increase with

decreasing cladding traverse speed. This occurred when the laser beam melts the preplaced powder in order to produce good bonding (Bruck, 1987).

The relationship between dilution percentage (D) and cladding rate (C_r) (mm^2/s) for premixed clad powders of Ni-10 wt% Al and Ni-30 wt% Al is shown in Fig. 4. The relationship between dilution percentage and cladding rate for premixed clad powder o Ni-10 wt% Al can be expressed as:

$$D = 2.72\ C_r^{0.9} \quad (2)$$

While for premixed clad powder of Ni-30 wt% Al this relationship can be expressed as:

$$D = 0.015\ C_r^{1.07} \quad (3)$$

The dilution percentage is increased with increasing cladding rate (increases in cladding traverse speed). This is because with increasing cladding rate, any small heat input with respect to the clad height at a given cladding rate is considered high; therefore, dilution is high. It is clear from Fig.6 that no decreasing in dilution percentage took place at high cladding rate as compared with the relationship between dilution percentage and cladding speed for premixed clad powder of Ni-30 wt% Al (Fig. 4). This is because at high cladding traverse speed, the magnitude of cladding rate decreases due to decrease in the clad width. As a result of dilution at higher cladding rate for premixed clad powder of Ni-30 wt% Al is low (19.7%) compared with previous dilution percentage (41%); it approached in magnitude of the cladding rate at cladding traverse speed of 3.2 mm/s which is 23.1%. Therefore, the decreasing in dilution percentage at high cladding rate does not appear on the graph (Fig. 4).

Conversely, the relationship between dilution percentage and specific energy (Fig. 5) shows that the dilution is increased exponentially with deceasing specific energy (increasing cladding speed). The relationship between dilution percentage (D) and specific energy (E) (J/mm^2) for premixed clad powder of Ni-10% Al can be expressed as:

$$D = 71.5\ e^{-0.009\ E} \quad (4)$$

While for premixed clad powder of Ni-30% Al this relationship can be expressed as:

$$D = 0.41\ e^{-0.0067\ E} \quad (5)$$

Increasing the dilution percentage with decreasing in specific energy is related to increase in the cladding traverse speed with decreasing in specific energy. Decreasing cladding traverse speed means that little mixing will take place between premixed clad powder and substrate. Therefore, dilution is low.

4. Conclusions

1) Laser cladding of inconel 617 substrate with Ni-10 wt% Al and Ni-30 wt% Al premixed clad powders is feasible to obtain new high quality surface layer.

2) Experiments on laser cladding indicate that single clad layers of Ni-10 wt% Al and Ni-30 wt% Al premixed clad powders with dilution ranging from 3.7 to 78.3% and 6.9 to 41% respectively can be obtained.

3) The results showed that dilution is dependent mainly on cladding traverse speed with respect to constant of other laser cladding process variables.

References

Adak, B., Nash, P and Chen, D. (2005). Microstructural characterization of laser cladding of Cu-30Ni, *J. Materials Science,* 40, 2051.

Bruck, G.J. (1987). High power laser beam cladding, *J of Metals,* 39, 10.

Das, S.K and Davis, L.A. (1988). High performance aerospace alloys via rapid solidification processing, *Materials Science Engineering,* 98, 1.

Jendrzejewskia, R., Condeb, A., de Damboreneab, J and Sliwinski, G. (2002). Characterization of the laser-clad stellite layers for protective coatings, *Materials Design,* 23, 83.

Liang, G.Y and Su, J.Y. (2000). The microstructure and tribological characteristics of laser-clad Ni–Cr–Al coatings on aluminum alloy, *Materials Science and Engineering A,* 290, 207.

Maiman, T.H. (1960). Stimulated optical radiation in ruby, *Nature,* 187, 493.

Manna, I., Majumdar, J.D., Chandra, B.R., Nayak, S and Dahotre, N.B (2006). Laser surface cladding of Fe–B–C, Fe–B–Si and Fe–BC–Si–Al–C on plain carbon steel, *Surface Coating Technology,* 201, 434.

Nenadovć, T.M (2002). Hyperfine surface structure, *Materiali in Technologije,* 36, 91.

Steen, W.M and Courtney, C.G.H. (1980). Hardfacing of nimonic 75 using 2 kW continuous wave CO_2 laser, *Metals Technology*, June, 232.

Yang, Y. (1999). Microstructure and properties of laser-clad high-temperature wear-resistant alloys, *Applied Surface. Science,* 140, 19.

Table 1. Chemical composition of inconel 617

Chemical composition, wt%							
Fe	Cr	Mo	Co	Ti	Si	Al	Ni
1.25	21.7	8.9	12.4	0.45	0.06	0.73	54.1

Table 2. Processing parameters studied

Power (p)	1.7-1.9 kW
Beam diameter (d)	5 mm
Traverse speed (V)	1-35 mm/s
Interaction time (t)	0.14-5 s
Power density ($4P/\pi d^2$) (P_A)	86-97 W/mm^2
Specific energy (P/dV)	9.7-380 J/mm^2
Powder feed rate (f)	8.9-10 g/min
Shrouding gas	Argon

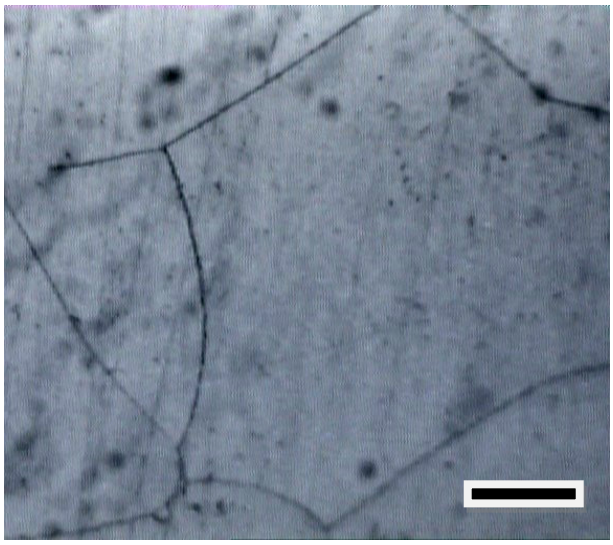

Figure 1. Microstructure of the inconel 617 substrate (marker is 15μm).

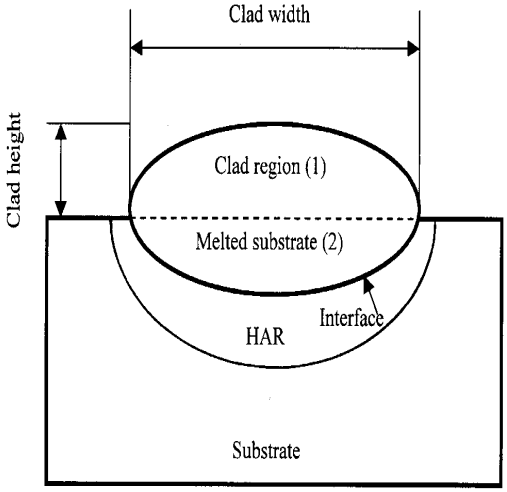

Figure 2. Schematic shape of the laser clad layer.

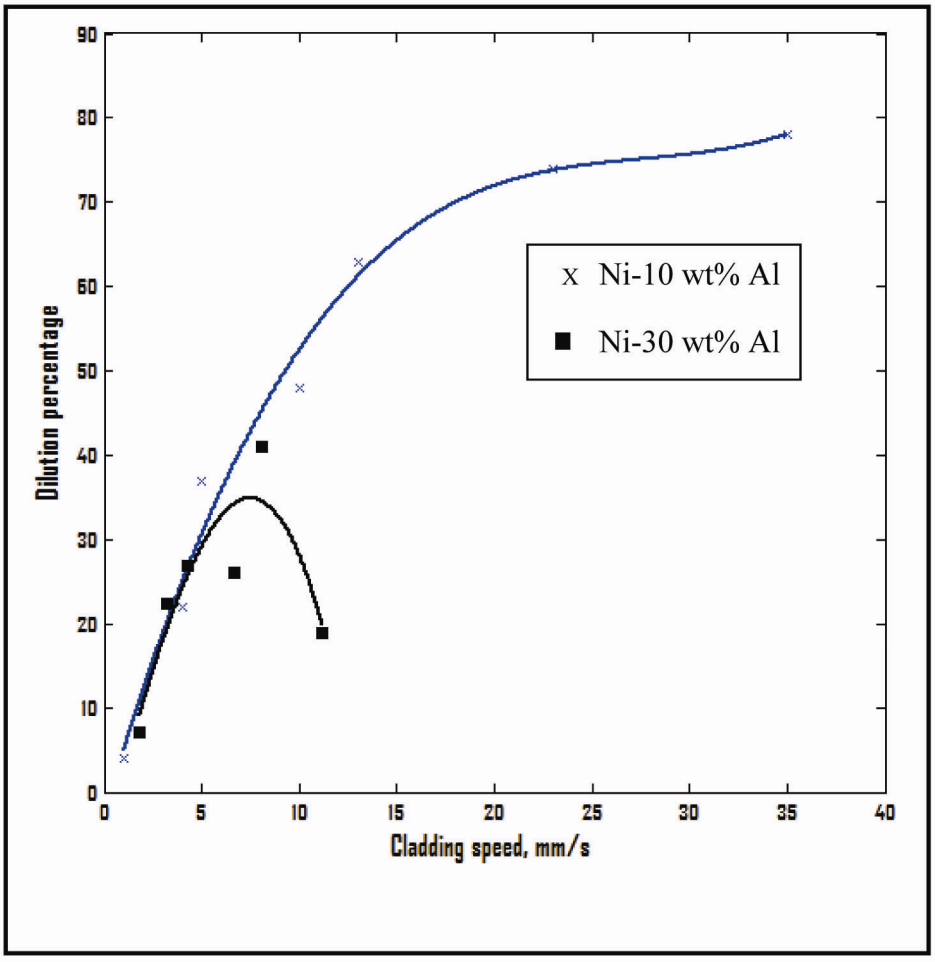

Figure 3. The relationship between dilution percentage and cladding traverse speed of laser cladded inconel 617 with Ni-10 wt% Al and Ni-30 wt% Al premixed powders

ISSN 1913-1844 E-ISSN 1913-1852

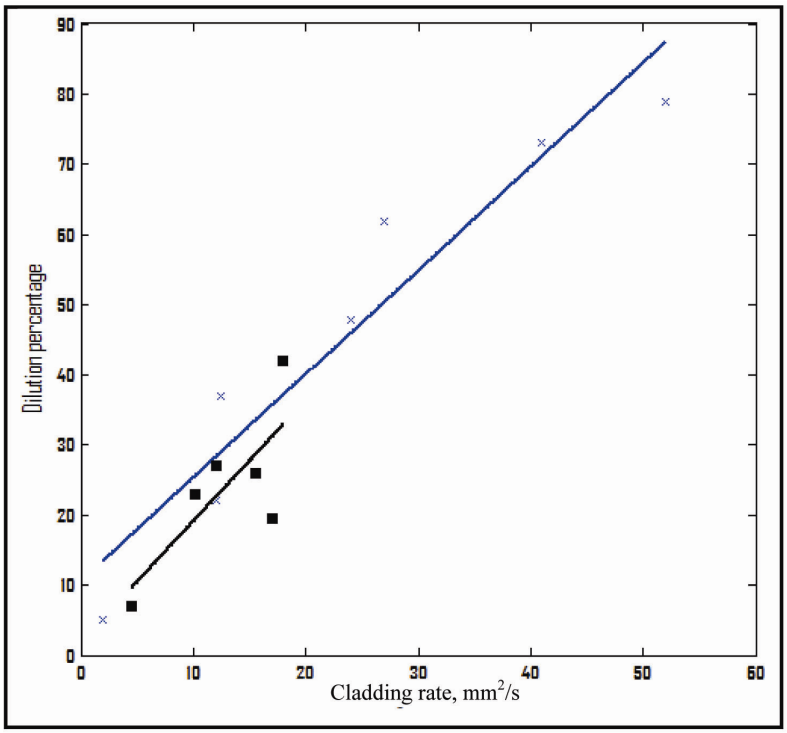

Figure 4. The relationship between dilution percentage and cladding rate of laser cladded inconel 617 with Ni-10 wt% Al and Ni-30 wt% Al premixed powders.

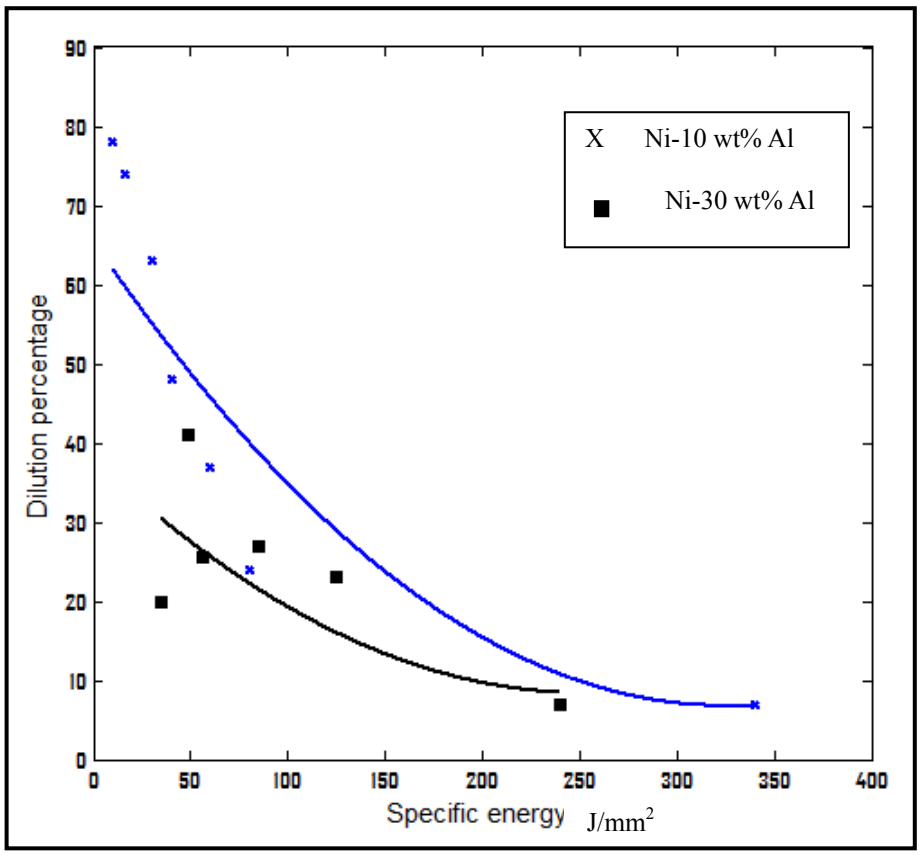

Figure 5. The relationship between dilution percentage and specific energy of laser cladded inconel 617 with Ni-10 wt% Al and 30 wt% Al premixed powders.

Design Lower Arm Using Optimum Approach

Adel Mahmoud Bash

Department of Mechanical Engineering, College of Engineering, Tikrit University, Salah al_deen, Iraq

Abstract

In the automotive industry, the riding comfort and handling qualities of an automobile are greatly affected by the suspension system. This paper presents the robust design of vehicle suspension arm using stochastic design improvement (SDI) technique based on Monte Carlo simulation. The main goal of this study is to determine the optimum design for the suspension arm. The structural model of the suspension arm was utilizing the Solid works and aluminum alloys (AA7075-T6) are selected as a suspension arm materials. The linear static stress distribution is investigated using the commercial Finite element analysis package, and dynamic analysis was performed using NASTRAN software. SDI has been performed to the design. A target output behavior is selected from the output variables available in the analysis. The result shows that the lower arm design has a higher capability to stand higher pressure as 9.18 MPa with the stress acted on lower arm is 41 MPa. The new parameter of material can be chose as optimum result for the lower suspension arm.

Keyword: Lower arm, SDI, FEM, Dynamic analysis

1. Introduction

Stress analysis activities vary depending on the function and maturity of the phase, an important benefit of performing stress analyses is the ability to determine design sensitivities and to conduct trade studies. (Conle and Mousseau 1991) used vehicle simulation and the finite element results to generate the fatigue life contours for the chassis components using automotive proving ground load history results combined with the computational techniques; They concluded that the combination of the vehicle dynamics modeling, finite-element analysis, and fatigue analysis are the viable techniques for the fatigue design of the automotive components. (Kim et al. 2002) were studied a method for simulating vehicles dynamic loads, but they add durability assessment, For their multibody dynamic analysis they use DADS and a flexible body model. Dynamic stress analysis was performed using MSC. NASTRAN. The fatigue life was then calculated using a local strain approach; The result fatigue life, shows the majority of the fatigue damage occurred over a frequency range that depend on terrain traveled (service or accelerated test course). (Gopalakrishnan and Agrawal 1993) carried out durability analysis of full automotive body structures using an integrated procedure, in which the dynamic simulation software ADAMS was used to generate loading histories, and the Inertia Relief Analysis of MSC.NASTRAN was used to analyze the model and to get displacements and stresses. Designing a robust suspension lower arm is crucial to the success of building the car and requires that suspension components have to be well engineered in aspects of both compactness and crashworthiness, which is defined as a measure of the whole vehicles or its components structural ability to plastically deform and yet maintain a sufficient survival space for its occupants in crashes involving reasonable deceleration loads (Praya and Belwefa 2004). Stochastic design improvement (SDI) is a fast and efficient method for improving the performance of a system. Can be specify the desired target behavior for a system and get multiple alternative solutions that satisfy the target. Most applications of robust design have been concerned with static performance in mechanical engineering and process systems (Zang et al., 2004) whereas the objective of robust design is to optimize the mean and minimize the variability that results from uncertainty represented by noise factors and to test the effect of the variability in different experimental factors using statistical tools. From a technical standpoint the Statistical process control (SPC) and Statistical experimental design (SED) are two methods has been used as a robust design of an automotive suspension arm to improve quality and productivity (Rahman, 1994).The inputs into such programs must include a complete description of the forces acting on the components via dynamic modeling (Frimpong et al., 2005). In this paper, finite element techniques have been used as a tool to model the mechanical properties of the suspension arm. Three-dimensional linear tetrahedron solid elements 10 nodes tetrahedral (TET10) used for the initial analysis based on the loading conditions. Convergence of stress energy was considered as the criteria to select the mesh size and predict the dynamic behavior of suspension arm; SDI has been performed to the design using robust design codes. A target output behavior is selected from the output variables available in the FEM. In the optimization process for the design all the parameters have been set as hard target for stress and design variable for material.

2. Optimization Technique

Optimization problems in practice depend mostly on several model parameters, noise factors, uncontrollable parameters, etc., which are not given fixed quantities at the planning stage. Due to several types of stochastic uncertainties (physical uncertainty, economic uncertainty, statistical uncertainty, and model uncertainty) these parameters are modeled by random variables having a certain probability distribution. In most cases at least certain moments of this distribution are known. Robust Design provides the means to quickly sort through this information and indicate the variables that have the most significant correlations, and therefore most impact the product's performance. Correlation is a concept different from of sensitivity in that collective changes in variable values are considered. Correlation between two variables expresses the strength of the relationship between these variables by taking into account the scatter in all the other variables in a system. It is possible to compute correlations between any pair of variables (input-output, output-output, etc.). Knowledge of the correlations in a system is equivalent to the understanding of how that system works. The above correlations are used in Robust Design for results interpretation and are labeled as linear and non-linear correlations on output plots. Pearson's correlation coefficient measures the linear correlation between variables. For two stochastic variables, x and y, their Pearson, or linear correlation is expressed as follows

$$r = \frac{\sum_i (x_i - u_x)(y_i - u_y)}{\sqrt{\sum_i (x_i - u_x)^2}\sqrt{\sum_i (y_i - u_y)^2}} \quad (1)$$

Where u is the mean value, the values of the Pearson correlation range from –1 to 1. A value close to either 1 or –1 indicates a strong linear correlation. Values close to zero indicate the variables are uncorrelated.

The Spearman rank correlation coefficient rs, is then computed as the linear correlation coefficient between the ranks Ri of the xis and the ranks Si of the yis, the rs is expressed as follows

$$r_s = \frac{\sum_i (R_i - u_r)(S_i - u_s)}{\sqrt{\sum_i (R_i - u_R)^2}\sqrt{\sum_i (S_i - u_S)^2}} \quad (2)$$

For the design of the lower arm suspension, the application of Stochastic Design Improvement (SDI) will be use which is in the MSC.Robust Design software. SDI is a fast and efficient capability to improve a system design so that its most probable behavior coincides with specified target values.

This process continues until either the target value or a physical limit for the design variable is reached. This is normally accomplished with 4 to 6 sets of 15 analysis runs. The key feature of SDI is that it operates on a full FE model, which incorporates tolerances, and not on a simplified surrogate. SDI surpasses classical optimization techniques in terms of performance and computational cost. Figure 1 shows the flows of steps that will be done in the SDI for the lower arm suspension design.

3. Motion for Suspension System of Automobile

Natural frequency is the rate of energy interchange between the kinetic and the potential energies of a system during its cycle motion. As the mass pass through the static equilibrium position, the potential energy is zero (Dimarogonas, 1996). The natural frequency is expresses as Eq. (3).

$$w_n = \sqrt{\frac{k}{m}} \quad (3)$$

Where: w is natural frequency
k is coefficient of spring
m is mass

The chassis natural frequency is used the suspension rate and chassis mass and expressed as in Eq. (4),

$$w_n = \sqrt{\frac{k_s}{m_c}} \quad (4)$$

where w_n is natural frequency for the car
k_s is coefficient of spring
m_c is mass of the car

For the wheel natural frequency ωw, it's necessary to take into account Ks and Kt because the wheel oscillates the suspension and tire springs. Although these two springs are on opposite side of the wheel/hub/knuckle mass, the mass would feel the same force if the two springs were in parallel on one side of the mass. In other words, the two springs, Ks and Kt, are in parallel and their composite rate is their sum.

$$w_w = \sqrt{\frac{k_s + k_t}{m_w}} \tag{5}$$

Where w_w is the natural frequency of the wheel

k_s is the coefficient of spring

k_t is coefficient of tire

m_w is mass of the wheel

3.1 Model Description

Vehicle suspension is a mechanism locating between the sprung mass (vehicle body) and the unsprung masses (wheels) of the vehicle. The suspension provides forces between these two masses of the vehicle according to certain state variables of the vehicle. A good car suspension system should have satisfactory road holding ability, while still providing comfort when riding over bumps and holes in the road. When the bus is experiencing any road disturbance the bus body should not have large oscillations, and the oscillations should dissipate quickly. A simple three-dimensional model of suspension arm was modeling by used Solid Works software as shown in Figure 2.

3.2 Mechanical Properties

Material model and material properties play an important role in the result of FE method. The material properties are one of the major inputs, which is definition of how the material behaves under the cyclic loading conditions. The materials parameters required depend on the analysis methodology being used. The mechanical properties of 7075-T6 aluminum alloy are shown in Table 1.

4. Results and Discussion

4.1 Modeling and Simulation

The lower arm suspension is one of the important parts in the suspension system. A specific area of constraint has been set into the design in order to get a precise result. TET10 has been used in the finite element modeling using MSC. PATRAN. These analyses were preformed iteratively at different mesh global length until the appropriate accuracy obtained. The convergence of the stresses was studied as the mesh global length was refined in the analysis. The mesh global length of 0.1 mm was chosen and the pressure of 8 MPa was applied at the end of the bushing that connected to the tire. The other two bushing that connected to the body of the car are constraint. The pressure that has been applied is based on (Al-Asady et al. 2008). The three-dimensional FE model, loading and constraints of suspension arm is shown in Figure 3.

4.2 Effects of the Mesh Types

The stress histories calculated using the linear static analysis method are usually the most accurate and are commonly used by members of the finite element community as a reference to evaluate the accuracy of the stochastic design improvement. The linear static stress analysis was performed utilizing MSC.NASTRAN to determine the stresses result from finite element model. The material models utilized of elastic and isotropic material. The tetrahedral element TET10 was use for the mesh analysis Figure 4. The convergence of the finite element model of the structure was tested for TET10 and 5 different mesh sizes. Figure 5 shows the von Mises stress contour for TET10 element. The linear elastic analysis results including maximum principal stress, von Mises stress, and Tresca stress are tabulated in Table 2. The convergence of the stress was considered as the main criteria to select the mesh type. The finite element mesh was generated using TET10 for various mesh global length. From the stress analysis, the result shows that the white area of the design is the lowest predicted stress acted on the lower arm suspension design. Therefore, the area can be made as a guide in the future process of modifying or optimizing the design. It is also important to make sure that the critical points on the design which have the highest predicted stress should be look carefully in the process of modifying and optimizing the design in order to avoid any failure in the future usage of the lower arm design.

Figure 6 shows the predicted results of stresses at the critical location of the suspension arm. It can be seen that the smaller the mesh size capture the higher predicted stresses. It is also observed that mesh size of 0.1 mm (54178 elements) has obtained the maximum stresses, which is almost flatter in nature. The maximum stress obtained of 50.3, 52.2 and 56.3 MPa for von Mises stress, Tresca and Maximum principal stress method respectively. The maximum principal stress method occurred highest stresses through the global length range. Thus TET10 and maximum principal stress method are selected for linear static and dynamic analyses of the

suspension arm. Thus TET10 at mesh size 0.1 and maximum principal stress method are selected for linear static and stochastic design improvement of the suspension arm.

4.3 Dynamic Analysis of Lower Arm

Dynamic analysis is focused on the eigen-frequencies and mode shapes. From a physical point of view an initial excitation of an undamped system causes to vibrate and the system response is a combination of eigenmodes, where each eigenmode oscillates at its associated eigen-frequency (Patrik, 2001). Modal analysis is usually used to determine the natural frequencies and mode shapes of a component. It can be used as the starting point for dynamic analysis. The finite element analysis codes usually used several mode extraction methods. The Lanczos mode extraction method is used in this study. Lanczos is the recommended method for the medium to large models. In addition to its reliability and efficiency, the Lanczos method supports sparse matrix methods that significantly increase computational speed and reduce the storage space. This method also computes precisely the eigenvalues and eigenvectors. The number of modes was extracted and used to obtain the suspension arm stress histories, which is the most important factor in this analysis. Using this method to obtain the first 10 modes of the suspension arm, which are presented in Table 3 and the shape of the mode are shown in Figure 7. It can be seen that the working frequency (80Hz) is far away from the natural frequency (233.26 Hz) of the first mode. A sample of the resulting eigenvalue/eigenvector from the suspension arm is shown in Table 4.

4.4 Stochastic Design Improvement

A stochastic simulation generates multiple scenarios of a model by repeatedly sampling values from the probability distributions for the uncertain variables. The stochastic simulation takes the uncertainty of variables into account to determine the level of uncertainty in the outputs. The more stochastic variables a model contains, the more realistic it is. From the Figure 8, the relative influence of tolerances in input variables on the scatter in a particular functionality (output) can be obtained. The pressure gives the largest influence on the stress value followed by the Poisson ratio, modulus of elasticity, and density respectively. This result is very logical and showed that the design is functioning correctly. Figure 9 shows ant hill scatter for stress against materials. It can be seen that there is less interaction (correlation) between them. Linear and non-linear correlation betwee them are obtained negative (linear cor.= -0.594 and non-linear cor. = -0.583). Figure 10-11 show the Ant hill correlation between the maximum principal stress and von Mises stress versus pressure respectively. It can be seen that the correlation between the stress and load scale factor are strongly correlation between them (linear cor. = 0.994 and non-linear = 0.988 for maximum principal stress and linear cor. = 1.0 and non-linear = 1.0 for von Mises stress. It is to be more dominant that's confirming the result in the pie chart Figure 8.

In the optimization process for the design all the bounds of function study have been set as follows.

1) Max SDI step is 5.
2) Design variable: Modulus of Elasticity, Poisson Ratio, Density, Pressure.
3) Hard target: Von Mises Stress (50.3MPa).

The results of SDI shows that there are multiple samples from the ant hill scatter plot that give the value of the parameter to use in the optimization process. So the outcome from the SDI had been selected and it can be shown in Table 5. Figure 12 show that lower arm design has a higher capability to stand higher pressure as 9.18 MPa with the stress acted on lower arm is 41 MPa.

5. Conclusion

An example was attempted on how robust design technique could be applied in the design stage of the product optimum process so as to maximize product reliability. A detailed model of suspension arm has been developed using finite element techniques. The tetrahedral elements (TET10) is used for the initial analysis then used for the solid mesh. Sensitivity analysis was performed to determine the optimum element size. It can be seen that the TET10 at mesh size 0.1 capture highest moment levels von Mises stress for this reason used to dynamic analysis. The results of the frequency are shown 10 modes and several deformation shapes and from the results proved that the control suspension arm model has been predicted the dynamic behavior. A robust design of lower arm suspension using stochastic optimization is presented. From the analysis, several conclusions can be drawn as follows; The design capability to endure more pressure with lower predicted stress is identified through the optimization process, A lower density and modulus of elasticity of material can be reconsidered in order to optimize the design, and The area of the design that can be altered for the optimization and modification is identified through the stress analysis result.

References

Al-Asady, N.A., Abdullah, S., Arrifin, A.K., Rahmman, M.M. and Beden, S.M. (2008). Improving the automotive lower suspension arm durability using finite element analysis, Seminar on Engineering Mathematics. Universiti Malaysia Pahang of Department of Mechanical and Materials Engineering.

Conle, F.A and Mousseau C.W. (1991). Using vehicle dynamic simulation and finite element result to generate fatigue life contours for chassis component. *International Journal of Fatigue,* 13(3): 195 - 205.

Dimarogonas, A. (1996). *Vibration for Engineers.* Second Ed. New York: Prentice Hall.

Frimpong, S., Yafei, H. and Awuah-Offei, K. (2005). Mechanics of cable shovel-formation interactions in surface mining excavations. *Journal of Terramechanics* 42: 15-33.

Gopalakrishnan, R., and H. N. Agrawal. (1993). Durability Analysis of Full Automotive Body Structures. SAE International Congress and Exposition, Detroit, MI, March.

Kim, H.S, Yim, H.J and Kim, C.M. (2002). Computational durability prediction of body structure in prototype vehicles. *International Journal of Automotive Technology,* 3(4): 129-136.

Patrik, H. (2001). *FE-adaptivity and a nonlinear eigenproblem algorithm.* Department of Structural Mechanics, Chalmers University of Technology, Sweden.

Praya, Prasad and jamel E. Belwefa. (2004). *Vehicle crashworthiness and occupant protection,* American Iron and steel institute 2000 Town center Southfield, Michigan 48075.

Rahman P. (1994). Robust Design of an Automotive Suspension System, M.S. Thesis. Michigan Technological University, USA, 1994.

Zang C., M.I. Friswell, and J.E. Mottershead. (2004). A review of robust optimal design and its application in dynamics, *Computers & Structures,* vol.83, no.4-5, pp. 315-326, 2004.

Table 1. Mechanical properties of aluminum alloy 7079-T6

Material	Young's Modulus (GPa)	Poisson's ratio	Tensile strength (MPa)	Yield strength (MPa)
Aluminum alloy AA7079-T6	72	0.33	503	572

Table 2. Variation of stresses concentration at the critical location of the suspension arm for TET10 mesh

Mesh size (mm)	Total nodes	Total Elements	Von Mises (MPa)	Tresca (MPa)	Max Principal Stress (MPa)
0.1	96080	54178	50.3	52.2	56.3
0.3	10041	4676	50.2	51.3	54.2
0.6	5889	2665	48.9	50.6	52.2
1.0	5436	2465	47.4	48.2	50.7
1.5	3186	1409	45.3	35.7	49.9

Table 3. Natural frequency of lower arm

No. of Mode	Natural Frequency (Hz)
1	233.26
2	424.88
3	889.65
4	1114.7
5	1388.4
6	1546.4
7	1660.6
8	2380.7
9	2498.3
10	2535.2

Table 4. Maximum displacements from modal analysis

Mode No	T1(μm)	T2(μm)	T3(μm)
1	146.89	5825.3	10135.5
2	629.77	6349.31	1088.46
3	1234.45	5807.32	950.36
4	1568.87	7615.65	1572.16
5	2854.58	1533.89	490.42
6	1377.12	6320.35	1781.14
7	1262.52	5506.094	1614.21
8	2178.52	5343.608	2623.39
9	1925.07	5991.516	2042.43
10	2586.68	4238.355	2572.20

Table 5. Comparison of the design parameter before and after optimization

Design parameter	FEM	SDI
Modulus of elasticity	71.7 GPa	69.1 GPa
Density	2.7 g/cc	2.489 g/cc
Poisson Ratio	0.33	0.3428
Pressure acted on the design	8MPa	9.18 MPa
Maximum von Mises stress	50.3MPa	41.0 MPa

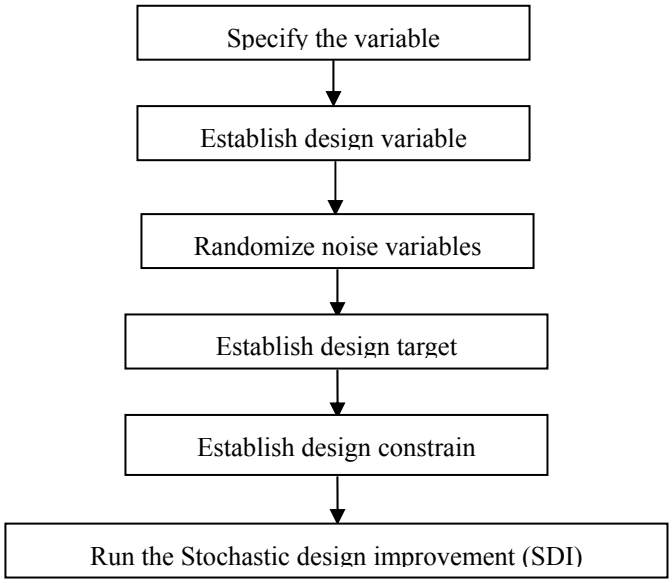

Figure 1. Flow chart of steps in SDI

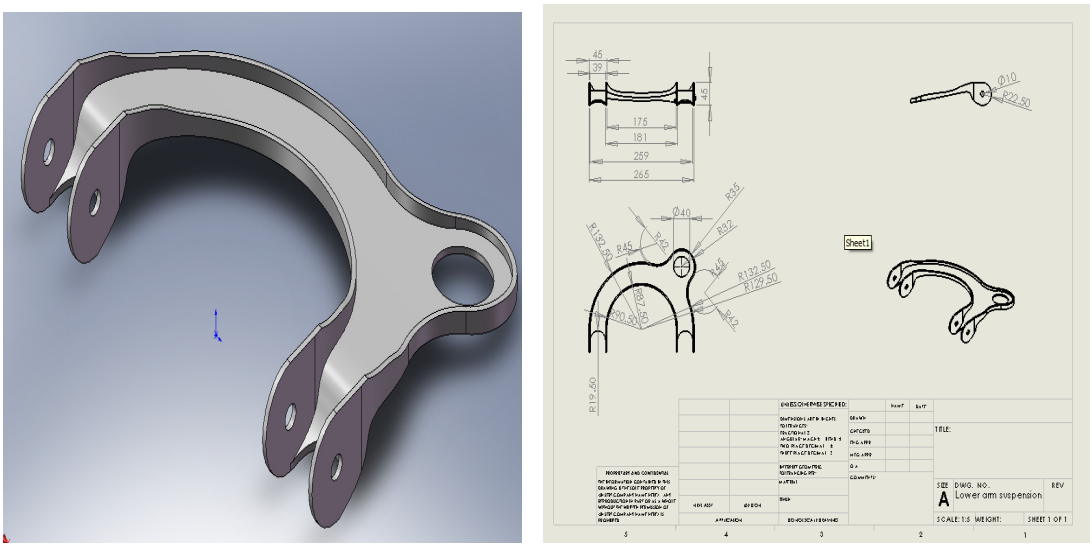

(a) Structural model (b) Overall dimension

Figure 2. Structural mode

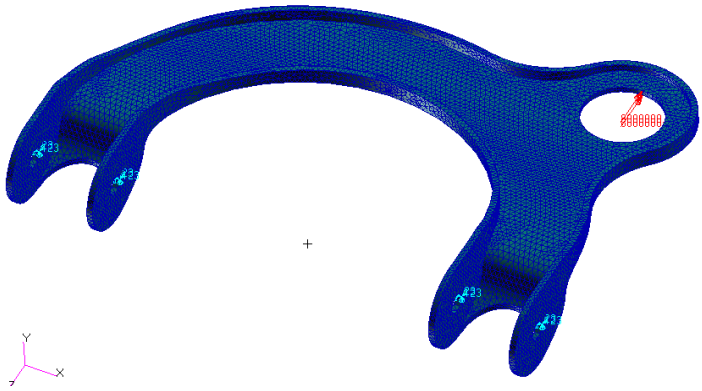

Figure 3. Three-dimensional FE model, loading and constraints

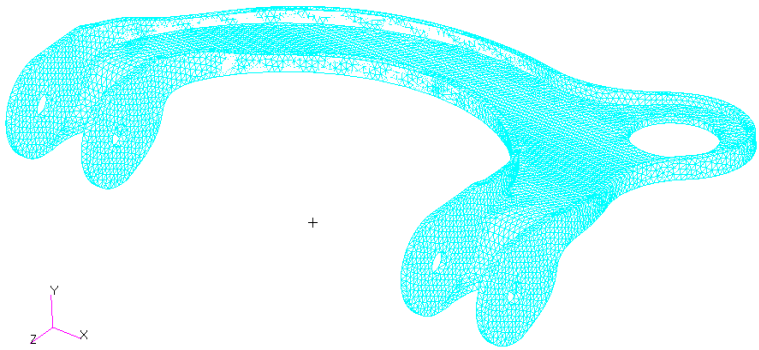

Figure 4. TET10, 54178 elements and 96080 nodes

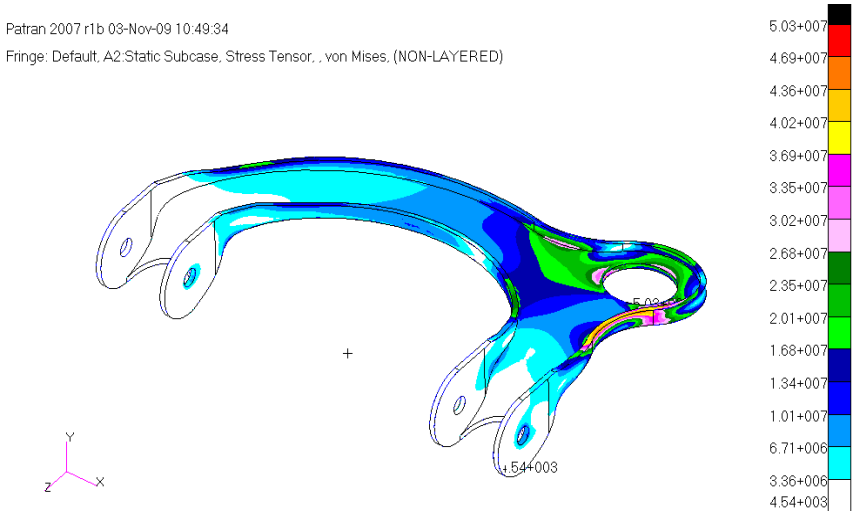

Figure 5. von Mises stresses contour for TET10

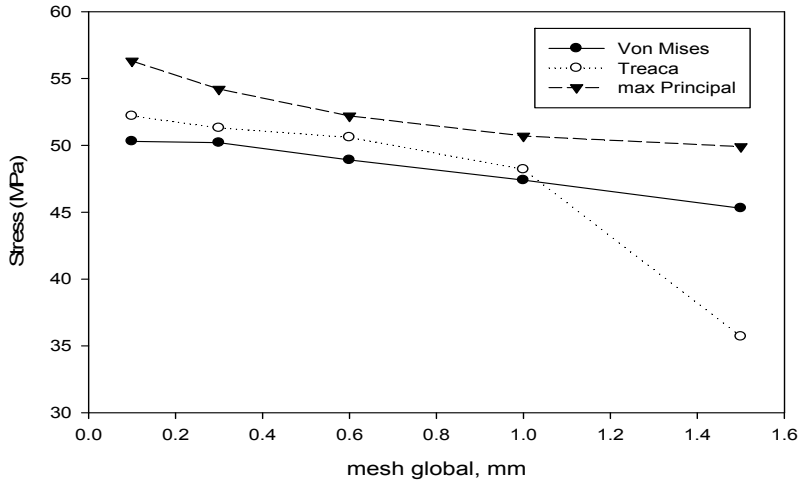

Figure 6. stress contour for TET10

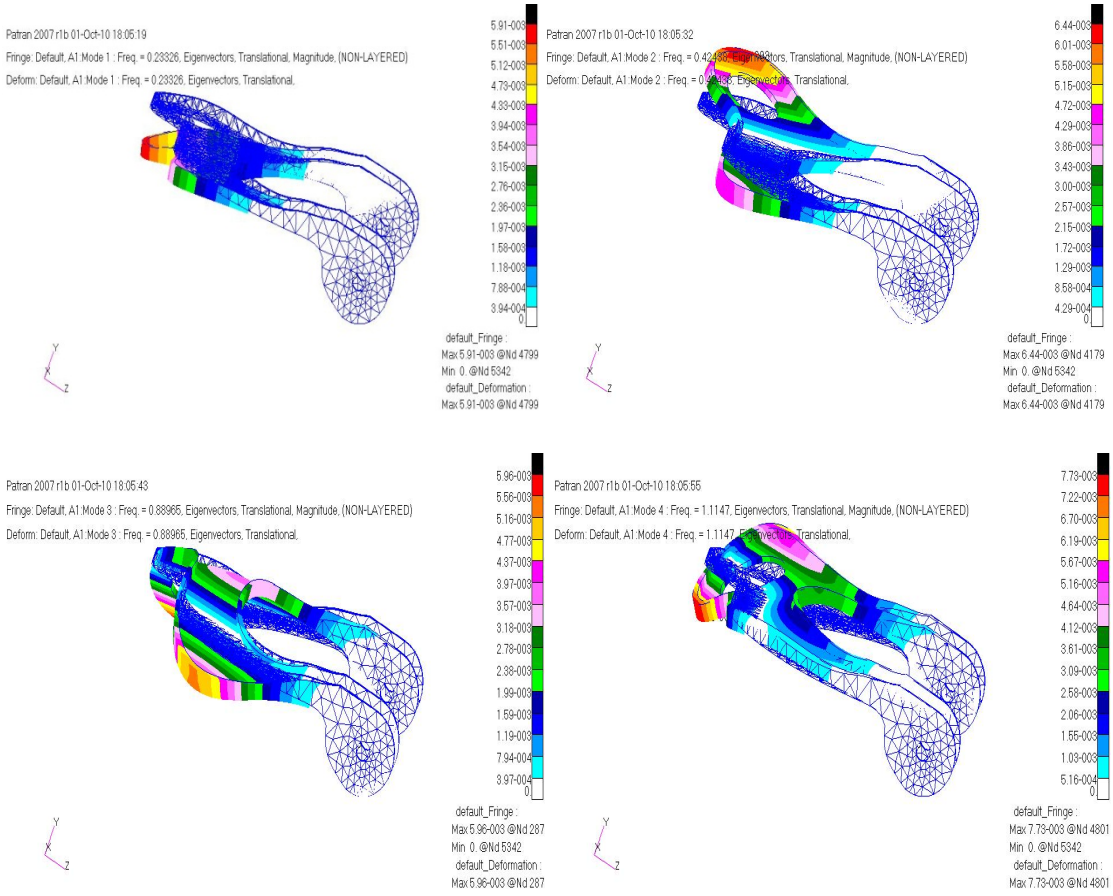

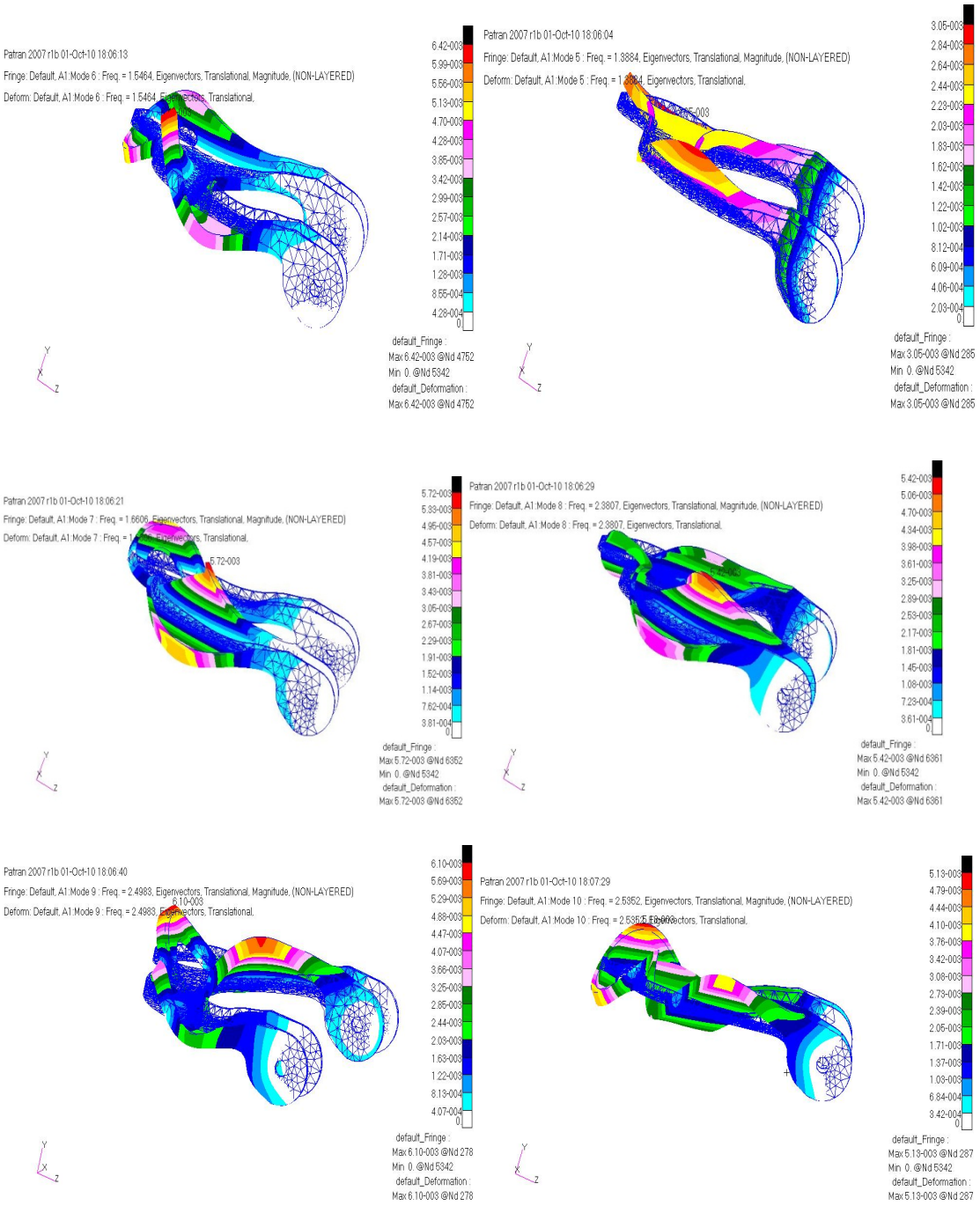

Figure 7. frequency mode shape of lower arm

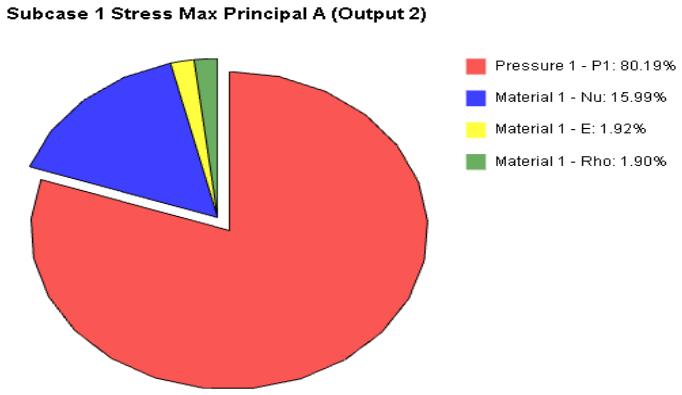

Figure 8. Pie chart of factors that influence to the stress value in the design

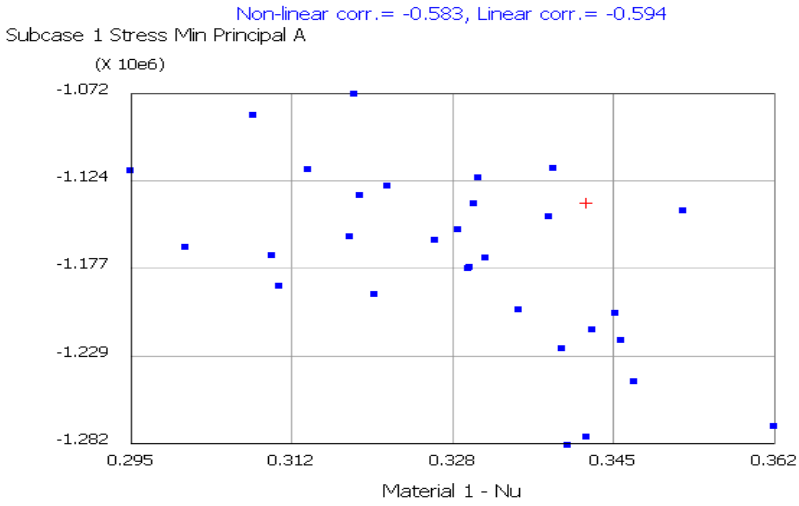

Figure 9. Ant hill scatter plot for stress VS Poisson ratio

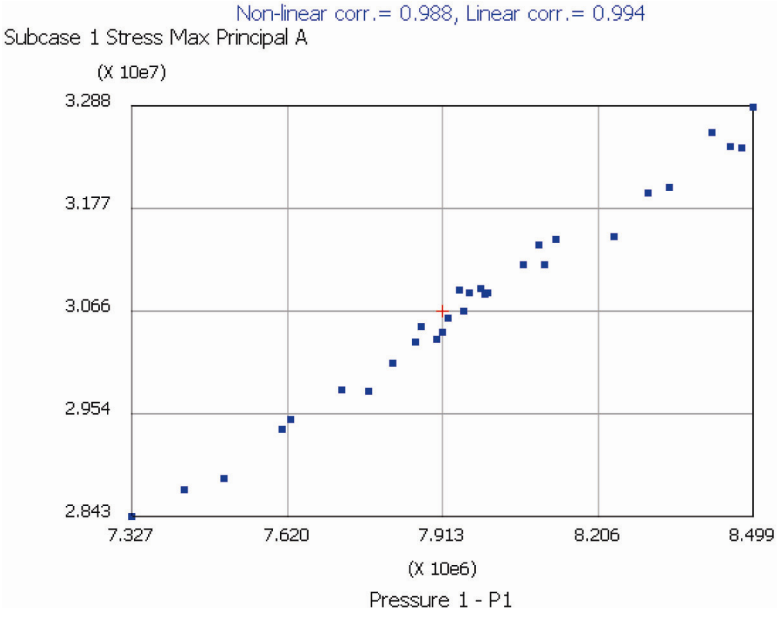

Figure 10. Ant hill scatter plot for stress VS pressure

 ISSN 1913-1844 E-ISSN 1913-1852

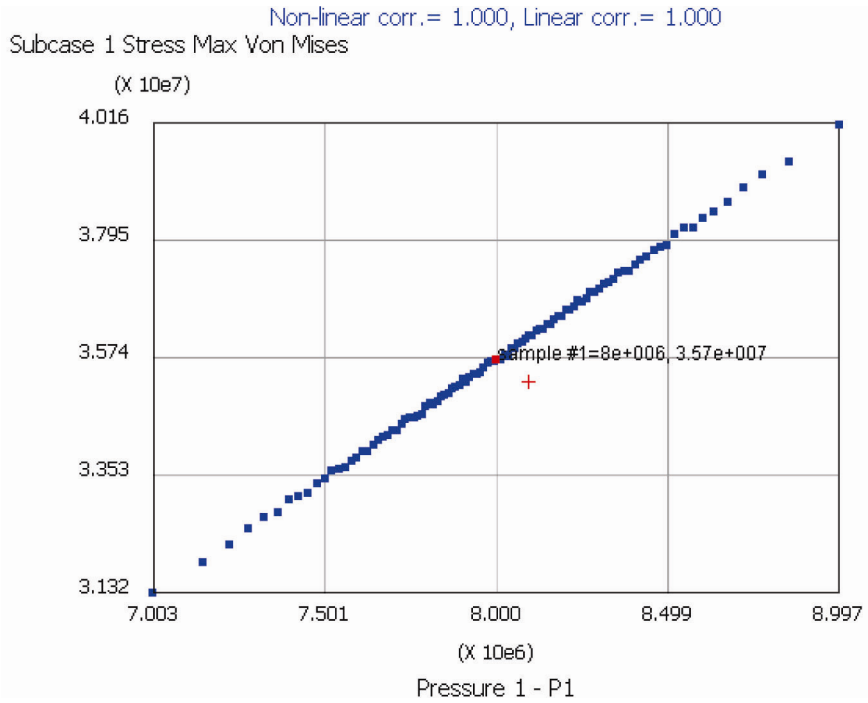

Figure 11. Ant hill scatter plot for stress VS pressure

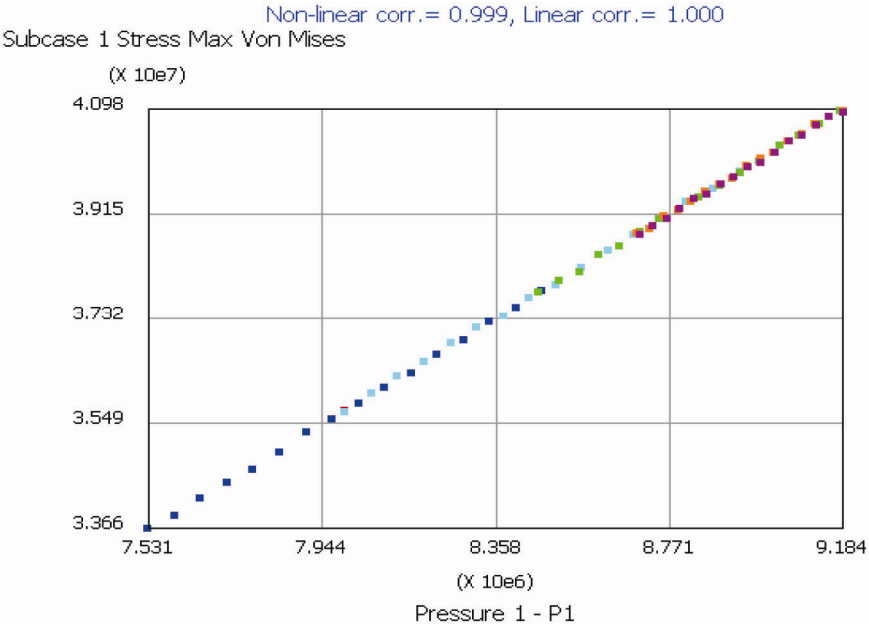

Figure 12. Ant hill scatter plot for stress VS pressure (After SDI)

Research on the Optimization Method of Virtual Enterprise's Task Scheduling Problems in Aluminum Industry

Erwei Yin, Fantian Zou & Fengxing Zou

College of Mechatronics Engineering and Automation, National University of Defense Technology

Changsha 410073, China

Project supported by the State Key Program of National Natural Science of China (Grant No. 60634020)

Abstract

Traditional research on production scheduling in aluminum industry, aimed to certain production process, simply pursued the output as the highest aim, scheduled based on experience, so that the result of scheduling cannot reach the global optimization, and cannot realize production scheduling and resource allocation with the aim of optimal energy consumption, resulting in the waste of energy. Taken the minimal sum of energy consumption in production, transport and stock as objective function and integrated with enterprise's experiences in production, the article establishes a model of virtual enterprise's task scheduling in aluminum industry and a hybrid distributed particle swarm optimization (PSO) algorithm is proposed to solve the problem. Finally, simulation experiment is carried out using industrial data and the result shows the optimized scheduling method has obvious optimal effect on reducing scheduling time, optimizing allocation of resources and so on, and thus the energy saving and consumption reducing purpose are obtained.

Keywords: Aluminum industry, Virtual enterprise, Task scheduling, Hybrid distributed particle swarm optimization (PSO) algorithm

1. Introduction

Aluminum industry is metallurgical process with the highest unit comprehensive energy consumption, and the level of production scheduling for aluminum industry also has direct connection to its energy consumption in the process of production(Chen Weiqiang, Wan Hong-yan, Wu Juanni. 2009). Traditional production scheduling in aluminum industry aimed to certain industrial process and the scheduling solution obtained often cannot reach global optimization. Virtual enterprise has such characteristics as flexible structure, prompt response and so on, which cater to fast-changing market opportunities, so more and more enterprises pay attention to it(Zhao Qiang, Xiao Renbin. 2009). Usually, the master of the alliance decomposes and mergers the productive task to several subtask firstly, and then chooses appropriate cooperative enterprises to undertake corresponding subtask, and finally finishes total productive task through cooperative enterprise's joint effort(Huang Aihua, Ye Fei.).

VE task scheduling model has the characteristics such as multiple target, multiple constraints, nonlinear and so on, which is a difficult problem of NP(Gao Yang, Jaing Zibin. 2007). The article takes the optimal energy consumption in production, transport and stock which VE uses to finish productive task in aluminum industry as objective function, establishes a nonlinear mathematical planning model and a hybrid distributed particle swarm optimization (PSO) algorithm is proposed to solve the problem(HDPSO). The approach effectively uses the fast and random global search capacity of genetic algorithm (GA) and parallel distributed positive feedback mechanism of particle swarm optimization (PSO). Through discretization, it avoid redundant search in the real number range. The effect is obvious. Simulation results shows the method can reach the goal of reducing scheduling time and saving energy and reducing consumption under the premise of satisfying VE's operation requirements for aluminum industry.

2. The description of problem and mathematical model

2.1 The description of problem

Because the consumption of primary aluminum is increasing quickly and the fixed cost for producing per ton aluminum is decreasing with the expansion of the scale of aluminum plant, the scale of construction of modern aluminum plant is still growing and thus consists large aluminum production bases, so that each base can be made up of complete aluminum industrial production system including mining station, aluminum oxide plant, electrolytic aluminum plant, aluminum processing plant and so on, from bauxite to alumina, and then from alumina electrolysis to aluminum, even to the products such as Aluminum sections, planks, wires(Zhang Zhaolu, Cui Zhaojie, Zhang Luqiang. 2009). Therefore, aluminum production system may be seen as a virtual enterprise of aluminum production. Each correlative mining station, aluminum oxide plant, electrolytic aluminum plant, aluminum processing plant is the node of virtual enterprise, which consist the supply chain alliance of virtual enterprise and provide conditions for realizing the production scheduling and optimization of aluminum production system.

 ISSN 1913-1844 E-ISSN 1913-1852

Now the process of aluminum production system is properly simplified, from mining bauxite to putting the products of aluminum on sale. All the process is classified roughly and mainly includes four sections as shown in figure 1.

In fact, the problem of virtual enterprise's production task scheduling in aluminum industry is similar to hybrid flow shop scheduling problem, but because the constraint relations between virtual enterprise's tasks are very complex, it is needed to be further extended so as to reach ideal goal of global optimization under the condition of ensuring time limit.

2.2 The establishment of the VE task scheduling model in aluminum industry

1) To make such assumptions about the model considering the characteristics of VE in aluminum industry:

① According to the difference of contract orders, the products are classified into several lots and the time that each lot is processed in different plants is known;

② Considering production capacity and resource conditions, each plant only processes one lot during the same period of time;

③ VE begins to operate from 0:00

1) Symbol definition:

N: the sum of lots to be processed;

S: the sum of productive tasks of virtual enterprise

M_j: the number of candidate enterprise for the productive task j

N_k: the number of the lot to be arranged to be produced in the enterprise k

x_{ijk}: 0-1 variable, if the task j of the lot i is processed in enterprise k, take 1, otherwise take 0;

s_{ijk}: the start time for the task j of the lot i in the enterprise k

c_{ijk}: the completion time for the task j of the lot i in the enterprise k

t_{ijkh}: the transportation time that the task j of the lot i is transported to the next task's enterprise h after it is processed in the enterprise k

e_{ijk}: the energy consumption that the task j of the lot i is processed in the enterprise k

q_{ijkh}: the energy consumption in transport that the task j of the lot i is transported to the next task's enterprise h after it is processed in the enterprise k

$\delta(x_{ijk},x_{i,j+1,h})$: 0-1 variable, take 1 if and only if x_{ijk} and $x_{i,j+1,h}$ are 1 at the same time, otherwise take 0;

K: stock energy consumption coefficient

T^*: the delivery date of the products

2) Objective function

At present, the simple pursuit of maximizing enterprises' interests has become the highest productive aim of many non-ferrous metallurgical enterprises. Because of the limits of theory, method and other aspects, production scheduling solutions only involves productive fees, and most of them aim to pursue output and carry out scheduling according to their experiences. The realization of the aim of output is often at the cost of sacrificing energy consumption, the efficiency of resource use is not improved substantially and the production scheduling and resource allocation aiming to optimal energy consumption cannot be achieved, leading to the waste of energy. Therefore, aiming to the optimized energy consumption for production task, material transport and stock respectively, the article adopts the form of weighted sum to set up the objective function.

$$\begin{aligned} f(X) = & \sum_{i=1}^{N}\sum_{j=1}^{S}\sum_{k=1}^{M_j} e_{ijk}x_{ijk} \\ & + \sum_{i=1}^{N}\sum_{j=1}^{S-1}\sum_{k=1}^{M_j}\sum_{h=1}^{M_{j+1}} q_{ijkh}\delta(x_{ijk}, x_{i,j+1,h}) \\ & + K\times[T^* - \max(c_{iN})] \end{aligned} \tag{1}$$

In the formula (1), the first term represents the energy consumption that virtual enterprise in aluminum industry finishes all the productive task; the second term represents the sum of energy consumption in transport between different productive tasks; the third term represents the stock energy consumption.

3) Constraint condition

① tasks assignment

$$\sum_{j=1}^{M_j} x_{ijk} = 1, \quad i \in \{1,2,\cdots N\}, j \in \{1,2,\cdots S\} \tag{2}$$

$$\sum_{j=1}^{M_j} N_k = N \tag{3}$$

The formula (2) shows each productive task of each lot must be produced in one candidate enterprise; the formula (3) shows the total number of the lot which assign to each parallel enterprise is *N*.

② the constraints of the processing sequence

$$\begin{cases} s_{i_1,j,k} < s_{i_2,j,k} \\ i_1 < i_2, \quad i_1, i_2 \in \{1,2,\cdots,N_k\}, j \in \{1,2,\cdots,S\} \end{cases} \tag{4}$$

The formula (4) shows the former the lot assigned to each enterprise ranks, the earlier it is processed.

③ the constraints of time

$$\begin{cases} c_{ijk} + t_{ijkh} \le s_{i,j+1,h} \\ i \in \{1,2,\cdots,N\}, j \in \{1,2,\cdots,S-1\} \end{cases} \tag{5}$$

$$c_{i_1 j} \le s_{i_2 j}, i_1 < i_2, i \in \{1,2,\cdots,N_k\}, j \in \{1,2,\cdots,S\} \quad (6) \quad T^* \ge \max(c_{iN}) \tag{7}$$

$$s_{ijk} \ge 0, \quad i \in \{1,2,\cdots,N\}, \quad j \in \{1,2,\cdots,S\} \tag{8}$$

The formula (5) shows each task of each lot has to start working only after the lot reaches the enterprise which undertakes the productive task; the formula (6) shows, for certain enterprise, the later lot has to start working only after the former one completes; the formula (7) shows the completion time of all the productive tasks cannot be later than the delivery time, otherwise it will lead to losing credit even contract default; the formula (8) shows the start time is nonnegative.

3. The design of HDPSO and the solutions to the problem

Particle swarm optimization (PSO) algorithm adopted velocity-position search model. The approach initialized randomly a group of particles, each particle represents a candidate solution in the solution space, all the particles have a fitness decided by the objective function, particles fly at a fixed speed in the search space, following the particle whose fitness is optimized at present can find the global optimal particle(I.Jacob Raglend, C.Raghuveer, G.Rakesh Avinash. 2010)(Angus F.M. Huang, Stephen J.H. Yang, Minhong Wang. 2010). Particles update themselves through tracking the most optimal solution *rbest* found by itself and *gbest* found by all the swarm. While finding out the two most optimal solutions, the particles update their velocity and position according to the formula as follows:

$$\begin{aligned} v_{id}(t+1) = {} & wv_{id}(t) + c_1 rand_1()(gbest_d - x_{id}(t)) \\ & + c_2 rand_2()(rbest_{id} - x_{id}(t)) \end{aligned} \tag{9}$$

$$x_{id}(t+1) = x_{id}(t) + v_{id}(t+1) \tag{10}$$

In the formula (9) and (10), v_{id} shows the velocity of the particle *i* in the space *d*, x_{id} shows the position of the particle *i* in the space *d*, c_1 and c_2 are constants, $rand_1()$ $rand_2()$ are random numbers evenly distributed in the interval [0,1].

3.1 The coding and decoding of particles

Because virtual enterprise task scheduling model in aluminum industry has high complexity and multiple constraint conditions, most of the existing scheduling methods only search in the real number space and the search efficiency is very low. (Wei Ou, Fengxing Zou, Zheng Gao. 2008) proposed a code matrix method based on genetic algorithm, which made use of matrix element and position information to deal with the constraint relations between different processes effectively. The article codes and decodes particles based on the method, and the code matrix is shown in the formula (11):

$$P_{N\times S} = \begin{bmatrix} p_{11} & p_{12} & \cdots & p_{1S} \\ p_{21} & p_{22} & \cdots & p_{2S} \\ \vdots & \vdots & \vdots & \vdots \\ p_{N1} & p_{N2} & \cdots & p_{NS} \end{bmatrix} \tag{11}$$

Each row of the matrix $P_{N\times S}$ corresponds to each lot and each row corresponds to a productive task. Matrix element p_{ij} is an integer in the interval $(1,M_j)$. When decoding, p_{ij} shows the enterprise of the task j of the lot i.

3.2 The discretization of PSO algorithm

Because virtual enterprise task scheduling model in aluminum industry the article proposes is an integer programming, but basic PSO algorithm adopts search in real number space and needs to carry out integer operation, this often leads to constraint dissatisfaction or keeping away optimal solution as well as high redundancy of the approach (Chen Ailing, Yang Genke, Wu Zhiming. 2006). Aim to the problem the article carried out discrete treatment for PSO algorithm. From the formula (9) and (10) we can know, when $x_{id}(t)$ and $v_{id}(t+1)$ are integers, it is also ensured that $x_{id}(t+1)$ is an integer. So only to ensure that $v_{id}(t+1)$ is integer all the time in the evolution. The formula (9) is improved as follows:

$$v_{id}(t+1) = \text{int}(wv_{id}(t)) + \phi_1 + \phi_2 \tag{12}$$

In the formula (12), when $gbest_d \geq x_{id}(t)$, ϕ_1 is an integer in the interval $[0, c_1(gbest_d - x_{id}(t))]$ according to a uniform probability distribution; When $gbest_d \leq x_{id}(t)$, ϕ_1 is an integer in the interval $[c_1(gbest_d - x_{id}(t)), 0]$ according to a uniform probability distribution; The calculation of ϕ_2 is the same as ϕ_1. The PSO approach after discretization can be shown by the formula (9) and (12).

3.3 The improvement based on inertia weight

Basic PSO algorithm sets inertia weight as a constant value. Bigger inertia weight has a strong global convergence capability and smaller inertia weight has a strong local convergence capability. For different problems, confirming the proportionate relationship between global search capacity and local search capacity is very important. Generally, in the process of solving the problem, thresholds of iteration should choose bigger inertia weight, with the increasing the number of iterations, search space is becoming small gradually, as well as inertia weight(S.H. Nabavi-Kerizi, M.Abadi, E. Kabir. 2010). It is an effective method to design inertia weight as self-adaptability reduces linearly. The article set inertia weight as

$$w(g) = w_0 - \frac{g}{g_{\max}} \times c \tag{13}$$

In the formula (13), w_0 is initial weight, set as the bigger value; g shows the evolutionary generation; g_{max} shows the biggest evolutionary generation; c shows decay factor.

3.4 The introduction of gene

The search efficiency of PSO algorithm is very high at the earlier stage of computation, but at the later stage, because individual differences decrease, it is easy for the approach to fall into local extreme values. Aiming to the characteristic, the article chooses suitable gene according to the differences of the scale of the problem, after all the individuals of each generation finish iterations, according to the fitness f_i of each particle and the relationship between the maximum f_{max} and minimum f_{min}, we can judge whether each particle carries out crossover operation. The rule of crossover is:

$$\begin{aligned} &IF \qquad f_i \in (f_{\min}, (f_{\min} + \frac{f_{\max} - f_{\min}}{MP} \times rand())) \\ &Exchange \qquad p_u \qquad p_v \qquad u \neq v \end{aligned} \tag{14}$$

In the formula (14), *rand*() is a random number in the interval [0,1], p_u、p_v represents arbitrary two rows of coding respectively, after crossover, the coding sequences ensures the validity of particles.

3.5 The choice of fitness function

Because the aim of virtual enterprise's task scheduling model in aluminum industry is to minimize the energy consumption, in order to meet the conditions that the fitness maximize when the particles optimizes, the article set the fitness function as reciprocal of $H(X)$. So the fitness of particles is:

$$H_{fit}(X) = 1/\min H(X) \tag{15}$$

From the formula (15) we can know, when the particles search out the optimized value, the energy consumption minimizes.

4. Simulation experience and the result analysis

Now take the example of certain large aluminum industry group. The numbers of candidate enterprises of each

task are 3,3,2,2 respectively. The performance index parameters of these candidate enterprises are shown in the table 1-3. The delivery time of the products is 100 days and the stock energy consumption coefficient $K = 5$. Assume the population size of PSO is 30, the largest iteration generation is 200, the initial weight is $w_0 = 1.2$, $c_1 = 1.8$, $c_2 = 1.8$.

In order to verify the optimized effect of the algorithm, the article did a lot of experiments. Each experiment calculates two sets of curves: one is basic PSO algorithm's optimal particle's fitness and average fitness variation curve; the other one is improved HDPSO algorithm's variation curve, of which one test result is shown in the figure 2.

From the figure we can know, compared basic PSO algorithm with HDPSO algorithm curves, the former has obvious prematurity, the approach falls into local optimal solution early, its global search capacity is too weak and redundancy is very high; for the later, the optimized effect with the improvement of inertia weight and introduction of mutation operator is very obvious so that the global search capacity becomes strong obviously, and the discretization of the algorithm makes its search redundancy reduces greatly. As shown in the figure 3,in the experiment, the optimal scheduling solution obtained by HDPSO algorithm had obvious optimal effect on productive task assignments and scheduling. The completion time is 106 days, which meet the requirements of delivery time. The simulation result showed adopting the optimized scheduling solutions can satisfy the requirements of aluminum production and achieved the aim to save energy and reduce consumption.

5. Conclusions

The research shows, it has been very limited for the space of improving enterprise's comprehensive benefits through one-side improving the production capacity and control level of the production equipments, but to realize optimized scheduling, allocate productive resource reasonably, improve flexibility of production system and the utilization efficiency of equipments and reduce the consumption of manpower, water and energy are importance to improve the key competition ability of enterprise and solve resource bottleneck problem. Aiming to virtual enterprise's task assignment problem in aluminum industry, the article took the minimized energy consumption as the objective function and established nonlinear planning model. Under the constraint conditions that the delivery time of products was satisfied, the model took the energy consumption in the production, transport and stock fully into account. Aiming to the characteristics, the article proposed a new improved HDPSO algorithm. Through a lot of experiments, the simulation results showed the structure of the optimization scheduling model is reasonable and satisfy the technological requirements: HDPSO algorithm can search out the optimal energy consumption scheduling solution quickly and the application in the virtual enterprise's task scheduling model in aluminum industry is feasible. The optimization scheduling method gives references to realize the optimized scheduling of all the process in aluminum industry and energy conservation and consumption reduction.

References

Angus F.M. Huang, Stephen J.H. Yang, Minhong Wang. (2010). Improving fuzzy knowledge integration with particle swarmoptimization. *Expert Systems with Applications.* 37 (2010): 8770–8783.

Chen Ailing, Yang Genke, Wu Zhiming. (2006). Hybrid discrete particle swarm optimization algorithm for capacitated vehicle routing problem. *Journal of Zhejiang University SCIENCE A,* 2006, 7(4): 607-614.

Chen Weiqiang, Wan Hong-yan, Wu Juanni. (2009). Life Cycle Assessment of Aluminium and the Environmental Impacts of Aluminium Industry. *LIGHT METALS,* 2009, 5:3-10.

Gao Yang, Jaing Zibin. (2007). Using HGA to Solve Production Planning in VE. *Control and Decision,* 2007, 22(8):931-938.

Huang Aihua, Ye Fei. (2002). Task Allocation and Harmonizing of Virtual Enterprise. *Journal of South China University of Technology (Natural Science Edition),* 2002, 30(5):1-4.

I.Jacob Raglend, C.Raghuveer, G.Rakesh Avinash. (2010). Solution to profit based unit commitment problem using particle swarm optimization. *Applied Soft Computing,* 10(2010): 1247-1256.

S.H. Nabavi-Kerizi, M.Abadi, E. Kabir. (2010). A PSO-based Weighting method for linear combination of neural networks. *Computers and Electrical Electrical Engineering,* 36(2010):886-894.

Wei Ou, Fengxing Zou, Zheng Gao. (2008). Flexible Flow-shop Scheduling Approach Based on Hybrid Particle Swarm Optimization. *The 20th Chinese Control and Decision Conference,* 2008: 946-951.

Zhang Zhaolu, Cui Zhaojie, Zhang Luqiang. (2009). The designing and planning of circular economy industry chain for aluminium industry. *China Mining Magazine,* 2009, 18(5): 25-28.

Zhao Qiang, Xiao Renbin. (2009). Task Scheduling of Virtual Enterprise Based on Multi-Agent Technology. *Journal of South China University of Technology (Natural Science Edition),* 2009, 37(2):20-24.

Table 1. the production schedule of candidate enterprise

lot	Task 1			Task 2			Task 3		Task 4	
	E_{11}	E_{12}	E_{13}	E_{21}	E_{22}	E_{23}	E_{31}	E_{32}	E_{41}	E_{42}
1	5	6	3	8	9	13	10	6	5	6
2	6	6	5	14	14	10	8	10	6	6
3	5	4	3	13	13	12	9	10	7	7
4	6	5	5	13	10	11	7	8	7	5
5	4	6	5	13	14	12	10	10	5	6
6	4	4	4	14	11	12	7	9	5	5
7	6	5	5	12	13	14	7	6	5	5
8	6	5	5	13	13	13	8	10	6	6
9	5	5	4	14	11	11	9	10	5	6
10	5	6	6	12	14	14	8	18	6	5
11	6	6	5	10	9	12	10	7	5	7
12	5	6	5	13	14	11	7	8	7	6

Table 2. the energy consumption of candidate enterprise in the production

lot	Task 1			Task 2			Task 3		Task 4	
	E_{11}	E_{12}	E_{13}	E_{21}	E_{22}	E_{23}	E_{31}	E_{32}	E_{41}	E_{42}
1	7.1	8.3	3.2	12.0	13.5	17.5	24.5	17.7	3.8	4.5
2	8.2	10.2	9.5	14.0	18.0	12.5	20.5	24.2	4.6	5.7
3	8.4	7.9	6.5	15.5	17.0	16.5	22.6	23.2	6.0	5.6
4	10.1	8.2	8.9	17.0	13.0	14.5	19.5	18.9	5.8	4.3
5	7.8	10.5	9.1	16.5	18.0	15.5	24.5	23.7	3.9	5.0
6	6.3	6.9	5.8	17.5	14.5	15.5	20.8	22.4	4.9	4.1
7	9.9	8.7	8.4	15.0	17.0	18.0	19.6	17.9	3.5	4.5
8	10.5	7.2	8.6	16.5	16.0	17.0	22.2	24.1	5.6	5.2
9	8.5	8.7	7.9	18.0	14.5	12.0	23.4	24.2	4.8	5.1
10	7.8	8.0	8.5	16.0	17.5	18.0	18.7	18.5	5.5	4.5
11	8.6	10.4	7.9	14.5	13.0	15.0	24.0	19.9	4.4	5.8
12	8.6	10.8	8.3	16.0	17.5	12.5	20.6	22.5	5.2	4.0

Table 3. The candidate enterprise's energy consumption in transport and schedule

candidate enterprise	energy consumption in transport			Transport time		
	$E_{i+1,1}$	$E_{i+1,2}$	$E_{i+1,3}$	$E_{i+1,1}$	$E_{i+1,2}$	$E_{i+1,3}$
E_{11}	1.3	1.0	0.6	2.5	2.0	1.5
E_{12}	0.6	0.9	1.2	1.5	2.5	3.0
E_{13}	1.4	1.1	0.9	3.0	2.5	2.5
E_{21}	3.2	2.1		3.0	2.5	
E_{22}	3.0	3.5		2.5	1.5	
E_{23}	2.5	4.0		2.0	2.5	
E_{31}	1.2	1.0		1.5	1.0	
E_{32}	2.2	2.4		2.5	2.0	

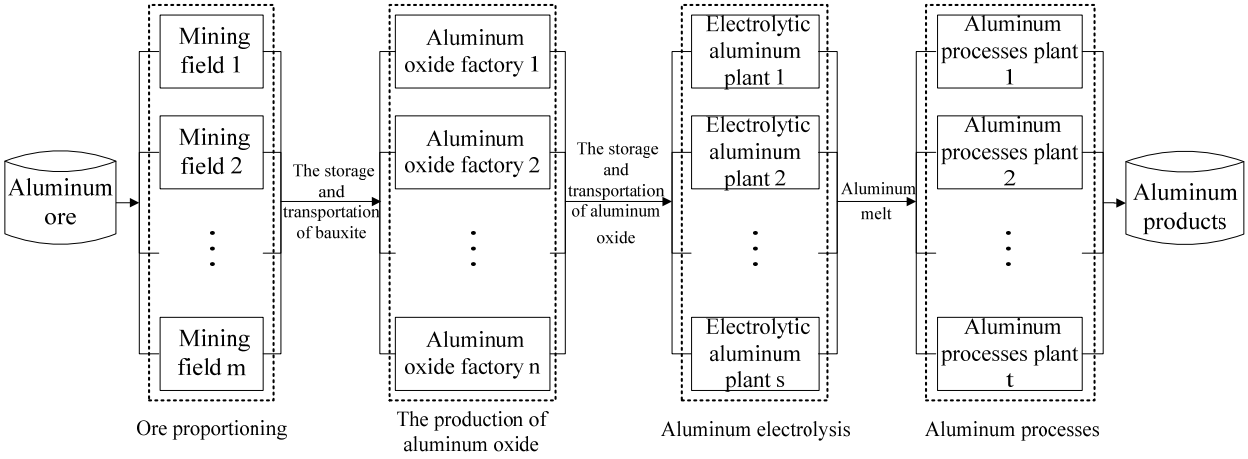

Figure 1. The production process flow chart of Aluminum industrial system

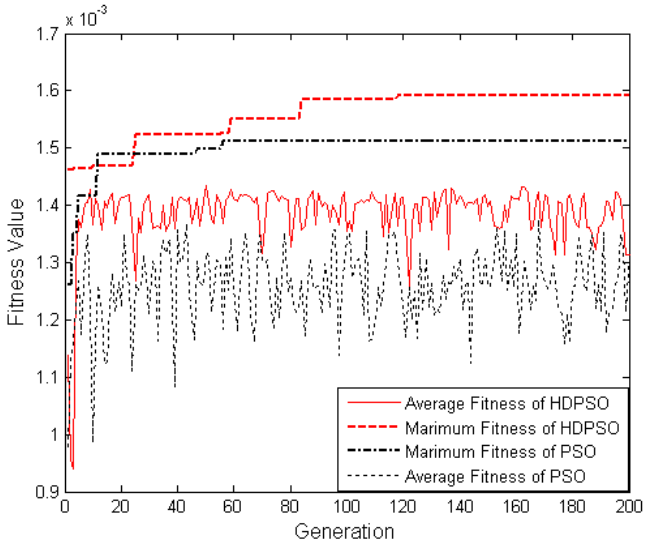

Figure 2. Particle's fitness maximum and average convergence curve

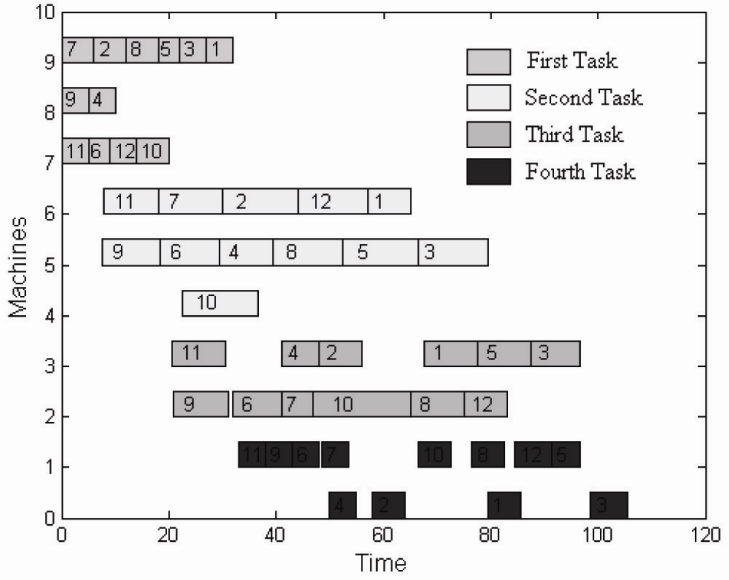

Figure 3. The Gantt chart of scheduling solutions through HDPSO approach

Design a PID Controller of BLDC Motor by Using Hybrid Genetic-Immune

Mohammed Obaid Ali, S. P. Koh & K. H. Chong

Department of Electronics and Communication Eng., University Tenaga Nasional

Selangor 43009, Malaysia

Asmaa Salih Hamoodi

College of Computers Science & Mathematics, University of Tikrit, Iraq

Abstract

In this paper hybridization between two optimization methods that are Genetic Algorithm (GA) and Artificial Immune System (AIS) is presented for determining the optimal proportional-integral derivative (PID) controller parameters, for speed control of a linear brushless DC motor. The brushless DC motor is modeled in Simulink and the Hybrid GA-AIS algorithm is implemented in MATLAB. The capability of overcoming the shortcomings of individual algorithms without losing their advantages makes the hybrid techniques superior to the stand-alone ones based on the dominant purpose of hybridization. The Hybrid GA-AIS method has superior features, stable convergence characteristic and good computational efficiency. The results that get it from hybridization are improved compares with that results can get from GA and AIS alone. The hybrid GA-AIS consists of two processes, the first one is a genetic algorithm (GA) is typically initialized population randomly. Hybridization is faster and more accurate compare with GA AIS alone.

Keywords: Hybrid, Genetic Algorithm (GA), Artificial Immune System (AIS), Optimization mathematical test functions, Brushless DC Motor

1. Introduction

Optimization is a computational science that studies techniques for finding the 'best' solutions. It has been widely employed in a large variety of fields, including transportation, manufacturing, physics, and medicine(Herskovits. J, Mappa. P, Goulart. E and Mota Soares. CM. 2005). The process of optimization lies at the root of engineering, since the classical function of the engineer is to design new, better, more efficient and less expensive systems as well as to devise plans and procedures for the improved operation of existing systems(Araujo.A.L, MotaSoares CM, Herskovits. J. and Pedersen. P. 2002).

The power of optimization methods to determine the best case without actually testing all possible cases comes through the use of a modest level of mathematics and at the cost of performing iterative numerical calculations using clearly defined logical procedures or algorithms implemented on computing machines (Dennis. J.E and Schnabel. R. 1983). The development of optimization methodology will therefore require some facility with basic vector–matrix manipulations, a bit of linear algebra and calculus, and some elements of real analysis (Auatt. S.S, Borges. L.A and Herskovits. J. 1996).

To apply the mathematical results and numerical techniques of optimization theory to concrete engineering problems, it is necessary to clearly delineate the boundaries of the engineering system to be optimized (Laporte, E. and LE Tallec .P. 2002), to define the quantitative criterion on the basis of which candidates will be ranked to determine the best, to select the system variables that will be used to characterize or identify candidates, and to define a model that will express the manner in which the variables are related (Dubeux V.J.C. 2005).

2. Artificial Immune System

The computational problems become more complex, people are seeking a new technique to these problems, turning often to nature for inspiration. Now there is a great deal of attention paid to the vertebrae immune system as a potential source of inspiration, where it is thought that different insights and alternative solutions can be gleaned, over and above other biologically inspired methods., computer scientists, and engineers developed solutions to such problems as distributed control and computer security. With the development of solutions to a wide variety of problems ranging from optimization, fault tolerance, data mining, bioinformatics, and robotic systems, The field of Artificial Immune Systems (AIS) is becoming more popular because of highly distributed, highly adaptive, self-organizing in nature, maintains a memory of past encounters and has the ability to continually learn about new encounters and AIS-based works spanning from theoretical modeling and simulation to wide variety of applications over the past few years, There was an increase of ever interest in the field of artificial immune systems (AIS) and applications among the many new works in this field of research (J. Timmis, T. Knight, L.N. de Castro and E. Hart. 2004)(Guan-Chun Luh a, Chung-HueiChueh. 2008)(Leandro. N. de Castro, Jon Timmis. Helder Knidel.Fernando Von Zuben. 2009).

The artificial immune system (AIS) implements a learning technique inspired by the human immune system which is a remarkable natural defense mechanism that learns about foreign substances, (Yang Liu, Bo Xue Tan, Xue Zhang. 2007). The AIS aim at using idea derived from immunology for the development of systems capable of perform different tasks in different areas of research (Leandro Nunes de Castro, Fernando J. Von Zuben. 2000).

Our immune system has as its main task the detection of the infectious foreign elements (called pathogens) that attack us, and defend us from them . Examples of such pathogens are bacteria and viruses. Any molecule that can be recognized by our immune system is called antigen. Such antigens provoke a specific response from our immune system. Lymphocytes are a special type of cells that play a major role in our immune system. Two types of lymphocytes exist: B cells (or B lymphocytes) and T cells (or T lymphocytes). Upon detection of an antigen, the B cells that best recognize (i.e., match) the antigen are cloned.

Some of these clones will be differentiated into plasma cells, which are the most active antibodies secretors, while others will act as memory cells. These cloned cells are subject to a high somatic mutation rate (normally called hypermutation) in order to increase their affinity level (i.e., their matching to the antigens). These mutations experienced by the clones are proportional to their affinity to the antigen. The highest affinity cloned cells experiment the lowest mutation rates, whereas the lowest affinity cloned cells have high mutation rates, Figure.1, show the Mechanism of Immune System. Due to the random nature of this mutation process, some clones could be dangerous to the body and are, therefore, eliminated by the immune system itself.

Plasma cells are capable of secreting only one type of antibody, which is relatively specific for the antigen. Antibodies play a key role in the immune response, since they are capable of adhering to the antigens, in order to neutralize and eliminate them. These cloning and hypermutation processes are collectively known as the clonal selection principle. It is worth noting, however, that the immune response is certainly more complex than the above explanation, in which we only focused on the B cells, in order to keep our discussion very short. Once the antigens have been eliminated by the antibodies, the immune system must return to its normal conditions, eliminating the in-excess cells.(Leandro Nunes de Castro, Fernando J. Von Zuben. 2000)

However, some cells remain in our blood stream acting as memory cells, so that our immune system can ‘remember’ the antigens that have previously attacked it. When the immune system is exposed again to the same type of antigen (or a similar one), these memory cells are activated, presenting a faster (and perhaps improved) response, which is called secondary response. Based on the previous (oversimplified) explanation of the way in which our immune system works, we can say that, from a computer science perspective, the immune system can be seen as a parallel and distributed adaptive system. Clearly, the immune system is able to learn; it has memory, and is able of tasks such as associative retrieval of information.

These features make immune systems very robust, fault tolerant, dynamic and adaptive. All of these properties make it very attractive to be emulated in a computer. Artificial Immune Systems (AIS) are composed of the following basic elements:

A representation for the components of the system (e.g., binary strings, vectors of real numbers, etc.).

A set of mechanisms to evaluate the interaction of individuals with their environment and with each other. Such an environment is normally simulated through an affinity function, which is based on the objective function(s) in the case of optimization problems.

Procedures of adaptation, that indicates the way in which the behavior of the system changes over time. These procedures of adaptation consist of, for example, mutation operators.

AIS are population-based meta-heuristics, and have been widely used for a wide variety of optimization and classification tasks.

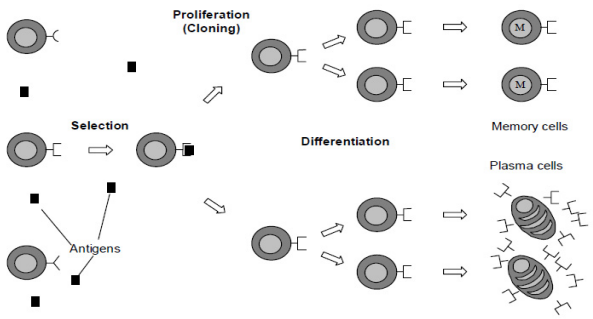

Figure 1. The Mechanism of Immune System(Leandro Nunes de Castro, Fernando J. Von Zuben. 2000)

3. Genetic Algorithm

A GA is an intelligent optimization technique that relies on the parallelism found in nature; in particular its searching procedures are based on the mechanics of natural selection and genetics. GAs was first conceived in the early 1970s by Holland. GAs is used regularly to solve difficult search, optimization, and machine-learning problems that have previously resisted automated solutions (Ian Griffin. 2003). They can be used to solve difficult problems quickly and reliably. These algorithms are easy to interface with existing simulations and models, and they are easy to hybridize. GAs includes three major operators: selection, crossover, and mutation, in addition to four control parameters: population size, selection pressure, crossover and mutation rate. Population-based optimization methods are addressed also. This paper is concerned primarily with the selection and mutation operators(Ian Griffin. 2003). There are three main stages of a genetic algorithm; these are known as *reproduction, crossover* and *mutation*. This will be explained in details in the following section.

A. Reproduction

During the reproduction phase the fitness value of each chromosome is assessed. This value is used in the selection process to provide bias towards fitter individuals. Just like in natural evolution, a fit chromosome has a higher probability of being selected for reproduction. An example of a common selection technique is the Roulette Wheel Selection method as shown in Figure 2.

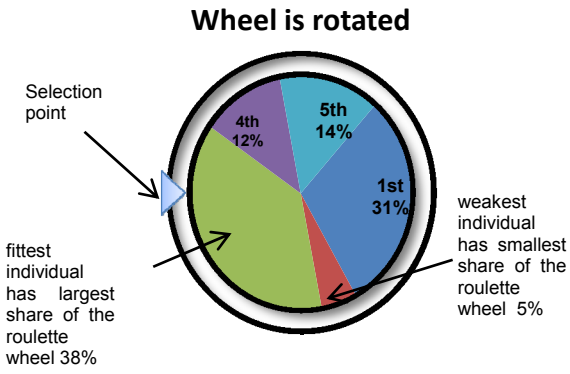

Figure 2. depiction of roulette wheel selection

Each individual in the population is allocated a section of a roulette wheel. The size of the section is proportional to the fitness of the individual. A pointer is spun and the individual to whom it points is selected. This continues until the selection criterion has been met. The probability of an individual being selected is thus related to its fitness, ensuring that fitter individuals are more likely to leave offspring. Multiple copies of the same string may be selected for reproduction and the fitter strings should begin to dominate. There are a number of other selection methods available and it is up to the user to select the appropriate one for each process. All selection methods are based on the same principal that is giving fitter chromosomes a larger probability of selection (Ian Griffin. 2003). Four common methods for selection are:

1) Roulette Wheel selection

2) Stochastic Universal sampling

3) Normalized geometric selection

4) Tournament selection

B. Crossover

One of the three basic operators in any genetic algorithm (GA) is crossover. Two chromosomes which are the parents that combined through crossover which is a genetic operator through mating to produce a new chromosome or offspring. The main point behind crossover is that it takes the best characteristics from each of the parents to form a new chromosome that may be better than both of the parents. According to a user-definable crossover probability, crossover occurs during evolution.

To produce better chromosomes, the crossover operations exchange certain parts of the two selected strings in an attempt to acquire the good parts of old chromosomes. Various crossover techniques exist for organisms which use different data structures to store themselves. Figure 3 show the kinds of crossover:

- Single-point crossover

- Two-point crossover

- Uniform crossover

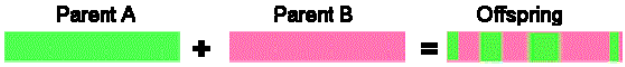

Figure 3. Illustration of crossover operation

C. Mutation

Using *selection* and *crossover* on their own will generate a large amount of different strings. However there are two main problems with this:

1) Depending on the initial population chosen, there may not be enough diversity in the initial strings to ensure the Genetic Algorithm searches the entire problem space.

2) The Genetic Algorithm may converge on sub-optimum strings due to a bad choice of initial population.

These problems may be overcome by the introduction of a mutation operator into the GA. Mutation is the occasional random alteration of a value of a string position. It is considered a background operator in the GA. The probability of mutation is normally low because a high mutation rate would destroy fit strings and degenerate the GA into a random search. Mutation probability values of around 0.1% or 0.01% are common, these values represent the probability that a certain string will be selected for mutation i.e. for a probability of 0.1%; one string in one thousand will be selected for mutation. Once a string is selected for mutation, a randomly chosen element of the string is changed or mutated. For example, if the GA chooses bit position 4 for mutation in the binary string 1011101, the resulting string is 1011001 as the fourth bit in the string is flipped as shown in Figure.4 (SAIFUDIN BIN MOHAMED IBRAHIM. 2005).

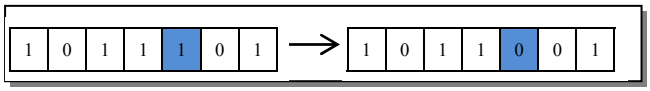

Figure 4. Illustration of mutation operation

4. Hybrid GA-AIS Mechanism

Optimization is the task of getting the best solution among the feasible solutions. There are many methods available to obtain an optimized solution.

The proposed algorithm contains two major processes which are the GA and AIS.

GA starts with procedure below:

1) Generate initial population of individuals randomly
2) Calculate the fitness values of the individuals in the current population.
3) Select individuals for reproduction.
4) Apply crossover and mutation operator.
5) Compute the fitness value of the individuals
6) Select the best individuals to create the new population.

Steps 3 to 6 are repeated until a pre-defined stopping criterion is attained

The second process (AIS) usually initializes with random population, the new technique that used here says that AIS uses the best population of GA as input to AIS procedures. Figure 5, shows the hybrid of GA-AIS.

AIS process start with procedures below:

1) Generate initial population of Ab from the last population of GA
2) Compute the fitness of each Ab.
3) Select *n* antibodies with best affinity.

4) Generate clones of selected set
5) Mutate clonal set affinity maturation
6) Calculate affinity clonal set
7) Select candidate(s) memory cells
8) Replace lowest *d* affinity antibodies.
9) Steps 3 to 6 are repeated until a pre-defined stopping condition is reached.

5. Test Function

Many novel algorithms are introduced to solve the optimization problem accordingly the researchers looking for various benchmark functions with various properties in order to make comparison and evaluate different algorithms. Many of these popular benchmark functions have some properties that have been exploited by some algorithms to achieve excellent results. this paper used eight test function that have various Rastrigin's function, Rosenbrock's valley function, Griewank's function, Ackley's function, Rotated hyper-ellipsoid function, Moved axis parallel hyper-ellipsoid function, Goldstein-Price's function, Sum of different power properties to compare between AIS, GA, and Hybrid AIS-GA. Below eight test functions (Fevrier Valdez,Patricia Melin. 2008):

1) Rastrigin's function Test

The Rastrigin function is a non-convex function used as a performance test problem for optimization algorithms. It is a typical example of non-linear multimodal function. Function definition:

$$f(x) = 10.n + \sum_{i=1}^{n} (x_i^2 - 10.\cos(2.\pi.x_i)) \qquad (1)$$

.Xi ϵ [-5.12, 5.12] It has a global minimum at X=0 where f(x)=0.

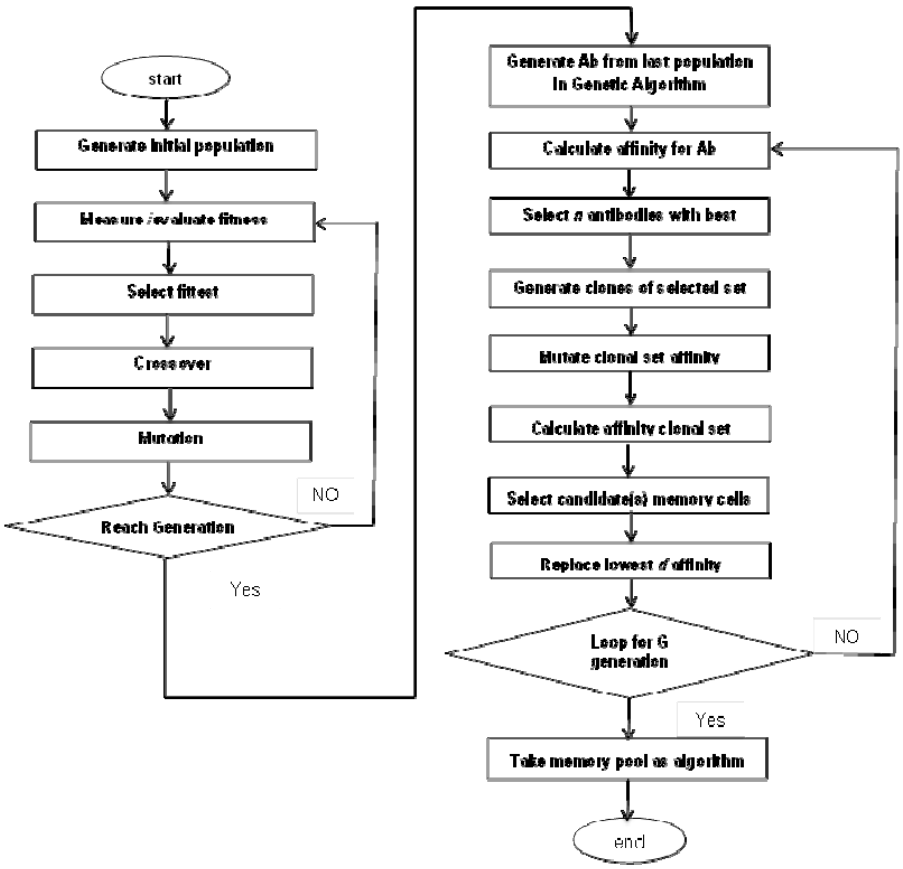

Figure 5. Whole flowchart shows the Hybrid GA-AIS

2) Rosenbrock's valley function (De Jong's function 2)

In mathematical optimization, the Rosenbrock function is a non-convex function used as a performance test problem for optimization algorithms introduced by Rosenbrock (1960)

Function definition:

$$f(x,y) = (1-x)^2 + 100(y-x^2)^2 \quad (2)$$

3) Griewank's Function

The mathematical formula that defines Griewank's function is:

$$f(x) = \frac{1}{4000}\sum_{i=1}^{n} X^2 - \prod_{i=1}^{n} \cos\left(\frac{X_i}{\sqrt{i}}\right) + 1 \quad (3)$$

4) Ackley's Function

Ackley's function, generalized to n dimensions by Bäck, is function definition:

$$f(x) = 20 + e - 20e^{-0.2\sqrt{\sum_{i=1}^{n} x_i^2}} - e^{\frac{1}{n}\sum_{i=1}^{n}\cos(2\pi x_i)} \quad (4)$$

5) Rotated hyper-ellipsoid function

An extension of the axis parallel hyper-ellipsoid is Schwefel's function1.2. It is continues, convex and unimodal.

Function definition:

$$f(x) = \sum_{i=1}^{n}\sum_{j=1}^{i} x_j^2 \quad (5)$$

6) Moved axis parallel hyper-ellipsoid function

This function is derived from the axis parallel hyper-ellipsoid.

Function definition:

$$f(x) = \sum_{j}^{n} 5i.x_j^2 \quad (6)$$

7) Goldstein-Price's function

The Goldstein-Price function [GP71] is a global optimization test function.

Function definition:

$$f(x1,x2) = (1+(x_1+x_2+1)^2 . (19-14x_1^2-14x_2+6x_1x_2+3x_2^2)) . (30+(2x_1-3x_2)^2.(18-32x_2+12x_1^2+48x_2-36x_1x_2+27x_2^2)) \quad (8)$$

8) Sum of different power function 9

The sum of different powers is a commonly used unimodal test function.

Function definition:

$$f(x) = \sum_{i=1}^{n} |x_i|^{(i+1)} \quad (9)$$

6. Simulation Results and Discussions

To testify the efficiency and effectiveness of Hybrid GA-AIS algorithm, several tests of the hybridization algorithm were made in the Matlab programming language. All the implementations were developed using a computer with processor Intel(R) Core (TH)2 Duo CPU T8100 that works to a frequency of clock of 2.10 GHZ, 4 GB of RAM Memory and Windows 7 operating system.

Experimental Results of the Artificial Immune System (AIS), Genetic Algorithm (GA) and Hybrid GA-AIS algorithm optimization methods. The results obtained after applying methods to the mathematical functions are shown on the table 1. Figure6 shows results of Rastrigin's Function.

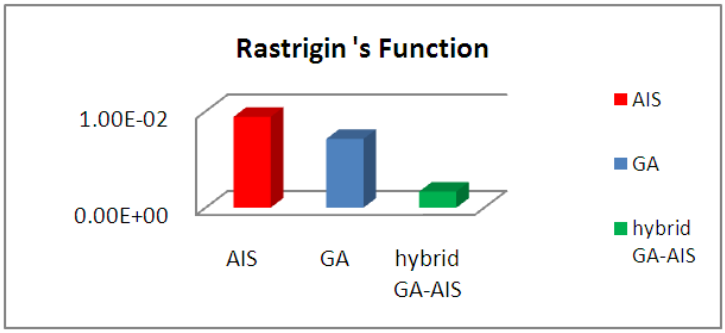

Figure 6. Chart shows Hybrid methods compared with AIS and GA for Rastrigin's function

Result obtained after applying the AIS, GA and Hybrid GA-AIS to the other functions in table 1 shows the AIS, GA, and Hybrid GA-AIS results.

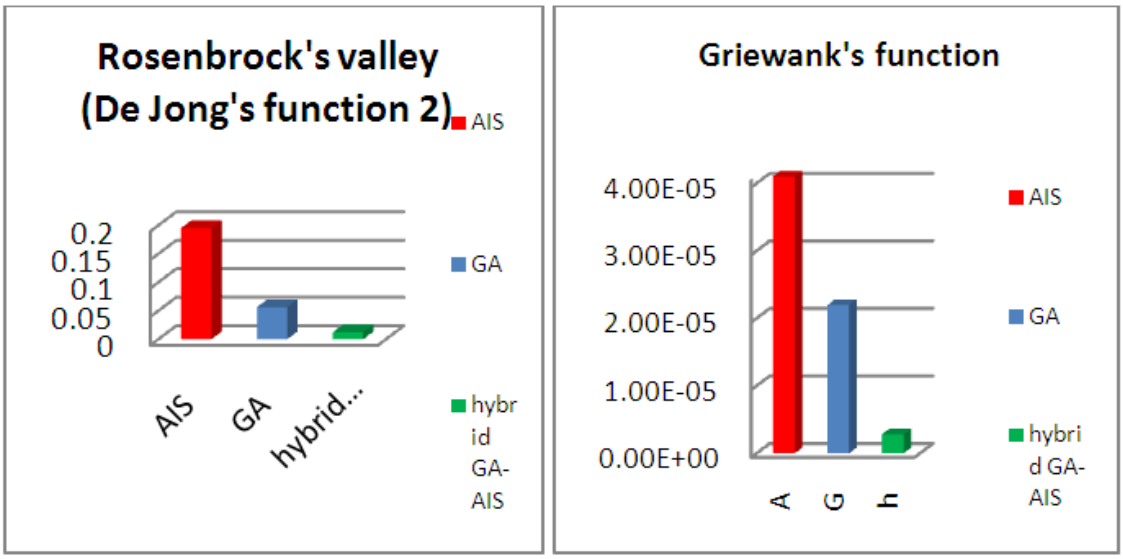

a b

Figure 7. Charts show Hybrid methods compared with AIS and GA of the
a) Rosenbrock's valley's function. b) Griewank's function.

Table 1. Show the values of AIS, GA and Hybrid for eight test functions

functions	no of G	Average of 20 times of trials final value of the objective function		
		AIS	GA	hybrid GA-AIS
Rastrigin 's Function	100	9.42E-03	7.14e-03	1.68E-03
Rosenbrock's valley	100	0.1952	0.05634	1.24E-02
Griewank's function	100	1.44E-03	2.20E-05	2.81e-06
Ackley's function	100	0.357205	1.39E-02	1.10e-03
Rotated hyper function	100	2.54E-03	3.53E-05	3.91e-06
Moved axis function	100	1.54E-01	2.94E-04	1.70e-05
Goldstein-Price's function	100	21.4622	7.624955	3.1179
Sum of different power	100	2.272E-03	7.37E-05	2.621e-06

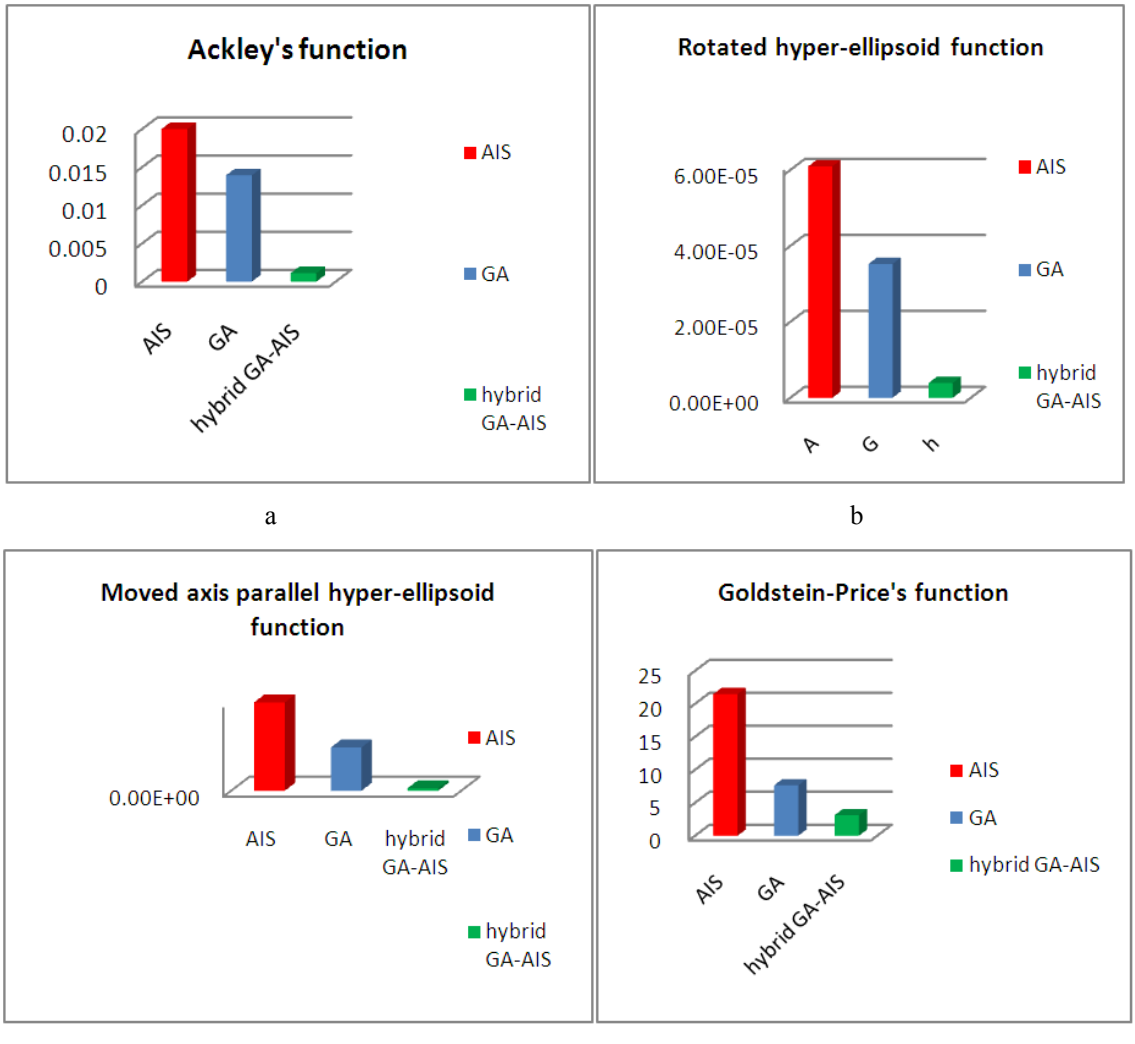

Figure 8. Charts Show Hybrid methods compared with AIS and GA for a) Ackley's function. b) Rotated hyper-ellipsoid function. c) Moved axis parallel hyper-ellipsoid function. d) Goldstein-Price's function.

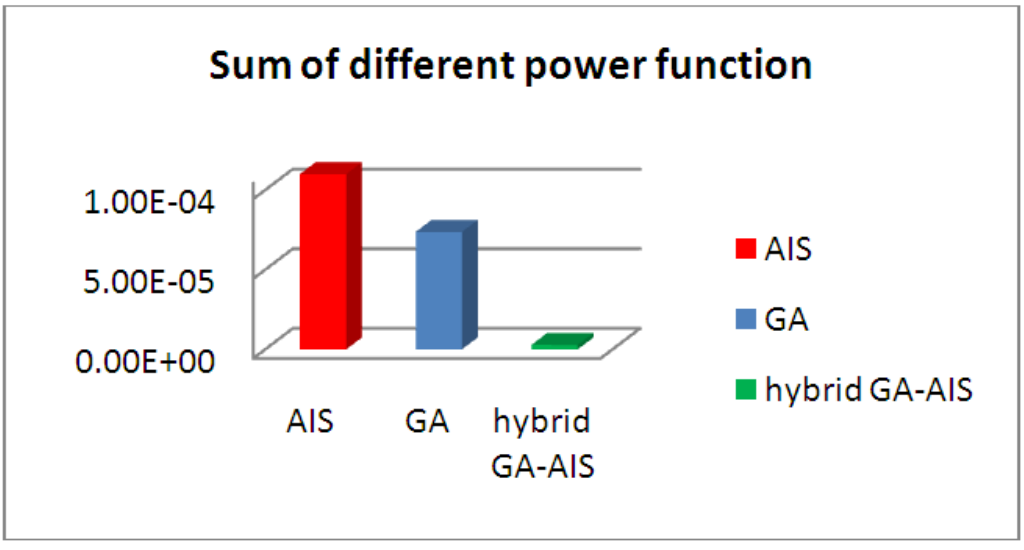

Figure 9. Chart shows Hybrid methods compared with AIS and GA Sum of different power function

ISSN 1913-1844 E-ISSN 1913-1852

7. Design a Pid Contrller of A Linear BLDC Motor

There are mainly two types of dc motors used in industry.

The first one is the conventional dc motor where the flux is produced by the current through the field coil of the stationary pole structure. The second type is the brushless dc motor (BLDC motor) where the permanent magnet provides the necessary air gap flux instead of the wire-wound field poles. Brushless DC motors are reliable, easy control, and inexpensive. Due to their favorable electrical and mechanical properties, high starting torque and high efficiency, the BLDCM are widely used in most servo applications such as actuation, robotics, machine tools, and so on. The design of the BLDCM servo system usually requires time consuming trial and error process, and fail to optimize the performance. In practice, the design of the BLDCM drive involves a complex process such as model, devise of control scheme, simulation and parameters tuning. The dynamic characteristics of BLDC motors are similar to permanent magnet DC motors. The characteristic equations of BLDC motors can be represented as (Fevrier Valdez,Patricia Melin. 2008):

$$V_{app}(t) = L\frac{di(t)}{dt} + R.i(t) + V_{emf}(t) \quad (10)$$

$$V_{emf} = K_{b.}W(t) \quad (11)$$

$$T(t) = K_{t.}i(t) \quad (12)$$

$$T(t) = J\ \frac{dw(t)}{dt}\ + D.w(t) \quad (13)$$

where v_{app} (t) is the applied voltage, ω (t) is the motor speed, L is the inductance of the stator, i(t) is the current of the circuit, R is the resistance of the stator, v_{emf} (t) is the back electromotive force, T is the torque of motor, D is the viscous coefficient, J is the moment of inertia, Kt is the motor torque constant, and Kb is the back electromotive force constant. Figure4.1 shows the block diagram of the BLDC motor. From the characteristic equations of the BLDC motor, the transfer function of speed model is obtained.

$$\frac{w(s)}{V_{app}(s)} = \frac{K_t}{LJS^2 + (LD + RJ)S + K_tK_b} \quad (14)$$

7. 1 PID Controller

Despite rapid evolution in control hardware, the proportional–integral–derivative (PID) controller remains the workhorse in process industries. The P action (mode) adjusts controller output according to the size of the error. The I action (mode) can eliminate the steady state offset and the future trend is anticipated via the D action (mode). These useful functions are sufficient for a large number of process applications and the transparency of the features leads to wide acceptance by the users

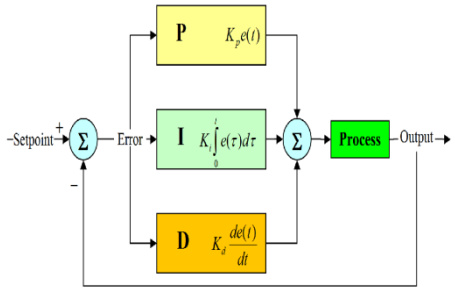

Figure 10. PID controller

In PID controller design methods, the most common performance criteria are IAE, ISE, MSE and ITAE performance criterion formulas are as follows:

$$IAE = \int_0^t |r(t) - y(t)|dt = \int_0^t |e(t)|dt \quad (15)$$

$$ISE = \int_0^t (e(t))^2 dt \quad (16)$$

$$MSE = \frac{1}{t}\int_0^t \big(e(t)\big)^2 dt \quad (17)$$

$$ITAE = \int_0^t t|e(t)|dt \quad (18)$$

8. Simulation Results and Analysis

A. Optimal Hybrid (GA-AIS)-PID Response

To control the speed of the BLDC motor at 1000 rmp, according to the trials, the following GA and AIS parameters are used to verify the performance of the Hybrid (GA-AIS)-PID controller parameters:

- Population size: 20;
- Total Iteration : 100;
- GA iteration : 50;
- AIS iteration : 50;
- Crossover rate : 0.8;
- Mutation : 0.2;

Figure 20 Step response of BLDC motor in GA based PID speed control

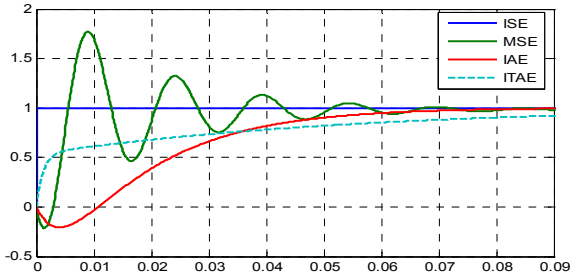

Figure 11. Step response for BLDC motor with PID controller optimized by GA method

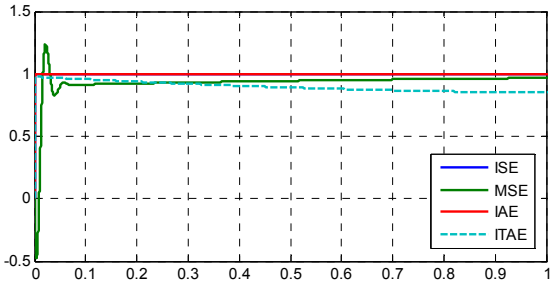

Figure 12. Step response for BLDC motor with PID controller optimized by AIS method

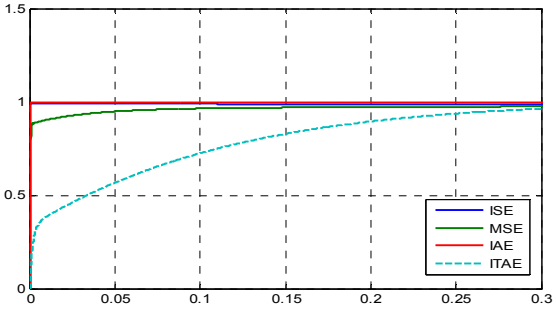

Figure 13. Step response for BLDC motor with PID controller optimized by Hybrid GA-AIS method

9. Conclusion

The analysis of the simulation results showed that the Hybrid GA-AIS optimization is better in terms evaluating the minimum value for eight mathematical test functions.

The obtained results for the hybrid AG-AIS are very good results compare to AIS and GA results (see TABLE.2). For the engineering problem its clear the improvement in the step response of the Hybrid GA-AIS optimization

method compare with GA step response and AIS step response in terms of Overshoot, Rising time and Setting time.

Acknowledgement

This paper was supported in part by grant from the Ministry of Higher education Malaysia.

References

Araujo.A.L, MotaSoares CM, Herskovits. J. and Pedersen. P. (2002). Development of a Finite Element Model for the Identification of Material and Piezoelectric Properties through Gradient Optimization and Experimental Vibration Data. *Composite Structures,* 58: 307 - 318. 2002.

Auatt. S.S, Borges. L.A and Herskovits. J. (1996). An Interior Point Optimization Algorithm for Contact Problems in Linear Elasticity. *Numerical Methods in Engineering, 855-861.* 1996.

Dennis. J.E and Schnabel. R. (1983). *Numerical Methods for Constrained Optimization and Nonlinear Equations.* Prentice Hall, New Jersey. (1983).

Dipankar Dasgupta. "Artificial Immune Systems" *A Bibliography COMPUTER SCIENCE DEPARTMENT THE UNIVERSITY OF MEMPHIS, USA*.2007

Dubeux V.J.C. (2005). Nonlinear Programming Techniques for Large Size Optimization, *D.Sc. Thesis, COPPE/Federal University of Rio de Janeiro, Mechanical Engineering Program, Rio de Janeiro, Brazil*. 2005.

Fevrier Valdez,Patricia Melin. (2008). COMPARATIVE STUDY OF PARTICLE SWARM OPTIMIZATION AND GENETIC ALGORITHMS FOR COMPLEX MATHEMATICAL FUNCTIONS. *Journal of Automation, Mobile Robotics & Intelligent System*.2008.

Guan-Chun Luh a, Chung-HueiChueh. (2008). A multi-modal immune algorithm for the job-shop scheduling problem. *Information Sciences journal homepage: www.elsevier.com/locate/ins.* (2008).

Herskovits. J, Mappa. P, Goulart. E and Mota Soares. CM. (2005). Mathematical programming models and algorithms for engineering design optimization. *Computer Methods in Applied Mechanics and Engineering, 194 (30): 3244-3268. 2005.*

Hongwei Mo. (2009). Harbin. Handbook of Research on Artificial Immune Systems and Natural Computing Applying Complex Adaptive Technologies. *Engineering University, China* 2009.

Ian Griffin. (2003). On-line PID Controller Tuning using Genetic Algorithms. *M.Eng. in Electronic Systems*. 2003.

J. Timmis, T. Knight, L.N. de Castro and E. Hart. (2004). An Overview of Artificial Immune Systems, *University of Kent.Canterbury.UK.* 2004.

Laporte, E. and LE Tallec .P. (2002). Numerical Methods in Sensitivity and Shape Optimization. *Birkhauser.* 2002.

Leandro Nunes de Castro, Fernando J. Von Zuben. (2000). The C lonal Selection Algorithm with Engineering Applications. *Workshop on Artificial Immune Systems and Their Applications, Las Vegas, USA, July* 2000.

Leandro Nunes de Castro, Fernando J. Von Zuben. (2000). The Clonal Selection Algorithm with Engineering Applications. *Workshop on Artificial Immune Systems and Their Applications, Las Vegas, USA.* 2000.

Leandro. N. de Castro, Jon Timmis. Helder Knidel.Fernando Von Zuben. (2009). Artificial Immune Systems. *structure, function, diversity and an application to biclustering. Springer Science Business Media B.V.* 2009.

Leontiev. A, Huacasi .W and Herskovits.J.(2002). An Optimization Technique for the Solution of Signorini Problem Using the Boundary Element Method. *Structural and Multidisciplinar Optimization, 24 (1): 72 - 77.* 2002

SAIFUDIN BIN MOHAMED IBRAHIM. (2005). THE PID CONTROLLER DESIGN USING GENETIC ALGORITHM. *Bachelor of Engineering (Electrical and Electronics) 27th October*, 2005.

Yang Liu, Bo Xue Tan, Xue Zhang. (2007). Position Accuracy Improvement of PMLSM System Based on Artificial Immune Algorithm. *IEEE International Conference on Mechatronics and Automation, Harbin, China.* 2007.

Screening of Myxobacteria Strains Producing Bioactive Substances against Breast Cancer

Hongpeng Wang

College of Life Science, Hebei University

Key Lab of Microbial Diversity Research and Application of Hebei Prov., Baoding 071002, China

Liping Zhang (Corresponding author)

College of Life Science, Hebei University

Key Lab of Microbial Diversity Research and Application of Hebei Prov., Baoding 071002, China

Tel: 86-312-507-9696 E-mail: zhlping@hbu.edu.cn

Nan Shi

College of Life Science, Hebei University

Key Lab of Microbial Diversity Research and Application of Hebei Prov., Baoding 071002, China

This research was financially supported by Hebei Province Basic Research Project titled "Extraction, purification and structure analysis of antitumor bioactive substances from myxobacteria" (Grant No. 09966430D).

Abstract

[Objective] To screen myxobacteria strains producing secondary metabolites with anti-cancer activity. [Method] Fermentation culture the stains of myxobacteria, extract secondary metabolites with methanol, and detect the antitumor activity of secondary metabolites from myxobacteria and its toxicity to normal cells with the modified MTT (3-[4,5-dimethythiazol-2-yl] -2,5-diphenyltetrazolium bromide) method. [Results] Inhibition rate of myxobacteria strain 93431 fermentation original solutions, 2 fold dilution and 10 fold dilution on MCF-7 cells was 53.32%, 49.35%, and 46.50%, respectively, and their inhibition rate on MRC cells was 2.95%, 5.90%, and 1.97%, respectively. [Conclusion] Secondary metabolites produced from strains 93431 could inhibit MCF-7 cells specifically while had little effects on MRC cells and the bioactive substances from its secondary metabolites could be natural target anti-cancer agents.

Keywords: Myxobacteria, Breast cancer, MTT method, Secondary metabolites

Myxobacteria were a kind of complicated gram-negative bacterium and could perform cooperative feeding, movement and development into fruit bodies. It has been more than 200 years of investigation ever since myxobacteria were discovered. It could result in rich secondary metabolites, and was one of the important sources to develop antimicrobial agents (Reichenbach, 2001, PP. 149-156). In the secondary metabolites of myxobacteria, most of them were compounds with novel structure, and possessed high pharmacological and biological activity (Gurmeet, 2006, PP. 235-242).

Cancer is one of the major diseases that seriously damaged to human health, and the approach to heal cancer has been the research attention all over the world. Currently, clinical chemotherapeutic drugs have huge toxicity, and could bring poor life quality to patients, such as nausea, vomiting; myelosuppression, serious impairment of cardinal physiological organs, such as heart, liver, kidney, nervous system and so on. Breast cancer is one of common malignant tumors in women. According to statistics, the global number of new diagnosis of breast cancer was more than 12 million cases with 5 million cases of mortality (Curtis, 1999, PP. 138-144). In recent years, incidence of breast cancer showed an increasing trend in China, and the age of onset tended to be younger and younger.

Due to the implementation of surgery, chemotherapy, radiotherapy and other treatments, the mortality of breast cancer began to decrease. However, a considerable proportion of patients would recur and transfer finally, and the patients had to need a permanent medication. Consequently, drugs against breast cancer with high efficacy

and low toxicity tended to be particularly critical. Myxobacteria were rich in metabolic pathways, could generate a large number of metabolites with novel structure and unique function, and thus could be the important source of anticancer bioactive substances (Gerth, 2003, PP. 233-253).

1. Materials and methods

1.1 Materials

1.1.1 Strains

20 strains used in the present study were isolated and preserved in our laboratory.

1.1.2 Cell lines

MCF-7 (human breast cancer) cell lines and MRC (human embryonic lung fibroblast) cell lines were offered as a gift from Collection Center of China Type Culture, Wuhan University.

1.1.3 Reagents and apparatus

CAS medium: 1% enzymatic casein, 0.1% $MgSO_4.7H_2O$, pH 7.2

VY/2 medium: 1% yeast extract, 0.1% $CaCl_2.2H_2O$, 0.5mg/L VB12, pH 7.2

D312 macroporous resin: Shandong Lukang Pharmaceutical Group Co., Ltd.

RPMI-1640 culture medium: Gibco, USA

FBS: Hangzhou Evergreen Biological Engineering Materials Co., Ltd.

CO2 incubator: Thermo HERA cell 150, Germany

ELISA analyzer: BMG FLUOstar OPTIMA, Germany

Automatic Centrifugal Concentrator: miVac QUC-23050-100, UK

Membrane rotary evaporator: Heidolph, LABOROTA 4000, German

Analytical HPLC: Hitachi L-2000, DAD detector, Japan

Column: Thermo ODS-2, 5μm, 250mm×4.6mm

1.2 Methods

1.2.1 Fermentation culture

Strains preserved in glycerol were inoculated into the slope of VY/2, and cultured in biochemical incubator at 28°C till fruit bodies. The resultant fruit bodies were selected to inoculate into sterile CAS medium, and then shaking cultured at 28°C at 200r/min. After seed fluid was completed and microscopic examination, 10% seed fluid was inoculated into VY/2 fermentation medium containing D132 macroporous resin by pipette, and shaking cultured for 7 days at 28°C at 200r/min.

1.2.2 Extraction of fermentation products

After centrifuging fermentation products and discarding fermentation solutions, the strains and resin were collected, added 10 times methanol of their volume and placed in shaking table. After overnight extraction and centrifugation, strains and resin were removed. Methanol extracts of fermentation products were gathered, and concentrated by automatic centrifugal concentrator. Therefore, crude extracts of fermentation products were obtained.

1.2.3 Fermentation activity and toxicity detection

Crude extracts were dissolved by PBS buffer containing containing 5% DMSO and 5% ethanol. After filtrated by 0.22 μm sterile membrane, the resultant solution was diluted into 1/2 and 1/10 of its stock solution by RPMI-1640 medium containing 10% fetal calf serum respectively.

Based on the MTT method established by Mosmann (1983, PP. 55-65), its modification was applied in the present paper. MCF-7 cells were harvested with 0.25% trypsin, and cell viability was measured by 0.4% trypan blue; when their viability were above 90%, they were counted, and diluted into a density of approximately 1×10^4/mL by RPMI-1640 medium containing 10% fetal bovine serum. Cells were seeded into 96-well plates, 180μL each well, and incubated for 24h at 37°C in a 5% CO_2 incubator. Before adding the sample into 96-well plates, RPMI-1640 medium was removed, plates were rinsed by PBS (enough to cover the cell surface) in order to discard suspended cells. Samples were undertaken 3 gradients and 4 replicates, and 20ml prepared samples were added into each well, 20μL 1mg/mL cisplatin as positive control and the same volume of RPMI-1640 medium as blank control, and incubated for another 24h continuously at 37°C in a 5% CO2 incubator. After

completion of the treatment, cells in 96-well plates were centrifuged for 10 min at 1000 r/min in order to discard samples and medium and washed with PBS, and 20μL of 5 mg/mL MTT was added to the cells and incubated for another 4 h at 37°C. After 4 h, 96-well plates were centrifuged at 1000 r/min in order to remove the uninvolved MTT and the precipitated formazan was subsequently dissolved in 200μL dimethyl sulfoxide (DMSO) and gently shaken for 10 min. The absorption was measured at 492nm, with ELISA analyzer (Germany).The inhibiting rate was calculated using the equation below (Wang, 2009, PP. 755-760):

Inhibiting rate = (1 - OD positive control/OD blank control) × 100%

Toxicity determination used MRC cell model, and the medium changed into DMEM containing 10% fetal calf serum. Method was the same with inhibition rate. Inhibition rate of samples on MRC cells were measured and calculated.

1.2.4 Analysis of bioactive substances in fermentation products

Fermentation solutions with higher inhibition rate on MCF and lower on MRC were selected, and analyzed by Thermo ODS-2 analytical HPLC to ascertain components of secondary metabolites in fermentation solutions. A gradient elution was carried out using the following solvent systems: mobile phase: solvent A, 20%-80% methanols; solvent B, water.

2. Results

2.1 Bioactivity and toxicity

OD_{492} values in the table were shown as the means and standard deviations of 4 replicates, and data was analyzed by SPSS 16.0 software. One-way ANOVA was used to test the significance of difference in measured variables between control and treatment in combination with Dunnett method. Results were listed in Table 1 in detail. As well known to us all, antitumor agents with potential development prospects should not only had strong inhibition effects on tumor cells, but also less toxicity to normal cells.

As seen from Table 1, the majority of myxobacteria fermentation metabolites could inhibit the growth of MCF-7 tumor cells in the present study. Among them, 16 strains had significant inhibition effects on MCF-7 tumor cells with positive rate over 80%, and inhibition rate of 9 strains attained more than 50%, accounting for 45% of the tested strains; Inhibition rate of myxobacteria strain 93431 fermentation original solution, 2 fold dilution and 10 fold dilution on MCF-7 cells was 53.32%, 49.35%, and 46.50%, respectively, and their inhibition rate on MRC cells was 2.95%, 5.90%, and 1.97%, respectively. Therefore, fermentation extracts of strain 93431 were selected to undertaken HPLC analysis to ascertain its secondary metabolites components with gradient elution.

2.2 Morphological variation of cells by inverted microscope

Normal MCF-7 cells attached to the wall to proliferate and showed an irregular multilateral angle with a large number of cells; in 96-well plates, after treated by strain 93431 fermentation solutions for 24h, cells in each group all had shrinkage, and separated from the surrounding cells. Nuclear contracted, cells that attached walls decreased, either suspension or shedding.

MRC cells attached to the wall to proliferate and showed a long-spindle with a large number of cells; in 96 well plates, after treated by strain 93431 fermentation solutions for 24h, a large majority of cells in each group showed a normal morphology, spreading and transparent.

2.3 Bioactive components separation by HPLC

Fermentation crude extracts of strain 93431 were undertaken HPLC analysis with gradient elution. Mobile phase and its proportion were listed in Table 2. Results showed that mixed components were easy to separate, and separation effects were listed in Figure 2. As seen from Figure 3, peaks at 38.65 min, 40.70 min, 43.63 min, 45.43 min, 48.06 min, 51.18 min, 64.54 min and 66.81 min represented secondary metabolites of strain 93431 fermentation products. Peaks at 8.75 min, 15.41min, 17.03 min and 23.75 min need further investigation to figure out.

3. Discussions

In the present study, using MCF-7 and MRC cell lines as an experimental model, we investigated the antitumor activity of secondary metabolites from myxobacteria and its toxicity to normal cells. Results indicated that myxobacteria strains 93431 had strong inhibitory effects on MCF-7 cells while had little toxicity to MRC cells. Accordingly, bioactive substances in strains 93431 fermentation products had selective inhibitory effects on tumor cells, and had potential development prospects. After HPLC analysis, results suggested that peaks at peaks at 38.65 min, 40.70 min, 43.63 min, 45.43 min, 48.06 min, 51.18 min, 64.54 min and 66.81 min represented

secondary metabolites of strain 93431 fermentation products, but they still need further separation and purification. In addition, functional targets of inhibiting tumor cell growth and its action mechanism still should need further investigation.

Streptomyces, fungi and bacilcus were recognized as the big three drug sources. Currently, bioactive substances such as heterocyclic, quinine, polyether, macrocyclic, vinyl, peptides and other types, nearly 400 kinds were discovered in myxobacteria. With the increasing discovery of more and more secondary metabolites with pharmacological and biological activity, myxobacteria exceeded bacilcus, and rose to the third place. Myxobacteria tended to be an important microbial resource, and would shed light on the screening and application of antitumor agents. Myxobacteria resources were abundant in China, but hard to isolate, purify and incubate. All those characteristics tended to be critical factors that impeded the research and development of myxobacteria. With the profound investigation of its metabolites, it would be certain to find some novel target antitumor agents with unique functions.

References

Curtis, M. (1999). Global Breast Cancer Mortality Statistics. *CA Cancer J Clin*, 49:138-144.

Gerth, K., Pradella, S., & Perlova, O., et al. (2003). Myxobacteria: proficient producers of novel natural products with various biological activities past and future biotechnological aspects with the focus on the genus Sorangium. *Biochemical Journal*, 106:233-253.

Gurmeet, K., & Melinda, H. (2006). Biological evaluation of tubulysin A: a potential anticancer and antiangiogenic natural product. *Biochemical Journal*, 396:235-242.

Mosmann, T. (1983). Rapid colorimetric assay for cellular growth and survival: Application to proliferation and cytotoxicity assays. *J Immunol Methods*, 55-65.

Reichenbach, H. (2001). Myxobacteria producers of novel bioactive substances. *Journal of Industrial Microbiology & Biotechnology*, 27:149-156.

Wang, D.H., & Tao, W.Y. (2009). Antitumor activity in vitro and volatile components of metabolites from myxobacteria Stigmatella WXNXJ-B. *African Journal of Microbiology Research*, 3(11):755-760.

Table 1. OD492 values and inhibition rate of bioactive substances

Strain	MCF-7 cells OD_{492} Values and inhibition rate (%)			MRC cells OD_{492} Values and inhibition rate (%)		
	Original solution	1/2 Original solution	1/10 Original solution	Original solution	1/2 Original solution	1/10 Original solution
92006	0.684±0.023* 15.10	0.496±0.026** 38.40	0.507±0.031** 37.05	0.249±0.008** 38.81	0.385±0.016 5.47	0.381±0.010* 6.33
92152	0.438±0.010** 45.67	0.689±0.041** 14.48	0.736±0.060 8.68	0.215±0.008** 47.17	0.247±0.009** 39.43	0.376±0.014* 7.60
92153	0.757±0.043 6.01	0.681±0.072** 15.47	0.731±0.056* 9.24	0.219±0.006** 46.22	0.368±0.009* 9.69	0.407±0.017 0.00
92154	0.491±0.011** 39.08	0.728±0.062* 9.65	0.772±0.038 4.16	0.232±0.007** 42.96	0.372±0.014* 8.65	0.407±0.011 0.00
92155	0.805±0.047 0.07	0.616±0.009** 23.59	0.793±0.040 1.53	0.236±0.006** 41.98	0.400±0.021 1.72	0.401±0.027 1.47
92163	0.792±0.009 1.69	0.780±0.007 3.17	0.758±0.009 5.91	0.305±0.010** 25.1	0.283±0.003** 30.37	0.296±0.006** 27.36
92213	0.725±0.041* 9.97	0.585±0.032** 27.40	0.549±0.012** 31.84	0.265±0.017 34.94	0.270±0.013 33.58	0.265±0.013 34.91
93428	0.527±0.025** 34.60	0.517±0.021** 35.84	0.529±0.016** 34.29	0.304±0.010** 25.30	0.324±0.022** 20.35	0.341±0.017** 16.15
93429	0.366±0.011** 54.63	0.355±0.016** 55.91	0.381±0.040** 52.68	0.259±0.013** 36.38	0.284±0.009** 30.25	0.400±0.018 1.79
93430	0.747±0.047 7.22	0.795±0.032** 1.47	0.714±0.020** 11.42	0.372±0.022* 8.70	0.405±0.016 0.02	0.406±0.009 0.25
93431	0.376±0.044** 53.32	0.408±0.014** 49.35	0.431±0.026** 46.50	0.395±0.006 2.95	0.383±0.011 5.90	0.399±0.013 1.97
93434	0.627±0.031** 22.21	0.338±0.034** 58.06	0.462±0.019** 42.67	0.246±0.022** 39.61	0.312±0.015** 23.46	0.378±0.024* 7.22
94236	0.336±0.042** 58.35	0.383±0.024** 52.45	0.395±0.014** 51.00	0.331±0.012** 18.69	0.361±0.031** 11.26	0.375±0.025* 7.85
94237	0.428±0.022** 46.91	0.425±0.021** 47.19	0.286±0.004** 64.55	0.222±0.007** 45.55	0.224±0.007** 44.90	0.326±0.023** 19.97
94238	0.359±0.035** 55.43	0.667±0.149** 17.18	0.507±0.106** 37.01	0.299±0.019** 26.60	0.332±0.026** 18.34	0.368±0.034* 9.48
94229	0.461±0.031** 42.76	0.335±0.023** 58.37	0.543±0.040** 32.55	0.229±0.009** 43.78	0.228±0.011** 43.99	0.314±0.020** 22.87
94231	0.376±0.046** 53.34	0.269±0.020** 66.55	0.350±0.028** 56.53	0.251±0.011** 38.30	0.309±0.023** 24.14	0.336±0.012** 17.52
94232	0.329±0.040** 59.11	0.302±0.024** 62.53	0.245±0.006** 69.57	0.278±0.014** 31.77	0.266±0.015** 34.55	0.315±0.006** 22.71
94241	0.684±0.044** 15.04	0.543±0.022** 32.59	0.806±0.052 0.00	0.239±0.006** 41.35	0.263±0.020** 35.39	0.255±0.009** 37.47
94242	0.521±0.028** 35.34	0.481±0.044** 40.29	0.615±0.017** 23.68	0.242±0.007** 40.64	0.244±0.004** 39.95	0.283±0.018** 30.38
CK	0.806±0.042			0.407±0.005		

Note: Data are means ±SD, n=4 (*, P<0.05 po0.05; **, (P<0.01).

Table 2. HPLC gradient elution parameters

Time (min)	Methanol (%)	Water (%)
0	20	80
20	20	80
60	60	40
80	80	20
90	100	0

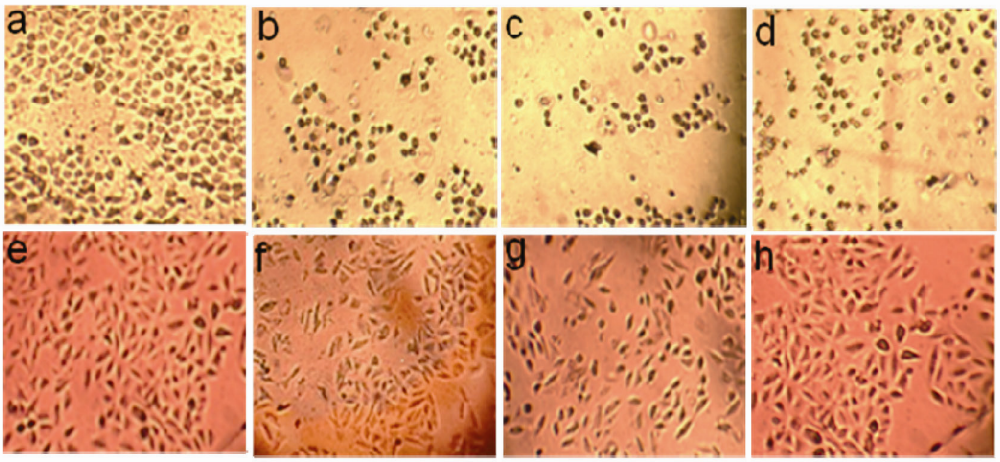

Note: a, MCF-7 cell; b, MCF-7 cells treated by fermentation original solution for 24h; c, MCF-7 cells treated by 1/2 fermentation original solution for 24h; d, MCF-7 cells treated by 1/10 fermentation original solution for 24h; e, MRC cell; f, MRC cells treated by fermentation original solution for 24h; c, MRC cells treated by 1/2 fermentation original solution for 24h; d, MRC cells treated by 1/10 fermentation original solution for 24h.

Figure 1. Cell morphological variation

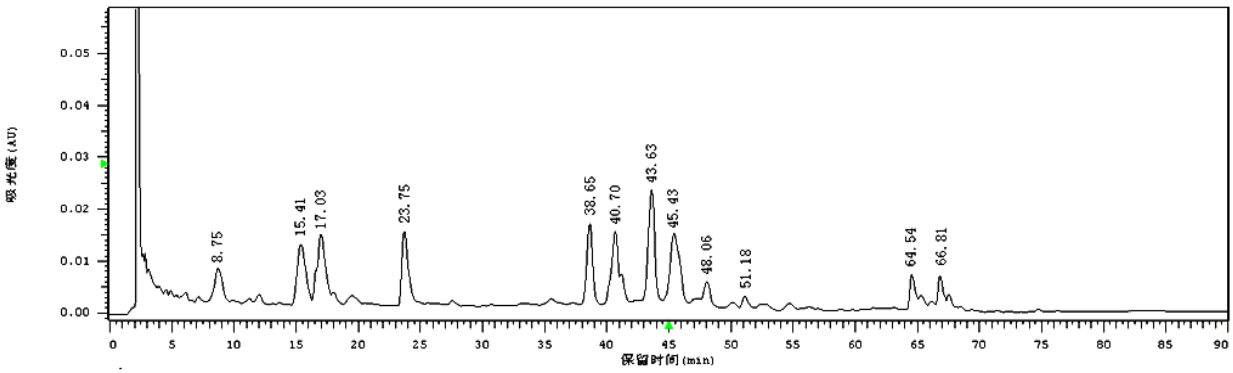

Figure 2. HPLC gradient elution chromatogram of strain 93431 fermentation products at 300 nm

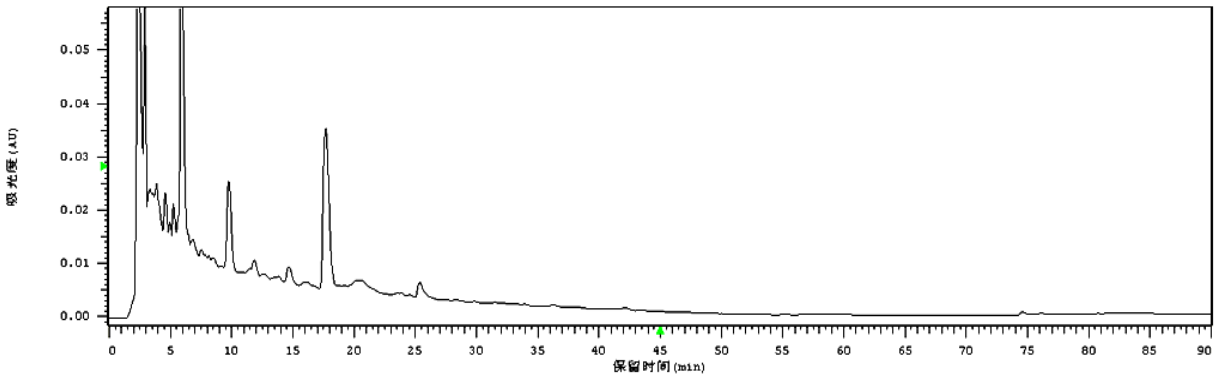

Figure 3. HPLC gradient elution chromatogram of blank medium at 300 nm

Simultaneous Removal of Lignin and 2,4-Dichlorophenol in Pulp and Paper Mill Wastewater Using a Supervibration-photocatalytic Reactor

Suchanya Thongkrua

Inter-department of Environmental Science, Graduate School, Chulalongkorn University

254 Phayathai Road, Pathumwan, Bangkok 10330, Thailand

Tel: 66-2-218-7666 E-mail: suchanya_9@yahoo.com

Chavalit Ratanatamskul (Corresponding author)

Department of Environmental Engineering, Chulalongkorn University

254 Phayathai Road, Pathumwan, Bangkok 10330, Thailand

Tel: 66-2-218-6678 E-mail: dr_chawalit@yahoo.com

Abstract

Advanced photocatalytic degradation of lignin and 2,4-dichlorophenol (2,4-DCP) was studied. The method used a newly developed supervibration-photocatalytic reactor based on the photocatalytic process combined with a supervibration agitator. Effects of operating conditions such as initial pH, UV intensity and supervibration frequency on removal efficiency were investigated. From the results obtained, removal efficiencies of lignin and 2,4-DCP were similar pattern. UV intensity and supervibration frequency in a low initial pH increased removal efficiencies of lignin and 2,4-DCP. The optimum operating condition for a supervibration-photocatalytic reactor was found at initial pH 5, 25.2mW/cm^2 UV intensity and 50Hz supervibration frequency. Under the optimum treatment condition, the reactor could simultaneously remove lignin and 2,4-DCP up to 75.1% and 94.1%, respectively within 420min.

Keywords: 2,4-Dichlorophenol, Lignin, Pulp and paper mill wastewater, Supervibration-photocatalytic reactor

1. Introduction

Pulp and paper mill has produced large volume of wastewater which are heavily loaded with organic maters such as biochemical oxygen demand (BOD), chemical oxygen demand (COD), chlorinated compounds, suspended solids, fatty acids, lignin and its derivatives, etc (Ali & Sreekrishnan, 2001, P175~196). Lignin is very complex and amorphous polymer which has been discharged from cooking and pulp bleaching processes as waste in effluent (Ksibi et al., 2003, P211~218). Pulp and paper mill effluent in Finland was found to contain 186~293mg/L of lignin material (Leiviskä et al., 2009, P3199~3206; Pessala et al., 2004, P319~330). The untreated wastewater causes a loss of aesthetic beauty in the receiving body of water (Pokhrel & Viraraghavan, 2004, P37~58). For instance, the dark brown color of these effluents inhibits the natural process of photosynthesis in streams due to absorbance of sunlight (Sahoo & Gupta, 2005, P1573~1578). Furthermore, many authors reported the presence of toxic species on aquatic organisms, such as growth inhibition and genotoxicity (Ali & Sreekrishnan, 2001, P175~196; Dekker et al., 2002, P374~380; Yakovleva et al., 2004, P242~246). Whereas, 2,4-DCP has been produced from pulp and paper making as a by-product of the chlorine pulp bleaching process (Pera-Titus et al., 2004, P219~256). It was found in aeration pond, treating pulp and paper mill wastewater in Selenga at 2.38mg/L (Batoev et al., 2005, P31~36). Previous studies reported the effects to organisms, such as growth inhibition in microorganisms (Matafonova et al., 2006, P209~212), growth inhibition (Scragg et al., 2003, P616~622) and physical changes (Sahinkaya & Dilek, 2009, P781~786) in aquatic organisms and effect on human erythrocytes (Bukowska et al., 2007, P238~244). Most wastewater treatments of pulp and paper mill are typically carried out using biological treatments but they can only remove small amounts of lignin (Leiviskä et al., 2009, P3199~3206) and 2,4-DCP (Kaigi et al., 2005, P191~196) and require long residence time. Therefore, powerful advanced oxidation processes are alternatives for effective treatment.

Photocatalysis involves the use of titanium dioxide (TiO_2) as a catalyst and ultraviolet light (UV) as an irradiation source. The UV light (wavelengths < 385nm) absorbed by the photocatalyst with energy higher than band gap energy of TiO_2 (3.2eV) excites an electron from the valence band to the conduction band, producing electron-hole pairs (e^-/h^+). During the process, hydroxyl radicals ($OH^\bullet$) are generated on the surface of TiO_2. Mechanisms of photocatalytic reaction are shown in equations (1)~(6).

$$TiO_2 + h\nu \longrightarrow h^+_{VB} + e^-_{CB} \quad (1)$$

$$h^+_{VB} + H_2O \longrightarrow OH^\bullet + H^+ \quad (2)$$

$$h^+_{VB} + OH^- \longrightarrow OH^\bullet \quad (3)$$

$$e^-_{CB} + O_2 \longrightarrow O_2^{\bullet-} \quad (4)$$

$$O_2^{\bullet-} + 2H_2O \longrightarrow 2H_2O_2 \quad (5)$$

$$H_2O_2 \longrightarrow 2OH^\bullet \quad (6)$$

Due to the high oxidation potential (2.8V), $OH^\bullet$ are the principal agents responsible for the oxidation of numerous aqueous organic contaminants and mineralize them into carbon dioxide (CO_2), water (H_2O) and other small molecules (Chen et al., 2004, P329~337; Kaneko & Okura, 2002; Zhou & Smith, 2002, P247~264). The effects of the form of TiO_2, TiO_2 dosages, initial pH, UV light, and initial concentration on removal of lignin (Dahm & Lucia, 2004, P7996~8000; Ksibi et al., 2003, P211~218; Portjanskaja & Preis, 2007, P1~7; Tanaka et al., 1999, P287~294) and 2,4-DCP (Bayarri et al., 2007, P231~239; Bayarri et al., 2005, P227~236; Chen et al., 2004, P329~337; Pandiyan et al., 2002, P149~155) using UV/TiO_2 have been continuously studied. González et al. (2010, P3493~3499) reported that an increase in suspended TiO_2 from 0 to 20mg/L caused an increase in the 2,4-DCP removal initial rate. Effect of UV on 2,4-DCP degradation was studied by Bayarri et al. (2007, P231~239), UV-ABC radiation could be more efficient than UV-A. Furthermore, Dahm & Lucia (2004, P7996~8000) found that at the highest light intensity level (445mW/cm^2), lignin removal occurred much faster than that at the lower illumination intensity. However, it is difficult for TiO_2 powder to disperse and be recycled in aqueous solution. TiO_2 should be coated on some carriers before use (Bao-xiu et al., 2007, P1020~1024).

In this study, the effects of operating parameters on the performance of a novel supervibration-photocatalytic reactor for simultaneous treatment of lignin and 2,4-DCP were investigated, focusing on removal efficiency to determine the optimum treatment condition.

2. Materials and methods

2.1 Chemicals

The chemicals used in the experiments were phosphoric acid (H_3PO_4) (A.R.), hydrogen peroxide (H_2O_2) (A.R.), hydrofluoric acid (HF) (A.R.), lignosulfonic acid sodium salt (analytical grade) and 2,4-DCP (99%) (Aldrich); sulfuric acid (H_2SO_4) (A.R.), methanol (HPLC grade) and acetonitrile (HPLC grade) (LAB-SCAN); sodium hydroxide (NaOH) (analytical grade) (CARLO ERBA).

2.2 Experimental set-up

The experiments were conducted in laboratory scale. The supervibration-photocatalytic reactor, developed in this study, is based on the photocatalytic process combined with a supervibration agitator in order to provide faster reaction and higher removal efficiency. The schematic diagrams of the supervibration-photocatalytic reactor including an agitated tank, a supervibration agitator and an ultraviolet light source and the supervibration agitator containing an eccentric motor, a shaft and multistage blade were shown in figure 1. All experiments were carried out in batch-mode operation using a rectangular reactor of 26.3 × 36.2 × 26.3cm^3 with 25liters capacity, made of stainless steel. The supervibration equipment consists of a set of four multistage blades with each size of 5cm × 8cm × 1mm. Micro-structured TiO_2 film with thickness of approximately 1μm as photo-catalyst coated on the surface of the multistage blade (titanium plate) was produced by low-voltage anodization process of titanium plate, described by Portjanskaja et al. (2009, P26~30). The plate oxidation was conducted in a dual-electrode reaction chamber, in which the titanium plate was used as the anode and a stainless steel plate of the same size was used as the cathode. Both electrodes were submerged in a mixture of electrolyte solution (H_2SO_4 (1.0M)-H_3PO_4 (0.3M)-H_2O_2 (0.6M)-HF (0.03M)) and a direct-current source was used to provide electric current (150~200V) between electrodes. The illumination was provided using four low-pressure 6W mercury lamps (Philip TUV-G6T5, 254nm), which were attached at the top cover of the agitated vessel. The vertical vibration generated from eccentric motor is transferred to the multistage blade through the shaft and the generated supervibrational energy is converted to fluid energy. Consequently, this agitator generates a powerful 3-dimensional agitating flow in the tank and the flow rate produced by the supervibration agitator is higher than that produced by the conventional rotary pump in the same condition of the electrical power source.

2.3 Experimental procedures

Wastewater samples with 218~290mg/L of lignin and 111~152μg/L of 2,4-DCP were supplied by the pulp and paper mill located at Kanchanaburi province in Thailand. Before treatment, the wastewater was precipitated with gravity followed by filtration using glass microfiber filters, GF/C and then pH was adjusted with NaOH and

H_2SO_4. The temperature of wastewater was kept at room temperature (30°C). The removal efficiencies of lignin and 2,4-DCP were studied under different initial pH (5, 6, 7, 8, 9), UV intensity (0, 6.3, 12.6, 25.2mW/cm^2 and supervibration frequency (0, 20, 30, 40, 50Hz). The effluent samples were taken at 15, 30, 60, 90, 120, 180, 300 and 420min for lignin analysis on UV-Visible spectrophotometer and 2,4-DCP analysis on HPLC.

Lignin concentration was analyzed by UV-Visible spectrophotometer, Model Helios Alpha, with detection wavelength of 700nm (Eaton et al., 2005). Whereas, 2,4-DCP was detected by HPLC Varian Prostar with column C 18 (4.6mm di × 250mm) and UV-Visible detector at wavelength of 280nm. A mixture of 25% of acetonitrile, 30% of methanol and 45% of water adjusted at pH 3 with H_2SO_4 was used in the mobile phase (1ml/min of flow rate) (Kinakul, 2002).

3. Results and discussion

3.1 Effect of pH

Wastewater samples were treated under five different initial pH levels as 5, 6, 7, 8 and 9. The supervibration-photocatalytic reactor was carried out with 6.3mW/cm^2 of UV intensity and 30Hz of supervibration frequency. The experimental data depicted in figure 2 show that the effect of initial pH on the removal efficiency of lignin and 2,4-DCP was similar trend. The maximum removal efficiencies of lignin and 2,4-DCP were obtained at initial pH 5. The ultimate lignin removal efficiencies were 28.6% (pH 5), 25.1% (pH 6), 18.5% (pH 7), 13.2% (pH 8) and 10.1% (pH 9) within 420min. Whereas, 2,4-DCP removal efficiencies of the reactor were 65.6% (pH 5), 61.2% (pH 6), 56.8% (pH 7), 55.2% (pH 8) and 50.8% (pH 9) in the same time. The results indicate that both lignin and 2,4-DCP removal efficiencies were increased with the decrease in the initial pH. Several researchers obtained similar results in which more lignin removal (Chang et al., 2004, P1011~1017; Ma et al., 2008, P998~1004; Portjanskaja & Preis, 2007, P1~7) and more 2,4-DCP removal (Bayarri et al., 2005, P227~236; Pandiyan et al., 2002, P149~155) were achieved with samples of lower pH level thus, the acidic conditions favor the lignin and 2,4-DCP decomposition. It may be because, under acidic conditions, a superoxide radical ($O_2^{\bullet-}$) will react with a hydrogen ion (H^+) and produce a perhydroxyl radical ($HO_2^{\bullet}$). Consequently, the $HO_2^{\bullet}$ can form hydrogen peroxide (H_2O_2), which in turn gives rise to the $OH^{\bullet}$ as shown in equations (7)~(10) (De Lasa et al., 1992).

$$O_2^{\bullet-} + H^+ \longrightarrow HO_2^{\bullet} \quad (7)$$

$$HO_2^{\bullet} + HO_2^{\bullet} \longrightarrow H_2O_2 + O_2 \quad (8)$$

$$H_2O_2 + e^- \longrightarrow HO^{\bullet} + OH^- \quad (9)$$

$$H_2O_2 + O_2^{\bullet-} \longrightarrow HO^{\bullet} + OH^- + O_2 \quad (10)$$

On the other hand, the point of zero charge (pzc) of TiO_2 is between pH 5.6 and 6.4. Therefore, depending on the pH, the TiO_2 surface will be charged positively (pH < pzc) and negatively (pH > pzc) that will have a significant effect on the adsorption properties of TiO_2. Molecules of lignin are negatively charge in alkaline solution, being repelled from the TiO_2 surface; which causes to reduce their adsorption. Also the accumulation of carbonate and bicarbonate ions, $OH^{\bullet}$ scavenger, could be the reason of decreased efficiency at alkaline pH (Portjanskaja & Preis, 2007, P1~7). In addition, 2,4-DCP is mostly in the un-ionized form under acidic pH values and then, it can be more easily adsorbed onto the TiO_2 surface, whereas for alkaline conditions, 2,4-DCP and TiO_2 surface are mostly charged negatively so can exist a repulsion between both compounds (Bayarri et al., 2005, P227~236; Pandiyan et al., 2002, P149~155).

3.2 Effect of UV intensity

In order to determine the effect of UV intensity, the experiments were performed by varying UV intensity as 0, 6.3 and 12.6mW/cm^2 at constant optimum initial pH 5 and 30Hz of supervibration frequency. Figure 3 reveals that lignin and 2,4-DCP removal efficiencies were increased greatly by the increase in UV intensity, thereafter it started decreasing slowly. Removal efficiencies of lignin with 6.3 and 12.6mW/cm^2 of UV intensity were 28.6% and 44.8%, respectively, and 65.6% and 73.2%, respectively for 2,4-DCP removal, after 420min. Whereas, the absence of UV light induced low lignin removal (6.2%) and 2,4-DCP removal (15.8%) in the same time of UV irradiation. It may be due to the photocatalytic degradation not occurring, but fluid energy converted from supervibration energy can break some molecules of the pollutants. The results indicate that an increase in UV intensity could enhance both lignin and 2,4-DCP removal. This is because when UV intensity is higher, the photonic flux irradiation will increase and the higher rate of hole production will occur. Thus, the rate of $OH^{\bullet}$ and the $O_2^{\bullet-}$ production increase, which would allow the degradation to be faster. Related results were previously observed by Dahm & Lucia (2004, P7996~8000). The results demonstrated lignin removal using a light intensity of 223~445mW/cm^2 and it was found that higher illumination intensity correlated well with higher initial

degradation rate and total lignin degradation. Furthermore, Bayarri et al. (2007, P231~239) reported that the photocatalytic degradation of 2,4-DCP was about 20% higher with UV-ABC than with UV-A. An increase in UV intensity always increases the reaction rate until the reaction is mass transfer limited (De Lasa et al., 1992).

3.3 Effect of supervibration frequency

The influence of supervibration frequency was also studied. Figure 4 illustrates the photodegradation efficiency of lignin and 2,4-DCP with five different supervibration frequency as 0, 20, 30, 40 and 50Hz in the presence of constant optimum initial pH (pH 5) and optimum UV intensity (12.6mW/cm^2). It indicated the effect of supervibration frequency on photocatalysis under the conditions used here. Although there was an absence of supervibration frequency (0Hz), the system could remove lignin and 2,4-DCP at 25.4% and 52.5%, respectively in 420min because of photocatalytic degradation (UV/TiO_2). When introducing the supervibration frequency into the system, the reactor was able to remove more lignin and 2,4-DCP. The removal efficiencies of lignin were 40.2% (20Hz), 44.8% (30Hz), 45.1% (40Hz) and 47.0% (50Hz) in the same time. For 2,4-DCP, the reactor could remove at 66.4% (20Hz), 73.2% (30Hz), 74.3% (40Hz) and 76.3% (50Hz), after 420min. Removal efficiencies of lignin and 2,4-DCP were increased as supervibration frequency increased. This is probably because, in the condition of higher supervibration frequency, the powerful 3-dimensional agitating flow in the reaction tank is higher. Therefore, the contact between pollutants and TiO_2 will be enhanced. In addition, the higher supervibration energy is converted to higher fluid energy and it may be more than chemical bond energy in pollutant structure; consequently, the breaking down of the lignin and 2,4-DCP molecules occurred. Additional experiment with increased UV intensity into the system was also performed. The results were found that, under conditions as UV intensity of 25.2mW/cm^2, initial pH 5, supervibration frequency of 50Hz, removal efficiencies of lignin and 2,4-DCP were up to 75.1% and 94.1%, respectively, after 420min. Portjanskaja & Preis (2007, P1~7) used mechanical agitation with magnetic stirrers in the UV/TiO_2 reactor for treatment of lignin. The system could degrade lignin not exceeding 50% after 25 hours when using 100mg/L of initial lignin concentration at pH around 8.0. Furthermore, Yang et al. (2008, P300~307) investigated degradation of 2,4-DCP in water using UV/TiO_2 and magnetic stirrers under conditions as 0.5mg/L of 2,4-DCP solution at initial pH 7 and 900μW/cm^2 of UV intensity. 2,4-DCP removal efficiency was around 53% within 120min, whereas present work using supervibration agitator could remove 2,4-DCP up to 77.9% in the same time. Therefore, the supervibration agitator in the present study has higher performance in lignin and 2,4-DCP removal than that of previous researches. This may be because the fluid flow rate produced by the supervibration agitator is higher than that produced by magnetic stirrers.

4. Conclusions

According to our study, a supervibration-photocatalytic reactor can effectively reduce pollutants as lignin and 2,4-DCP in wastewater and can be concerned as a new alternative technology for real world application. The optimum operating condition for a supervibration-photocatalytic reactor was found at initial pH 5, 25.2mW/cm^2 UV intensity and 50Hz supervibration frequency. Under the optimum treatment condition, the reactor could simultaneously remove lignin and 2,4-DCP up to 75.1% and 94.1%, respectively within 420min.

Acknowledgements

The authors are grateful to THE 90th ANNIVERSARY OF CHULALONGKORN UNIVERSITY FUND (Ratchadaphiseksomphot Endowment Fund) for financial support.

References

Ali, M., & Sreekrishnan, T. R. (2001). Aquatic toxicity from pulp and paper mill effluents: a review. *Advances in Environmental Research*, 5, 175~196.

Bao-xiu, Z., Xiang-zhong, L., & Peng, W. (2007). Degradation of 2,4-dichlorophenol with a novel TiO_2/Ti-Fe-graphite felt photoelectrocatalytic oxidation process. *Journal of Environmental Sciences*, 19, 1020~1024.

Batoev, V. B., Nimatsyrenova, G. G., Dabalaeva, G. S., & Palitsyna, S. S. (2005). An assessment of contamination of the Selenga River Basin by chlorinated phenols. *Chemistry for Sustainable Development*, 13, 31~36.

Bayarri, B., Abellán, M. N., Giménez, J., & Esplugas, S. (2007). Study of the wavelength effect in the photolysis and heterogeneous photocatalysis. *Catalysis Today*, 129, 231~239.

Bayarri, B., Giménez, J., Curcó, D., & Esplugas, S. (2005). Photocatalytic degradation of 2,4-dichlorophenol by TiO_2/UV: kinetics, actiometries and models. *Catalysis Today*, 101, 227~236.

Bukowska, B., Michalowicz, J., Krokosz, A., & Sicińska, P. (2007). Comparison of the effect of phenol and its derivatives on protein and free radical formation in human erythrocytes (*in vitro*). *Blood Cells, Molecules, and Diseases*, 39, 238~244.

Chang, C.-N., Ma, Y-S., Fang, G-C., Chao, A. C., Tsai, M-C., & Sung, H-F. (2004). Decolorizing of lignin wastewater using the photochemical UV/TiO_2 process. *Chemosphere*, 56, 1011~1017.

Chen, C., Lei, P., Ji, H., Ma, W., & Zhao, J. (2004). Photocatalysis by titanium dioxide and polyoxometalate/TiO_2 cocatalysis: intermediates and mechanistic study. *Environmental Science & Technology*, 38, 329~337.

Dahm, A., & Lucia, L. A. (2004). Titanium dioxide catalyzed photodegradation of lignin in industrial effluents. *Industrial & Engineering Chemistry Research*, 43, 7996~8000.

Dekker, R. F. H., Barbosa, A. M., & Sargent, K. (2002). The effect of lignin-related compounds on the growth and production of laccases by the ascomycete, *Botryosphaeria* sp. *Enzyme and Microbial Technology*, 30, 374~380.

De Lasa, H. I., Dogu, G., & Ravella, A. (1992). *Chemical reactor technology for environmentally safe reactors and product*. London: Kluwer Academic.

Eaton, A. D., Clesceri, L. S., Rice, E. W., & Greenberg, A. E. (2005). *Standard methods for the examination of water and wastewater*. (21st ed.). American Public Health Association.

González, L. F., Sarria, V., & Sánchez, O. F. (2010). Degradation of chlorophenols by sequential biological-advanced oxidative process using *Trametes pubescens* and TiO_2/UV. *Bioresource Technology*, 101, 3493~3499.

Kaigi, F., Eker, S., & Uygur, A. (2005). Biological treatment of synthetic wastewater containing 2,4-dichlorophenol (DCP) in an activates sludge unit. *Journal of Environmental Management*, 76, 191~196.

Kaneko, M., & Okura, I. (2002). *Photocatalysis science and technology*. Tokyo: Kodansha.

Kinakul, S. (2002). *High performance liquid chromatographic analysis of phenolic compounds and photooxidation of chlorophenols using titanium dioxide as photosensitizer*. Master Thesis, Khon Kaen University, Thailand.

Ksibi, M., Amor, S. B., Cherif, S., Elaloui, E., Houas, A., & Elaloui, M. (2003). Photodegradation of lignin from black liquor using a UV/TiO_2 system. *Journal of Photochemistry and Photobiology A: Chemistry*, 154, 211~218.

Leiviskä, T., Rämö, J., Nurmesniemi, H., Pöykiö, R., & Kuokkanen, T. (2009). Size fraction of wood extractives, lignin and trace elements in pulp and paper mill wastewater before and after biological treatment. *Water Research*, 43, 3199~3206.

Ma, Y-S., Chang, C-N., Chiang, Y-P., Sung, H-F., & Chao, A. C. (2008). Photocatalytic degradation of lignin using Pt/TiO_2 as the catalyst. *Chemosphere*, 71, 998~1004.

Matafonova, G., Shirapova, G., Zimmer, C., Giffhorn, F., Batoev,V., & Kohring, G.-W. (2006). Degradation of 2,4-dichlorophenol by *Bacillus* sp. Isolated from an aeration pond in the Baikalsk pulp and paper mill (Russia). *International Biodeterioration & Biodegradation*, 58, 209~212.

Pandiyan,T., Rivas, O. M., Martínez, J. O., Amezcua, G. B., & Martínez-Carrillo, M. A. (2002). Comparison of methods for the photochemical degradation of chlorophenols. *Journal of Photochemistry and Photobiology A: Chemistry*, 146, 149~155.

Pera-Titus, M., García-Molina, V., Baños, M. A., Giménez, J., & Esplugas, S. (2004). Degradation of chlorophenols by means of advanced oxidation processes: a general review. *Applied Catalysis B: Environmental*, 47, 219~256.

Pessala, P., Schultz, E., Luukkainen, S., Herve, S., Knuutinen, J., & Paasivirta, J. (2004). Lignin as the cause of acute toxicity in pulp and paper mill effluents. In D. L. Borton, T. J. Hall, R. P. Fisher, & J. F. Thomas (Eds.), *Pulp & paper mill effluent: environmental fate & effects* (pp. 319~330). Lancaster: DEStech Publication.

Pokhrel, D., & Viraraghavan, T. (2004). Treatment of pulp and paper mill wastewater- a review. *Science of the Total Environment*, 333, 37~58.

Portjanskaja, E., & Preis, S. (2007). Aqueous photocatalytic oxidation of lignin: the influence of mineral admixtures. *International Journal of Photoenergy*, 1~7.

Portjanskaja, E., Stepanova, K., Klauson, D., & Preis, S. (2009). The influence of titanium dioxide modifications

on photocatalytic oxidation of lignin and humic acids. *Catalysis Today*, 144, 26~30.

Sahinkaya, E., & Dilek, F. B. (2009). The growth behavior of *Chlorella vulgaris* in the presence of 4-chlorophenol and 2,4-dichlorophenol. *Ecotoxicology and Environmental Safety*, 72, 781~786.

Sahoo, D., & Gupta, R. (2005). Evaluation of ligninolytic microorganisms for efficient decolorization of a small pulp and paper mill effluent. *Process Biochemistry*, 40, 1573~1578.

Scragg, A. H., Spiller, L., & Morrison, J. (2003). The effect of 2,4-dichlorophenol on the microalga *Chlorella* VT-1. *Enzyme and Microbial Technology*, 32, 616~622.

Tanaka, K., Calanag, R. C. R., & Hisanaga, T. (1999). Photocalalyzed degradation of lignin on TiO_2. *Journal of Molecular Catalysis A: Chemical*, 138, 287~294.

Yakovleva, Y. N., Ostrovskaya, R. M., & Novikova, L. N. (2004). Assessment of genotoxicity of lignin substances as risk factors for aquatic ecosystems. *Russian Journal of Ecology*, 35, 242~246.

Yang, Q., Choi, H., Chen, Y., & Dionysiou, D. D. (2008). Heterogeneous activation of peroxymonosulfate by suppored cobalt catalysts for the degradation of 2,4-dichlorophenol in water: the effect of support, cobalt precursor, and UV radiation. *Applied Catalysis B: Environmental*, 77, 300~307.

Zhou, H., & Smith, D. W. (2002). Advanced technologies in water and wastewater treatment. *Journal of Environmental Engineering and Science*, 1, 247~264.

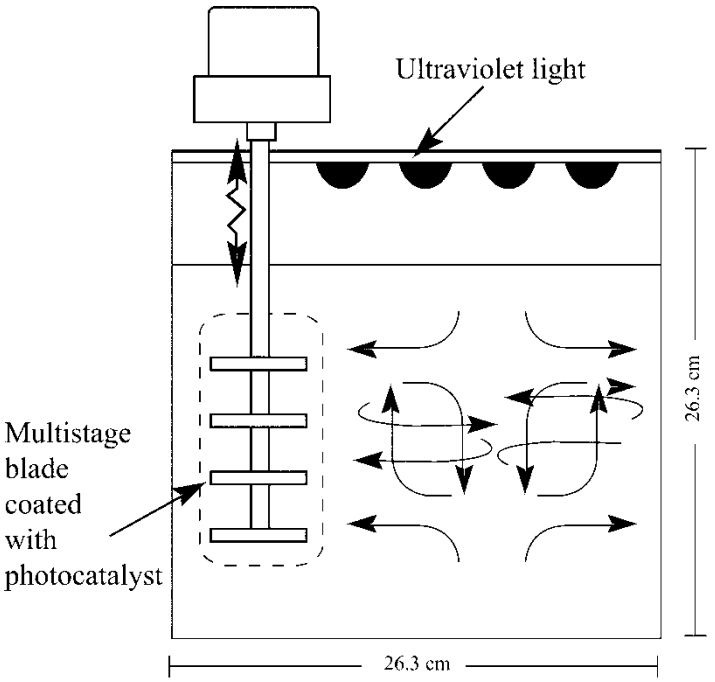

(a)

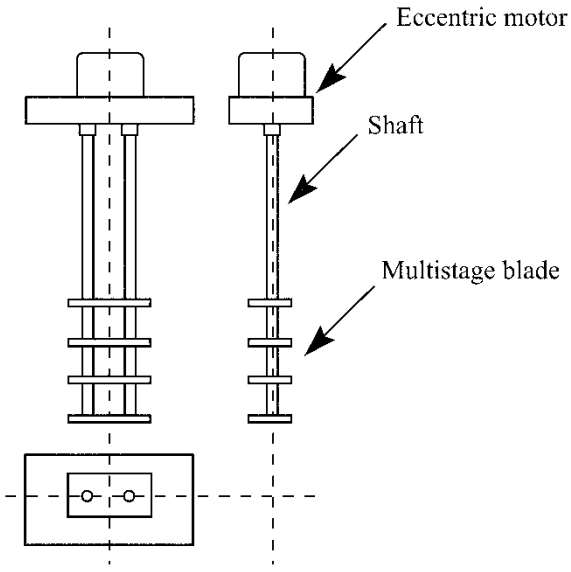

(b)

Figure 1. The schematic diagrams of the supervibration-photocatalytic reactor (a) and the supervibration agitator (b)

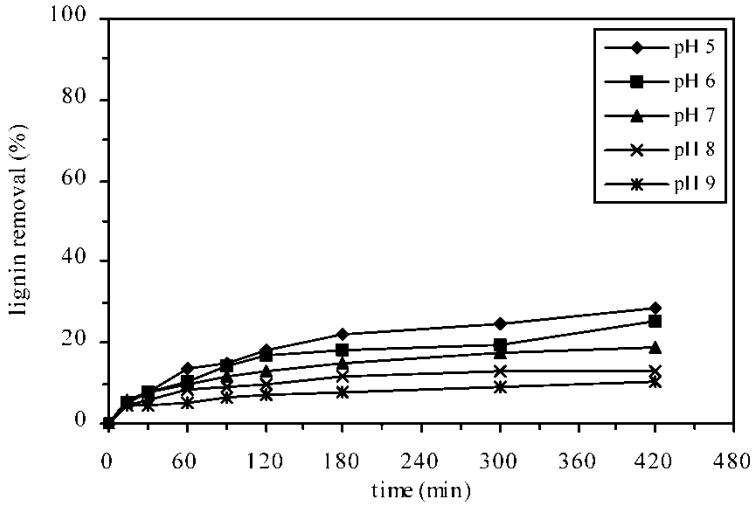

(a)

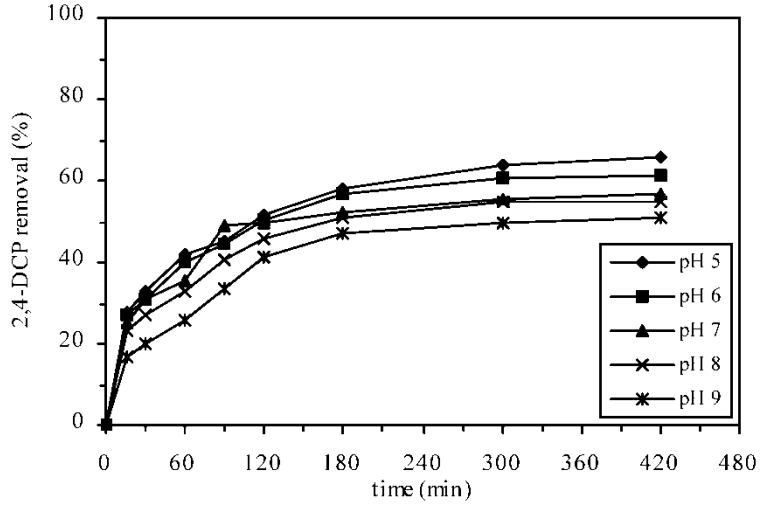

(b)

Figure 2. The effect of initial pH on removal efficiency of lignin (a) and 2,4-DCP (b)

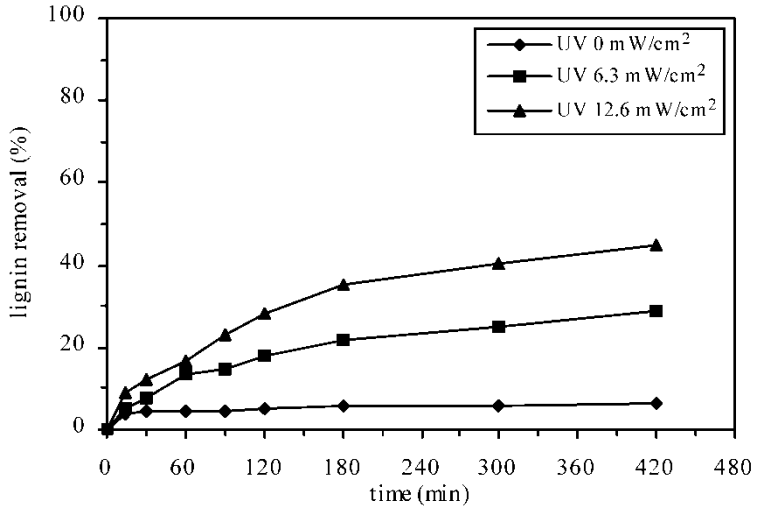

(a)

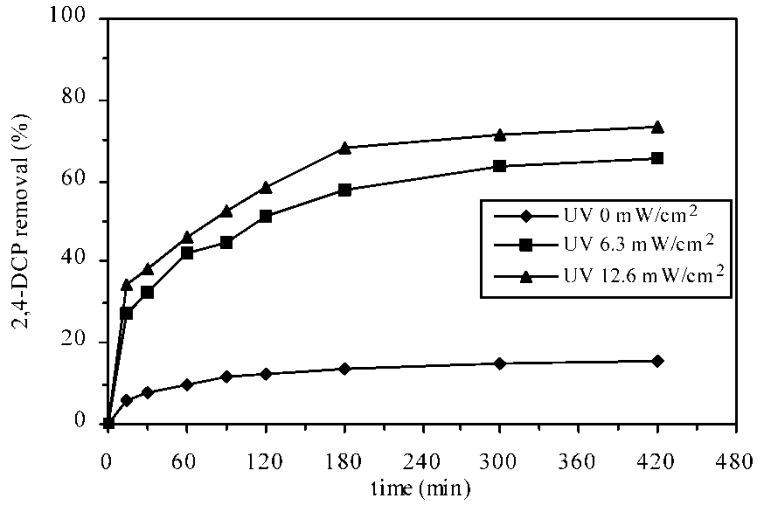

(b)

Figure 3. The effect of UV intensity on removal efficiency of lignin (a) and 2,4-DCP (b)

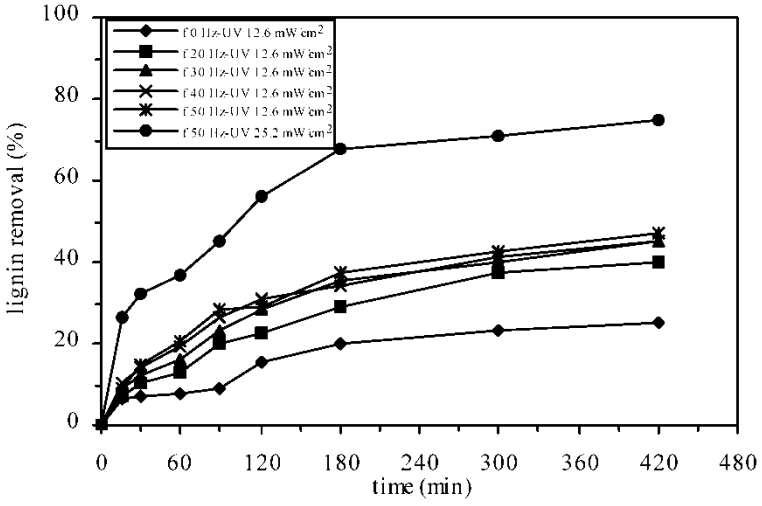

(a)

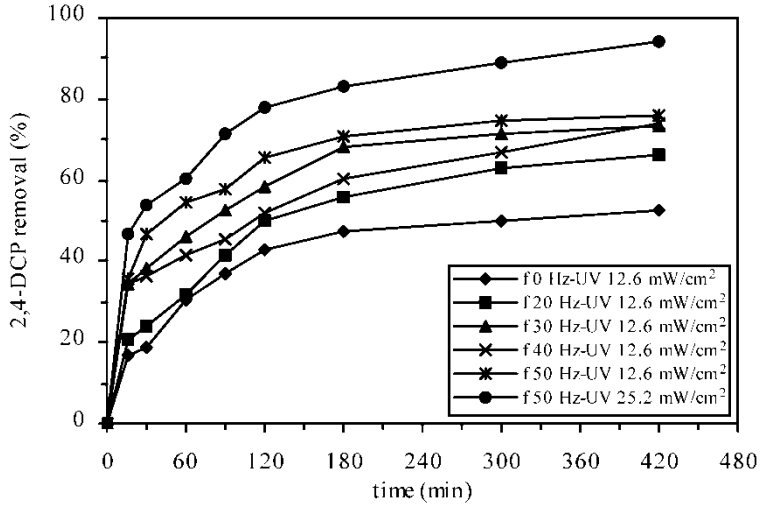

(b)

Figure 4. The effect of supervibration frequency on removal efficiency of lignin (a) and 2,4-DCP (b)

ISSN 1913-1844 E-ISSN 1913-1852

Design of the Robust Controller of the APT Fine Tracking System Based on the Structured Singular Value Theory

Mingqiu Li & Hongzuo Li

Institute of Electronic and Information Engineering, Changchun University of Science and Technology

Changchun 130022, China

Tel: 86-431-8558-2437 E-mail:limingqiu2003@126.com

Abstract

APT (Acquisition, Pointing, Tracing) system is the important component of the space laser communication system, and its tracing accuracy is mainly determined by the fine tracing subsystem. To enhance the tracing accuracy and robustness of the APT system, the robust control technology based on the structured singular value theory (μ integration) is adopted in the design of the controller of the APT fine tracing subsystem, and the mathematical model of the augmented object of the fine tracing subsystem based on μ integration is established, and the robust H_∞ controller is designed by the D-K iterative method in this article, and the bandwidth of the fine tracing subsystem could achieve 318 Hz, which could satisfy the requirements of the APT system to the bandwidth of the fine tracing subsystem. The equivalent sine simulation of the system indicates that the system tracing accuracy is better than 0.6 μrad.

Keywords: Laser communication, Compound axis system, Fine tracing subsystem, Robust control, μ integration

1. Components of the APT system

The components of the compound axis APT system are seen in Figure 1, and the coarse tracing subsystem includes the gimbal servo turntable and the coarse-tracing CCD, with the characteristics such as wide dynamic range, narrow control bandwidth, lower resonance frequency, and it could accomplish the initial orientation of the laser axis and realize the capture and coarse tracing. The main components of the fine tracing subsystem are the fast steering mirror and the fine tracing detector, and the fine tracing subsystem could further correct the residual error which could not be compensated by the coarse tracing loop, to satisfy the aiming and tracing accuracy required by the system (Toyoda Masahiro, 2006, P.4-12 & Tzung-Hsien Ho, 2005, P.81-92 & T. Tolker-nielsen, 2002, P.6-20 & Liu, 2006, P.103-103).

2. Mathematical model of the fine tracing subsystem

The executive component of the fine tracing subsystem is the two-dimensional fast steering mirror, and its mathematical model is

$$G_F(s)=\frac{\omega_n^2}{s^2+2\zeta\omega_n s+\omega_n^2}=\frac{8.2\times10^7}{s^2+1.3\times10^4\times s+8.2\times10^7}$$

The fine tracing imaging system is the CCD camera with the frame frequency of 1600 Hz, and its mathematical model could equal a delay factor, and the delay time is determined by the frame frequency of the fine tracing CCD camera.

3. Design of the robust controller based on the structured singular value theory (μ integration)

3.1 Establishment of the fine tracing system augmented object model based on μ integration

The robust control structure of the fine tracing subsystem is seen in Figure 2, and $K(s)$ is the transfer function of the system controller, and θ_i is the target visual axis, and θ_o is the visual axis of fine tracing. d_1 is the main disturbance acting on the visual axis of fine tracing, d_2 and z_2 are evaluation signals of the system to the multiplicative perturbing robustness, z_3 is the evaluation signal to the control signal of system, z_1 is the evaluation signal to the response of the system to the disturbance, W_1 is the weighted function to measure the disturbance performance of the system, W_2, W_3 and W_4 respectively are the weighted functions of multiplicative perturbing, disturbance perturbing, and control signal. $\Delta(s)$ is multiplicative perturbing, and $\|\Delta\|_\infty<1$. The augmented object model of the fine tracing system based on μ integration obtained from Figure

2 is seen in Figure 3.

3.2 Selection of the weighted function

The selection of the weighted function is the core approach of the robust controller design based on μ integration, and the weighted function determines the robust stability and the robust tracing performance of the system, and through repeated adjustment, the weighted function is

$$\omega_1(s) = \frac{0.782s + 100}{s + 0.00009}$$

$$\omega_2(s) = \frac{33.3s^3 + 3.567\times10^5 s^2 + 1.9\times10^9 s + 5.417\times10^{12}}{s^3 + 3.967\times10^4 s^2 + 4.042\times10^8 s + 6.708\times10^{12}}$$

$$\omega_3(s) = 0.24$$

$$\omega_4(s) = \frac{9.98s + 1.412\times10^4}{s + 1.298\times10^5}$$

3.3 The μ integration of controller

The design target of the robust controller based on μ integration is to design the robust H_∞ controller $K(s)$ by the μ theory, and minimize the μ value of the closed-loop transfer function $F(G,K)$ from d to z, i.e. minimize $\mu_\Lambda(M(j\omega))$, and $M(s) = F(G,K)$ (Mei, 2008, P.96-100).

When designing the controller of the APT fine tracing subsystem by the D-K iterative method, the value of μ obtained through three times of iteration equals the norm of H_∞, and the iterative process ends. The order of controller and the μ values of the corresponding controllers are seen in Table 1.

From Table 1, the values of μ of the third iteration and the second iteration are very close with the norm of H_∞, because the order of the controller obtained in the third iteration is higher. So the result of the second iteration is the final controller, and the relationship between the structured singular value and the frequency is seen in Figure 4, and the peak value of μ is 0.413, and the mathematical model of the 13-order controller after two iterations is

$$K(s) = \frac{914.669\,(s+6e6)\,(s+1.35e5)\,(s+3.36e4)\text{^}2\,(s+724.6)\,(s+347.2)}{(s+6.001e006)\,(s+3.458e004)\,(s+3.264e004)\,(s+6152)\,(s+1868)\,(s+638.8)} \cdots$$
$$\cdot\frac{(s+309.6)\,(s+289.5)\,(s\text{^}2+6087s+1.998e008)\text{^}2}{(s+309.5)\text{^}2\,(s+0.0001)\,(s\text{^}2+5760s+1.939e008)\,(s\text{^}2+6475s+2.056e008)}$$

3.4 Analysis of the simulation of the APT fine tracing system based on robust H_∞ controller

Through designing the robust controller by the μ theory, the step response and the closed-loop frequency characteristic curve of the fine tracing system respectively are seen in Figure 5 and Figure 6, and the bandwidth of the fine tracing subsystem is 2000 rad/s (318.3 Hz), and the adjustment time is 0.0045s, and the overshoot is zero, which all could satisfy various index requirements of the system.

4. Simulation of the tracing performance of the compound axis APT system

The simulation analysis of the tracing performance of the APT system is implemented by adding equivalent sin signal to the APT signal. According to the maxim work speed and the accelerated speed required by the system, the amplitude of the equivalent sin signal is 0.0262 rad, and the frequency is 2 rad/s (Hu, 2005, P.7-9 & Fu, 1998, P.5-10 & Wu, 2008, P.41-47).

From the simulation result, the responses of the APT system based on the robust control and the system based on the routine compensation respectively are the curve 1 and the curve 2 in Figure 7. The part error enlargement figure of the APT system based on the robust control is Figure 8. The result shows that the robust control based on μ integration could enhance the tracing accuracy of the system, and the tracing accuracy of the system is better than 0.6 μrad.

5. Conclusions

In this article, the μ integration method is used to design the robust H_∞ controller of the APT fine tracing subsystem, which could make the system bandwidth achieve 318 Hz. By the equivalent sin simulation of the APT system, the result shows that robust control technology based on μ integration could make the tracing accuracy of the fine tracing system exceed 0.6 μrad.

References

Fu, Chengyu, Ma, Jiaguang & Ye, Buxia et al. (1998). Application of the Compound Axis Control System. *Opto-Electronic Engineering.* No.25(4). P.5-10.

Hu, Qinggong & Wang, Kejia. (2005). Design 0f atmosphere laser communication APT system and fine tracking system simulation. *Application science and technology.* No.32(12). P.7-9.

Liu, Ximin, Sun, Liren & Sun, Jianfeng. (2006). Bandwidth Design of Composite Axis System in Satellite Laser Communication. *Acta Optica Sinica.* No.26(1). P.103-103.

Mei, Shengwei, Shen, Tielong & Liu, Kangzhi. (2008). *Theory and Application of Modern Robust Control.* Beijing: Tsinghua University Press. P.96-100.

Wu, Qiong. (2008). *Study on the Fine Tracking Control Technology of the Laser Communication APT System in Free Space.* Changchun: Master's Degree Thesis of Changchun University of Science and Technology. P.41-47.

Toyoda Masahiro. (2006). Acquisition and tracking control of satellite-borne laser communication systems and simulation of downlink fluctuations. *Optical Engineering (S0091-3286).* No.45(3). P.4-12.

T. Tolker-nielsen, G. Oppenhauser. (2002). In-orbit test result of an operational optical inter-satellite link between ARTEMIS and SPOT4,*SILEX.Proc.SPIE.* Vol.4635. P.6-20.

Tzung-Hsien Ho, Stuart D. Milner, Christopher C Davis. (2005). Fully optical real-time pointing, acquisition and tracking system for free space optical link. *Proc.SPIE.* Vol.5712. P.81-92.

Table 1. D-K iterative result

Iterative times	Orders of controller	μ	H_∞ Norm
1	10	0.488	1.598
2	13	0.409	0.413
3	16	0.396	0.396

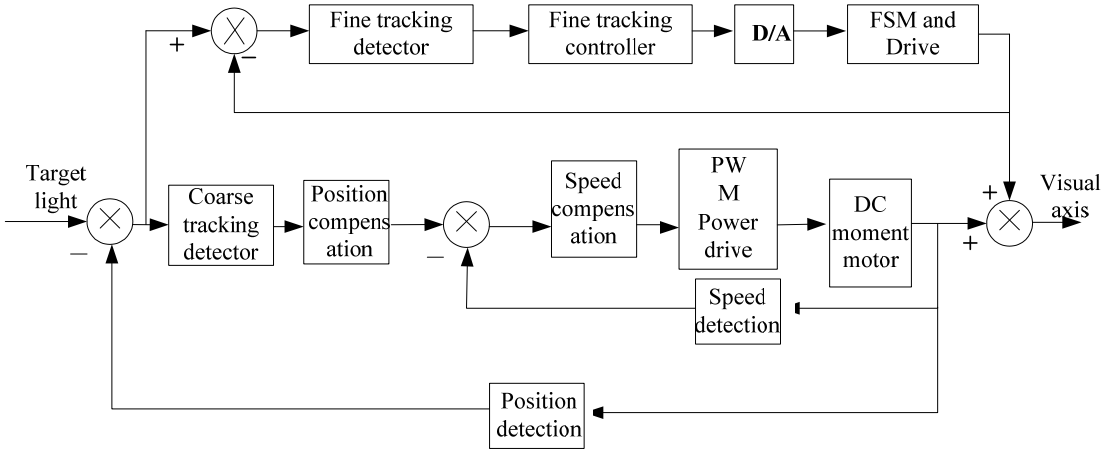

Figure 1. Block Diagram of the APT System

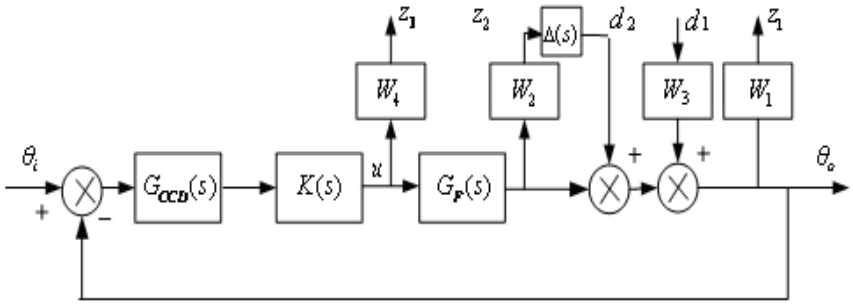

Figure 2. Robust Control Structure of the Fine Tracking Subsystem

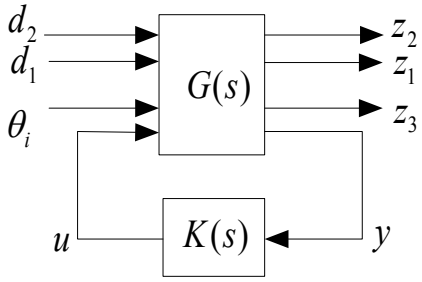

Figure 3. Augmented Object Model of the Fine Tracking System

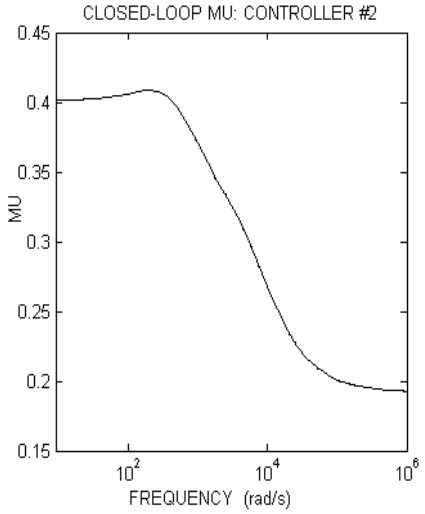

Figure 4. Structured Singular Value of the System

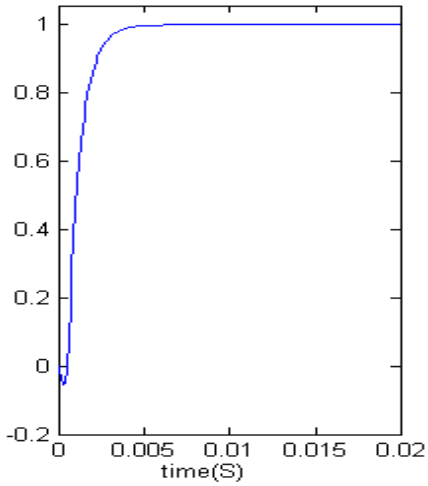

Figure 5. Step Response of the Fine Tracking System

 ISSN 1913-1844 E-ISSN 1913-1852

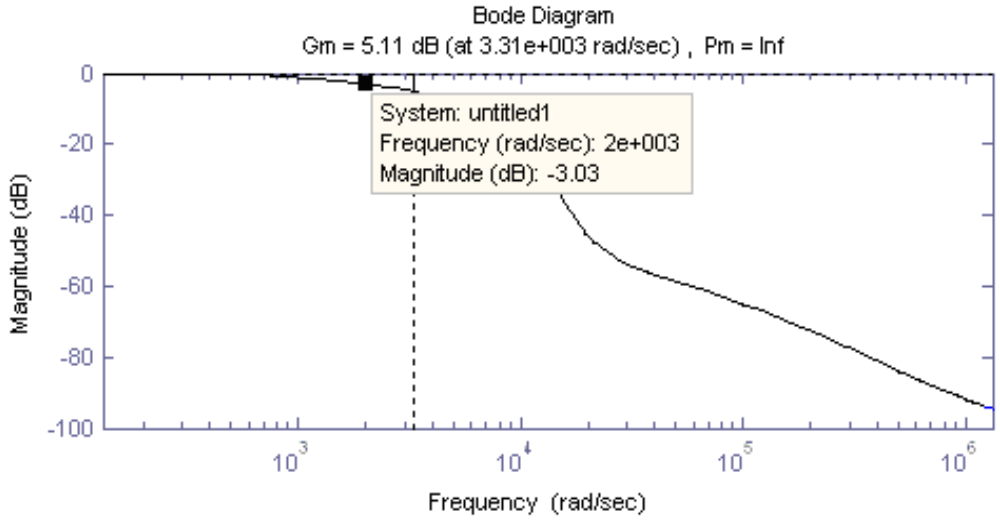

Figure 6. Closed-loop Magnitude-frequency Characteristic of the After-compensation Fine Tracking Subsystem

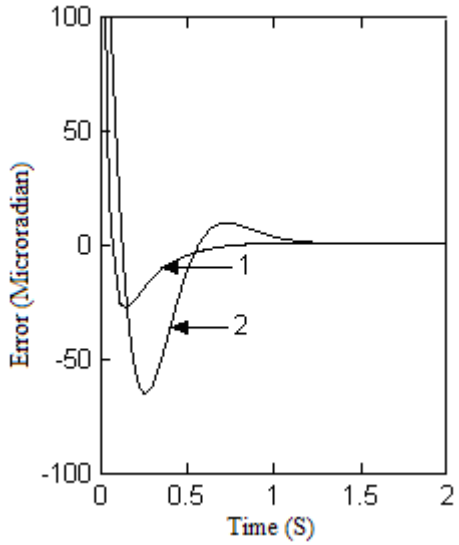

Figure 7. Equivalent Sine Simulation Result of APT System

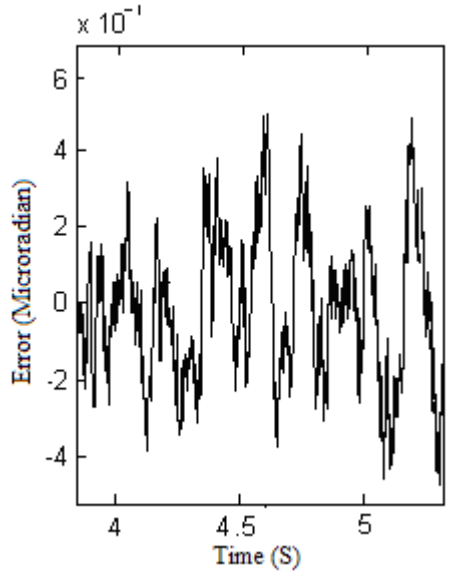

Figure 8. Part Enlargement of Error

Design and Fabrication of Nanostructures Silicon Photodiode

Alwan M. Alwan (Corresponding author) & Allaa A.Jabbar

School of Applied Sciences, University of Technology, Baghdad, Iraq

E-mail: alkrzsm@yahoo.com

Abstract

A highly sensitive (metal/nanostructure silicon /metal) photodiode has been fabricated from rapid thermal oxidation (RTO) and rapid thermal annealing (RTA) processes, of nanostructure porous silicon prepared by laser assisted etching.

Photoresponse was investigated in the wavelength range (400-850nm). A responsivity of (3A/W) was measured at (450 nm) with low value of dark current of about (1 μA /cm^2) at 5 volt reverse bias.

Keywords: Porous silicon, Photoelectrochemical etching, Dark current, Photocurrent, Sensitivity, XRD

1. Introduction

Since the discovery of effective visible photoluminescence (PL) at room temperature from highly porous silicon (psi), a great deal of attention has been paid to its electronic properties because of the potential applications in Si-based optoelectronics(O. Klima, P. Hlinomaz, A. Hospodkova, J. Oswald, and J. Kocka. 1993)(P. Hlimonaz, O. Klima, A. Hospodkova, E. Hulicius, J. Oswald, E. Sipek, and J. Kocka, 1994); (psi) has many unique characteristics such as direct and wide modulated energy band gap , high resistivity , vast surface area-to-volume ratio and the same single-crystal structure as bulk silicon .Those advantages make it a suitable material for photodetectors(Nobuyoshi Koshida and Hideki Koyama. 1992)(Zhiliang Chen, Gijs Bosman and Romulo Ochoa. 1993).

(Psi) photodetector manufactured through conventional method is found to have several shortcomings, such as unstable optical and electrical characteristics, insufficient light sensitivity, insufficient low dark-current and insufficient photo-current, hence the application range for (psi)photodectors is somewhat limited (Ming-Kwei Lee. 1998).

According to the paper published in 1992 by Petrova-Koch et, it was note that (psi) surface also contain unstable Hydrogen-passivated surface as they tend to form a recombination centers that would reduce the life time of the carriers , which further reduce the (psi) photodetectore's photo-current and light sensitivity and causes instability to (psi)photodetectors. (RTO) and (RTA) are utilized to improve the stability of (psi)photodetector, enhance photodetectore's photo-current, and reduce dark-current of photodetectors at the same time and expend the application of (psi) photodetectors(M. K. Lee, Y. H.Wang, and C. H.Chu. 1994).

2. Experimental

The samples were prepared using silicon wafers, (111) oriented, with n-doping, and resistivity of (1.5-4.5 Ω.cm), 508 μm thickness. After cutting into (1×1.5 cm2)specimens and standard cleaning steps , we prepared porous silicon structures by photoelectrochemical etching (PECE) .In this technique the samples are dipped into mixture of HF:Ethanol (1:1) for 20 minutes with anodization current density that was varied from 10 to 40 mA/cm2 . In order to achieve significant hole current in n-type silicon, external illumination was used (Red 650 nm). Typical (PECE) apparatus are schematically shown in Fig (1).

The porous layer was then rapid-thermal-oxidized (750°C, 50 sec) to form partial SiO_2-layer and subsequently rapid-thermal-annealed at 750°C for 15 sec.

The (RTO) system as shown in figure (2) was built in laboratory and it consists from tungsten halogen photo optic lamp at 1000 Watt power. The as-prepared samples were introduced into quartz tube and the etched side was positioned directly above the halogen lamp .The quartz tube is open for allowing air to enter (dry oxygen source).

The (RTA) system as shown in figure (3) was also built in laboratory. The (RTA) system allows tungsten lamp annealing by swiftly raising the temperature to reache 750oC in 15 sec.It consists of a small vacuum chamber (quartz tub) pumped by an ordinary rotary pump (minimum pressure reached is about 10-2torr). Annealing is carried out by placing the sample (etching side) on the tube directly above the lamp .There is also a thermocouple placed at the end of the tube and attached to the surface of the sample. When the temperature reads 750oC, the power is turned off and sample is allowed to cool. Finally it is removed when the temperature reads room temperature.

 ISSN 1913-1844 E-ISSN 1913-1852

3. Results and Discussion

Figure (4) shows the dark current of PSi photodetector (before RTO and RTA processes) via preparation current density. We can see that the dark current decreased from (1660 μm/cm^2) at etching current density 10 mA/cm2 and reached to smaller value(1 μm/cm2) at etching current density 30 mA/cm^2, The decrease in dark current for four etching current density is due to decrease in thermally generated carriers so that the conductivity and dark current were reduced. We could observe the increase in dark current at etching current density 40 mA/cm^2. It could be caused by the defects or tunneling centers (M.Lee,Y.Wang and C.Chu. 1997).

We observed decreasing dark current with increasing etching current density after rapid thermal oxidation and rapid thermal annealing processes as shown in Fig (5), and at etching current density (40mA/cm2), the dark current varied from (2600-3) μm/cm2. That decrease is due to the increase of oxide thicknesses that reduce the tunneling probability of thermally generated carriers, so the dark current are reduce.

From figure (6) , We found that the photocurrent at preparation current density 10 mA/cm2 is higher than at 20,30 mA/cm2, that means that photocurrent decreases with increasing preparation current density because the increasing value of resistivity is due to increasing the psi layer thickness , but as shown in the same figure, there is increase in photocurrent at etching current 40 mA/cm2, This may due to the excessive etching process which leads to increase of porosity of the porous silicon layer and hence improve the sensitivity of the formed junction between the crystalline silicon and the Psi layer .

Figure (7) shows the current–voltage curve. Typical diode behavior can be seen. When illuminated with white light, the current for reverse bias of less than –1 V is increased about thirteen orders of magnitude demonstrating the high sensitivity of the photodetector(L. A. Balagurov, S. C. Bayliss, S. Y. Adrushin, A. F. Orlov, B. Unal, D. G. Yarkin, and E. A. 2001).

Generally the forward current shows presence of distinguish stable region .First region at low voltage (Vf < 1 volt), the recombination current is dominant, because the concentration of charge carriers is greater than the concentration of intrinsic (np > ni2), therefore for equilibrium case recombination process will take place, this means that each excitation electron from valance band to conduction band will recombine with a hole in valance bond. Second region at high voltage(Vf > 1volt) shows forward current increase exponentially with the applied voltage because the applied voltage exceeds the potential barrier .This voltage gives the electron enough energy to overcome the barrier height and that is what called diffusion current (V.A. Vikulov V.V. Korobtsov. 2009) .In the reverse bias , also there are two regions, one at low voltage, where the current increases with the applied voltage and the generated current is dominant. In the second region, the current is dependent on voltage and the diffusion current is dominant.

Figure (8) illustrates the measured sensitivity (R_λ) as a function of various incident wavelengths. From this figure (8) we can see that the spectral responsivity of structures measured in the wavelength range from (400-850) nm .We notice that the observed photo responsivity is shifted towards shorter wavelength in agreement with the assumption that the emission is related to quantum size effects (A.Akram. 2008). For longer wavelengths (700-900)nm, we can see that the value of responsivity decreased away from the responsivity top, that decrease in responsivity is attributed to the incident photon energy not being enough to generate electron –hole pairs (M.Lee,Y.Wang and C.Chu. 1997).

This large variation in the sensitivity with the incident photo energy is due to the variation in absorption depth which is a function of wavelength of the incident light , where the absorption of short wavelength occurs within the (Psi) layer and the large wavelength is absorbed at the interface of silicon and (Psi)(Svechnikov S.V., Kaganovich E.B., and Manoilv E.G, Semicond. 1998).

Figure (9) shows the X-ray diffraction of PSi at 30 mA/cm^2 etching current density. From this measurement, we can observe apparent new small peak at new diffraction angle, this may be attributed to new nanostructure which was different in morphology.

The morphological phase of nano (PSi) layer (crystalline or amorphous) will give good concept for electrical behavior of this material (P. Balk. 1965). The nanocrystallite size can be calculated by employing Scherer's formula as shown in the equation below:

$$L = \frac{0.9\lambda}{B\cos\theta_B}$$

Where L is the nanocrystallite size for PSi layer in (nm), λ is the wavelength in (nm) of employed radiation, B (radians) is the full width half maximum (FWHM), θ_B (radians) is the diffraction angle and 0.9 is the value of shape factor (B. D. Cullity. 1967).

The morphological properties of the porous silicon sample prepared at current 30mA/cm2 is shown in figure (10) .From this figure, we can see that the pore size varied from (0.1~1μm), while the average silicon sizes in the porous layer is less than (0.4 μm).

4. Conclusion

In this paper, the treatments of RTO and RTA processes have been used to enhance the photoresponsivity and reduce the dark current to(3 μA /cm2) at preparation current density (40 mA/cm2). The device is very stable and the reproducibility is good due to a stable surface on the PS layer and it can be concluded from I-V characteristic, of our devices which shows rectifying behavior.

The optimized RTA-RTO-PS photodetector has the performance of temperature 750°C (under 100 mW/cm illumination). A high response of 3 A/W can be obtained under a 5W (810 nm) laser diode illumination.

Acknowledgment

This work was supported and sponsored in part by the School of Applied Sciences/UOT/Baghdad-IRAQ.

References

A.Akram. (2008). Thesis, RTO effect on PS prepared by Stain Etching, Univ. Technology, Iraq, (2008).

B. D. Cullity. (1967). *Elements of X-Ray diffraction,* Addison-Wesley Publishing, Company, Inc. America, (1967).

L. A. Balagurov, S. C. Bayliss, S. Y. Adrushin, A. F. Orlov, B. Unal, D. G. Yarkin, and E. A. (2001). Petrova, Solidstate Electron. 4, 1607 (2001).

M. K. Lee, Y. H.Wang, and C. H.Chu. (1994). High-Sensitivity Porous Silicon Photodetectors Fabricated Through Rapid Thermal Oxidation and Rapid Thermal Annealing. *IEEE journal of quantum electronics,* VOL.33, NO 12, Decembr(1994).

M.Lee,Y.Wang and C.Chu. (1997). IEEE QE.33 (12)(1997)2199.

Ming-Kwei Lee. (1998). National Science Conuncil,Taiwan. METHOD TO IMPROVE THE SHORT CIRCUTE OF THE POROUS SILICON PHOTODETECTOR Mar. 13, 1998 .

Nobuyoshi Koshida and Hideki Koyama. (1992). Visible electroluminescence from porous silicon, *Appi. Phys. Lea.,*Vol. 60, pp. 347-349, Jan 1992.

O. Klima, P. Hlinomaz, A. Hospodkova, J. Oswald, and J. Kocka. (1993). *J. of Non-Cryst. Solids,* 961, pp. 164 ñ 166 (1993).

P. Balk. (1965). *The Electrochem. Soc. Meeting,* Buffalo, NY, Oct. 10-14, 1965.

P. Hlimonaz, O. Klima, A. Hospodkova, E. Hulicius, J. Oswald, E. Sipek, and J. Kocka. (1994). *Appl. Phys. Lett.,* 64, p. 3118 (1994).

Svechnikov S.V., Kaganovich E.B., and Manoilv E.G, Semicond. (1998). *Phys. Quan. & Optoelc.* 1, 1998,P.13

V.A. Vikulov V.V. Korobtsov. (2009). Thin Solid Films, Elsevier B.V. Elsevier B.V. 517, 3912–3915, 4 February, (2009).

Zhiliang Chen, Gijs Bosman and Romulo Ochoa. (1993). Visible light emission from heavily doped porous silicon homojunction pn diodes, *Appl. Phys. Lett.,* Vol. 62, pp.708-710, Feb 1993.

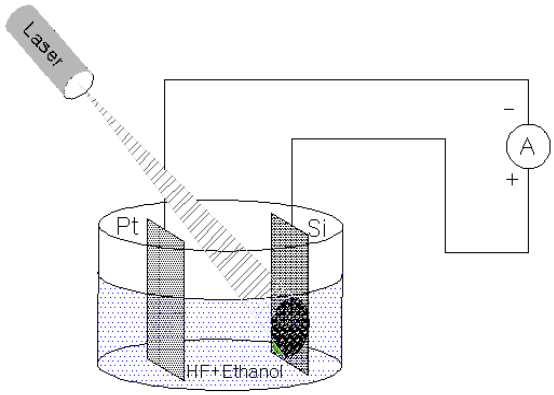

Figure 1. Schematic diagram of the photoelectochemical etching system

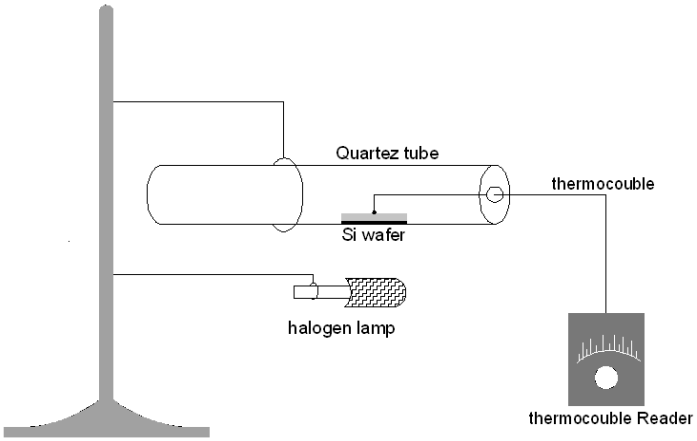

Figure 2. Schematic diagram of rapid thermal oxidation system

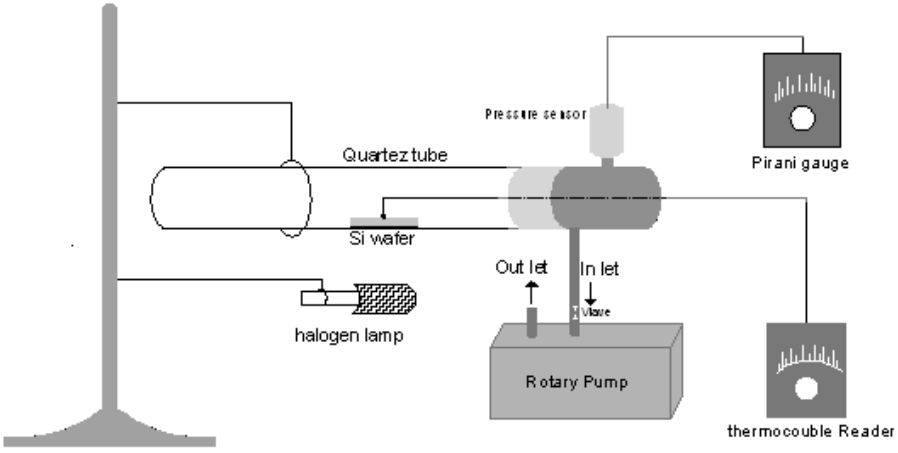

Figure 3. Schematic diagram of the rapid thermal annealing system

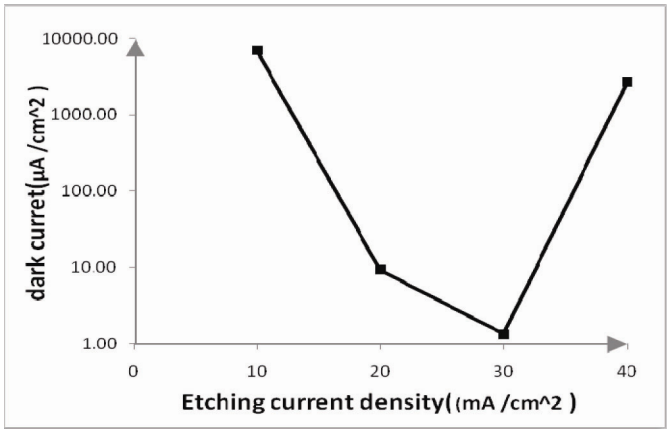

Figure 4. the dark current at different etching current density (10, 20, 30, 40 mA/cm^2) ,under reverse bias 5V

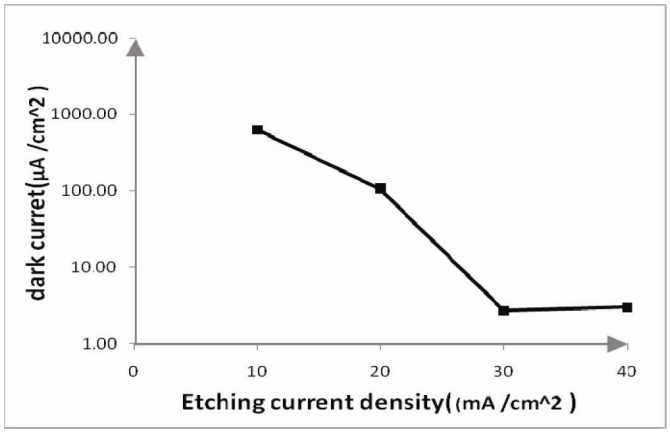

Figure 5. the dark current at different etching current density (10,20,30,40 mA/cm^2) , after RTO and RTA processes,(100 sec) and (15 sec) sequently, under reverse bias 5V

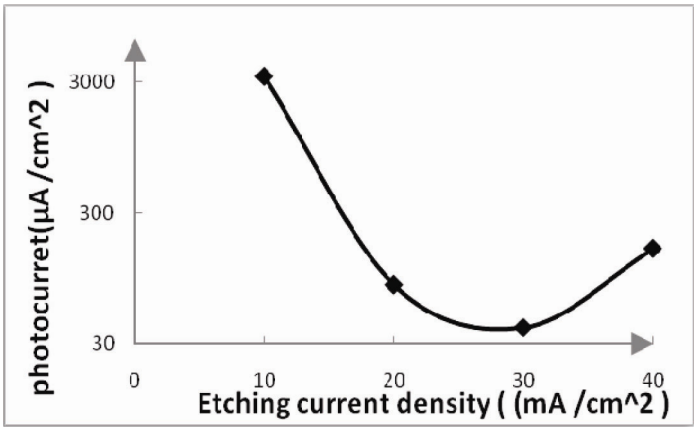

Figure 6. shows the variation of photo current as a function to the preparation current density at specific illumination power 200mW/cm^2

 ISSN 1913-1844 E-ISSN 1913-1852

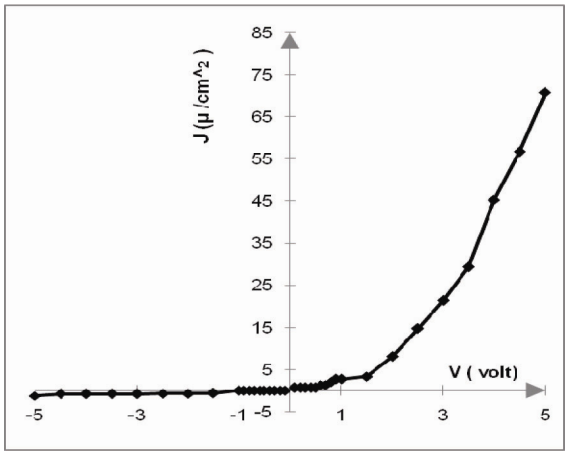

Figure 7. the (I – V) characteristics for (metal/nanostructure silicon /metal) photodiode at etching current density (30 mA/cm^2), under reverse bias 5V and illumination power 200 mW/ cm^2

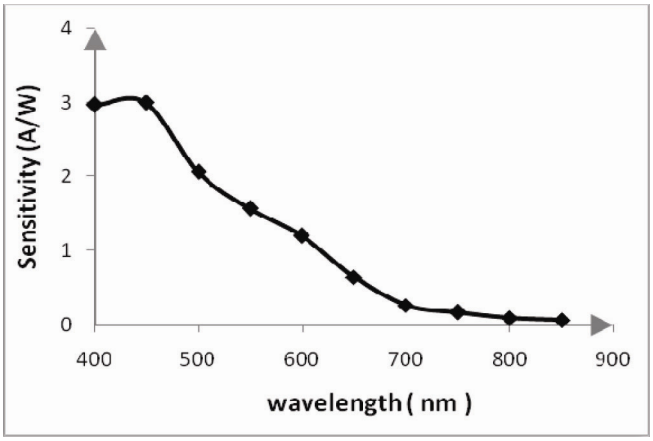

Figure 8. the sensitivity as a function of various wavelength (400-850)nm ,for Psi sample prepared at (30 mA/cm^2)

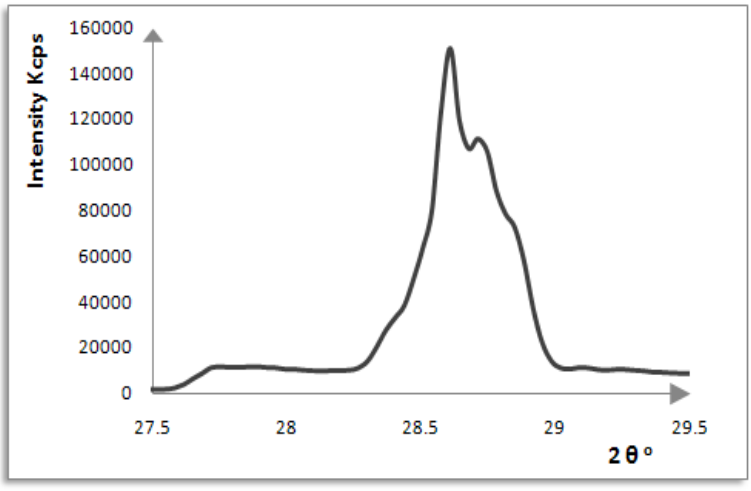

Figure 9. X-ray diffraction for porous silicon at 30 mA/cm^2 etching current density

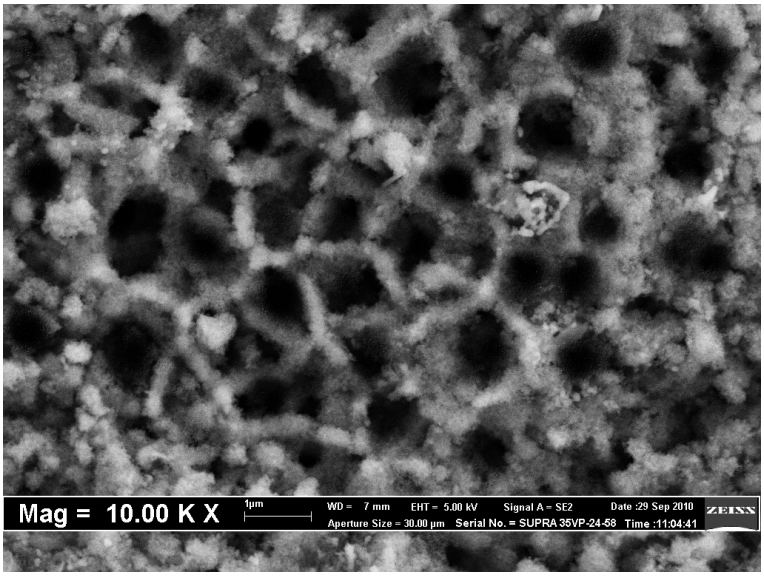

Figure 10. the SEM image of porous silicon sample prepared at etching current of (30 mA/cm^2)

ISSN 1913-1844 E-ISSN 1913-1852

Explore of Modern Family in the Waste Disposal Methods

Caifeng Chen
College of Mechanical Engineering, University of Shanghai for Science and Technology
516 Jun Gong Road, Shanghai 200093, China
Tel: 86-21-5527-0638 E-mail: chencaifeng@usst.edu.cn

Xinhua Wang
College of Mechanical Engineering, University of Shanghai for Science and Technology
516 Jun Gong Road, Shanghai 200093, China
Tel: 86-21-5527-3617 E-mail: wangxinhua@hotmail.com

Abstract

In this paper we proposed the development scheme of the modern family's kitchen waste processing machine combined with automatical crush, dewatering, drying, granulation and sterilization, and discussed the proper way of process to reduce, recycle and reuse the modern family's kitchen waste by analyzing the production condition, present process and processing technology.

Keywords: Kitchen waste, Crush, Dewater, Drying

1. Introduction

Shanghai, for example, the daily waste in shanghai is more than million tons, and increases by 10% according to statistics. The cook waste accounts for 40% of the total. There are about 7 million families in Shanghai, every family produces the cook waste more about 1.5~2kg, the daily waste in shanghai is more about 1200 tons accordingly, the family is the main source of the city's waste. For the big population, fast urbanization and high comprehensive handling charges in China, it is imperative to control the cook waste from the source and realize "reduce no harm resource".

The kitchen waste is produced easily rotten wastes by family. The common components are food remainder, waste oils and greases, dishes vegetable leaves and leftovers for fruit peel organic waste etc. The Characteristics of the cook waste is oily and wet, rotten easily, nutrient, and with existence of the virus and pathogens microorganisms, it is difficult to the collect, transport and handle. Some waste disposal facilities have been used at home and family, they are mainly mechanical facilities (principle of rapid speed and crystal), heat facilities (Heat carbonization principle) and biological facilities (Bacteria groom principle) etc. The equipment exists some problem or inconvenience in use so that they might be promoted difficultly.

(1) Mechanical equipment: This is suspended at the bottom of the kitchen sink, and the cook rubbish goes from the bottom of the kitchen sink into the downfall container, finally drain away the downfall rubbish from the water pipe, but this rubbish is easily clogged in the water pipe, and it is easy to gather dirt, to distribute smells and breed insects in the inside wall of downfall warehouse. The sink is easier to shape and it may lead to leakage and blow out the electrical motor.

(2) Heating equipment: A processing time is very long, and usually continues two to four hours. It also consumes large electricity and stores difficultly; it is going to wash by hand the oil of the cook rubbish and then put the waste broken or filter water by hand before drying, and finally dries it. It is inconvenient and even has some cumbersome.

(3) Biological device the user needs displace the bacteria regularly, it not only displaces difficultly but also biological bacteria easily make the user fear. Its price is also too high to go into average homes of the city.

therefore, the article proposes the scheme of the automation process equipment for the cook rubbish of modern urban families Integrating with downfall, dehydrated, drying and making particles, disinfection and storage (abbreviation for the kitchen waste processor), it can automatically process the domestic food waste safely and conveniently, and after handling they turn into dry Powder or particles and are turned into raw materials of organic and feed to realize the purpose of "reduce no harm resource" for cook rubbish.

2. The Structure design of the cook rubbish processor

2.1 Design requires

Based on the situation of about 1.5~2 kg made by the daily waste in shanghai and the requirements for high efficiency and low energy consumption, the technological requirements for the remainder processor is that the processing waste for a time is 1.0 kg, the smash cavity is 2.5 L, the volume of microwave drying Cavity is 3.5 L, the volume of the storage for drying material is 5 L, for 5. The drinking water for a time is Less than or equals 7L, the electricity consumption for a time is Less than or equals 0.5 degrees, and a single processing time is Less

than or equals 45 minutes.

2.2 Overall structure design

The waste processor consists of three parts and four devices. The three parts are smash mechanism, dewater and mechanism for delivering material and mechanism for drying up and making particles. The four devices are the washing and reverse rushing device with the high pressure mist and water, the sensing device of temperature and humidity, device for drying and disinfecting with microwave and purification device for waste fumes.

2.3 Smash mechanism

The highest hardness for the remainder is poultry bones and teeth; we usually impact them with the hammer for pieces fully, as shown in figure 2. It is equipped with fix teeth and crystal knife plate with multiple functions in the downfall cavity and it is equipped with two moving hammer on the crystal knife plate. The remainders go to the downfall room from the entrance; the spinning knife plate driven by the motor turns the two moving hammer and fix teeth into spinning knife groups. The rubbish is broken into pieces by the joint action of compressing, impacting, grinding, splitting, and cutting and then drains by the crystal force of the teeth and goes into dewater mechanism from channels.

2.3.1 Structural design of the Centrifugal plate

The centrifugal knife plate is the key components of the smash mechanism as shown in figure 2. The requirements for it are resisting to corrosion and high hardness, strength and stiffness, so we choose Martensitic stainless steel material, the diameter of the centrifugal knife plate is 120 mm referring to the structural dimension of the kitchen sink on test.

2.3.2 Force analysis for the centrifugal knife plate and the determination of power

Based on the actual applied load of the centrifugal knife plate, we idealize the knife plate to the cardboard rotating by the central axis. There are fluid resistance, resistance when breaking the waste (cut, tear and wear) resistance and fluid pressure.

(1) Fluid resistance F_1: According to the following formula, calculate the moment-of-fluid resistance on the centrifugal knife plate:

$$M = 3.87R^3 + \frac{1}{2}\rho\mu\sqrt{(\gamma / u_1 R)^{\frac{1}{2}}}$$

In the formula above, viscosity γ =0.01cm/s, fluid density ρ = 1.0x103kg/m3, Poisson ratio μ=0.5N/m, radius of the centrifugal knife plate R = 0.06m, line speed u1 =ωR, angular velocity angel Speed ω = 2πn/60rad/s, rotating speed of the Crushing motor n= 2800r/min, Calculation: the moment-of-fluid resistance M = 0.12N.m, so fluid resistance F1 = 2 N.

(2) Resistance from the waste F_2: Through testing on the common poultry bones and scraps from the waste, work out the biggest resistance by testing F_2 = 11.5N.

(3) Fluid pressure F_3: In formula, the fluid depth h is 150 mm, fluid pressure q can be calculated, q =ρgh =1.0x103x9.8x0.15 = 1470 N/m^2, so fluid pressure $F_3 = qA = q\pi R^2$ = 1470xπx0.06^2 =16.6 N.

(4) The overall resistance to overcome F: $F = F_1 + F_2 + F_3$ = 2 + 11.5 + 16.6 =30.1 N

(5) Determining power of downfall electrical motor P_w

When the downfall knife plate working, the resistance to overcome is F, rotating speed of the centrifugal knife plate n= 2800 r/min, so line speed V =15.5 m/s, so the working power of knife plate $P_w = FV$ = 468 W.

2.4 Dehydration and delivering material mechanism

The mature method for processing kitchen waste utilizes comprehensively comminuting and suppressing and dehydrating and dry technology. The machine chooses a spiral squeezing mechanism to divide solid and liquid for squeezing continuously, the design adopts a small power electrical motor (25w motor of dehydration), and it rotates at a low speed and has low energy consumption and noise reduction.

The spiral squeezing mechanism is shown as in figure 3, it consists of the cylinder shell and rotating shaft. It is fitted with a filter net in the cylinder shell. The spiral blade pushes the material from the feed holes to the export. Since the entrance volume of spiral shaft and shell is reduced gradually, the materials are squeezed, the liquid is drained through the filter hole, and then the solid materials go to the drying mechanism from the hole of draining material.

2.5 Dry, mixture and particle made mechanism

The volume of the mechanism is so big that it is placed at the bottom of the machine to ensure stability of the whole machine and., as shown in figure 1, the structure of the mixture axis is shown in figure 3, the blade is welded in the stir bar, the process is better to mix fully in drying up under high temperature and materials are heated uniformly. The heat way by microwave can ensure the disinfection effectiveness.

3. Process automatically in the cook waste

In the test, after placing the remainder in the downfall cavity, press down “run” key, the device will start

automatically and end after 45 minutes. The whole process as the following:

1) Empty food waste into the smash cavity;

2) Wash away food grease with high pressure misty water;

3) Drain grease to drainage;

4) Grid food waste by injecting water;

5) Deliver particles and dewater by centrifugal force;

5) Drain waste gas to drainage;

7) Dry and grid materials and deliver automatically;

8) Wash out cavity and drain water;

9) Store materials to storage box;

4. Conclusion

The cost of the development programme for the kitchen waste processor in the article is about half of that of biological processor, and convenient in using and compact in structure. The drying grainy can be turned into the raw materials for organic fertilizer and feed, thus reduce environment pollution and threaten of the kitchen waste and produce good social significance.

Acknowledgment

This work is supported by Shanghai Leading Academic Discipline Project, Project Number: J50503.

References

Zhang, Xianhui, Zhang, Bo & Yi, Xiaohong. (2005). Discussion on Method of food wastes Disposal. *Environmental Science and Mangement.* 2006(2) 141~142.

Wang, Xianhui, Li,Guangwei, Meng, Hong & Zhao Guojue. (2005). Discussion on Treatment Status of Food Residue. *Enviornmental Sanitation Engineering.*2005(4). 41~43.

Zeng, Qigao. (2008). Design of Control System for Remainder Processor Based on the PLC. *Electrical and mechanical engineering technology*. 2008(12). 28~29.

Zhang, Xinhui, Zhang, bo & Yi, xiaohang. (2006). Explore for handling the cook rubbish. *Environmental science and manage*. 2006 (2).

Song sixin. (2006). Design and study for moving components of smash processor based on adams and ansys. *Beijing university of chemical journal*. 2006 (5).

Xin, Xiaomu. (2008). Cleaner Production and Analysis of Urban Domestic Waste treatmenys. *Journal of meteorology and environmen*t. 2008(4). 50~53.

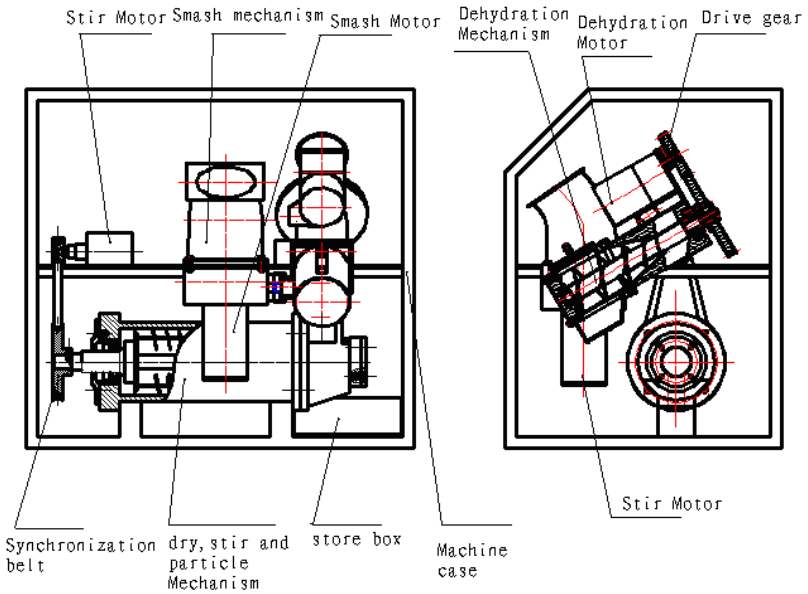

Figure 1. Diagram of internal structure layout

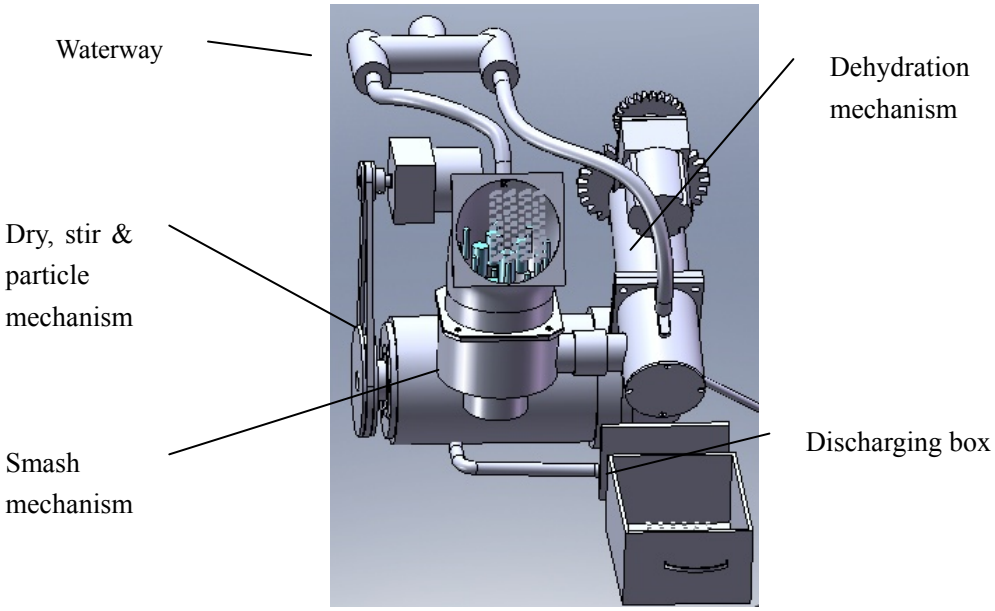

Figure 2. 3d graphics of internal structure layout

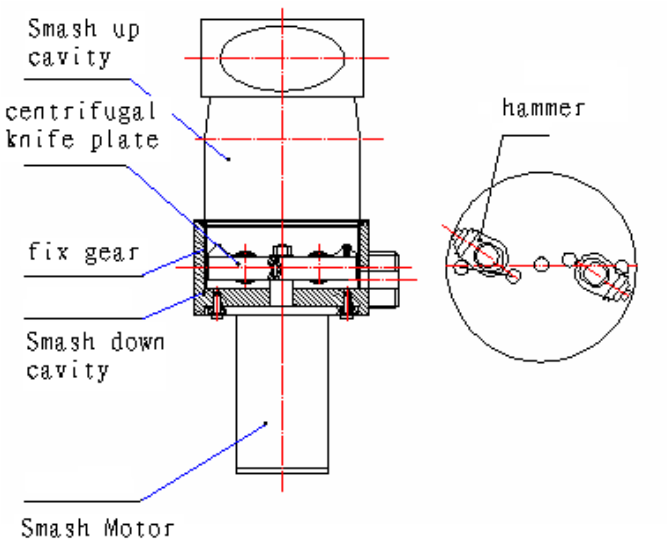

Figure 3. Diagram of the comminuting mechanism

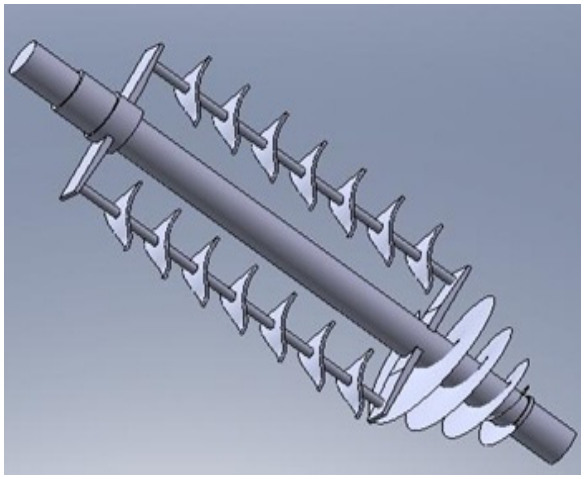

Figure 4. Diagram of the stir shaft

ISSN 1913-1844 E-ISSN 1913-1852

Enhanced Spectral Utilization of 3G WCDMA-Based FDD Mode in the Uplink Transmission

Joseph Isabona
Department of Basic Sciences, Benson Idahosa University
PMB. 1100, Benin City, Benin, Nigeria
Tel: 23-4-703-918-1006 E-mail: josabone@yahoo.com

Moses Ekpenyong
Department of Computer Science, University of Uyo
PMB. 1017 520003, Uyo, Akwa Ibom State, Nigeria
Tel: 23-4-803-793-3961 E-mail: ekpenyong_moses@yahoo.com, mosesekpenyong@gmail.com

Samuel Azi
Department of Physics, University of Benin
PMB. 1100, Benin City, Benin, Nigeria
Tel: 23-4-803-239-5000 E-mail: ugochukwuazi@gmail.com

Abstract

The economic value on network capacity has made it a major determinant in the design of any generation of mobile technologies. For any multi-user cellular system, the measure of its economic usefulness is the peak load that can be supported within a given quality and service (QoS) availability. In this paper, we improve upon the existing Wideband Code Division Multiple Access (WCDMA) user capacity expressions in single and multi cell environments for the uplink, by integrating new parameters that affect the system. Specifically, we study and report the effect of multi-user detection and adaptive antenna gain on WCDMA users' capacity in the presence of loading, voice activity, sectorization, power control factor and bandwidth efficiency.

Keywords: Multiuser detection, Adaptive antenna gain, Network capacity, WCDMA, QoS

1. Introduction

Recently, the telecommunication industries have witnessed a phenomenal growth in the development and deployment of wireless services. This is evident from the proliferation of cellular data services and emerging wireless multimedia applications. This proliferation has opened up new research avenues and calls for the re-examination of some fundamental issues in wireless cellular networks. One major fundamental issue to address is the provision of higher capacity cellular systems with guaranteed QoS to meet its daily service demands for both commercial and residential subscribers. Although the second generation (2G) wireless systems such as the Global System for Mobile Communications (GSM) and IS-95, are successful in many countries (Jin and Yu-Dong, 2003), they still do not meet the requirement of high speed data and user capacity in densely populated areas.

Higher system capacity, better QoS and flexible accommodation of diverse wideband services such as video and multimedia services with different transmission rates are required in third generation (3G) wireless communication systems (Kim and Adachi, 2001). Code Division Multiple Access (CDMA) has been chosen as the radio interface technology for 3G systems (IEEE Comm. Magazine, 1999), unlike Frequency Division Multiple Access (FDMA) and Time Division Multiple Access (TDMA), which primarily are either bandwidth or dimension limited in capacity (Gilhousen, Jacobs, Padovani, Viterbi, Weaver and Wheatley, 1991). Some benefits offered by this technology include high data rates, universal and low-cost terminals, global standard, seamless roaming and interoperability. The technology is used in Ultra High Frequency (UHF) cellular phone systems within 800MHz – 1.9GHz frequency range.

Contrary to FDMA and TDMA systems, the main limiting factor for capacity expansion in WCDMA system is the interference (De Sousa, De Lima, Rodrigues, Cavalcanti and Braga, 2003). Each user acts as an interference source to other users in the system. As such, a reduction in interference will directly increase the capacity.

Emerging technologies such as directional adaptive antenna, rake receivers, and multi-user detection, could lead to a significant reduction in the interference and result in many fold capacity increase (Tse and Hanly, 1999, Ammer, 2004, Amitava and Saha, 2004). Capacity estimation is therefore an important element in the design of CDMA systems and in the performance evaluation of emerging technologies.

Several attempts at formulating, modeling and evaluating capacity equations for WCDMA cellular networks have been made. In CDMA performance evaluations, the user capacity is used to measure the CDMA system, with continuously active users (Kim and Honig, 2000). By user capacity, we refer to the number of users a CDMA system can support at a desired signal-to-noise ratio (SNR) satisfying certain conditions (Alma, 2008). In Gilhousen *et. al* (1991), the CDMA uplink user capacity is estimated considering voice traffic only, where strength-based power control (Xia, Shroff and Chong, 2001, Isabona and Ekpenyong, 2009, El-Osery and Abdullah, 2000) is assumed and the total other-cell interference, I_{other}, is modeled as a Gaussian noise. I_{other} increases with the number of active users per cell, K, which decreases the SNR. The effect of rake receiver and antenna diversity on reverse link user capacity is presented in Kim and Adachi (2001), where the received signals at different antenna groups are assumed to be independent of each other. Also, modification and throughput optimization of WCDMA capacity equations are studied in Alma (2008), Ekpenyong, Isabona and Akpaeti (2009). However despite its advantages, there still remain challenges (complexities associated with detection and degradation in performance) in the design of WCDMA receivers, arising from Multiple Access Interference (MAI), which limits the system's capacity.

In this paper, we modify the existing WCDMA capacity expressions for the uplink transmission, integrating more parameters, which affect its operations. A closed-form equation relating multi-antenna gain, multi-user detection, power factor, sectorization factor, voice activity factor, bandwidth efficiency factor, target SNR and CDMA processing gain is presented and studied through extensive computer simulation to estimate the uplink user capacity.

2. System Model for Uplink Capacity

The capacity of a CDMA cell is determined by the balance between the required signal-to-noise-ratio (SNR) for each user, and the spread spectrum processing gain. The notation that determines the merit of a well-designed digital receiver is the dimensionless SNR given in equation (1):

$$\frac{\varepsilon_b}{N_0} \equiv \frac{Energy\ per\ bit}{Power\ spectral\ density\ noise + Interference} \tag{1}$$

The "noise" part of the SNR in a spectrum system is actually the sum of the thermal noise and the other-user Interference. The energy-per-bit, ε_b is related to the signal power P_r, and data rate, R_b as given in equation (2):

$$\varepsilon_b = \frac{P_r}{R_b} \tag{2}$$

The noise-power spectral density, N_0, is the ratio of the total interference power, I to the transmission bandwidth W, as expressed in equation (3):

$$N_0 = \frac{I}{W} \tag{3}$$

Given the above relations, the bit-energy-to-noise density can be rewritten as:

$$\varepsilon_b \big/ N_0 = \left(\frac{P_r}{F}\right)\left(\frac{W}{R_b}\right) \tag{4}$$

where the ratio $\frac{W}{R_b}$ indicates the processing gain of the system.

Let us consider a single cell load with K users that are in power control with the base station. Following the derivation in Garg and Johnson (2000), the total interference power for user i, is composed of the received signal power P_{rj} from all users in the cell:

$$I = \sum_{j=1, j\neq i}^{K} \frac{P_{ri}}{W} + N_{th} \tag{5}$$

where N_{th} is the thermal noise. If the power of signals of all active users have the same value, equation (5) simplifies to

$$I = \frac{(K-1)P_r}{W} + N_{th} \tag{6}$$

Substituting equation (6) into (4), the ε_b / N_0 on the uplink, allotted to an arbitrary user is

$$\frac{\varepsilon_b}{N_o} = \frac{W}{R} \cdot \frac{P_r}{N_{th}W + (K-1)P_s} \tag{7}$$

Ignoring the thermal noise N_{th} and solving for K in equation (7), yields the network capacity (number of users) in the system

$$K = 1 + \frac{PG}{\varepsilon_b / N_0} \tag{8}$$

where $PG = W/R$.

Equation (8), which defines the number of simultaneous active users, is the basis for the WCDMA capacity. If we take into account the background thermal noise N_{th} over the full bandwidth N_0W (see equation (7)), then the number of active users is reduced by the inverse of the signal-to-noise-ratio (SNR) in the total system bandwidth. Thus

$$K = 1 + \frac{PG}{\varepsilon_b / N_0} - \frac{N_{th}W}{P_r} \tag{9}$$

3. Impact of Different Parameters on the Capacity Model

The analysis takes into account a number of capacity influencing factors such as loading factor, sectorization, voice activity factor, power factor and the effect of intra and inter interference. This paper does not explicitly address modulation techniques and their performance; rather, it assumes an efficient modulation and forward error correcting coding for given channels under established conditions, which the receiver achieves an acceptable level of performance, particularly in terms of the maximum number of users supported per cell.

3.1 Loading

Equation (9) is an effective model that describes the number of active users a single WCDMA cell can support, without any interference from neigbouring cells. To roughly include the effects from surrounding cells, we require the introduction of a loading factor η. This term indicates the increase in interference above the inverse of the factor (1 + η), known as the frequency reuse factor *F*. *F* is related to the loading factor η, by

$$F = \frac{1}{1+\eta} \tag{10}$$

For a single cell, the reuse factor is unity and the loading is zero. When multiple cells are considered, cell loading increases while *F* decreases. If we include the loading factor η from other cells, equation (7) becomes

$$\frac{\varepsilon_b}{N_0} = PG \frac{P_r}{N_{th}W + (K-1)P_r(1+\eta)} \tag{11}$$

Again, we can solve for K:

$$K = 1 + PG\left(\frac{1}{\varepsilon_b / N_0 (1+\eta)}\right) - \frac{N_{th}W}{P_r(1+\eta)} \tag{12}$$

with $W/R = PG$

3.2 Antenna sectorization

Let N_s represent the number of sectors in the cell-sector antenna. The use of sectorization and directional antennas could increase the capacity because it reduces interferences (Tse and Hanly, 1999). For instance, a cell site with three directional antennas, each having a perfect beam-width of 120^o, has interference which is one-third of the interference in the case of an omni-directional antenna.

3.3 Voice activity factor

CDMA use speech coding, reducing the rate of the speech coder with voice activity detection along with variable rate transmission, could decrease the multiple access interference. By employing a variable rate vocoding, the

system reduces the total interference power by the voice activity factor *v*. In Ammer (2004), the voice activity factor of human speech is approximately 42%.

3.4 Power factor

Because the performance of WCDMA system is interference limited, we require accurate power control (Suyeb, Jasvir and Mian, 2006, Ernestina, 2005). An increasing power control error will reduce the system's capacity. The value of the power control error will depend on the system implementation and on the algorithm used in the control. This could be defined using a log-normal distribution with suitable power correction factor α_p (Karimm and Sarraf, 2005). So, we modify equation (11) to account for the effect of the voice activity factor, *v*, power factor, α_p and antenna sectorization, N_s, to have

$$\frac{\varepsilon_b}{N_0} = \frac{N_s \alpha_p}{v} \frac{PG}{(K-1)(1+\eta) + \frac{N_{th}W}{P_r}} \tag{13}$$

We then extract a parametric formula for the capacity, thus

$$K = \frac{N_s \alpha_p}{v}\left[\frac{PG}{\varepsilon_b / N_0 (1+\eta)}\right] - \frac{N_{th}W}{P_r(1+\eta)} + 1 \tag{14}$$

3.5 Bandwidth efficiency factor

The bandwidth efficiency factor β_F is introduced here because the individual users in a cell do not necessarily take the entire frequency band available to the system. Thus, if there are *K* users inside the cell, which are homogeneously distributed over the frequency carriers of the cell, the number of users of the same frequency band is K/β_F and the number of interferers from the cell is given by

$$\frac{K}{\beta_F} - 1 \tag{15}$$

This transforms equation (13) into

$$\frac{\varepsilon_b}{N_0} = \frac{N_s \alpha_p}{v} \frac{PG}{\left(\frac{K}{\beta_F} - 1\right)(1+\eta) + \frac{N_{th}W}{P_r}} \tag{16}$$

Taking into account the bandwidth efficiency factor, β_F with other capacity enhancement parameters, we obtain an expression for K:

$$K = \beta_F\left[1 + \frac{PG}{\varepsilon_b / N_0}\left(\frac{1}{1+\eta}\right)\frac{\alpha_p N_s}{v}\right] - \frac{N_{th}W}{P_r(1+\eta)} \tag{17}$$

We are interested in equations (8), (9), (12), (13) and (17).

4. The Impact of More Capacity Improvement Parameters on WCDMA Capacity Model

The use of various interference elimination methods could increase system capacity. Some of the methods include use of directional antenna processing system, rake receivers, multi-user detection, etc.

4.1 Adaptive antenna

Interference due to other users can be reduced by replacing an omni-directional antenna with a directional antenna. For instance, a cell site with three directional antennas, each having a perfect beam-width of 120^o has interference which is one-third of the interference in an omni-directional antenna (Alma, 2008). Use of adaptive (multi) antenna system with the above assumptions will increase the WCDMA capacity, so the parameter A_d, which describes antenna gain of referent users to antenna gain of its jammers ratio could be input directly into equation (16). We now modify equation (17) as another suggested expression to show the impact of the usage of multi antenna system (A_d) on the overall capacity, thus

$$K = \frac{B_r A_d \alpha_p N_s}{V_f}\left[PG\left(\frac{1}{\varepsilon_b / N_0 (1+\eta)}\right)\right] - \frac{N_0 W}{\Pr(1+\eta)} + 1 \tag{18}$$

A_d could be easily related with the number of antenna elements B, as

$$a_b[dB] = 10\log B$$

where a_b is the antenna gain expressed in dB.

4.2 Multi-user Detection (MUD)

A major technological difficulty in CDMA systems is the 'near far' problem (i.e. strong signal swamping weaker signal) and Multiple Access Interference (MAI). MUD provides a means of reducing the effect of multiple interference and hence increases the system's capacity. The optimum multi-user detector for asynchronous multiple access Gaussian channels is obtained in Ammer (2004), where the 'near far' problem suffered by the convectional CDMA receiver, accounts for the presence of other interference in the channel. Thus

$$\frac{\varepsilon_b}{N_0}\frac{PG}{(1-\beta)I_{Intra} + I_{Inter} + \frac{N_{th}W}{P_r}} \tag{19}$$

where β denotes the capacity enhancement parameter of the multi-user detection technique. We assume here that the multi-user receiver accepts only those users (Intra-cell users) whose interference the MUD has cancelled. This implies that in a practical system, the capacity will be limited by the efficiency of the algorithm and the inter-cell interference. If Intra cell interference I_{Intra} is taken to be $(K-1)P_r$, equation (19) yields

$$\frac{\varepsilon_b}{N_0} = \frac{PGP_r}{(1-\beta)(K-1)P + I_{Inter-cell} + N_{th}} \tag{20}$$

The Inter-cell interference is proportional to Intra-cell interference by the relation

$$Inter = \eta Intra = \left(\frac{1}{F} - 1\right)Intra \tag{21}$$

Substituting equation (21) into (20), we have

$$\varepsilon_b \Big/ N_0 = \frac{PGP_r}{(1-\beta)(K-1)P_r + \left(\frac{1}{F}-1\right)(K-1)P_r + N_{th}W} \tag{22}$$

since $I_{Intra} = (K-1)P_r$.

From equation (22), the uplink network capacity to meet required ε_b / N_0 becomes

$$K = \frac{\frac{\beta_F N_S \alpha_P}{V}\left[1 + PG\left(\frac{1}{\varepsilon_b / N_0(1+\eta)}\right)\right] - \frac{\beta_F N_{th}W}{P_r(1+\eta)}}{(1+\beta) + (\frac{1}{F} - 1)} \tag{23}$$

4.3 Capacity gain

An analytical capacity gain estimation with multi-user detection is derived in this section. The total noise level spectral density N_0 at the base station generated by thermal noise N_{th} of all interferers from inside the cell I_{Intra} plus noise generated by all interferers from outside the I_{Intra} is

$$\begin{aligned} N_0 &= N_{th} + I_{Intra} + I_{Inter} \\ &= (1+\eta)Intra + N_0 \end{aligned} \tag{24}$$

The noise-rise is defined as the ratio of the total noise level spectral density to the thermal noise:

$$Noise\,rise = \frac{N_0}{N_{th}} \tag{25}$$

The wideband interference after MUD can be written as

$$N_{0(total,MUD)} = (1+\eta-\beta)I_{Intra} + N_{th} \tag{26}$$

where we assume that *MUD* is able to cancel part of the intra-cell interference I_{Intra}. The cancelled part is denoted by

$$\beta \quad = MUD\ efficiency \tag{27}$$

When evaluating the capacity gain, we assume that the mobile transmission power remains constant, i.e. the coverage of the cell is not affected. This requires that the interference power after multi-user detection, $N_{0(total,MUD)}$ remains the same as without multi-user detection $N_{0(total)}$.

$$N_{0(total,MUD)} = N_{0(total)} \tag{28}$$

The capacity gain can be obtained using equations (23) and (25)

$$(1+\eta-\beta) \bullet Capcity\ gain \bullet I_{Intra} + N_{th} = (1+\eta)I_{Intra} + N_{th} \tag{29}$$

Solving equation (29) yields the capacity gain:

$$Capacity\ gain = \frac{1+\eta}{1+\eta-\beta} \tag{30}$$

4.4 Coverage gain

The coverage gain is evaluated with the assumption that the number of active users remains constant, i.e. the capacity of the cell is not affected. The coverage gain is defined as the decrease in the active user output power, which alternatively could be used to extend the cell range. The noise power $N_{0(total,MUD)}$ after MUD is derived as follows

$$N_{0(total,MUD)} = (1+\eta-\beta)\frac{I_{Intra}}{Coverage\ gain} + N_{th} \tag{31}$$

The coverage gain is equal to the reduction in the noise power after MUD:

$$Coverage\ gain = \frac{N_{0(total)}}{N_{0(total,MUD)}}$$

$$Coverage\ gain = \frac{(1+\eta).I_{Intra} + N_{th}}{(1+\eta-\beta).\frac{I_{Intra}}{Coverage\ gain} + N_{th}} \tag{32}$$

$$Coverage\ gain = \frac{(1+\eta).\frac{I_{Intra}}{N_{th}} + 1}{(1+\eta+\beta).\frac{1}{Coverage\ gain} \bullet \frac{I_{Intra}}{N_{th}} + 1}$$

Merging equations (24) and (25) gives

$$\frac{I_{Intra}}{N_{th}} = \frac{Noise\ rise - 1}{1+\eta} \tag{33}$$

Solving for *Coverage gain* using equations (32) and (33) gives

$$Coverage\ gain = 1 + \frac{\beta(Noise\ rise - 1)}{1+\eta} \tag{34}$$

5. System Performance and Discussion of Result

Empirical data used for simulating the impact on WCDMA capacity, including its system design parameters are shown in Table 1. Some of these values have been used in Alma (2008), Isabona (2008), Isabona and Ekpenyong (2009), to obtain a fairly improved performance. The empirical data were gathered from real life simulation experiments using well established conditions.

Fig. 1 illustrates how number of active users varies with the signal-to-noise ratio (SNR), in the presence of other parameters. When we isolate other parameters and consider the impact of processing gain and the SNR on the system, the system supports only 11 users at ε_b / N_0 = 9dB for voice applications, without any performance effecting parameter. Due to the loading factor on desired users by neighbouring cells, the capacity of the system degrades to about 5 users. After the introduction of induced capacity enhancement parameters such as sectorization, voice activity factor, power control factor and adaptive antenna gain, the system performance improves, thus supporting 15, 17, 21 and 25 users, with all the enhancement parameters. Also, with power and bandwidth efficiency factors, the system supports 12 and 14 users respectively. The improvement in system performance with adaptive antenna leads other parameters (see Fig. 1.). The improvement in SNR is about 3dB with two antenna elements, 6dB with four elements, 8dB with six elements and 9dB with eight elements. Obviously, the implementation of multi-antenna system will reduce the average interference level from all users particularly, so the total channel capacity increases.

The expression in equation (17) could also be applied when comparing values of WCDMA capacity depending on SNR of the different antenna gain ratio. This is shown in Fig. 2. Therefore, for a desired SNR of 9 or 6dB (for a BPSK or QPSK with coherent detection), the number of simultaneously active users for one service is 20 for A_d=2.5, for instance.

Fig. 3 shows the users capacity enhancement with and without MUD. A comparison of the combined effects of various parameters with the capacity enhancement MUD technique (β) in multi cell environments is shown in Fig. 4. This technique minimizes the multiple access interference and increases the performance up to 22 users per cell, considering same set of parameters in Fig. 3. To study the impact of different operations scenario, different multi-user detection factor is assumed to represent different multi-path propagation. The effect is shown in Fig. 4. We observe in Fig. 4 that, when MUD is increased, more users can access the same channel bandwidth simultaneously. This is represented using equation (23).

Assuming a MUD factor of 60% and typical macro cellular other-to-own cell interference ratio of 0.65, we obtain a capacity gain of 65%. The capacity gain as a function of efficiency is shown in Fig. 5. In a micro cellular environment, the cells tend to have a higher isolation, making other-to-own cell interference ratio smaller. With a cell interference ratio of 0.3, and assuming a MUD of 70%, a capacity gain of 80% is obtained in micro cellular environments.

The coverage gain as a function of the initial noise rise is shown in Fig. 6, assuming a MUD factor of 65% and other-to-own cell interference ratio of 0.65. The coverage gain of the MUD receiver improves the coverage from 1.2dB to 2dB. This is shown in Fig. 7. Here a link level improvement of 1dB can be used to increase the cell area by 15%.

Capacity is related to the spectral efficiency (SE) of a system, as well as the amount of traffic offered by each user. The spectral efficiency (Hosham, Salim and Hessein, 2008) is given by

$$SE = Network\ capacity \times (\Pr oces \sin g\ gain)^{-1}[{}^{(b/s)}\!/\!_{(Hz)}] \tag{35}$$

From the results shown in Fig. 8, it is clearly observed that the various capacity enhancement parameters have potentially increased the spectral efficiency. We attribute this to the reduced interference, which allows the users to operate at higher rate.

6. Conclusion and Outlook

Enhanced spectral utilization allows the maximum number of users with adequate signal strength in a CDMA cell. This paper has modified the basic expression of WCDMA capacity with elements that impact significantly on it. A modified expression for WCDMA computation has been proposed. The use of multi antenna (adaptive) system and multi user detection as methods for increasing the system capacity are strongly recommended as promising solutions for future generation mobile communication systems (for both macro and micro cellular environments) to provide improved system performance and dependable quality of service to both residential and commercial subscribers (or end-to-end users).

So far, our CDMA system capacity modeling optimization approach considers the various parameters such as MUD, adaptive antenna, etc., which constitute the main features of the physical layer. We also assumed efficient coding and modulation. In reality, however, time varying channel conditions could cause the propagated signal to fluctuate at some degree. Though this can be resolved through efficient coding and modulation methods, is beyond the scope of this paper and is slated for a future paper.

References

Alma, S. R. (2008). The Modification of WCDM Capacity equation. 16th Telecommunication Forum, Telfor. 266 – 269.

Amitava, M. and Saha, D. (2004). Approaches for Radio Resource Management in Mobile Wireless Networks: Current Status and Future Issues. Technical reports (University of New South Wales. School of Computer Science and Engineering); UNSW-CSE-0404.

Ammer, C. (2004) Multiuser Detection Techniques for UMTS. *Bechtel Telecommunication Journal.* 2(2): 1-2.

De Sousa, V. A., De Lima, C. H. M, Rodrigues E. B, Cavalcanti F. R. P and Braga A. R. (2003): Coverage and Capacity of WCDMA Systems with Beam and Steering Antenna. Vehicular Technology Conference, VTC – 2003 Fall, 2:826 – 830.

Ekpenyong, M., Isabona J., and Akpaeti, A. (2009): Robust Modelling and Throughout Optimization in CDMA Networks. *Journal of Applied Science and Engineering Technology.* 3: 5-12.

El-Osery A, and Abdullah C. (2000). Distributed Power Control in CDMA Cellular Systems. *IEEE Antennas and Propagation Magazine.* 42(4): 152-159.

Ernestina, C. (2005) Spread Spectrum Technique and Their Applications to Wireless Communications. *IETE Journal of Research,* 15(1): 5-18.

Garg V. K. and Johnson K. U. (2000). IS-95 CDMA and CDMA 2000. Upper saddle Rius. NJ Prentice Hall.

Gilhousen K S., Jacobs, I. M., Padovani, R. Viterbi, A. J., Weaver, L. A. and Wheatley, C. E. (1991): On the capacity of a cellular CDMA System. IEEE Transactions on Vehicular Technologies. 40(2): 303 – 312.

Hosham S. S. and Hessein B. (2008). Performance Enhancement of GSM Cellular Phone Network using Dynamic Frequency Hopping, *Engineering and Technology.* 26(3): 365 – 375.

IEEE Communication Magazine (1999). Special Issue on Wideband Code Division Multiple Access WCDMA 36.

Isabona J. (2008). Transmit Power Control in Multimedia CDMA Cellular System. M.Sc. Thesis, University of Uyo, Nigeria.

Isabona, J. and Ekpenyong, M. (2009) Performance Evaluation of Coverage Capacity Interaction in CDMA Wireless Networks. *Journal of the Nigerian Mathematical Society.* 28: 153 – 167.

Jin Y. and Yu-Dong Y. (2003). Reverse Link Capacity of SIR-based Power Controlled CDMA Systems with Antenna Arrays. *Wireless Communications and Mobile Computing.* 3: 759-772.

Karim M. R. and Sarraf, M. (2002). W-CDMA and CDMA 2000 for 3G Mobile Networks, McGraw-Hill, New York.

Kim D. K. and Adachi F. (2001) Theoretical analysis of reverse link capacity of an SIR-based power-controlled cellular system in a multipath fading environment. *IEEE Transactions on Vehicular Technologies.* 50(2): 452-464.

Kim J. B. and Honig M. L. (2000). Resource Allocation for multiple classes of DS – CDMA traffic. *IEEE Transaction on Vehicular Technologies.* 49(2): 506-519.

Suyeb A. K, Jasvir S. and Mian M. (2006): Capacity Analysis of WCDMA in forward Link FDD Mode System, 3rd IEEE Mobility Conference, organized by Rangsit University, Bangkok, Thailand, 25 – 27.

Tse D. N. C. and Hanly, S. V. (1999). Linear Multiuser Receivers, Effective Interference, Effective Bandwidth and User Capacity. *IEEE Transactions on Information Theory.* 45(2): 641 – 657.

Xia O. M., Shroff N. B. and Chong E. K. P. (2001). Resource Management in Power – Controlled Cellular *Wireless Communications and Mobile Computing.* 1(2): 185-199.

Table 1. Factors which impact on WCDMA capacity and its system design parameters.

Parameter	Empirical values
Correction factor of power control α_p	2.50
Voice activity factor, v	0.40
Frequency reuse factor, F_r	0.60
User data rate, R	64 Kbps
SNR (ε_b/N_0)	1-10 dB
Chip rate, W	3.84 Mcps
Capacity enhancement using MUD technique	0.20, 0.40, 0.60
Adaptive antenna gain, A_d	1.90
Loading factor, η	0.65
Sectorization gain, N_s	1.50

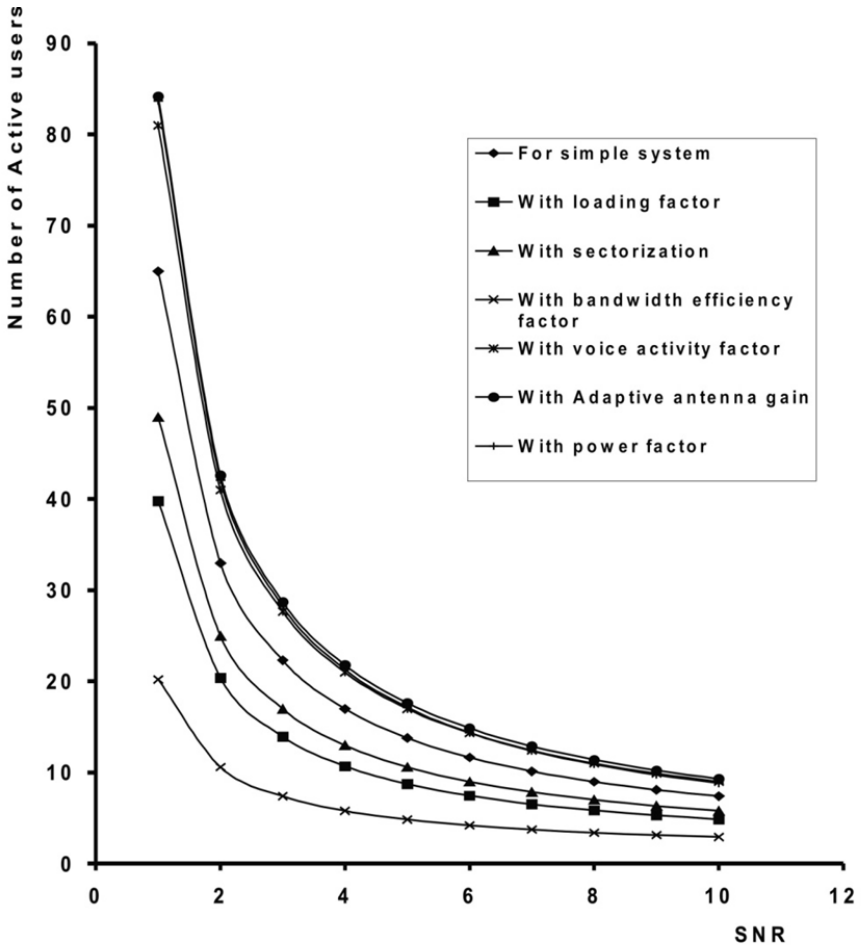

Figure 1. Effect of variable factor on users' capacity at varying SNR conditions

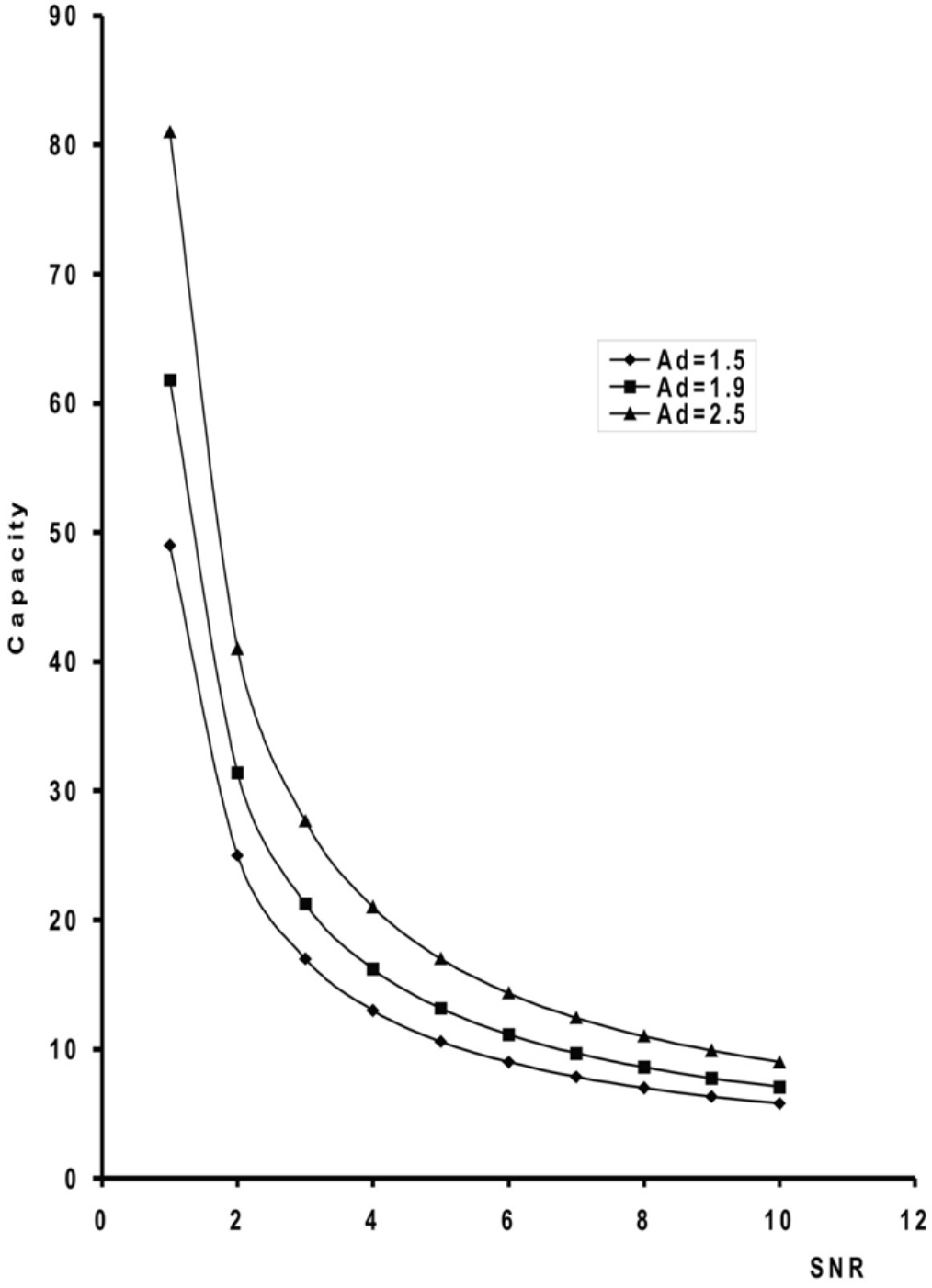

Figure 2. Comparison of different values of adaptive antenna gain (Ad) factor for voice applications on number of active users with varying SNR conditions

 ISSN 1913-1844 E-ISSN 1913-1852

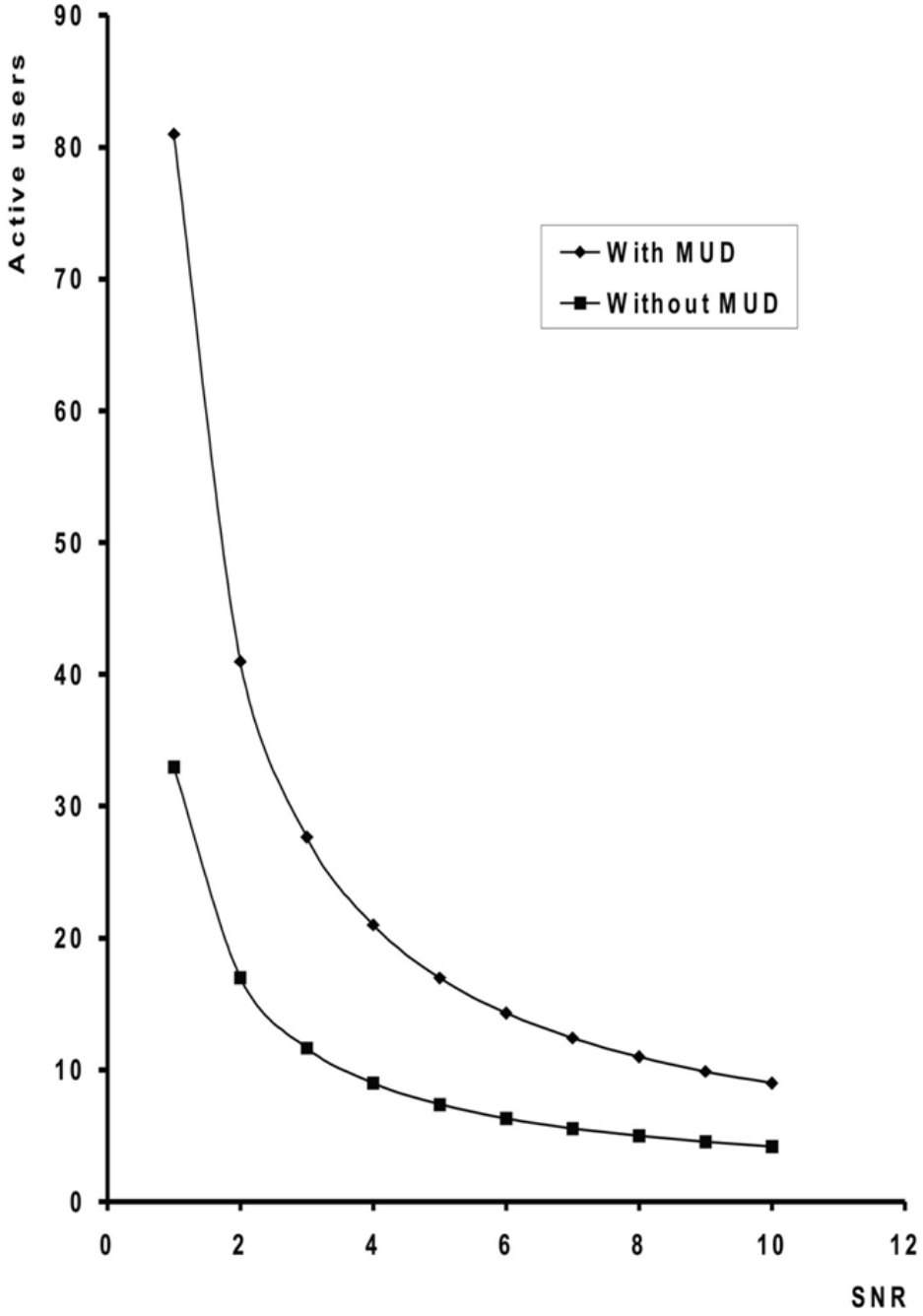

Figure 3. Effect of MUD on system capacity at varying SNR conditions for voice applications

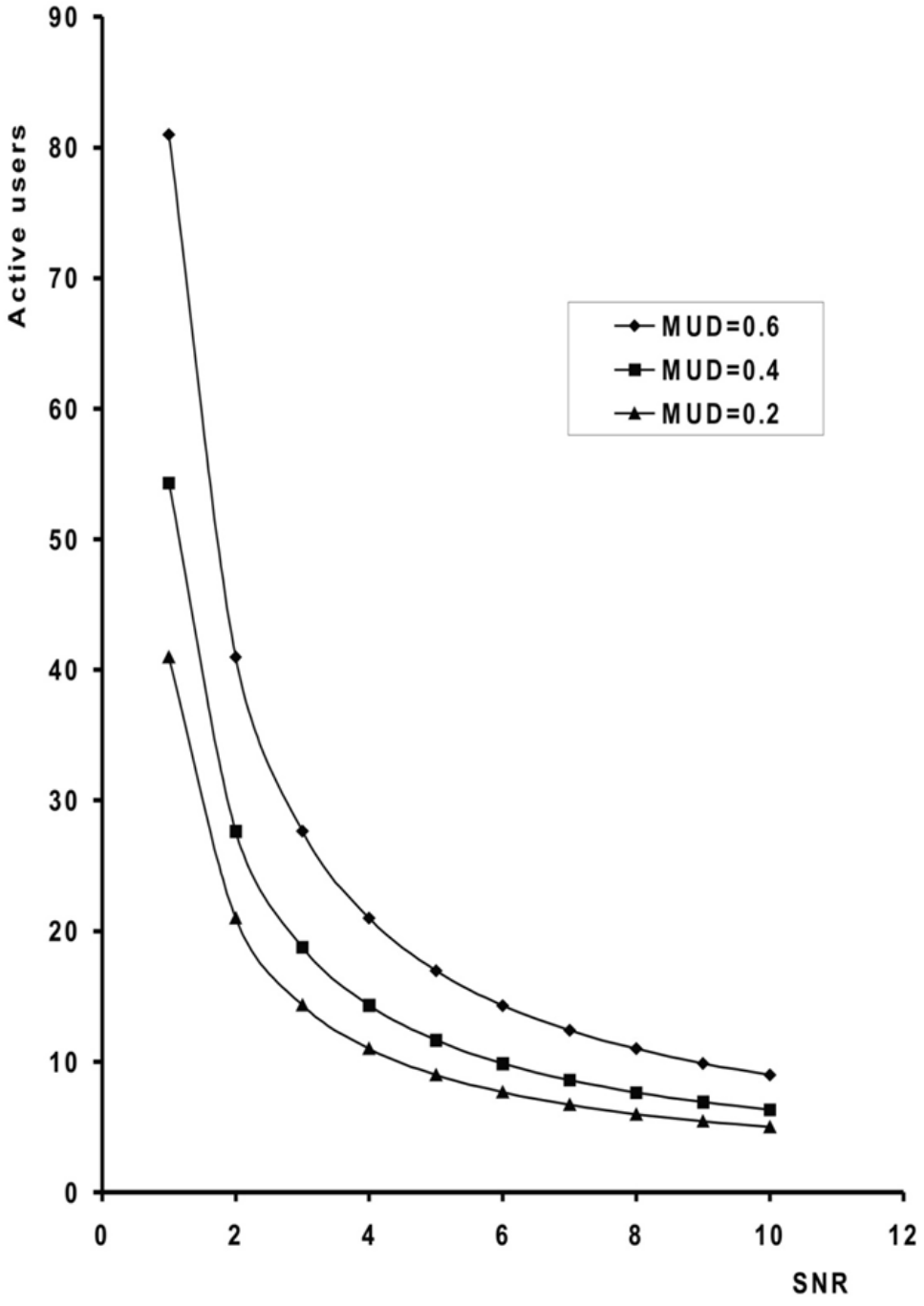

Figure 4. Comparison of different values of MUD factor with voice applications on number of active users with varying conditions of SNR

 ISSN 1913-1844 E-ISSN 1913-1852

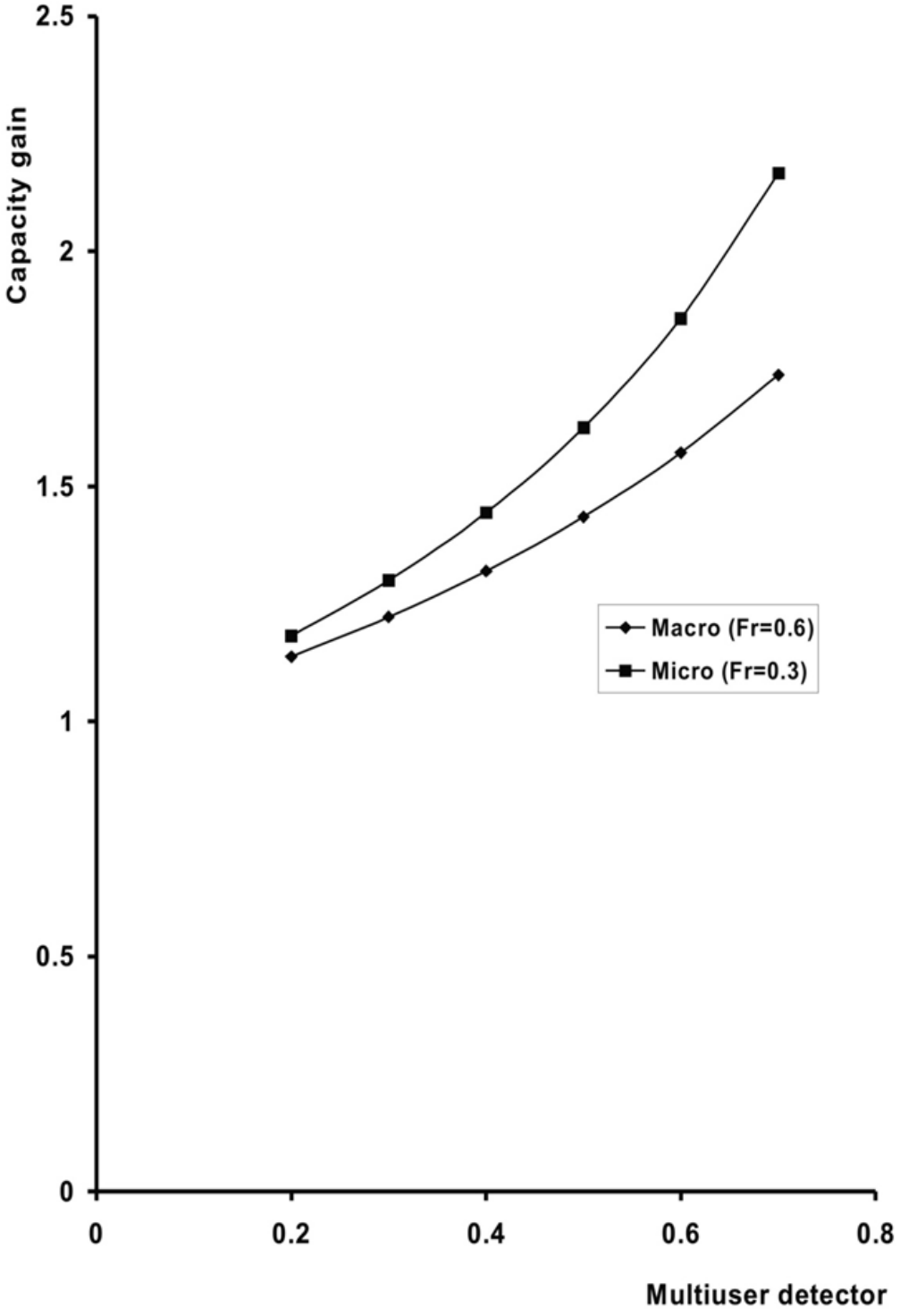

Figure 5. capacity gain with MUD for micro and macro cellular environments

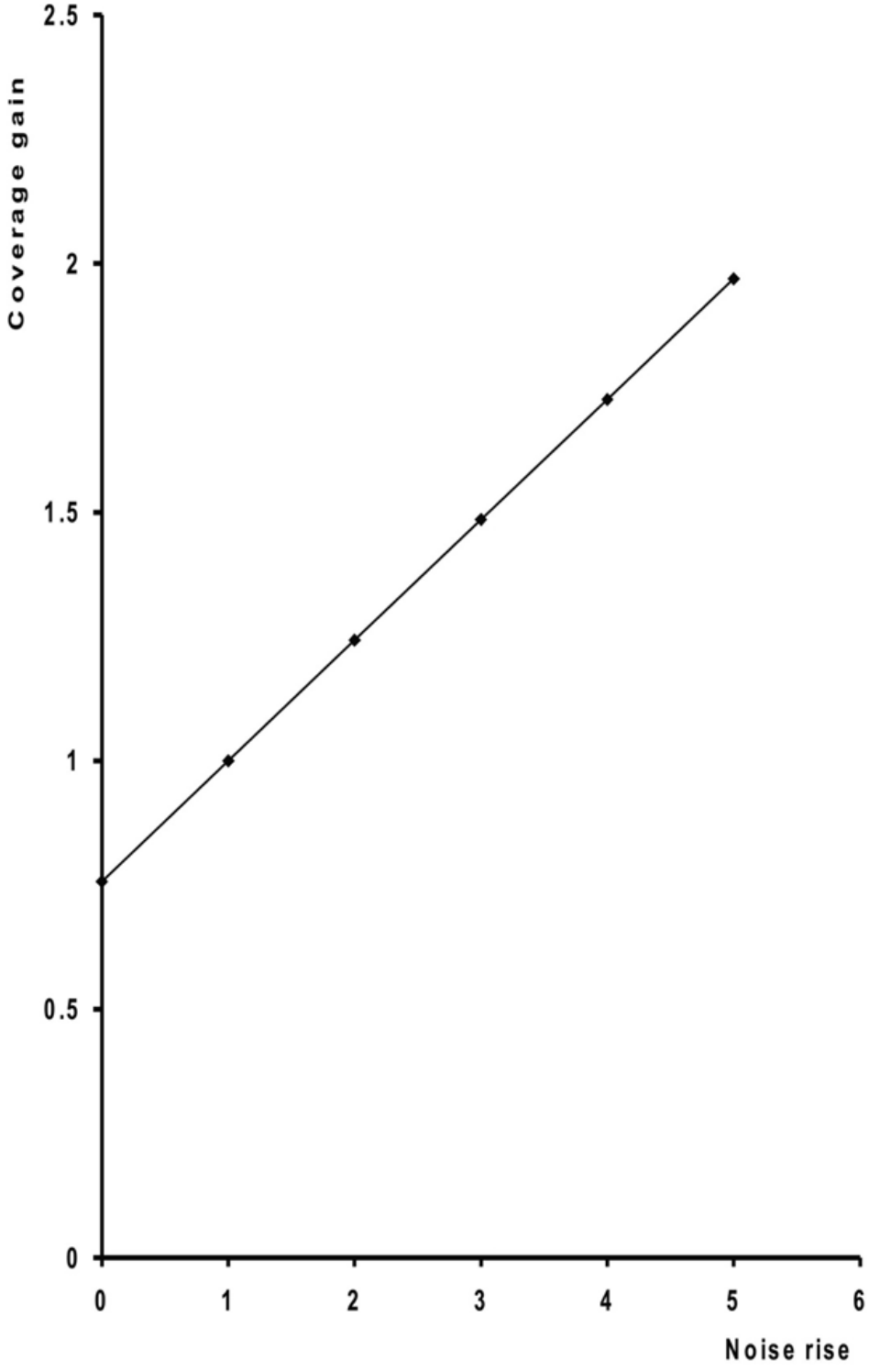

Figure 6. Coverage gain as a function of noise rise

 ISSN 1913-1844 E-ISSN 1913-1852

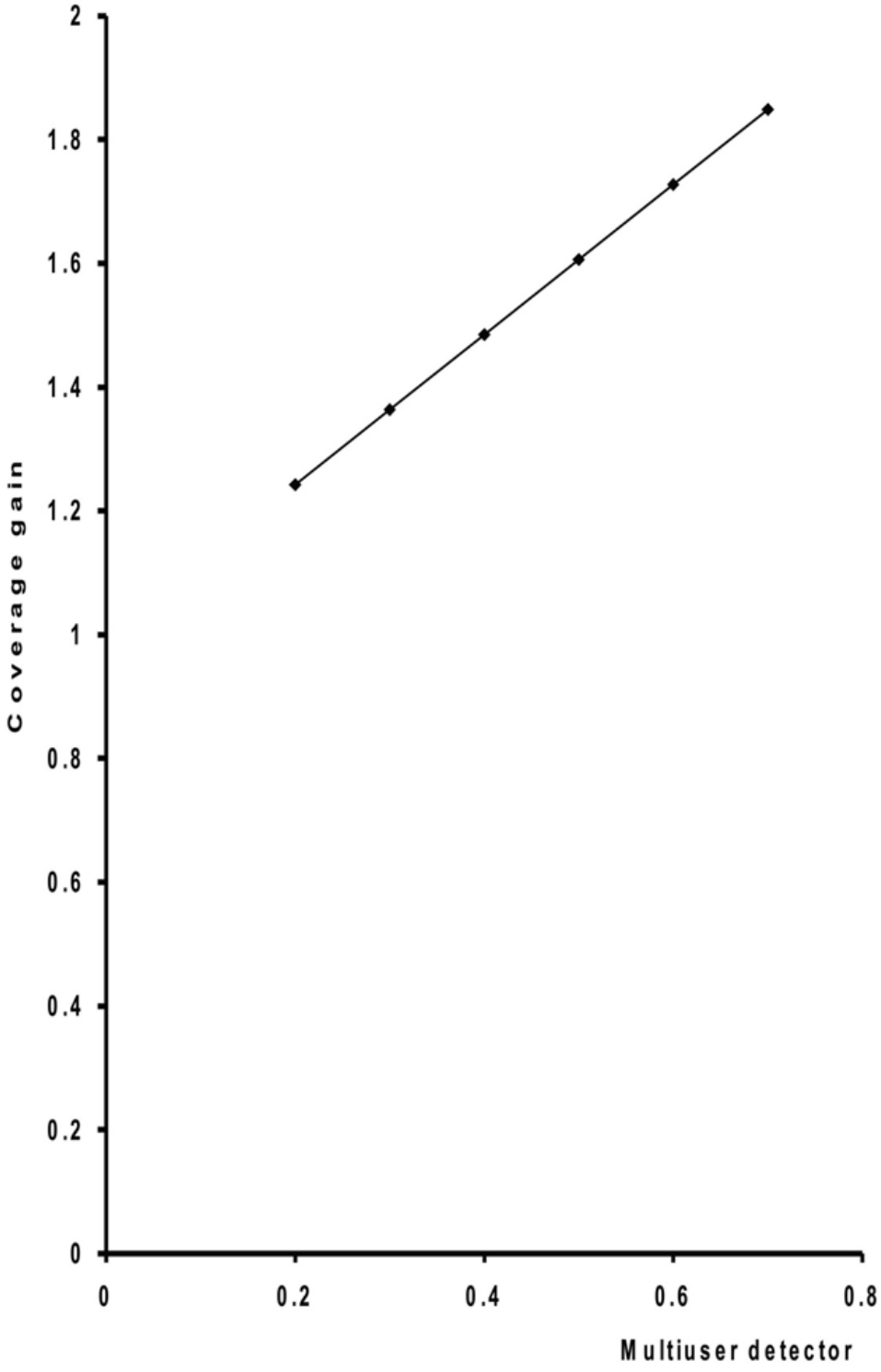

Figure 7. Coverage gain as a function of MUD

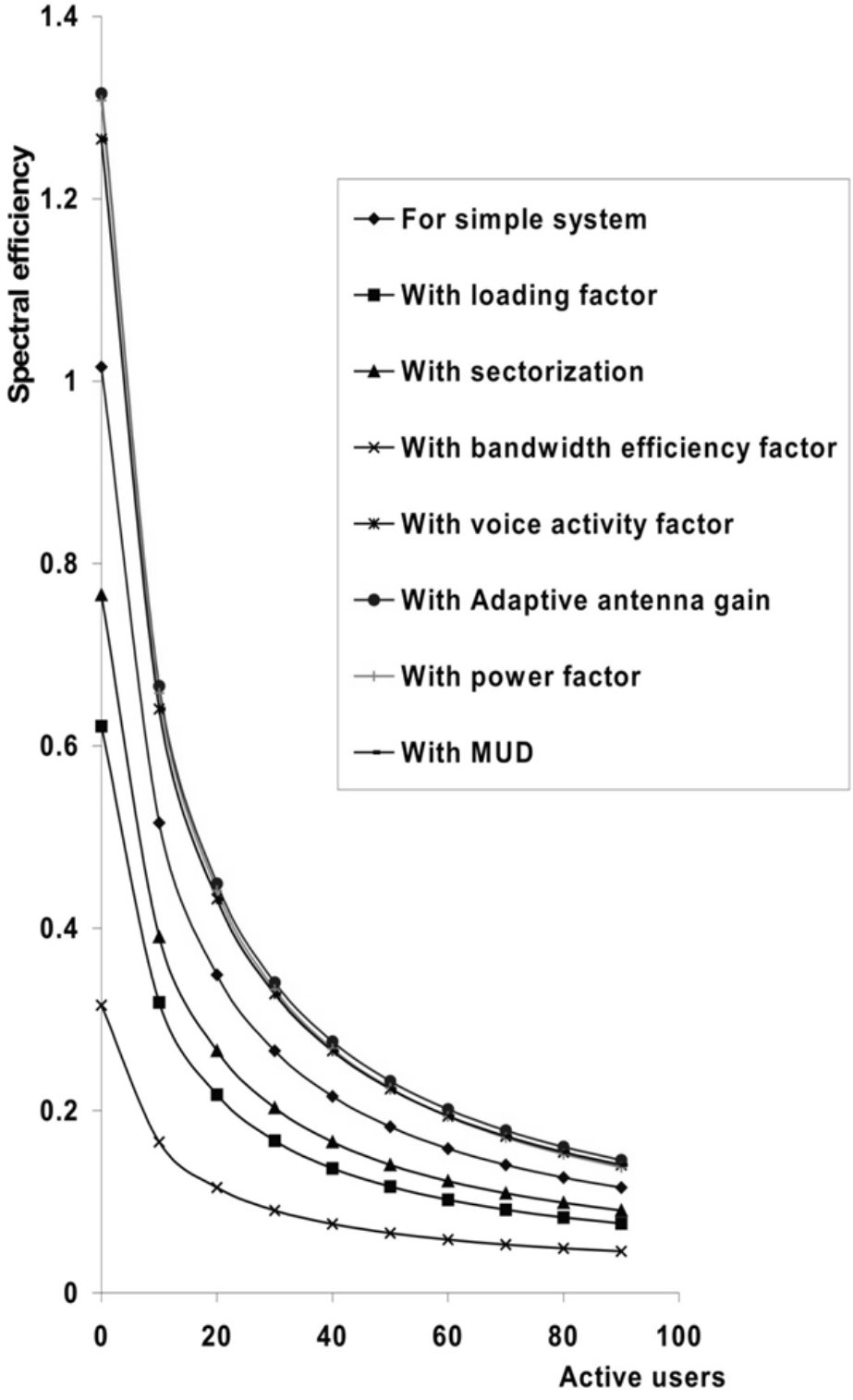

Figure 8. Spectral efficiency as a function of number of active users

 ISSN 1913-1844 E-ISSN 1913-1852

Theoretical Foundation for Energy Structure Adjustment

Zhiquan Wu
School of Energy & Power Engineering
North China Electric Power University, Beijing, China
&
China National Water Resources & Electric Power Materials & Equipment Co., Ltd
Beijing, China
Tel: 86-10-5196-1658 E-mail:zhiquanwu@tom.com

Shaoxiang Zhou, Liansuo An, Guoqing Shen & Hailin Shi
School of Energy & Power Engineering
North China Electric Power University, Beijing, China
Tel: 86-10-6177-2825 E-mail: zxs@ncepu.edu.cn

The research is supported by the 'Study on the Beijing Energy Saving and Emission Reduction Support System Based on Energy Saving Potentials' of the special funds of Beijing Co-construction.

Abstract

Application of unit fuel consumption has been explored deeply based on the second law analysis of thermodynamics to meet the strategy demand of optimizing energy structure adjustment. Theory of unit consumption analysis has been used in this paper to explore the theoretical foundation of energy structure adjustment. It has been proved that value of fuel exergy varies when two fuel exergy assessment methods are used separately. It can be obtained that coal utilization corresponds to the lowest second law efficiency while H_2 or CH_4 the highest according to the calculations. Thus, to increase the percentage of natural gas in regional energy consumption will lead to higher regional second law efficiency. And theoretical energy saving potential can be obtained from the departure of practical unit fuel consumption (UFC) to theoretical UFC.

Keywords: Energy structure, Energy utilization efficiency, Evaluate, Theory of unit fuel consumption, Fuel exergy

1. Introduction

About 90% of the world energy supplies are provided by fossil fuels, with the associated emissions causing local, regional, and global environmental problems. Long-term projections indicate that world energy demand may increase dramatically, with most of this increase taking place in developing countries, while fossil fuels reserves are limited and gradually decreasing because of the enormous energy consumption in economic growth and social development. This has been reported previously (Marc and Ibrahim, 2001, pp.3-13; GUO, Chai and XI, 2008, pp.38-43). In addition, other energy resources like nuclear energy and renewable energy account for less than 10% of the total energy consumption in the world, although lots of measurements have been carried out to prompt research and application of these energy resources. To solve these problems, researchers suggest more concern and devotion on how to improve energy utilization efficiency for social sustainability.

Zaltu and Arif (2007, pp.1-29) reported that energy structure and its supply modes exert great influence on the efficiency of energy resource utilization. Energy structure is among key factors influencing energy utilization efficiency. Obviously, to adjust the energy structure and its supply modes will be an efficient and effective way to improve the efficiency of energy resource utilization. So the theoretical foundation for adjusting energy structure will be studied here.

Exergy analysis is a key tool in evaluating the efficiency of energy resource utilization, and has been widely used by researchers in assessing how efficiently energy is used in sectors, local, regional systems, discussed previously (Wall, 1990, pp.435-444). Then, what will happen if exergy analysis is adopted in studying the effectiveness that energy structure and its supply modes is used to evaluate the exergy utilization efficiency of

regional system? Here, the foundation of adjusting energy structure and its supply modes will be studied.

2. Exergy and Exergy analysis

Exergy is defined as the maximum amount of work that can be produced by a system or a flow of matter or energy as it comes to equilibrium with a reference environment. Exergy is a measure of the potential of the system or flow to cause change, as a consequence of not being completely in stable equilibrium relative to the reference environment. Unlike energy, exergy is not subject to a conservation law. Rather exergy is consumed or destroyed, due to irreversibilities in any real process. Bejan et al. (1996,pp.71-90) reported that the exergy consumption during a process is proportional to the entropy created due to irreversibilities associated with the process.

The second law of thermodynamics, i.e., exergy analysis, takes the entropy portion into consideration by including irreversibilities. It's a method that uses the conservation of mass and conservation of energy principles together with the second law of thermodynamics for the analysis, design and improvement of energy and other systems. During the past decades, exergy related studies have received tremendous amount of attention from various disciplines ranging from chemical engineering to mechanical engineering, from environmental engineering to ecology and so on, discussed by Ibrahim (2002,pp.137-149). The exergy method is useful for improving the efficiency of energy resource use, for it quantifies the locations, types, and magnitudes of wastes and losses. In general, more meaningful efficiencies are evaluated with exergy analysis identifies accurately the margin available to design more efficient energy systems by reducing inefficiencies. Many engineers and scientists suggest that thermodynamic performance is best evaluated using exergy analysis because it provides more insights and is more useful in efficiency improvement efforts than energy analysis.

Exergy analysis has been used not only in assessing the energy resource efficiency of process and links in practical systems, which has been reported previously (Irfan, Nevin and Ibrahim 2010,pp.:451-460; Leyla, Arif and Ibrahim, 2007,pp.1185-1192; Samuel and Silvio, 2008,pp.153-162), but also of sectors and regional systems, because the latter combines micro thermodynamic and macro decision making and research about this gradually become a trend. Tens of countries have carried out energy resource efficiency evaluation researches based on exergy analysis for sectors, local and regional systems and society. The approaches used to analyze energy utilization of countries or societies may be grouped into three types, namely Reistad's approach, Wall's approach and Sciubba's approach, discussed in Zaltu and Arif (2007, pp.1-29). There are some differences when compared the three approaches.

3. Unit fuel consumption analysis of energy utilization and energy saving potential

Unit fuel consumption analysis (UFCA) proposed by Professor Song Zhi-ping (1992, pp.15-21), is a analysis method for energy system based on exergy and exergy economics. It belongs to exergy analysis. According to second law of thermodynamics, the exergy balance equation for any energy use process could be stated as follows:

$$B^s \cdot e_f = P \cdot e_p + \Sigma B_i \cdot e_f \tag{1}$$

where ef, ep stand separately for specific exergy of fuel and product, with unit kW·h/kg, P is product, Bs is standard coal consumption and ΣB_i is the sum of additional fuel consumption corresponding to exergy consumption of links in a process.

Apparently, (1) could be written as:

$$b = \frac{B^s}{P} = \frac{e_p}{e_f} + \frac{\Sigma B_i}{P} = b^{\min} + \Sigma b_i \tag{2}$$

$$b^{\min} = e_p / e_f \tag{3}$$

Where b_{min} is theoretical unit fuel consumption (TUFC) of a product, depending on natural qualities of a product not production process, Σb_i is the sum of additional unit fuel consumption, depending on production modes and flow path.

Second law efficiency (e.g., exergy efficiency) for energy use could be attained according to (1):

$$\eta_{ex} = \frac{P \cdot e_p}{B^s \cdot e_f} = \frac{e_p / e_f}{B^s / P} = \frac{b^{\min}}{b} \tag{4}$$

As is known, second law efficiency is the fundamental efficiency of energy use process. Equation (3) makes it possible for second law efficiency to apply statistics analysis, which is an important development for second law

analysis, more details referred to Zhou's (2008, pp.42-44; 2004,pp. 1219-1226).

According to (2) and (4), theoretical energy saving potential could be derived:

$$\Delta b_{\max} = b - b^{\min} \tag{5}$$

The value of theoretical energy saving potential makes it definitely to tell us what is the object we've devoted to, however, it doesn't mean it's easy to calculate this value. For example, the unit fuel consumption(UFC) of power supply for the most advanced 1000MW super-critical coal-fired generation sets so far is about 280 g/(kW·h), which means quantity of energy saving potential, compared to 122.9 g/(kW·h) which is the theoretical unit fuel consumption. Nevertheless, this potential is very hard to be excavated. Other generation systems like combined cycles and fuel cells should be integrated while to break through the present situation.

According to Statistics Express of China Electricity Council, the average UFC of electricity for electric networks is 342 g/(kW·h). It's easy to dig the real energy saving potential comparing with that of 1000MW super-critical coal-fired generation sets. The real energy saving potential is defined as the ratio of real unit fuel consumption to advanced UFC for product in the world:

$$\Delta b_{re} = b - b^{ad} \tag{6}$$

Song (1985, pp.399) reported that energy saving and emission reduction viewed from end product and its unit fuel consumption, explored the problem of establishing unified evaluation indicator system, which provided the foundation of energy saving potential analysis for energy-consumed devices, companies and region systems.

But there is still shortage in applying UFC based on end-use product aiming at energy structure adjustment, since theoretical energy saving potential calculated by (5) varies from different unit fuel exergy e_f in (4) and thus different b_{min}.

Scientific measures for adjusting energy structure could be presented only by comprehensively analyzing the basic theory and real energy saving potential, which will prompt national economic structure adjustment and low-carbon economy development.

4. Fuel exergy

Fuel exergy is the maximum work theoretically according to the definition in thermodynamics, and fuel exergy could be approximatively expressed:

$$e_f^0 = q_{h,f}^0 + T_0 \Delta s_R^0 + R_M T_0 \sum_{pr} \alpha_j \ln \frac{p_0}{p_{0j}} \tag{7}$$

Where subscript j stands for reactant except of fuels and resultants of standard reaction, pr stands for fuel combustion resultants, p_{0j} is sub-pressure of resultants in air. T_0, p_0 stand for air temperature and pressure in ambient condition separately, $q_{h,f}^0$ is gross heat of the fuel, Δs_R^0 is standard reaction entropy, which could be calculated:

$$\Delta s_R^0 = \sum_j \alpha_j s_j^0 \tag{8}$$

where s_j^0 is absolute entropy of resultants, referred to Wu's (2010, adopted). Table 1 listed basic thermal physics qualities of some pure fuels, from Zhou, Hu and Song (2006, pp:549-552).

There is much difficulty to precisely calculate fuel exergy because fuel exergy in (7) is derived under the assumptions of ideal gas, and the composition of real fuels varies and is much different from ideal gas. To simplify the calculation of fuel exergy, researcher Zoran Rant, from Slovenia, who firstly brought up the concept of exergy, suggested some ways to evaluate fuel exergy for gas, liquid and solid fuels according to the gross heat and low heat value of fuels.

$$e_f^0 = \begin{cases} 0.950\, q_{h,f}^0, & \text{for gas fuel} \\ 0.975\, q_{h,f}^0, & \text{for liquid fuel} \\ q_{l,f}^0 + r_{f,g} \cdot x, & \text{for solid fuel with moistue content x} \end{cases} \tag{9}$$

Where $r_{f,g}$ is latent heat of vaporization of water in ambient temperature.

Exergy is the capacity of work for working medium in thermodynamics, and electricity is the best quality of work and is considered as 100% exergy, thus there's much intuitive for converting fuel exergy to equivalent electricity.

$$e_f^e = \frac{e_f^0}{3600} \quad [\text{kW·h/kg}] \tag{10}$$

According to (4), the specific exergy of fuels vary because of different kinds of fuels, which means second law efficiency could be different. If high quality clean energy is used improperly, additional consumption will occur although its high thermal efficiency. For example, although the thermal efficiency (first law efficiency) of natural gas used in boiler is larger than normal coal-fired industrial boiler, in some area natural gas is directly used in heat supply for residents in winter, which results low efficiency. Moreover, wrong decisions which were unpractical and lacked long-term insight have been made during power industry development history. The reasons of making lapse are superficially resource and environment conditions, but the real and fundamental reason is that the evaluation of energy utilization efficiency is only carried out using the first law of thermodynamics, and the second law efficiency (4) is the nature respond to energy utilization. So far, thermal efficiency of energy utilization defined in nation regulation is based on the low heat value of standard coal, which ignores the difference of resource qualities could different energy efficiency. It means that the adjustment of energy structure lacked scientific theory guidance, and this should be changed as soon as possible.

5. Specific exergy and theoretical unit fuel consumption of electricity and heat

5.1 specific exergy of electricity and heat

Electricity and heat are mainly two modes of energy use, and almost each product would consume directly or indirectly these two energy. Here, only the specific exergy of electricity and heat are explored, those of other products could be determined by thermodynamics.

specific exergy of electricity:

$$e_p = 1 \quad [\text{kW·h/kW·h}] \tag{11}$$

For heat production, when average thermodynamics temperature of desired heat is $\overline{T}_h$, Zhou (2007) considered that the specific exergy could be:

$$e_p = (1 - \frac{T_0}{\overline{T}_h}) \quad [\text{kW·h/kW·h}_\text{h}] \tag{12}$$

Or,
$$e_p = 278(1 - \frac{T_0}{\overline{T}_h}) \quad [\text{kW·h/GJ}] \tag{12a}$$

where T_0 is ambient temperature.

5.2 Theoretical unit fuel consumption of electricity and heat

Thus, theoretical lowest UFC of standard coal, fuel oil and natural gas for electricity generation could be:

$$b_e^{\min} = e_p / e_f^e = 1 / e_f^e \quad [\text{kg/kW·h}] \tag{13}$$

If the fuels listed above are used to supply heat, the corresponding theoretical lowest UFC are:

$$b_h^{\min} = \frac{e_p}{e_f^e} = \frac{278}{e_f^e}(1 - \frac{T_0}{\overline{T}_h}) \quad [\text{kg/GJ}] \tag{14}$$

LHV is widely used in energy statistics in China, and therefore, all energy consumption should converted as low heat value (LHV) of fuels, and the theoretical lowest UFC of electricity generation and heat supply($b_e^{\min ce}$ and $b_h^{\min ce}$), based on LHV, would be equal to values from (13) and (14) times corresponding conversion factor to standard coal.

6. Analysis of fuel exergy

The theoretical lowest UFC of electricity generation and heat supply (other products are similar) is different because fuels used have different qualities. The higher qualities of fuels have, the lower of theoretical lowest UFC for a product is, according to (13) and (14). And in terms of (4), more scientific energy utilization technologies are needed to be developed in order to reach high second law efficiency.

For example, for fuel oil and natural gas, viewed from the second law efficiency, if these two kinds of fuel are used in electricity generation, gas-steam combined cycle or even fuel cell technology is needed in order to reach higher exergy efficiency; thus, it's an improper mode of energy use if these two kinds of fuel are directly used in heat supply.

Obviously, the second law efficiency analysis based on energy utilization is important in guiding theoretically energy structure adjustment and energy utilization efficiency improvement.

Nevertheless, the value of fuel exergy is very difficult to be calculated because of complex composition of practical fuels. For example, oil, which mainly consists of alkane, arene, alkene, cyclane, doesn't have molecular

formula. Even light oil products whose main components are pentane and hexane doesn't have molecular formula. Here, pure material fuels like H2, CH_4, C, and $C5H_{12}$, are chosen as examples in order to clearly understand fuel exergy and its impact on the second law of energy utilization.

Values of fuel exergy, corresponding gross heat, theoretical lowest UFC for electricity generation are obtained from (7) and listed in Table 2. In general, value of fuel exergy under atmospheric environment is higher than the gross heat value of the fuel except H2, which is probably connected with water assembly parameters, because only water has phase change and lead to big error when H2 is assumed to be ideal gas.

The fuel exergy for electricity generation is larger while the quality of fuel is higher if these pure material fuels are used to generate electricity, e.g. the number of fuel needed for power generation is less. Therefore, C is the fuel with the highest second law efficiency, others are less efficient. In other words, more advanced technologies are demanded in order to achieve more efficient energy utilization when other kinds of fuel are used. For example, the second law efficiency for oil-fired boiler than that of coal-fired boiler while the energy efficiency between these two kinds boiler is the same. The situation that fuel oil is widely used in other fields gives a big attack in its application in power generation less.

Equation (9) is computation method based on manually correction and it fits practical application and people's understanding of fuel quality. The quality of real fuel corresponding to pure material pure listed in Table 3 like coal, oil, natural gas and H_2, is improved step by step when used, while the quality of light oil is equal to that of natural gas.

H_2 fuel produces water when combusted and is considered to be an ideal clean energy resource, therefore, more attention should be paid on the technologies of energy use. It can be concluded from ratios in Table 3 that the second law efficiency of H_2 is 12.9% higher than that of C fuels in order to maintain the equality of these two efficiencies when H_2 is used for power generation.

Of course, different kind of fuel has different qualities. So it's of realistic and theoretical significance to carry out qualities evaluation of fuel for energy structure adjustment.

7. Conclusions

The efficiencies for different fuels used differ largely, for example, the efficiency of coal used is the lowest among several fuels studied above, while that of natural gas is highest. Therefore, when energy demand is determined, we could adjust energy structure in order to achieve the highest energy utilization efficiency.

The higher quality of fuel is, the larger value of specific exergy is, and the less fuel consumed. It should be established on the base of fuel exergy analysis for optimal use of different types of fuel.

It would provide decision support for building scientific and reasonable energy structure combined with research on market regulation systems based on the actual situation of local economy development and actual demand of energy consumption.

Energy utilization efficiency was defined on account of low heat value of standard coal so far in China, which ignores the probability that different quality of energy resource may produce diverse energy efficiency. Energy structure adjustment lack scientific theoretical guidance, which is badly in need of change.

It must be declared that the fuel exergy for simple and pure matter could be easily obtained according to part 5, thus its lowest TUFC for electricity generation and heat supply and the value of energy saving could also be attained. It would take lots of effort to analysis how to obtain the fuel exergy of different kinds of compounds since the compositions are unstable and complex.

References

GUO Ju-e, Chai Jian and XI You-min. (2008). Effect of the primary energy consumption structure change to the energy use per unit of GDP. *China Population, Resource and Environment*, 1, 38-43

Ibrahim Dincer. (2002). The role of exergy in energy policy making. *Energy Policy*, 30, 137-149.

Irfan Kurtbas, Nevin Celik and Ibrahim Dincer. (2010). Exergy transfer in a porous rectangular channel. *Energy*, 35, 451-460.

Leyla Ozgener, Arif Hepbasli and Ibrahim Dincer. (2007). Exergy analysis of two geothermal district heating systems for building applications. *Energy Conversion and Management*, 48, 1185-1192.

Marc A. Rosen and Ibrahim Dincer. (2001). Exergy as the confluence of energy, environment and sustainable development. *Exergy In*t. J.1,3-13.

Samuel José Sarraf Borelli and Silvio de Oliveira Junior.(2008). Exergy-based method for analyzing the composition of the electricity cost generated in gas-fired combined cycle plants. *Energy*, 33(2): 153-162.

Song Zhiping and Wang Jiaxuan. (1985). *The Principle of Energy- Saving*, Electric Press, 399.

Song Zhiping. (1992). Consumption Rate Analysis: Theory and Practice. *Proceedings of the CSEE*. 12, 15-21.

Wall G. (1990). Exergy conversion in the Japanese society. *Energy,* 15, 435-44.

Wu Zhi-quan, Zhou Shao-xiang, An Lian-suo and Shi Hai-lin. (2010). Energy saving and emission reduction evaluation system based on unit fuel exergy of end-use product. *Chinese Journal of Power Engineering*, adopted.

Zafer Utlu and Arif Hepbasli.(2007). A review on analyzing and evaluating the energy utlizaiton efficiency of countries *Renewable and Sustainable Energy Reviews*, 11,1-29.

Zhou Shaoxiang, Hu Sangao and Song Zhiping. (2006). Comparison of the Theory of the Unit Fuel Consumption Analysis and the Method of Structural Coefficients. *Journal of Engineering Thermophysics*, 27, 549-552.

Zhou Shaoxiang, Hu Sangao and Song Zhiping. (2008). Specific Fuel Consumption Analysis and Efficiencies of Energy Utilizations, *China Energy*, 30, 42-44.

Zhou Shaoxiang. (2004). The Unified Benchmark Evaluating the Thermodynamic Performance of Energy Utilization Systems. *Proceedings of 17th ECOS International Conference*, Guanajuato. México, 1219-1226.

Table 1. mole mass, gross heat and low heat value and absolute entropy of pure fuels

fuels	RMW**	$q^0_{h,f}$	$q^0_{l,f}$	s^0_R	CF***
unit	kg/kmol	MJ/kmol	MJ/kmol	k/(mol·K)	-
H_2(g)	2.0159	286.0	240.80	130.57	4.07569
CH_4(g)	16.043	890.001	799.599	186.15	1.70059
C_5H_{12}(l)	72.151	3515.702	3244.402	262.7	1.53429
C(s)	12.0112	406.898	406.898	5.740*	1.15588

Note: g, l, s stand for gas, liquid, solid collection condition separately;

*-carbon dates of graphite structure; **- relative molecule weight; ***- factors that particular fuel converts to standard coal

Table 2. exergy values of different fuels from Eq. (7)

fuel	e^o_f	e^e_f	$e^o_f / q^0_{h,f}$	$b_e^{\min ce}$	ratio*
unit	MJ/kg	kW·h/kg	-	kg_{ce}/(kW·h)	-
H_2	138.60	38.50	0.9769	0.1059	1.150
CH_4	57.73	14.37	0.9326	0.1183	1.029
C_5H_{12}	47.89	13.30	0.9828	0.1153	1.056
C	34.18	9.49	1.0089	0.1218	1

Table 3. exergy values of different fuels from (9)

fuel	e^o_f	e^e_f	$e^o_f / q^0_{h,f}$	$b_e^{\min ce}$	**ratio***
unit	**MJ/kg**	**kW·h/kg**	**-**	**kg_{ce}/kW·h**	**-**
H_2	134.78	37.44	0.95	0.1089	1.129
CH_4	52.702	14.64	0.95	0.1162	1.058
C_5H_{12}	47.509	13.20	0.975	0.1163	1.057
C	33.877	9.410	1	0.1229	1

Note: *- is ratio of the theoretical lowest unit fuel consumption for a specific fuel to the theoretical lowest unit fuel consumption of C.

Moisture-Depend some Postharvest Properties of Two Varieties of Safflower

(*Darab* and *Goldasht*)

Javad Tarighi (Corresponding author)
Department of Agricultural Machinery Engineering, Faculty of Agricultural Engineering and Technology
College of Agricultural and Natural Resources, University of Tehran
P.O. Box 4111, Karaj 31587-77871, Iran
Tel: 98-935-211-2286 E-mail: Javad_tarighi63@yahoo.com

Asghar mahmoudi
Department of Agricultural Machinery Engineering, Faculty of Agricultural Engineering
University of Tabriz, Iran

Meysam Karami Rad
Department of Agricultural Machinery Engineering, Faculty of Agricultural Engineering and Technology
College of Agricultural and Natural Resources, University of Tehran

Abstract

The moisture-dependent physical properties are important to investigate for designing the post harvest equipments of the product .This study was carried out to determine the effect of moisture content on some physical properties. Four levels of moisture content ranging from 4-22% d.b (wet basis) and 4-22% d.b. for Darab and Goldasht, respectively was used. The average length, width, thickness, geometric mean diameter, equivalent diameter, arithmetic diameter, sphericity, thousand grain mass, angle of repose, grain volume, surface area and aspect ratio ranged from 7.52 to 7.89 mm, 3.95 to4.48 mm, 3.36 to 3.70 mm, 4.51 to 4.99 mm and 4.52 to5.00 mm, 4.89 to 5.36 mm, 60% to 63%, 32.2 to40.7 gr, 43º to 51º, 34.83 to 47.43 mm^3, 57.28 to 70.38 mm^2, 52.57% to 56.74% as the moisture content increased from 4 to 22% d.b. for Darab and from 7.41 to 7.67 mm, 4.59 to 4.74 mm, 3.57 to 3.84 mm, 4.93 to 5.18 mm, 4.88 to 5.12 mm, 5.17 to 5.41 mm, 66.37% to 68.56%, 50.50 to 59.2 gr, 47° to 56°, 40.76 to 53.12 mm^3, 62.27 to 72.38 mm^2, 64.22% to 62.95% with increase in moisture content from 4 to 22% d.b. for Goldasht. Goldasht has higher static angle of repose than Darab in all moisture content levels. As the moisture content increased, the bulk density was found to decrease from 547 to 520 kgm^{-3} and from 640 to 601 kgm^{-3} for Goldasht and Darab, respectively whereas true density and porosity were found to decrease from 1070 to 1010 kgm^{-3} and 48.87% to 48.51% for Goldasht and from 940 to 850 kgm-3, 31.91% to 29.29% for Darab. The static coefficients of friction on various surfaces, namely, galvanized metal, plywood and plastic also increased linearly with an increase in moisture content. For galvanized metal and plastic Darab was higher correlated with moisture content than Goldasht.

Keywords: Safflower, Physical properties, Moisture content, Darab variety, Goldasht variety

Introduction

The safflower is a plant that has the scientific name of Carthamus tinctorius L. The safflower which belongs to the Composite family is cultivated in several parts of the world due to its adaptability at different environmental conditions. In the past, safflower was planted in order to provide the pigment for using in dyeing machine. Today, in addition to that application, its seed is used for the production of seed oil. In order to design equipment for the handling, conveying, separation, drying, aeration, storing and processing of safflower grains, it is necessary to determine their physical properties as a function of moisture content. The knowledge of some important physical properties such as shape, size, volume, surface area, thousand grain weights, density, porosity, angle of repose, of different grains is necessary for the design of various separating, handling, storing and drying systems (Sahay and Singh, 1994). The size and shape are, for instance, important in their electrostatic separation from undesirable materials and in the development of sizing and grading machinery (Mohsenin, 1986). The shape of the material is important for an analytical prediction of its drying behavior. (Esref and Halil, 2007).

Bulk density, true density, and porosity (the ratio of intergranular space to the total space occupied by the grain) can be useful in sizing grain hoppers and storage facilities; they can affect the rate of heat and mass transfer of moisture during aeration and drying processes. Grain bed with low porosity will have greater resistance to water vapor escape during the drying process, which may lead to higher power to drive the aeration fans. Cereal grain kernel densities have been of interest in breakage susceptibility and hardness studies. The static coefficient of friction is used to determine the angle at which chutes must be positioned in order to achieve consistent flow of materials through the chute. Such information is useful in sizing motor requirements for grain transportation and handling (Ghasemi Varnamkhasti *et al*., 2007). The design of storage and handling systems for buckwheat requires data on bulk and handling properties, friction coefficients on commonly used bin wall materials (galvanized steel, plywood, and concrete), and emptying and filling angles of repose (Parde *et al.*, 2003). Theories used to predict the pressures and loads on storage structures (Janssen, 1895) require bulk density, angle of repose, and friction coefficients against bin wall materials. Also the design of grain hoppers for processing machinery requires data on bulk density and angle of repose. An example of the use of various bulk and handling properties of grains in the design of storage structures is given by Singh and Moysey (1985). The angle of repose determines the maximum angle of a pile of grain with the horizontal plane. It is important in the filling of a flat storage facility when grain is not piled at a uniform bed depth but rather is peaked (Mohsenin, 1986). Hence, current study was conducted on investigate some moisture dependent physical properties of safflower grain namely, dimensions, geometric mean, equivalent and arithmetic diameter, sphericity, thousand kernel weight (TKW), surface area, bulk density, true density, porosity, static angle of repose and static coefficient of friction against different materials.

Notations

L length, mm	Φ static coefficient of friction
W width, mm	θs static angle of repose, deg
T thickness, mm	ε porosity, %
S surface area, mm^2	Dg geometric mean diameter, mm
R^2 correlation determination	Dp equivalent diameter, mm
R_a aspect ratio	Da arithmetic diameter, mm
M moisture content, %	V volume, mm^3
Mi initial moisture content, %	Sp sphericity**,** %
Mf final moisture content, %	ρb bulk density**,** kgm-3
Wt total weight of sample, g	ρt true density, kgm-3
ΔWw weight of required water, g	

1. Materials and Methods

Two of popular varieties of cleaned safflower were obtained from Plant and Seed Institute in Karaj, Iran. The initial moisture content of seeds was determined by oven method (Tabatabaeefar, 2003) and in order to achieve the desired moisture level as 4,12, 16, and 22 (%d.b), the rewetting formula was used Eq.(1), and to allow the moisture be absorbed by samples were placed in refrigerator.

$$\Delta W_w = W_t \frac{(M_f - M_i)}{(100 - M_f)} \tag{1}$$

A digital caliper was used to determine length, width, and thickness of about 20 randomly selected grains of each sample. The geometric mean, Dg, equivalent, Dp, and arithmetic diameter, Da, in mm was calculated by considering prolate spheroid shape for a safflower grain and hence Eq (2), Eq (3) and Eq (4), respectively (Mohsenin, 1986).

$$D_g = (LDT)^{\frac{1}{3}} \tag{2}$$

$$D_p = \left[L \frac{(W+T)^2}{4} \right]^{\frac{1}{3}} \tag{3}$$

$$D_a = \frac{(L+W+T)}{3} \tag{4}$$

The sphericity (Sp) defined as the ratio of the surface area of the sphere having the same volume as that of grain to the surface area of grain, was determined using following formula (Mohsenin, 1986).

$$S_p = \frac{(LDT)^{\frac{1}{3}}}{L} \tag{5}$$

Thousand kernel weight (TKW) was measured by counting 100 seeds and weighing them in an electronic balance to an accuracy of .001 and then multiplied by 10 to give mass of 1000 kernels. Jain and Bal (1997) have considered grain volume, V and surface area, S may be given by:

$$V = 0.25\left[\left(\frac{\pi}{6}\right)L(W+T)^2\right] \tag{6}$$

$$S = \frac{\pi BL^2}{(2L-B)} \tag{7}$$

where

$$B = \sqrt{WT} \tag{8}$$

The aspect ratio (Ra) was calculated by (Omobouwajo *et al*., 1999).

$$R_a = \frac{W}{L} \tag{9}$$

The true density is a ratio of mass sample of grains to its pure volume. It was determined by the toluene displacement method (Mohsenin, 1986). Bulk density is the ratio of the mass sample of grains to its total volume. It was determined by filling a predefined container with from a constant high, striking the top level and then weighing the constants (Dashpande *et al.*, 1993). The porosity is the ratio of free space between grains to total of bulk grains. That was computed as:

$$\varepsilon = \frac{\rho_k - \rho_b}{\rho_k} \times 100 \tag{10}$$

The coefficient of static friction was determined with respect to different surfaces: plywood, plastic and galvanized metal. A hollow metal cylinder (Fig. 1) of diameter 75mm and depth 50mm and open at both ends was filled with the seeds at the desired moisture content and placed on adjustable titling surface such that the metal cylinder did not touches the surface. Then the surface was raised gradually until the filled cylinder just started to slide down (Razavi and Milani, 2006).

The static angle of repose is the angle with the horizontal at which the material will stand when piled. This was determined by using the apparatus (Fig. 2) consisting of a plywood box of 140-160-35mm and two plates: fixed and adjustable. The box was filled with the sample, and then the adjustable plate was inclined gradually allowing the seeds to follow and assume a natural slope (Tabatabeefar, 2003). Finally, the data were analyzed statistically and figures were plotted using Excel software 2007.

2. Results and discussion

A summary of the dimensions of Darab cultivar is shown in Table 1. All dimensions were increased with an increase in moisture content from 4% to 22% d.b. The increasing trend in axial dimensions, with gain in moisture content, was due to filling of capillaries and voids upon absorption of moisture and subsequent swelling (Table 1).

One thousand kernel weight (TKW) was increased significantly at 5% level of probability from 32.2 to 40.7 g as the moisture content increased from 4 - 22 d.b.(Fig. 3). Linear Relationship for one thousand kernel weight based on moisture content, M, was determined as follows:

(for Darab)	M*(1000)*= 0.471M + 30.51	$R^2 = 0.995$	(1)
(for Goldasht)	M(1000)= 0.479M + 49.00	$R^2 = 0.978$	(2)

The surface area of safflower grains increased from 57.28 to 70.38 mm^2, when the moisture content of grains increased from 4 to 22% d.b for Darab and from 62.27 to 72.38 when the moisture content of grainsa increased from 4 to 22% d.b for Goldasht. Milani *et al*. (2007) reported an increased in surface area of cucurbit seeds of three varieties at different moisture contents in the range of 5.18 - 42.76% d.b.

For Darab the sphericity of safflower grains increased from 0.60 to 0.63 with an increase in moisture content from 4 to 22% d.b. but for Goldasht the sphericity of safflower grains increased from 0.66 to 0.68 with an increase in moisture content from 4 to 22% d.b. The volume and aspect ratio of safflower grains have the same behavior. From table 1 it can be seen that geometric mean diameter, equivalent diameter and arithmetic diameter have the same behavior with increase in moisture content for both Darab and Goldasht. In this regard Esref and Halil (2007) found similar result for white speckledred kidney bean grains. The values of the bulk density for different moisture levels linearly decreased from 640 to 601 kg m^{-3} for Darab and from 547 to 520 kg m^{-3} for Goldasht (Fig. 4). The bulk density of seed was found to bear the following relationship with moisture content:

(for Darab) $\rho_b = -2.204M + 654.2$ $R^2 = 0.857$ (3)

(for Goldasht) $\rho_b = -1.491M + 556.6$ $R^2 = 0.862$ (4)

The above equations show that changing in moisture content has a greater impact on values of bulk density of Darab grains and equation 1 has greater slope. The decrease in bulk density for Goldasht grains is more linear than Darab ($R^2_{eq2} > R^2_{eq1}$). A similar decreasing trend in bulk density has been reported by Gupta and Das (1997) for corn seed. Whereas Parde *et al*. (2003) reported that the standard bulk density of Koto buckwheat increased significantly from 603.90 to 612.90 kgm^{-3} with an increase in moisture content from 14.8 to 15.8 %. With a further increase in moisture content, the standard bulk density decreased significantly.The true density and the moisture content of grain can be correlated as follows:

(for Darab) $\rho_t = 0.013M^2 - 3.609M + 1083$ $R^2 = 0.992$ (5)

(for Goldasht) $\rho_t = -0.375M^2 + 5.051M + 923.8$ $R^2 = 0.942$ (6)

For both Darab and Goldasht true density values decrease with increase in moisture content but the decrease is polynomial. It can be noted that Goldasht has greater true density than Darab in all moisture content levels (Fig. 5).

(for Darab) $\varepsilon = 0.001M^2 - 0.100M + 32.32$ $R^2 = 0.99$ (7)

(for goladasht) $\varepsilon = 0.010M^2 - 0.281M + 49.80$ $R^2 = 0.865$ (8)

The porosity of Darab safflower grains decreased polynomialy at the 5% level of probability from 31.91% to 29.29% with the increase in moisture content from 4 – 22% d.b. but for Goldasht the increase is not as much linear R^2=0.865 (Fig. 6). Goldasht has greater values of porosity in all moisture content levels. Moisture content has greater impact on porosity of Darab grains (from 31.90 to 29.29 d.b). The relationship between porosity and moisture content can be represented by the following polynomial equations:

The static coefficient of friction of safflower grains on three surfaces (plastic, plywood and galvanized metal) against different levels of moisture content are presented in Fig. 7. It was observed that the static coefficient of friction increased (probability < 0.05) with increase in moisture content for all the surfaces. This is due to the increased adhesion between the grains and the material surfaces at higher moisture values. Increases of 52.7%, 52.6% and 67.6% were recorded in the case of plastic, plywood and galvanized metal for Darab but for Goldasht the values of 22.2%, 83.3% and 60% were obtained, respectively, as the moisture content increased from 4 – 22% d.b. for Darab and Goldasht. For both variety at all moisture contents, the least static coefficient of friction was on galvanized metal. This may be owing to smaller cohesive force between grains and the galvanized metal than the other materials used . The relationships between static coefficient of friction and moisture content on plastic, plywood and galvanized metal can be represented by the following equations:

For Darab	$\varphi_{wood} = 0.010M + 0.337$	$R^2 = 0.978$	(9)
	$\varphi_{galv} = 0.012M + 0.295$	$R^2 = 0.992$	(10)
	$\varphi_{plas} = -0.000M^2 + 0.023x + 0.271$	$R^2 = 0.996$	(11)
For Goldasht	$\varphi_{wood} = 0.013M + 0.264$	$R^2 = 0.948$	(12)
	$\varphi_{galv} = 0.010M + 0.261$	$R^2 = 0.984$	(13)
	$\varphi_{plas} = -0.000M^2 + 0.023M + 0.281$	$R^2 = 0.832$	(14)

Similar results were found by Sahoo and Srivastava (2002) for okra. Parde *et al*. (2003) reported that the friction coefficient against plywood, galvanized steel and concrete surfaces for the Koto buckwheat cultivar increased significantly 0.26 to 0.31, 0.25 to 0.29 and 0.38 to 0.43 respectively, with increase in moisture content from 14.8 % to 17.9 %. The authors continued for significantly increasing the moisture content variation required more than 1 %. The experimental results for the static angle of repose with respect to moisture content are shown in Fig. 8. The values of the static angle of repose were found to increase significantly at the 5% level of probability from

43º to 51° and from 47º to 56° for Darab and Goldasht respectively. The static angle of repose for safflower has the following relationships with its moisture content.

(for Darab) $\theta st = 0.432M + 40.15$ $R^2 = 0.842$ (15)

(for Goldasht) $\theta st = 0.517M + 44.26$ $R^2 = 0.939$ (16)

Figure 8 shows that Goldasht has the greater static angle of repose in all moisture content levels and the increase in static angle of repose is more linear for Goldasht than Darab. From equations (15) and (16), it can be resulted that increase in moisture content has greater impact on static angle of repose of Goldasht (m=.517). Tabatabeefar (2003) found that the values of dynamic angle of repose for corn increased from 34.7º to 45° in the moisture range of 0 to 22% d.b. Parde *et al*., (2003) reported that the emptying angle of repose for Koto buckwheat cultivar remained constant at about 23.5° from 14.8 to 15.8% mc and then increased significantly and the filling angle of repose did not differ significantly at 14.8 to 16.6% but increased significantly to 28.4° at 17.9%.

Conclusions

All the studied physical properties of safflower grains depend on their moisture contents. The following conclusions are drawn from the investigation on physical properties of two varieties of safflower grains for moisture content range of 4 to 22% d.b. for Darab The average length, width, thickness, geometric mean diameter, equivalent diameter, arithmetic diameter, sphericity, thousand grain mass, angle of repose, grain volume, surface area, bulk density, true density, porosity, and aspect ratio, for safflower grains ranged from 7.52 to 7.89 mm, 3.95 to4.48 mm, 3.36 to 3.70 mm, 4.51 to 4.99 mm and 4.52 to5.00 mm, 4.89 to 5.36 mm, 60% to 63%, 32.2 to40.7 gr, 43º to 51º, 34.83 to 47.43 mm^3, 57.28 to 70.38 mm^2, 640 to 610 kgm^3,940 to 850 kgm^3,31.91% to 29.29% and 52.57% to 56.74% and from 7.41 to 7.67 mm, 4.59 to 4.74 mm, 3.57 to 3.84 mm, 4.93 to 5.18 mm, 4.88 to 5.12 mm, 5.17 to 5.41 mm, 66.37% to 68.56%, 50.50 to 59.2 gr, 47° to 56°, 40.76 to 53.12 mm^3, 62.27 to 72.38 mm2, 547 to 520 kgm^3, 1070 to 1010 kgm^3,48.87% to48.51%, 64.22% to 62.95% for Goldasht in the moisture content increase from 4 to 22% d.b respectively. The change in moisture content has greater impact in the bulk density of Goldasht was higher correlated with moisture content than Darab but for true density and porosity Darab has higher correlation with moisture content. The static coefficient of friction on various surfaces increased linearly with increase in moisture content. For Darab the galvanized metal as a surface for sliding offered the maximum friction followed by plywood and plastic but for Goldasht plywood shows the maximum friction while the static coefficient of friction for galvanized metal and plastic is almost the same.

References

Altuntas, E., & Yildiz, M. (2005). Effect of moisture content on some physical and mechanical properties of faba bean (Vicia faba L.) grains. *Journal of Food Engineering*, 78, 174–183.

Vursavus, K., & Ozguven, F. (2004). Mechanical behaviour of apricot pit under compression loading. *Journal of Food Engineering*, 65, 255–261.

Olaniyan, A. M., & Oje, K. (2002). Some aspect of the mechanical properties of shea nut. *Biosystems Engineering*, 81, 413–420.

Guner, M., Dursun, E., & Dursun, I.G. (2003). Mechanical behaviour of hazelnut under compression loading. *Biosystem Engineering*, 85(4), 485–491.

Oloso, A. O., & Clarke, B. (1993). Some aspects of strength cashew nuts. *Journal of Agricultural Engineering Research,* 55, 27–43.

Esref, I., & Halil, U. (2007). Moisture-dependent physical properties of white speckled red kidney bean grains. *Journal of Food Engineering*, 82, 209–216.

Gupta, R.K., & Das, S.K. (1997). Physical properties of sunflower seeds. *Journal of Agricultural Engineering Research*, 66, 1–8

Jain, R.K., & Bal, S. (1997). Properties of pearl millet. *Journal of Agricultural Engineering Research*, 66, 85–91.

Janssen, H.A. (1895). Versuche uber getreidedruck in silozellen. Z. vereines Deutscher Ingenieure, 39, 1045-1049.

Ghasemi Varnamkhasti, M., Mobli, H., Jafari, A., Rafiee, S., Heidary Soltanabadi, M. & Kheiralipour, K. (2007). Some Engineering Properties of Paddy (var. Sazandegi). *International Journal of Agricultural and Biology*, 5, 763-766.

Milani. E., Seyed, M., Razavy, A., Koocheki, A., Nikzadeh, V., Vahedi, N., MoeinFard, M. & GholamhosseinPour, A. (2007). Moisture dependent physical properties of cucurbit seeds. Int. *Agrophysics*, 21, 157-168.

Mohsenin, N.N. (1986). *Physical Properties of Plant and Animal Materials*, (2nd ed). New York: Gordon and Breach Science Publishers.

Omobuwajo. O.T., Akande, A.E. & Sann, A.L. (1999). Selected physical, mechanical and aerodynamic properties African Breadfruit (Treculia Africana) seeds. *Journal of Food Engineering*, 40, 241-244.

Ozarslan, C. (2002). Physical properties of cotton seed. *Bio-systems Engineering*, 83, 169–174.

Parde, S.R., Johal, A., Jayas, D.S. & White, N.D.G. (2003). Physical properties of buckwheat cultivars. *Canadian Bio-systems. Engineering*, Technical Note.

Razavi, S., & Milani, E. (2006). Some physical properties of the watermelon seeds. *African Journal of Agricultural Research*, 13, 65–69.

Sahay, K.M. & Singh, K.K. (1994). *Unit Operations of Agricultural Processing*. (1st ed). New Delhi: Vikas Publishing House Pvt.

Sahoo, P.K., & Srivastava, A.P. (2002). Physical properties of okraseed. *Bio-systems Engineering*, 83, 441–448.

Sheperd, H., & Bhardwaj, R.K. (1986). Moisture dependent physical properties of pigeon pea. *Journal of Agricultural Engineering Research*, 35, 227 – 234.

Singh, D., & Moysey, E.B. (1985). Grain bin wall pressures. Theoretical and experimental. *Canadian Agricultural Engineering*, 27, 43-48.

Tabatabeefar, A. (2003). Moisture-dependent physical properties of wheat. International. *Agrophysics* ,17, 207–211.

Table 1. Some physical properties of Darab variety dependent on moisture content.

MC (%)	L (mm)	W (mm)	T (mm)	D_g (mm)	D_p (mm)	D_a (mm)
4	7.52±0.62	3.95±0.54	3.36±0.32	4.51±0.54	4.52±0.56	4.89±0.38
12	7.75±0.57	4.22±0.45	3.46±0.23	4.76±0.63	4.78±0.64	5.15±0.66
16	7.78±0.56	4.43±0.37	3.71±0.23	4.95±0.31	4.97±0.32	5.30±0.34
22	7.89±0.41	4.48±0.61	3.70±0.19	4.99±0.31	5.00±0.32	5.36±0.30

Table 2. Some physical properties of Goldasht variety dependent on moisture content.

MC (%)	L (mm)	W (mm)	T (mm)	D_g (mm)	D_p (mm)	D_a (mm)
4	7.41±0.34	4.59±0.31	3.57±0.32	4.93±0.29	4.88±0.28	5.17±0.27
12	8.08±0.44	4.96±0.38	4.05±0.26	5.45±0.32	5.38±0.31	5.70±0.32
16	7.78±0.48	4.63±0.32	3.74±0.33	5.13±0.33	5.08±0.32	5.40±0.34
22	7.67±0.32	4.74±0.27	3.84±0.19	5.18±0.19	5.12±0.18	5.41±0.18

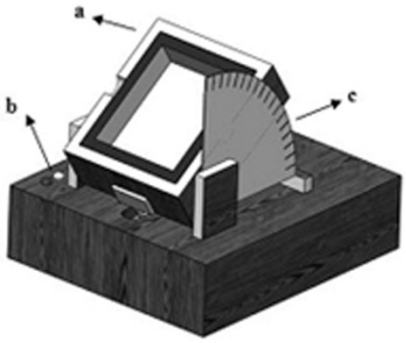

Figure 1. Apparatus to determine empting angle of repose

Figure 2. Apparatus to determine coefficient of static friction

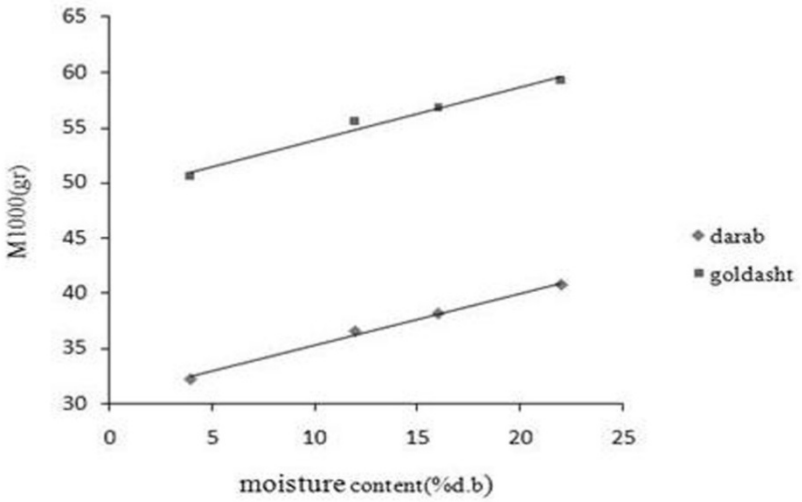

Figure 3. Effect of moisture content on M(1000): Goldasht (□) and Darab (◊)

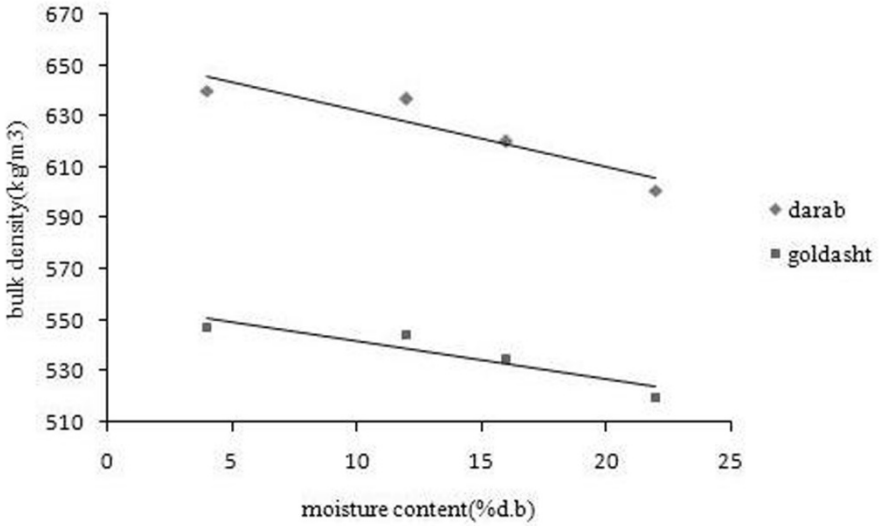

Figure 4. Effect of moisture content on bulk density: Goldasht (□) and Darab (◊)

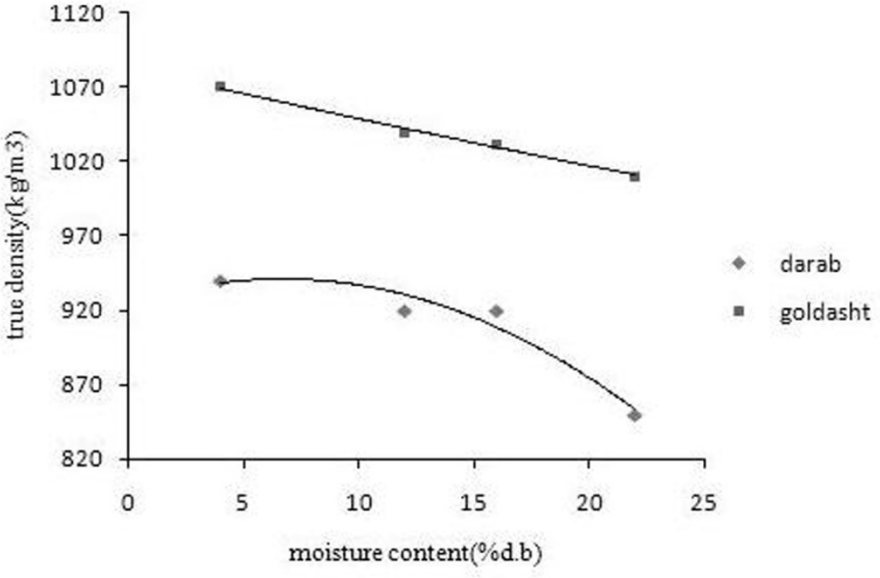

Figure 5. Effect of moisture content on true density: Goldasht (□) and Darab (◊)

 ISSN 1913-1844 E-ISSN 1913-1852

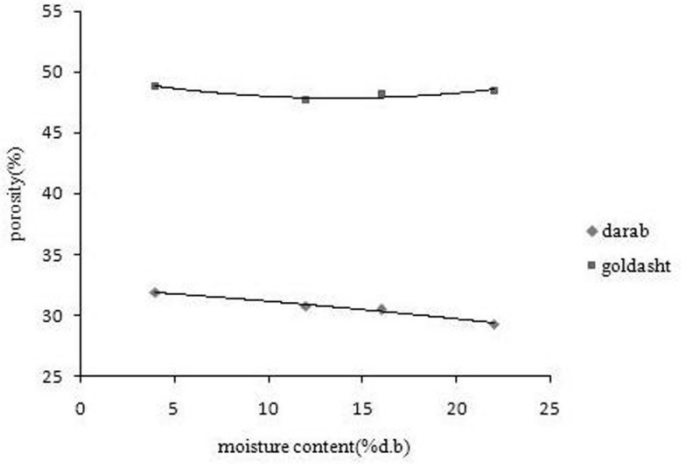

Figure 6. Effect of moisture content on porosity: Goldasht(□) and Darab (◊)

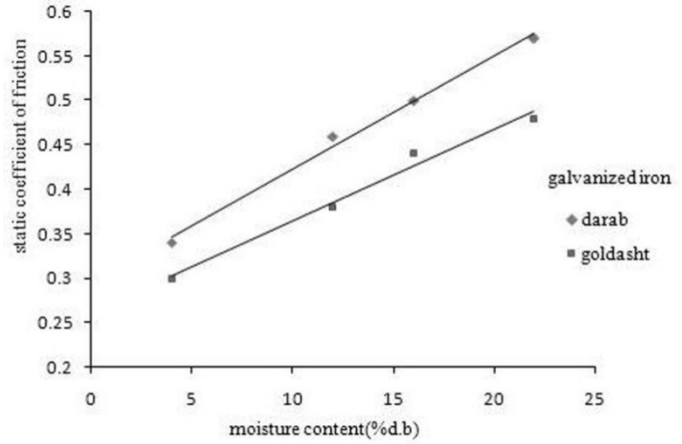

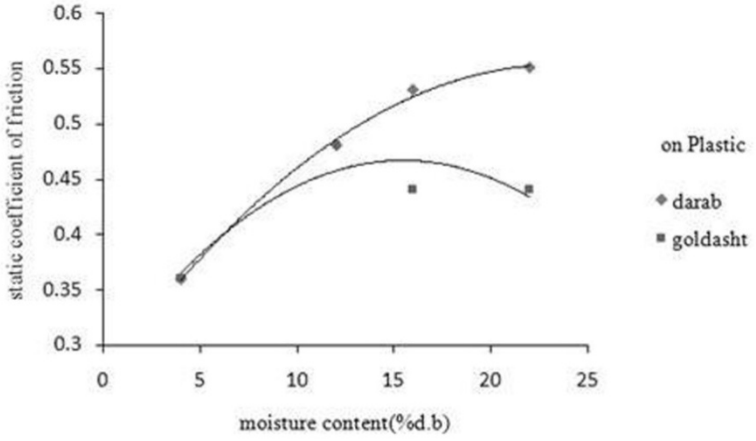

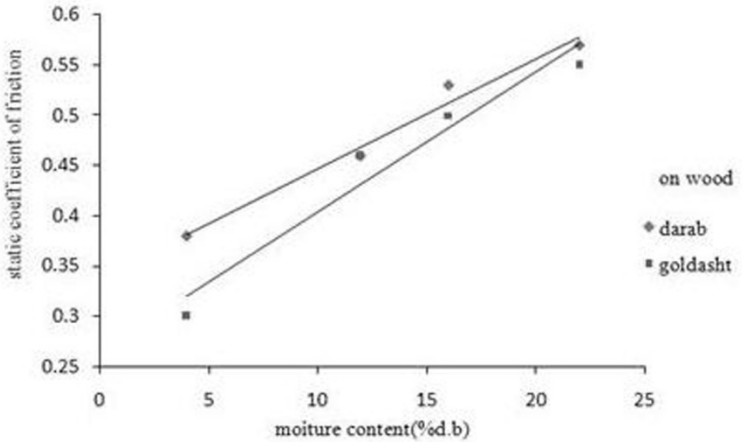

Figure 7. Effect of moisture content on static coefficient of friction: Goldasht(□) and Darab (◊)

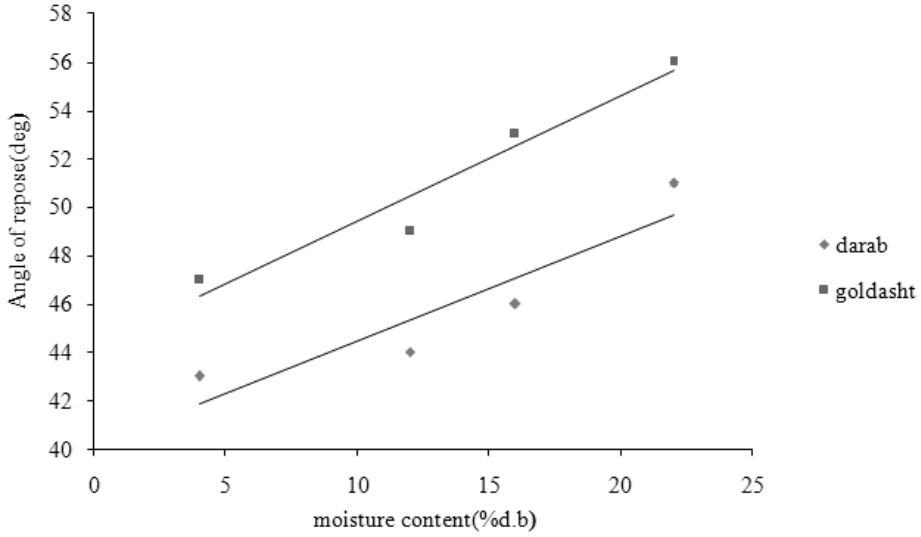

Figure 8. Effect of moisture content on static angle of repose: Goldasht (□) and Darab (◊)

ISSN 1913-1844 E-ISSN 1913-1852

An Analysis on Supply and Demand of Athletes' Accidental Injury Commercial Insurance in China

Houzhong Jin, Xuan Jia & Hongquan Li

Sports Economics and Management School, Central University of Finance and Economics

Beijing 100081, China

E-mail: jinhouzhong@126.com

Abstract

Through establishing supply and demand curve and its equilibrium, we shall analyze the supply and demand characteristics of athletes' accident commercial insurance in China. Subsequently, we shall discuss the influence of market, policy, law and other means of regulation on supply and demand equilibrium, so as to provide with theoretical support to Athletes' accident commercial insurance in China.

Keywords: Athlete, Accidental injury, Commercial insurance

Fund Project: Education Science Layout Project of China (GLA102024)

The insurance service of 2008 Olympic Games has tested China's sports insurance industry, which is also a significant opportunity for drawing on international experience and developing sports insurance, including athletes' accident insurance. However, compared to developed countries, China still has a long way to go on sports insurance (Feng, 2009). At present, China's athletes' accident commercial insurance represents as: oversupply of low-rate products and short supply of high-rate products, so nonequilibrium of supply and demand presents. Through establishing supply and demand curve and its equilibrium, we shall analyze the supply and demand characteristics of athletes' accident commercial insurance in China. Subsequently, we shall discuss the influence of market, policy, law and other means of regulation on supply and demand equilibrium, so as to provide with theoretical support to athletes' accident commercial insurance in China.

1. Current status of supply and demand of athletes' accident commercial insurance in China.

Athletes' accident commercial insurance is one type of personal accident insurance for individual athlete, which mainly provides with insurance service to athletes for personal training and match. Currently, among athletes' accidental injuries in China, "although minor injury accounts for biggest percentage, disability and serious injury have almost reached 30%, which means serious injuries have produced adverse effects on approximate one-third athletes for their personal health and being engaged in sports. Moreover, over 70% of Chinese athletes have been injured to different extent." (Wang et al, 2007) However, relevant research shows, among 3800 investigated athletes, "insured athletes account for only 32.2%, while the number of non-insured ones is high to 55.3% which is far more than that of insured. In addition, 12.5% of athletes are in unclear status. So the insurance level of Chinese athletes is extremely low." (Wang et al, 2007) The reasons should be that, firstly, the design of insurance policy is lack of pertinence, which can't meet the requirements of athletes for elusion of vocational risks; secondly, insurance depth and density are below average level, which results in difficulty of price dependence; thirdly, insurance fund is dependent on government for long term, but market, policy and law have inadequate regulations.

2. Analysis on supply and demand of athletes' accident commercial insurance in China

2.1 Analysis on price-supply and –demand

Herein we shall analyze price-supply curve and price-demand curve. See Figure 1, Q is the quantity of unit homogeneous product of athletes' accident commercial insurance; P is the price of unit homogeneous insurance product; Es is the corresponding insurance product; Ed is the demand elasticity of price. In Figure 1 (a), Q stays at A when P is low. According to law of great numbers, when P slightly increases, amplitude of Q is less than that of P by increasing 1 unit of Q, i.e. $Es < 1$ as P is low, due to high increase of marginal cost. When P is high to E, Q is high also. According to law of great numbers, when P slightly decreases, Q marginal cost to Q production cost by decreasing 1 unit of Q can be neglected, and $Es > 1$.

In Figure 1 (b), when P is high, Q is low to F. When P decreases, Q will increase correspondingly. According to law of great numbers, here consumers are risk haters, and other risk subjects still choose saving, social insurance and self-protection to take risks. When amplitude of Q is less than change of P, $Ed= (\Delta Q/Q)/ (\Delta P/P) <1$. P is low, while Q stays high at A. When P gradually decreases, anticipated consumers at corresponding positions are

enlarged into broader risk subjects. According to law of great numbers, when amplitude of Q is more than change of P, Ed= (ΔQ/Q)/ (ΔP/P)>1. In Figure 2, E is the equilibrium of P and Q, which is an ideal state of market supply and demand. Pe is equilibrium price, and Qe is equilibrium quantity.

2.2 Supply analysis

Supply of athletes' accident commercial insurance means the quantity of insurance products that insurer is willing to and can sell at possible price for athletes' unit homogeneous products within certain period. It consists of two factors. One hand, insurer is willing to sell insurance products. On the other hand, insurer is able to supply insurance. Its influential factors are mainly composed of insurance premium rate, cost and market monopoly degree. Due to late start of athletes' accident commercial insurance in China and immature managerial technique, insurance suppliers highly measure premium rate of unit homogeneous product of athletes' accident commercial insurance than real level, considering risk apportionment and corporate sustainable running. Shown as Figure 3, real supply curve stays at S^1, and meets supply curve d at E^1. Premium rate price of unit homogeneous product, Pe^1 is high, while quantity of market deal Qe^1 is low. If S^1 moves left to S, unit homogeneous insurance premium rate will decrease, quantity of market deal will increase, and market supply and demand will go to ideal E.

If unit homogeneous product cost of China's athletes' accident commercial insurance decreases through cost adjustment, supply curve will vertically go up to S^2 from S^1 on condition of same quantity Q. Thus, price falls to Pe^2, and deal quantity increases to ideal E^2 where Qe^2 and demand curve d meet. The other influential factors are comparatively low opening-up degree of China's insurance market, so few suppliers, small insurance variety, too much restriction to insurance capital and market channel, and high barrier to entry and exit. See Figure 4.

2.3 Demand Analysis

Demand of athletes' accident commercial insurance refers to the quantity of insurance products that athletes are willing to and can buy at possible price for unit homogeneous insurance products during sports training and match within certain period. It consists of two factors as well. One hand, athletes have purchase desire. On the other hand, athletes are able to buy them. Its influential factors are athletes' income, price of substitutes and complementary products of commercial insurance, and athletes'' preference and anticipation to risks. As far as income is concerned, Chinese athletes' income mainly comes from basic salary and subsidy. There is a big gap compared to few Olympic champions or excellent athletes who achieved world or national award (Liu & Sun, 2009). As for price of substitutes and complementary products, there are two pieces of source, i.e. excellent athletes' mutual insurance by Sports Insurance Department of China Sports Foundation, athletes' injury insurance, etc. In fact, the former is just a kind of pension which comes from athletes' individual paid premium, collection of relevant activities and social donation and help. With regards to preference and anticipation, athletes' welfare after retirement during planned economy time has been abolished, so athletes are not optimistic to the future after retirement (Zhang & Cao, 2005). In Figure 5, with the restriction of income level, substitutes and future anticipation, the real demand of athletes' accident commercial insurance Qe^1 is less than potential demand Qe, and market price Pe^1 is lower than ideal price Pe.

3. Analysis on supply and demand equilibrium of athletes' accident commercial insurance in China

3.1 Supply and demand equilibrium condition

It is assumed that an insured of athletes' accident commercial insurance has wealth w, its utility is $u(w)$, and random loss is X. Maximum premium he is willing to pay in order to avoid loss X is $G=nP_{max}$ (n is quantity of unit homogeneous insurance products; P is price of unit homogeneous insurance products). An insurer of athletes' accident commercial insurance has wealth w_1, and its utility function is $u_1(w_1)$. If he accepts insurance, he will confront random loss and make reparations. Minimum premium he charges is $H=nP_{min}$.

If $E[x]=\mu$, based on Expected Utility Theory, $G \geq \mu, H \geq \mu$ (1)

For insured, $u(w-G)=E[u(w-X)]=\int_0^{\infty} u(w-x)f(x)dx$ (2)

$f(x)$ is density function of risk X, for insurer, $u_1(w_1)=E[(w_1+H-X)]=\int_0^{\infty} u_1(w_1+H-X)f(x)dx$ (3)

Therefore, only if real charged premium is between G and H, insured and insurer will both be satisfied. Here insurance policy is feasible, i.e. satisfying general equilibrium conditions: H<P<G. So (H/n) <Pe< (G/n), Qe=n.

3.2 Supply and demand equilibrium

Combining Figure 2 and conditions of athletes' accident commercial insurance policy, we obtain general

equilibrium supply and demand curve and its point of equilibrium; see point E in Figure 6.

3.3 High premium rate-high risks supply and demand equilibrium

Owing to few risk subjects of athletes' accident commercial insurance products of high premium rate-high risks, here on selling n units of athletes' accident commercial insurance products, insurer achieves utility $u_1(w_1) = E[(w_1 + H - X)] = \int_0^\infty u_1(w_1 + H - X) f(x)dx$. Because of big X, with the decrease of n, X is approximately equal to H on condition of few buyers. So insurer's utility approximately goes to zero. Insurer's supply Qs^1 will stay at low level. However, at the same price, demand Qd^1 is large, consequently, demand exceeds supply. See Figure 7 (a).

3.4 Low premium rate-low risks supply and demand equilibrium

Due to large quantity of risk subjects of athletes' accident commercial insurance products of low premium rate-low risks supply and demand equilibrium, it is easy to use law of great numbers to determine rate. Once accidents happen, they will bring small loss to insurer, simultaneously, insurer will take fewer risks of adverse selection. Here regarding to insurer, on selling n units of athletes' accident commercial insurance products, insurer achieves utility $u_1(w_1) = E[(w_1 + H - X)] = \int_0^\infty u_1(w_1 + H - X) f(x)dx$. Product X of low premium rate-low risks is small. With the increase of n, H=nP increases and insurer's utility increases as well. Therefore, at the same market price, supply is high to Qs^2, while demand is low to Qd^2. See Figure 7 (b).

4. Supply and demand adjustment of Athletes' Accident Commercial Insurance in China

4.1 Market adjustment

Market adjustment consists of production cost adjustment and information cost adjustment. Through improving market regulation system, we should remove various barriers to resource flowing in sports insurance market, and reduce material cost of athletes' accident commercial insurance products. A variety of marketing channels need to be developed so as to reduce operating cost of insurance companies. Talents specializing sports insurance should be introduced in order to strengthen theoretical research on market rules and characteristics of sports insurance, especially athletes' accident commercial insurance. Accumulation of sports vocational insurance data has to be consummated for the purpose of solving current problems, i.e. few categories of insurance, high premium rate and lack of individual terms. According to different sports items, guaranteed emphasis of individual athletes' accident commercial insurance products should be established. Different premium rate and compensation range also need to be determined. We should determine disclaimer range scientifically, so that athletes' accident commercial insurance will more accord with athletes' injury characteristics, which are different from ordinary medical treatment and personal accident commercial insurance products. Meanwhile, labor cost should be reduced, so that the supply and demand of homogeneous insurance policy at the same price will increase.

4.2 Policy adjustment

In Nov. 2006, China State Sports Administration, Ministry of Finance and Ministry of Labor and Social Security together issued "On further strengthen social security of athletes", in which athletes' basic pension insurance, basic medical insurance, unemployment insurance and injury insurance are definitely stipulated, and Chinese athletes' social security is specified from system perspective (Zhou, 2008). The Chinese government should implement special supportive policies to sports insurance, especially athletes' accident commercial insurance. They can reduce sales tax; for instance, reduce sales tax of athletes' accident commercial insurance from ordinary rate 8% to 3%. Insurance of the athletes at provincial, municipal and national level should be tax free. Meanwhile, income tax of athletes' accident commercial insurance companies needs to be derated. Derated tax can be added to capital so that the utilization and turnover rate of insurance funds will be promoted. "Thus, insurance premium rate will be reduced and insurance fee will decrease, so that the shortage of insurance capital can be relieved" (Zhang et al, 2008).

4.3 Law adjustment

Along with the marketized reform of sports, China's relevant departments and industry associations should establish related rules, and regulate the minimum insurance and guarantee terms in the contracts between club and athletes. The responsibility range of match undertakers should be stipulated in the form of legislation. Moreover, examination procedure of sponsored insurance needs to be specified in order to ensure insurance types, insurance range, security level and diversity of insurance capital source. As for system level, we should discover the development system beneficial to athletes' accident commercial insurance. For those projects with marketization difficulty, compulsory insurance can be properly popularized to establish long-effect sustainable policy and capital support in the form of legislation.

References

Feng Shuoan. (2009). Problems and countermeasures of China's Sports Insurance. *Social Sciences Review.*

2009.24 (9):49-51.

Liu Ping & Sun Fuqiang. (2009). Human capital return and allocation model on Chinese athletes. *Journal of Shenyang Institute of Physical Education*. 2009.28 (2):7-10, 16.

Wang Xiuxiang et al. (2007). Survey and analysis on Chinese athletes' disability. *Liaoning Normal University (Natural Science)*. 2007.30 (2):241-243.

Wang Xiuxiang et al. (2007). Investigation and analysis on athlete disability insurance. *Physical Education*. 2007.14 (5):35-37.

Zhang Guimin & Cao Jihong. (2005). On China's athletes training system transformation. *Journal of Shenyang Institute of Physical Education*. 2005.24 (5):1-3, 6.

Zhang Mingbo et al. (2008). Suggestion on promoting athletes' insurance in China. *Finance and Economy*. 2008. (9):89-90.

Zhou Fei. (2008). On marketization of athletes' insurance. *Sports Technology Literature*. 2008.16 (2):103-105.

(a) (b)

Figure 1. Supply and Demand Curve of Athletes' Accident Commercial Insurance in China

(a: Price-Supply Curve; b: Price-Demand Curve)

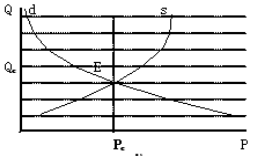

Figure 2. Equilibrium of Supply and Demand

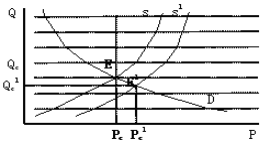

Figure 3. Supply Change 1

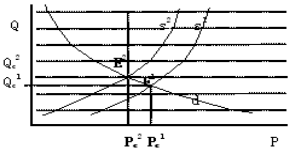

Figure 4. Supply Change 2

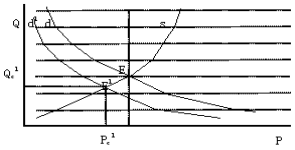

Figure 5. Demand Change

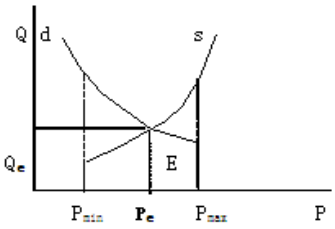

Figure 6. Supply and Demand Equilibrium of Athletes' Accident Commercial Insurance in China

(a) (b)

Figure 7. Supply and Demand Equilibrium of Athletes' Accident Commercial Insurance in China

(a: High premium rate-high risks supply and demand equilibrium; b: Low premium rate-low risks supply and demand equilibrium)

Modeling of Soil Cation Exchange Capacity Based on Fuzzy Table Look-up Scheme and Artificial Neural Network Approach

Ali Keshavarzi (Corresponding author)
Department of Soil Science Engineering, University of Tehran
P.O.Box: 4111, Karaj 31587-77871, Iran
Tel: 98-261-223-1787 E-mail: aliagric@gmail.com, alikeshavarzi@ut.ac.ir

Fereydoon Sarmadian
Department of Soil Science Engineering, University of Tehran
P.O.Box: 4111, Karaj 31587-77871, Iran
Tel: 98-261-223-1787 E-mail: fsarmad@ut.ac.ir

Reza Labbafi
Department of Agricultural Machinery Engineering, University of Tehran
P.O.Box: 4111, Karaj 31587-77871, Iran
Tel: 98-261-280-8138 E-mail: Rezalabbafi@ut.ac.ir

Majid Rajabi Vandechali
Department of Mechanics, Islamic Azad University
Jouybar Branch, Jouybar, Iran
E-mail: majid_r_v@yahoo.com

Abstract

In this study, a new approach is proposed as a modification to a standard fuzzy modeling method based on the table look-up scheme. 70 soil samples were collected from different horizons of 15 soil profiles located in the Ziaran region, Qazvin province, Iran. Then, neural network model (feed-forward back propagation network) and fuzzy table look-up scheme were employed to develop a pedotransfer function for predicting soil CEC using easily measurable characteristics of clay and organic carbon. In order to evaluate the models, root mean square error (RMSE) and R^2 were used. The value of RMSE and R^2 derived by ANN model for CEC were 0.47 and 0.94 respectively, while these parameters for fuzzy table look-up scheme were 0.33 and 0.98 respectively. Results showed that fuzzy table look-up scheme had better performance in predicting and modeling of soil cation exchange capacity than artificial neural network.

Keywords: Fuzzy table look-up scheme, Artificial neural network, Cation exchange capacity, Pedotransfer function, Ziaran

1. Introduction

Cation exchange capacity (CEC) is among the most important soil properties that is required in soil databases (Manrique et al., 1991), and is used as an input in soil and environmental models (Keller et al., 2001). CEC is the amount of negative charge in soil that is available to bind positively charged ions (cations). CEC is used as a measure of fertility, nutrient retention capacity and the capacity to protect groundwater from cation contamination (Akbarzadeh et al., 2009). CEC buffers fluctuations in nutrient availability and soil pH. Soil components known to contribute to CEC are clay and organic matter and to a lesser extent, silt (Seybold et al., 2005). Although CEC can be measured directly, its measurement is especially difficult and expensive in the Aridisols of Iran because of the large amounts of calcium carbonate (Carpena et al., 1972) and gypsum (Fernando et al., 1977).

1.1 Pedotransfer function

The term of pedotransfer function (PTF) was coined by Bouma (1989) as translating data we have into what we need. The most readily available data come from soil survey, such as field morphology, texture, structure and pH.

Pedotransfer functions add value to this basic information by translating them into estimates of other more laborious and expensively determined soil properties. These functions fill the gap between the available soil data and the properties which are more useful or required for a particular model or quality assessment. Various PTFs have been developed to estimate CEC from basic physical and chemical soil properties (Breeuwsma et al., 1986; Manrique et al., 1991; Bell & Van Keulen, 1995; McBratney et al., 2002). In most of these models, CEC is assumed to be a linear function of soil organic matter and clay content (Breeuwsma et al., 1986; McBratney et al., 2002). Results show that greater than 50% of the variation in CEC could be explained by the variation in clay and organic carbon content for several New Jersey soils (Drake and Motto, 1982), for some Philippine soils (Sahrawat, 1983), and for four soils in Mexico (Bell and Van Keulen, 1995). Only a small improvement was obtained by adding pH to the model for four Mexican soils (Bell and Van Keulen, 1995). In B horizons of a toposequence, the amount of fine clay was shown to explain a larger percent of the variation in CEC than the total clay content (Wilding and Rutledge, 1996). Vos et al. (2005) used 12 PTFs and Brazilian's database for prediction of bulk density. Their results showed that the separation of subsoil data from topsoil data did not increase the accuracy of prediction. Similarly, Heusher et al. (2005) and Kaur et al. (2002) reported that the soil texture and organic matter content were the main parameters for estimating of bulk density. Najafi and Givi (2006) used the ANNs and PTFs methods for prediction of soil bulk density. They pointed out that the ANNs are able to predict the soil bulk density better than the PTFs. Amini et al. (2005) estimated the cation exchange capacity in the central of Iran using soil organic matter and clay contents. They used the ANN and five experimental models that were on the basis of regression methods for their predictions. They showed that a neural network PTF with eight hidden neurons was able to predict CEC better than the regression PTFs. Also the ANN model significantly improved the accuracy of the prediction by up to 25%. They concluded that network models are in general more suitable for capturing the non-linearity of the relationship between variables. Jain and Kumar (2006) indicated that the ANN technique can be successfully employed for the purpose of calibration of infiltration equations. They had also found that the ANNs are capable of performing very well in situations of limited data availability.

1.2 Fuzzy inference systems

Fuzzy inference is the process of formulating the mapping from a given input to an output using fuzzy logic. The mapping then provides a basis from which decisions can be made, or patterns discerned. Fuzzy inference systems have been successfully applied in fields such as automatic control, data classification, decision analysis, expert systems and computer vision (Sun, 2009). Because of its multidisciplinary nature, fuzzy inference systems are associated with a number of names, such as fuzzy rule-based systems, fuzzy expert systems, fuzzy modeling, fuzzy associative memory, fuzzy logic controllers and simply (and ambiguously) fuzzy systems. It is well known that many elements of land properties have uncertainties. Uncertainty is inherent in decision-making processes, which involve data and model uncertainty. These range from measurement errors, to inherent variability, to instability, to conceptual ambiguity or to simple ignorance of important factors (Keshavarzi et al., 2010). Fuzzy set theory has been widely used in soil science for soil classification and mapping, land evaluation, fuzzy soil geostatistics, soil quality indices (Chang and Burrough, 1987; Burrough, 1989; Zhu et al., 1996; McBratney and Odeh, 1997; McBratney et al., 2003; Zhang et al., 2004; Lagacherie, 2005). McBratney and Odeh (1997) showed the potential of fuzzy set theory in soil science, such as mapping and numeric classification, land use evaluation, modeling and simulation of physical processes. Enea and Salemi (2001) and Klingseisen et al. (2007) used fuzzy logic for evaluating environmental impacts. Metternicht and Gonzalez (2004) presented a fuzzy exploratory model for the prediction of soil erosion hazards. Sadiq and Rodriguez (2004) evaluated and predicted the performance of slow sand filters using fuzzy rule-based modeling. Tran et al. (2002) developed a fuzzy rule-based model to improve the performance of the revised universal soil loss equation (RUSLE). Their approach consisted of two approaches: (1) Multi-objective fuzzy regression (MOFR); and (2) Fuzzy rule-based modeling (FRBM). Tayfur et al. (2003) studied a fuzzy logic algorithm to estimate sediment loads from bare soil surfaces. Predicting the mean sediment loads from experimental runs, the performance of the fuzzy model was compared with that of the artificial neural networks (ANNs) and the physics-based models. The results showed that the fuzzy model performed better under very high rainfall intensities over different slopes and over very steep slopes under different rainfall intensities. Zhu et al. (2010) presented a method to construct fuzzy membership functions using descriptive knowledge. Construction of fuzzy membership functions is accomplished based on two types of knowledge: 1) knowledge on typical environmental conditions of each soil type and 2) knowledge on how each soil type corresponds to changes in environmental conditions. In this study, a new approach is proposed as a modification to a standard fuzzy modeling method. This new method takes randomness into account by considering the statistical properties of training dataset. The method discussed here is called table look-up scheme. The idea is based on all available input-output data pairs (Jang et al., 1997; Liu et

al., 2003), a rule-base will be build. Then the unknown system between the input-output can be approximated using this rule-base.

Hence, the present study was carried out with objective to compare of ANNs model and fuzzy table look-up scheme for estimating and modeling of soil cation exchange capacity using some easily measurable soil parameters in Ziaran region.

2. Materials and methods

2.1 Site description

The study was carried out in Ziaran region, Qazvin province in Iran. The research commenced in 2008 and ended in 2009. The land investigated in the research is located between latitudes of 35°58′ and 36°4′ N and between longitudes of 50°24′ and 50°27′ E which has the area about 5121 hectares. The average, minimum and maximum heights points of Ziaran district are 1204, 1139 and 1269 meters above sea level, respectively (Fig1). The soil moisture and temperature regimes of the region by means of Newhall software are Weak Aridic and Thermic, respectively. Based on soil taxonomy (USDA, 2010), this region has soils in Entisols and Aridisols orders.

2.2 Data collection and soil sample analysis

After preliminary studies of topographic maps (1:25000), using GPS, studying location was appointed. 70 soil samples were collected from different horizons of 15 soil profiles located in Ziaran region in Qazvin Province. Measured soil parameters included texture (determined using Bouyoucos hydrometer method), Organic Carbon (O.C) was determined using Walkley-Black method (Nelson and Sommers, 1982) and CEC (cation exchange capacity in Cmolc kg^{-1} soil) determined by the method of Bower (Sparks et al., 1996).

2.3 Methods to fit PTFs

2.3.1 Artificial neural network

Neural classifiers can deal with numerous multivariable nonlinear problems, for which an accurate analytical solution is difficult to obtain (Park et al., 2010). An artificial neural network is a highly interconnected network of many simple processing units called neurons, which are analogous to the biological neurons in the human brain. Neurons having similar characteristics in an ANN are arranged in groups called layers. The neurons in one layer are connected to those in the adjacent layers, but not to those in the same layer. The strength of connection between the two neurons in adjacent layers is represented by what is known as a ‘connection strength’ or ‘weight’. An ANN normally consists of three layers, an input layer, a hidden layer, and an output layer. In a feed forward network, the weighted connections feed activations only in the forward direction from an input layer to the output layer. On the other hand, in a recurrent network additional weighted connections are used to feed previous activations back into the network. The structure of a feed-forward ANN is shown in Figure 2. This ANN is a popular neural network which known as the back propagation algorithm introduced by Karaca and Ozkaya (2006). This ANN had *k* input and one output parameters. They used this ANN for accurate modeling of the leachate flow-rate. They also reported that the input parameters, number of neurons at the hidden and output layer should be determined according to currently gathered data. Moreover, an important step in developing an ANN model is the training of its weight matrix. The weights are initialized randomly between suitable ranges, and then updated using certain training mechanism (Pachepsky et al., 1996: Schaap et al., 1998; Minasny et al., 1999).

In the feed-forward networks, error minimization can be obtained by a number of procedures including Gradient Descent (GD), Levenberg–Marquardt (LM) and Conjugate Gradient (CG). BP uses a gradient descent (GD) technique which is very stable when a small learning rate is used, but has slow convergence properties (Omid et al., 2009). Several methods for speeding up BP have been used including adding a momentum term or using a variable learning rate. In this study, LM algorithm in the sense that a momentum term is used to speeding up learning and stabilizing convergence is used.

2.3.2 Membership functions and fuzzy table look-up scheme

A general fuzzy system has the components of fuzzification, fuzzy rule-base, fuzzy output engine and defuzzification. Fuzzification converts each piece of input data to degrees of membership by a look-up in one or more several membership functions. The key idea in fuzzy logic is the allowance of partial belongings of any object to different subsets of a universal set, instead of completely belonging to a single set. Partial belonging to a set can be described numerically by a membership function, which assumes values between 0 and 1 inclusive. Intuitions, inference, rank ordering, angular fuzzy sets, neural networks, genetic algorithms and inductive

reasoning can be among many ways to assign membership values or functions to fuzzy variables. Especially, the intuitive approach is used rather commonly because it is simply derived from the innate intelligence and understanding of human beings. Fuzzy membership functions may take on many forms, but in practical applications simple linear functions such as triangular ones are preferable (Tayfur et al., 2003). MFs for the corresponding inputs are recommended by MATLAB (7.8) as triangular membership function. There are five steps in generating fuzzy rules with fixed membership functions. Consider the design of a fuzzy system with two inputs (x_1, x_2) and one output (y) system. Further, there are *n* data points in the training set.

Step1: Define the fuzzy partition of the input and output variables:

Six and three fuzzy sets are selected to form the partition of this range, respectively. This means the degree of membership can be evaluated for any input values. The fuzzy partition for the output is assumed to have the five fuzzy sets.

Step2: Generate one fuzzy rule for each of the *n* input-output pairs:

These results are in the initial fuzzy rule base (Eq.1) (Mendel, 2001; Liu et al., 2003):

$$(x_1^{\,p}, x_2^{\,p}, y^p) \Rightarrow Fuzzy\ Rule \quad p = 1,2,...,n \tag{1}$$

From this input-output pair, one fuzzy rule can be generated. One may be reminded of the facts that the fuzzy sets may overlap. Now the question is how to assign the appropriate membership functions to the variables in each data pair. The common practice is that the fuzzy variable is assigned the membership function that produces the maximum membership value.

Step 3: Calculate the degree for each fuzzy rule resulted from rules:

The number of fuzzy rules generated by the input-output pairs is usually large. Inconsistent and redundant rules are inevitable. One is then confronted with the task of eliminating the inconsistency and redundancy.

Step 4: Create the final fuzzy rule base by removing inconsistent and redundant rules:

In the standard approach, the rule having the largest degree is adopted. As an improvement, a new selection approach is proposed here to remove inconsistency and redundancy. The notion of reliability factor is introduced. Specifically, for each given set of *k* rules with the same antecedent parts, the reliability factor is defined as (Liu et al., 2003):

$$\text{Reliability Factor}\,(RF) = \frac{K_1}{K} \tag{2}$$

Where:

k_1=Number of redundant rules,

k =Total number of the redundant and inconsistent rules having the same antecedent part.

The reliability factor is then used as a weighting factor for computing the effective degree for each rule degree as follows (Liu et al., 2003):

$$\text{Effective Degree}\,(D_{eff}) = D * RF \tag{3}$$

Table 1 shows the example of reliability factors for the inconsistent and redundant rules itemized. The final fuzzy rule-base can now be compiled by choosing the rules with the largest effective degrees. For the redundant and inconsistent rules in table 1, the effective degree is given by (Liu et al., 2003):

$$D_{eff}(\max) = \max(D_{eff(i)}), \quad i = 1,2,...,n \tag{4}$$

Where: D_{eff} = effective degree, and *n* is the number of membership function.

Step 5: Determine the overall fuzzy system:

Up to this point, the membership functions are defined in step1 and the fuzzy rule-base is compiled in step 4. In this paper, Mamdani's inference scheme is adopted for its simplicity (Fig 3). In carrying out fuzzy inference (reasoning), mathematical operations on the membership functions are invariably required. Any T-norm or S-norm can be used to define the operations involving membership function. In addition, any defuzzification scheme such as the centroid method can be selected. This essentially completes the design procedure in modeling a fuzzy system. In summary, the modified table-look-up scheme offers an effective method for removing inconsistency and redundancy in the process of assembling fuzzy rules. In this study, MATLAB 7.8 software was used for the design and testing of ANN models and fuzzy table look-up scheme.

2.3.3 Performance criteria

The performance of the models was evaluated by a set of test data using the root mean square error (RMSE) and the coefficient of determination (R^2) between predicted and measured values. The RMSE is a measure of accuracy and reliability for calibration and test data sets (Wösten et al., 1999) and is defined as:

$$RMSE = \sqrt{\frac{1}{n}\sum_{k=1}^{n}(z_o - z_p)^2} \quad (5)$$

Where: Z_o is observed value, Z_p is predicted value, and n is number of samples.

3. Results and discussion

3.1 Data summary statistics

Data summary of train and test are presented in Tables 2 and 3, respectively. Data subdivided into two sets: 20% of the data for testing and the remaining 80% of the data were used for training or calibrating. Some soil parameters including clay and organic carbon were input data for prediction of CEC. However, clay and organic carbon were considered as inputs for prediction of CEC. Amini et al. (2005) stated that CEC has high correlation with these inputs. They found that inputs like sand and silt can not improve accuracy of prediction of CEC. Simple linear correlation coefficients (r) between CEC and independent variables were also calculated (Table 4). As Table 4 illustrates correlations between O.C and CEC and between clay and CEC were positive and highly significant. For example the correlation coefficients between CEC and clay content ($r = 0.92^{**}$) is more than between CEC and O.C content ($r = 0.56^{*}$). Positive correlation between CEC, O.C and clay content is related to existence of negative charges on these properties (Manrique et al., 1991; Bell and Van Keulen., 1995; Noorbakhsh et al., 2005). However with regarding to these correlation coefficients, both of them are suitable for developing PTFs for prediction of CEC in soils of Ziaran region.

3.2 Developing PTFs using Artificial Neural Network

After determining of linear correlation coefficients, performance of artificial neural networks was developed for test data set. In the present study for predicting soil CEC we did not increase the input date for constructing artificial neural network. Because according to findings of Lake et al. (2009) and Amini et al. (2005) increasing the number of inputs will decrease the accuracy of the estimations. For example for predicting a soil characteristics if just one types of the input data have low correlation coefficients with output data, the accuracy of the model will automatically decrease. The input data in this model were consisted of the percentages of clay and organic carbon. After determination the complexes of training and testing data, in the next step the various models of neural network having one hidden layer and 1-10 neurons in this layer were made. Then, the optimum structures of network by means of coefficient of determination and RMSE criteria were determined. The RMSE values for various numbers of neurons related to studied soil parameter are presented in the Figure 4. As shown in this Figure, the minimum level of RMSE for CEC is related to the network having seven neurons in the hidden layer. Also, with regarding to this figure can be realize that with increasing the number of neurons, the efficiency of models will decrease and hence, the best efficiency is related to the networks having optimum numbers of neurons. The levels of RMSE and R^2 for CEC were 0.47 and 0.94 respectively. Schaap et al. (1998) confirmed applicability of ANNs and concluded that accuracy of these models depend on number of inputs. One of the advantages of neural networks compared to traditional regression PTFs is that they do not require a priori regression model, which relates input and output data and in general is difficult because these models are not known (Schaap and Leij, 1998). The scatter plot of the measured against predicted CEC for the test data set is given in Figure 5. So that according to this diagram, the best fitted line has the angle of near to 45° that shows the high accuracy of estimation by the neural network model.

3.3 Developing PTFs using Fuzzy Table Look-up Scheme

Fuzzy rule-base contains fuzzy rules that include all possible fuzzy relations between inputs and outputs. These rules are expressed in the IF-THEN format. In the fuzzy approach there are no mathematical equations and model parameters, however, all the uncertainties and model complications are included in the descriptive fuzzy inference procedure in the form of IF-THEN statements (Tayfur et al., 2003). In this study, fuzzy rules relating the clay and organic carbon contents to soil CEC were inferred from the training data. The antecedent part of the rule (the part starting with IF, up to THEN) included a statement on the clay and organic carbon contents while the consequent part (the part starting with THEN, up to the end) included a statement on soil CEC. For example 'IF the (Clay is Low) and the (O.C is Medium), THEN the (CEC is High)'. Table 5 summarizes the fuzzy rules

constructed in this study. Fuzzy inference engine takes into account all the possible fuzzy rules in the fuzzy rule-base and learns how to transform a set of inputs to corresponding outputs. A general structure of fuzzy system is demonstrated in fig 6. In the main, each fuzzy system consists of three main sections, fuzzifier, fuzzy data base and defuzzifier. At first, input information is made as fuzzy data after bypassing the fuzzifier sections, in which the precise amount value becomes as fuzzy value by membership functions (Fig 7). Defuzzification converts the resulting fuzzy outputs from the fuzzy inference engine to a number. There are several defuzzification methods, such as the weighted average, maximum membership, average maximum membership, and center of gravity, etc. In this study, the centroid method is employed. Later, fuzzy parameters are entered to the fuzzy data base. Fuzzy data base includes two main sections, fuzzy rule-base and inference engine. In fuzzy rule-base, rules related to fuzzy propositions are described. Thereafter, analysis operation is applied by fuzzy inference engine. There are two main fuzzy inference engine-Sugeno and Mamdani- for this purpose. In this paper, Mamdani's inference scheme is adopted for its simplicity (Fig 3) and used for predicting mentioned parameter. Then, the optimum structures of fuzzy table look-up scheme by means of coefficient of determination and RMSE criteria were determined. The levels of RMSE and R^2 for CEC were 0.33 and 0.98 respectively. In addition, the levels of coefficient of determination and RMSE derived by fuzzy inference system for studied soil parameter had higher values than those derived by artificial neural network (Table 6) which is in line with the work done by Akbarzadeh et al. (2009). The fuzzy inference system for CEC was more suitable for capturing the non-linearity of the relationship between variables. The scatter plot of the measured against predicted CEC for the test data set in fuzzy table look-up scheme is given in figure 8. So that according to this diagram, the best fitted line has the angle of near to 45° that shows higher accuracy of estimation by fuzzy table look-up scheme than neural network model. Liu et al. (2003) found that the modified table look-up scheme can predict the time series more accurately when noise was added to the time series. Akbarzadeh et al. (2009) in their study showed that a hybrid method (ANN and Fuzzy model) predicted soil CEC with very high accuracy. Burrough et al. (1992) demonstrated that fuzzy classification produced a superior number of available areas for agriculture compared to conventional Boolean classification. Zorluer et al. (2010) investigated the application of a fuzzy rule-based method for determination of clay dispersibility. In this study, a fuzzy logic approximation method was developed to combine the different results of the double hydrometer, pinhole, Na (%)-TDS and ESP-CEC methods into a single value. This new method was applied to the dispersibility test results of 29 samples, and it gave more reliable and objective results for identifying the dispersibility of the clay soil. Fernández et al. (2009) worked with fuzzy rules-based on classification systems using a preprocessing step to deal with class imbalance. Their aim was to analyze the behavior of fuzzy rule-based classification systems in the framework of imbalanced datasets through the application of an adaptive inference system with parametric conjunction operators. The empirical results showed that the use of these parametric conjunction operators resulted in a higher performance for all datasets with different imbalanced ratios.

4. Conclusion

In this study, artificial neural network model (feed-forward back-propagation network) and fuzzy table look-up scheme were employed to develop a pedotransfer function for predicting soil cation exchange capacity by using available soil properties. This network was consisted of one hidden layer, a sigmoid activation function in hidden layer, and a linear activation function in output layer and Levenberg-Marquardt training algorithm used due to efficiency, simplicity and high speed. Fuzzy inference system is a rule-based system consists of three conceptual components. There are: a rule-base, contains fuzzy IF-THEN rules, a database, defines the membership function and an inference system, combines the fuzzy rules and produces the system results. First phase of fuzzy logic modeling is the determination of membership functions of input-output variables, second is the construction of fuzzy rules and the last is the determination of output characteristics, output membership function and system results. For predicting the soil property by means of PTFs, the input data were consisted of the percentages of clay and organic carbon for CEC. The performance of the neural network model and fuzzy table look-up was evaluated using a test data set. Results showed that fuzzy table look-up scheme had better performance in predicting soil CEC than neural network model. The fuzzy table look-up scheme for this parameter was more suitable for capturing the non-linearity of the relationship between variables. With regarding to the evaluation criteria, the results of this study revealed that the fuzzy table look-up scheme had superiority to the artificial neural networks for prediction of mentioned soil parameter. This is a crucial result because, since ANN- PTFs formed from local data produce more accurate predictions than those built from data spread from a wider area, the concept of data conservation becomes a critical factor in ANN-PTF construction. However, due to difficulties of direct measurement of soil parameters, we recommend using of neuro-fuzzy models in the future studies for obtaining the logical equations of other soil parameters, especially soil hydraulic properties, in each area and also we recommended testing mentioned formula for CEC in other regions.

References

Akbarzadeh, A., Taghizadeh Mehrjardi, R., Rahimi Lake, H., & Ramezanpour, H. (2009). Application of Artificial Intelligence in Modeling of Soil Properties (Case Study: Roodbar Region, North of Iran). *Environ Research J*., 3(2), 19-24.

Amini, M., Abbaspour, K. C., Khademi, H., Fathianpour, N., Afyuni, M., & Schulin, R. (2005). Neural network models to predict cation exchange capacity in arid regions of Iran. *Eur. J. Soil Sci.,* 53, 748-757.

Bell, M. A., & Van keulen, J. (1995). Soil pedotransfer functions for four Mexican soils. *Soil Sci Soc. Am. J.,* 59, 865-871.

Bouma, J. (1989). Using soil survey data for quantitative land evaluation. *Advances in Soil Science,* 9, 177-213.

Breeuwsma, A., Wosten, J. H. M., Vleeshouwer, J. J., Van slobbe, A. M., & Bouma, J. (1986). Derivation of land qualities to assess environmental problems from soil surveys. *Soil Sci Soc. Am. J.,* 50, 186-190.

Burrough, P. A. (1989). Fuzzy mathematics methods for soil survey and land evaluation. *Journal of Soil Science*, 40, 447-492.

Burrough, P. A., MacMillian, R. A., & Van Deusen, W. (1992). Fuzzy classification methods for determining land suitability from soil profile observations and topography. *Journal of Soil Science*, 43, 193-210.

Carpena, O., Lux, A., & Vahtras, K. (1972). Determination of exchangeable calcareous soils. *Soil Sci.,* 33, 194-199.

Chang, L., & Burrough, P. A. (1987). Fuzzy reasoning: a new quantitative aid for land evaluation. *Soil Survey and Land Evaluation*, 7, 69-80.

Drake, E. H., & Motto, H. L. (1982). An analysis of the effect of clay and organic matter content on the cation exchange capacity of New Jersey soils. *Soil. Sci.,* 133, 281-288.

Enea, M., & Salemi, G. (2001). Fuzzy approach to the environmental impact evaluation. *Ecological Modelling*, 136, 131-147.

Fernández, A., Jesus, M. J., & Herrera, F. (2009). On the influence of an adaptive inference system in fuzzy rule based classification systems for imbalanced data-sets. *Expert Systems with Applications*, 36, 9805-9812.

Fernando, M. J., Burau, R. G. & Arulanandam, K. (1977). A new approach to determination of cation exchange capacity. *Soil Sci Soc. Am. J.,* 41, 818-820.

Heusher, S. A., Brandt, C. C. & Jardin, P. M. (2005). Using soil physical and chemical properties to estimate bulk density. *Soil Sci. Soc. Am. J.,* 69, 51-56.

Jain, A., & Kumar, A. (2006). An evaluation of artificial neural network technique for the determination of infiltration model parameters. *Appl. Soft Comput.,* 6, 272–282.

Jang, J. S. R., Sun, C. T., & Mizutani, E. (1997). *Neuro-Fuzzy and Soft Computing: A Computational Approach to Learning and Machine Intelligence*. Prentice-Hall, Inc., Upper Saddle River, NJ, USA.

Karaca, F., & Ozkaya, B. (2006). NN-LEAP: A neural network-based model for controlling leachate flow-rate in a municipal solid waste landfill site. Environ. *Modell. Software.,* 21, 1190-1197.

Kaur, R., Kumar, S., & Gurung, H. P. (2002). A pedotransfer function soil data and its comparison with existing PTFs. *Aust. J. Soil Res.,* 40, 847- 857.

Keller, A., Von Steiger, B., Vander Zee, S. T. & Schulin, R. (2001). A stochastic empirical model for regional heavy metal balances in agroecosystems. *Journal of Environmental Quality.,* 30, 1976-1989.

Keshavarzi, A., Sarmadian, F., Heidari, A., & Omid, M. (2010). Land suitability evaluation using fuzzy continuous classification (a case study: Ziaran region). *Modern Applied Science*, 4(7), 72-81.

Klingseisen, B., Metternicht, G., & Paulus, G. (2007). Geomorphometric landscape analysis using a semi-automated GIS-approach. *Environmental Modelling and Software*, In Press.

Lagacherie, P. (2005). An algorithm for fuzzy pattern matching to allocate soil individuals to pre-existing soil classes. *Geoderma,* 128, 274-288.

Lake, H. R., Akbarzadeh, A., & Taghizadeh Mehrjardi, R. (2009). Development of pedotransfer functions (PTFs) to predict soil physico-chemical and hydrological characteristics in southern coastal zones of the Caspian Sea. *Journal of Ecology and the Natural Environment.,* 1(7), 160-172.

Liu, X., Kwan, B. W., & Foo, S. Y. (2003). Time Series Prediction Based on Fuzzy Principles. *Proc. 'Huntsville Simulation' Conf*, October 8, Huntsville, AL.

Manrique, L. A., Jones, C. A., & Dyke, P. T. (1991). Predicting cation exchange capacity from soil physical and chemical properties. *Soil Sci. Soc. Am. J.,* 50, 787-794.

McBratney, A. B., Mendonca, M. L., & Minansy, B. (2003). On digital soil mapping. *Geoderma*, 117, 3-52.

McBratney, A. B., Minasny, B., Cattle, S. R., & Vervoort, R. W. (2002). From pedotransfer function tosoil inference system. *Geoderma,* 109, 41-73.

McBratney, A. B., & Odeh, I. O. A. (1997). Application of fuzzy sets in soil science: fuzzy logic, fuzzy measurements and fuzzy decisions. *Geoderma*, 77, 85-113.

Mendel, J. M. (2001). *Rule-Based Fuzzy Logic Systems*. Prentice-Hall, Inc., Upper Saddle River, NJ, USA.

Metternicht, G., & Gonzalez, S. (2004). FUERO: foundations of a fuzzy exploratory model for soil erosion hazard prediction. *Environmental Modelling and Software*, 20 (6), 715-728.

Minasny, B., McBratney, A. B., & Bristow, K. L. (1999). Comparison of different approaches to the development of pedotransfer functions for water retention curves. *Geoderma*, 93, 225- 253.

Najafi, M., & Givi, J. (2006). Evaluation of prediction of bulk density by artificial neural network and PTFs. 10th Iranian Soil Science Congress. Karaj., pp: 680-681. (in Persian)

Nelson, D. W. & Sommers, L. E. (1982). Total carbon, organic carbon, and organic matter. In: Page, AL, Miller, RH, Keeney DR (Eds.), *Methods of Soil Analysis*. Part II, 2nd ed. American Society of Agronomy, Madison, WI, USA. pp. 539-580.

Noorbakhsh, F., Jalalian, A., & Shariatmadari, H. (2005). Prediction of cation exchange capacity with using some soil properties. *Iranian Journal of Science and Technology of Agriculture and Natural Resources*, 3, 107-117 (In Persian).

Omid, M., Baharlooei, A., & Ahmadi, H. (2009). Modeling drying kinetics of pistachio nuts with multilayer feed-forward neural network. *Drying Tech*., 27, 1069-1077.

Pachepsky, Y. A., Timlin, D., & Varallyay, G. (1996). Artificial neural networks to estimate soil water retention from easily measurable data. *Soil Sci. Soc. Am. J.,* 60, 727-733.

Park, B. J., Pedrycz, W. & Oh, S. K. (2010). Polynomial-based radial basis function neural networks (P-RBFNNs) and their application to pattern classification. *Applied Intelligence.,* 32, 27-46.

Sun, R. (2009). Data Mining Based on Fuzzy Rough Set Theory and Its Application in the Glass Identification. *Modern Applied Science*, 3(8), 100-105.

Sadiq, R., & Rodriguez, M. J. (2004). Fuzzy synthetic evaluation of disinfection by-products: a risk-based indexing system. *J Environ Manage,* 73, 1-13.

Sahrawat, K. L. (1983). An analysis of the contribution of organic matter and clay to cation exchange capacity of some Philippine soils. *Commun. Soil Sci. Plant Anal.*, 14, 803-809.

Schaap, M. G., & Leij, F. J. (1998). Using neural networks to predict soil water retention and soil hydraulic conductivity. *Soil Till. Res.,* 47, 37-42.

Schaap, M. G., Leij, F. J., & Van Genuchten, M. Th. (1998). Neural network analysis for hierarchical prediction of soil hydraulic properties. *Soil Sci. Soc. Am. J.,* 62, 847-855.

Seybold, C. A., Grossman, R. B., & Reinsch, T. G. (2005). Predicting Cation Exchange Capacity for soil survey using linear models. *Soil Sci. Soc. Am. J.,* 69, 856-863.

Sparks, D. L., Page, A. L., Helmke, P. A., Leoppert, R. H., Soltanpour, P. N., Tabatabai, M. A., Johnston, G. T., & Summer, M. E. (1996). *Methods of soil analysis*. Soil Sci. Soc. of Am. Madison, Wisconsin.

Tayfur, G., Ozdemir, S., & Singh, V. P. (2003). Fuzzy logic algorithm for runoff-induced sediment transport from bare soil surfaces. *Advances in Water Resources*, 26, 1249-1256.

Tran, L.T., Ridgley, M. A., Duckstein, L., & Sutherland, R. (2002). Application of a fuzzy logic-based modeling to improve the performance of the revised universal soil loss equation. *Catena*, 47(3), 203-226.

USDA. (2010). Soil Survey Staff. *Keys to Soil Taxonomy*. 11 th edition.

Vos, B. D., Meirvenne, M. Quataert, V., Deckers, P. J., & Muys, B. (2005). Predictive quality of pedotransfer

functions for estimating bulk density of forest soils. *Soil Sci. Soc. Am. J.,* 69, 500-510.

Wilding, L. P., & Rutledge, E. M. (1966). Cation exchange capacity as a function of organic matter, total clay, and various clay fractions in a soil toposequence. *Soil Sci. Soc. Am. Proc.,* 30, 782-785.

Wösten, J. H. M., Lilly, A., Nemes, A., & Le Bas, C. (1999). Development and use of a database of hydraulic properties of European soils. *Geoderma,* 90, 169-185.

Zhang, B., Zhang, Y., Chen, D., White, R. E., & Li, Y. (2004). A quantitative evaluation system of soil productivity for intensive agriculture in China. *Geoderma,* 123, 319-331.

Zhu, A. X., Band, L. E., Dutton, B., & Nimlos, T. (1996). Automated soil inference under fuzzy logic. *Ecological Modelling,* 90, 123-145.

Zhu, A. X., Yang, L., Li, B., Qin, C., Pei, T., & Liu, B. (2010). Construction of membership functions for predictive soil mapping under fuzzy logic. *Geoderma,* 155, 164-174.

Zorluer, I., Icaga, Y., Yurtcu, S., & Tosun, H. (2010). Application of a fuzzy rule-based method for the determination of clay dispersibility. *Geoderma*, In Press.

Table 1. Example of reliability factors and effective degrees for redundant and inconsistent rules

x_1	x_2	y	*Degree*	*RF*	D_{eff}
A	B	C_1	D_1	3/6	D_1*3/6
A	B	C_1	D_2	3/6	D_2*3/6
A	B	C_1	D_3	3/6	D_3*3/6
A	B	C_2	D_4	2/6	D_4*2/6
A	B	C_2	D_5	2/6	D_5*2/6
A	B	C_3	D_6	1/6	D_6*1/6

Table 2. Statistics of training data set for cation exchange capacity

	Soil parameter	Min	Max	Mean	Std
Training set	CEC ($Cmol^cKg^{-1}$)	7.42	20.45	15.87	2.64
	Clay (%)	3.20	56.80	23.85	12.05
	O.C (%)	0.04	1.10	0.36	0.23

Table 3. Statistics of testing data set for cation exchange capacity

	Soil parameter	Min	Max	Mean	Std
Testing set	CEC ($Cmol^cKg^{-1}$)	11.10	19.69	16.02	2.21
	Clay (%)	7.20	48.00	23.79	11.79
	O.C (%)	0.09	0.76	0.32	0.20

Table 4. Simple linear correlation coefficients (r) between CEC and independent variables

	CEC ($Cmol^cKg^{-1}$)	Clay (%)	O.C (%)
CEC ($Cmol^cKg^{-1}$)	1	0.92^{**}	0.56^{*}
Clay (%)	0.92^{**}	1	0.22^{*}
O.C (%)	0.56^{*}	0.22^{*}	1

* Correlation is significant at the 0.05 level

** Correlation is significant at the 0.01 level

Table 5. Fuzzy rules relating the clay and organic carbon contents to soil CEC (L= Low; M= Medium; H= High; V=Very)

Rule No.	*IF*	*Clay (%)*	*and*	*O.C (%)*	*THEN*	*CEC ($Cmol^c Kg^{-1}$)*
1	IF	VVL	and	L	THEN	L
2	IF	VL	and	L	THEN	M
3	IF	VL	and	M	THEN	M
4	IF	VL	and	H	THEN	M
5	IF	L	and	L	THEN	H
6	IF	L	and	M	THEN	H
7	IF	L	and	H	THEN	H
8	IF	H	and	L	THEN	VH
9	IF	H	and	M	THEN	VH
10	IF	H	and	H	THEN	H
11	IF	VH	and	L	THEN	VH
12	IF	VH	and	M	THEN	VH
13	IF	VH	and	H	THEN	VH
14	IF	VVH	and	M	THEN	VH

Table 6. Statistical parameters in test stage for different methods based on pedotransfer functions

Statistical parameters	Artificial Neural Network	Fuzzy Table Look-up Scheme
RMSE	0.47	0.33
R^2	0.94	0.98

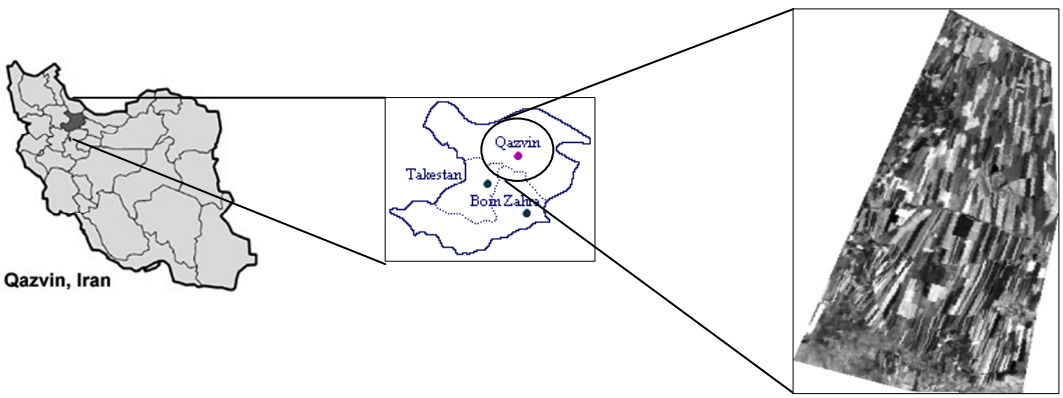

Figure 1. Location of the study area

ISSN 1913-1844 E-ISSN 1913-1852

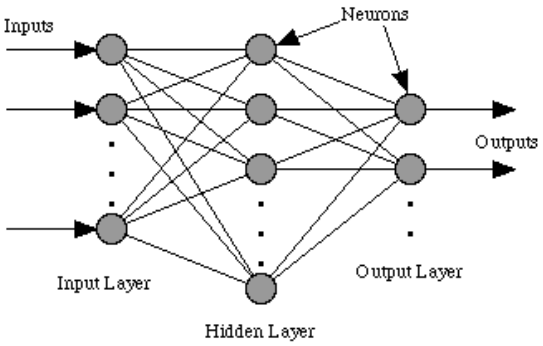

Figure 2. Structure of feed-forward ANN

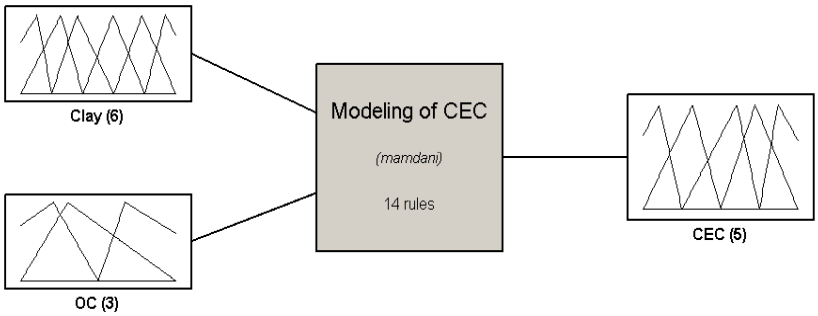

Figure 3. Structure of FIS Recommended model

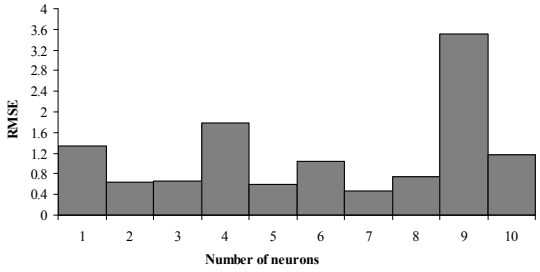

Figure 4. RMSE values for 1-10 neurons in hidden layer (cation exchange capacity)

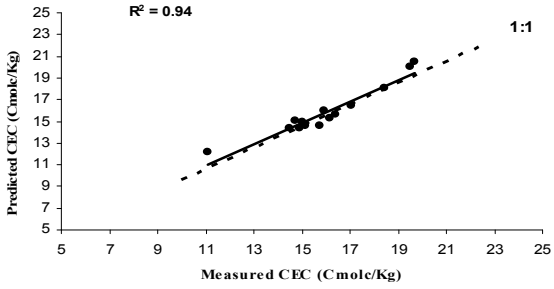

Figure 5. The scatter plot of the measured versus predicted CEC (ANN)

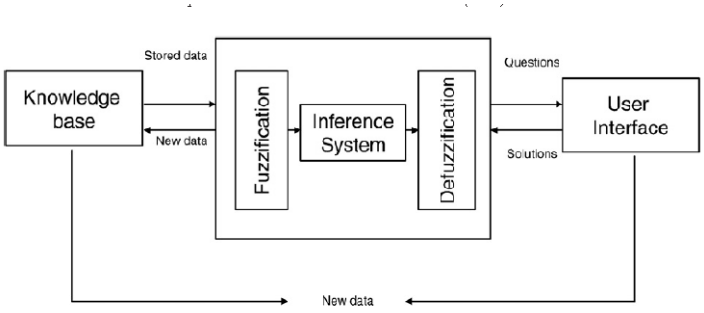

Figure 6. The general structure of the fuzzy inference system

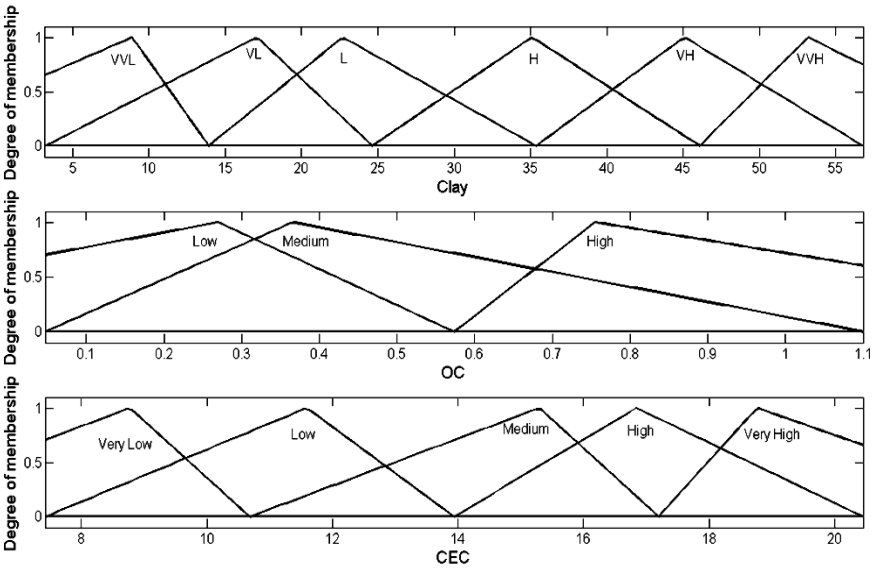

Figure 7. Fuzzy membership functions for input-output

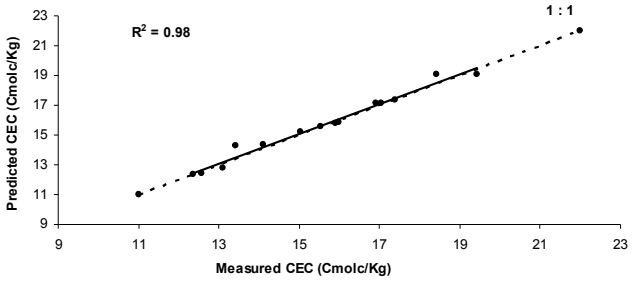

Figure 8. The scatter plot of the measured versus predicted CEC (Fuzzy Table Look-up Scheme)

Research on Grid Architecture and Its Application

Qinghai Bai
College of Computer Science and Technology
Inner Mongolia University for Nationalities
Tongliao 028043, China
Tel: 86-475-239-5155 E-mail: baiqh68@163.com

Ying Zheng
Editorial Department of Journal
Inner Mongolia University for Nationalities
Tongliao 028043, China
E-mail: mindaxuebao@163.com

Foundation item: National Natural Science Foundation of China (authorization number: 60873235, 60473099) and the New Century Excellent Researcher Award Program from Ministry of Education of China (authorization number: NCET-06-0300)

Abstract

With the application of grid computing in more and more industries and departments, the research on the application of grid computing has become a hot topic. The article described the principles and concept of grid computing, discussed two kinds of important grid architecture: Five-Level Sandglass Architecture and Open Grid Services Architecture (OGSA), studied and found the application of grid in genome annotation and geology disaster modeling, the application of SGE in financial analysis and integrated circuit design. The authors analyzed applicable field of grid and the benefit brought by grid to distributed application, and then put forward some suggestions for building grid, which is of significance in the development and popularization of grid computing technology.

Keywords: Grid computing, Grid architecture, Grid application

1. Introduction

With the deep development of science and technology, people desire computer system with higher computing ability. Under the condition a new network computing mode appear, which is a computing mode based on dynamic, heterogeneous and cross-domain collaborative sharing of resource and problem solving(Foster I , Kesselman1 C. 1999). This is grid computing, in brief, grid.

The concept of grid computing was first proposed in the I-WAY project. Although research on grid computing has been more than ten years, until now the differences about the concept of grid still exist. In 2001, Foster, Kesselman and Tuecke defined grid as: coordinated sharing of resource and solve problem in dynamic, multi-institutional virtual organizations. (Foster, I., Kesselman, C., Tuecke, S. 2001). More comprehensive description is that grid is an environment integrating computation and resources, which can integrate the whole internet into huge super computer in order to realize overall integration and sharing of all kinds of related wide resources including computation resource, storage resource, data resource, information resource, knowledge resource, specialist resource and equipment resource et.al. worldwide. Grid computing put forward collaborative and seamless resource sharing and computing problem. Grid computing system integrates distributed heterogeneous resource geographically into a virtual super computer(I. Foster, C. Kesselman. 2004) through network, which is used for large-scale, distributed and high-performance computation. Grid computing provide huge computing ability for users through resource sharing and virtualization.

Since then people carried out all-round theoretical research and specific practice for grid computing, which caused the attention of all the countries' institutions. Currently grid has become a hot topic in the research area globally and developing grid has been known as one of the core task of internet(Xu, Zhiwei, Feng, Baiming & Li, wei. 2004).

2. Grid Architecture

Grid architecture is the technology how to build grid, which gives the basic components and functions of grid, describes the relations between each part of grid and their method of integration and depicts the mechanism which supports grid to operate effectively. Until now comparatively important grid architecture includes mainly: the one is five-Level Sandglass Architecture put forward by Foster in 2001 (Foster, I., Kesselman, C., Tuecke, S.

2001); and the other one is open Grid Services Architecture (OGSA), which is put forward by Foster et.al combining Web Service, under the influence of industrial circles represented by IBM, after considering the development and influence of Web technology.

2.1 Five-Level Sandglass Architecture

Five-Level Sandglass Architecture is architecture with very wide influence. Its main characteristics is simplicity, which main stresses on qualitative descriptions but not specific protocol definition, therefore, it is easy to understand it as a whole.

In Five-Level Sandglass Architecture, the most important idea is centralized on protocol but also emphasizes the importance of service and API (Application Programming Interfaces) and SDK(Software Development Kits).

Five-Level Sandglass protocol model originates from the grid research project Globus of national laboratory in America and is centralized on Intergrid protocol. The five layers of the Sandglass model are as follows from bottom to top: Fabric, Connectivity, Resource, Collective and Application

Here are described the characteristics and functions of the five layers respectively below:

(1) Fabric

The fundamental function of fabric is to control local resources, including query mechanism (for example, find the information such as the structure and state of resources) and the resource management ability to control service quality et.al and provide connector to visit the upper resources. The resources of fabric are very extensive and they may be computation resources, storage system, directory, network resource, sensors and so on. The richer of the functions the resources of fabric provide, the more of the high-level sharing operation the resources of fabric supports, for example, if resource layer supports the function of advance reservation, it will be very easy to realize cooperation scheduling services of resources in higher layers. Otherwise to realize this kind of service will need large extra spending.

(2) Connectivity

The fundamental function of Connectivity is to realize mutual communication. It defines core communication and authentication protocol, which is used for the network transaction processing of grid. Communication protocol allows exchange data between the resources of fabric and the requirements include the functions such as transmission, routing, nominate et.al. Actually most of the protocol is extracted from TCP/IP protocol stack. Authentication protocol is based on communication service and the functions it provides includes: single sign-on, proxy, the integration with local security method and trust mechanism based on users.

(3) Resource

The fundamental function of resource is to realize the sharing of single resource. The protocol defined by resource layer includes security initialization, monitoring, sharing operation to control single resource, auditing and pay fees et.al. It ignores overall situations and atomic operation which crosses distribution resources integration.

(4) Collective

The fundamental function of collective is to coordinate the sharing of all kinds of resources. Collective protocol and service describes the generality of resources, including directory service, collaborative allocation and scheduling and proxy service, monitoring and diagnosing service, data duplicating service, programming system under the support of grid, load management system and coordinated allocation work frame, software discovery service, cooperation service et.al. They show how to interact with each other between different resource collections but don't involve the specific characteristics of resources.

(5) Application

Application exists in virtual organizational environment. Application can be structured according to the service defined by any layer. Each layer defines protocol in order to provide visit to related services, which includes resources management, data access, resource discovery et.al. In each layer, API can be defined as specific realization of the information about service transferring protocol which carry out specific operations.

A small number of core protocols form the bottleneck in the hierarchical structure of protocol, which have to realize the mapping from the higher-level protocol (the top of the Sandglass) to core protocol as well as from core protocol to lower level protocol(the bottom of the Sandglass) at the same time. The numbers of core protocols cannot be too many so that core protocols become the bottleneck of the hierarchical structure of protocol. Resource and connective layers consists the bottleneck of the core. The protocols of these layers are designed that they can adapt to different kinds of resources defined by fabric layer. Therefore, they may be used to build the services of collective layer and special applications.

The projects which use the grid include: Information power grid of National Aeronautics and Space Administration (NASA), National Technology grid of The National Science Foundation, Vega Grid and China Grid.

2.2 Open Grid Services Architecture (OGSA)

The most fundamental idea of OGSA is centralized on service. In the architecture of OGSA, all the grid resources exist in the form of service and the sharing of resource is embodied by the sharing of service in OGSA architecture. The abstraction from resource to service integrates resource, data and information et.al effectively, which is more beneficial for the realization of dynamic sharing mechanisms between virtual organizations.

OGSA put forward the concept of grid service, which is a kind of web service and provide a group of connectors. These connectors are well-defined and comply with specific management so as to solve the problems such as service discovery, the creation of dynamic service, lifecycle management and notification et.al. Grid service finishes different functions through defining connectors and service data is the information about the examples of grid service.

In OGSA, everything is seen as grid service so grid is extensible set of grid service. Grid service can be integrated by different way in order to satisfy the needs of virtual organizations. Virtual organizations can be defined partially according to the services they operate and share by themselves(Du, Zhihui, Chen, Yu & Liu, Peng. 2002). The main layers of OGSA are:

(1) Resource layer. It includes physical resources and logical resources. Physical resources include storage, network, computer, display device, server and other related local services. Logical resources provide extra functions and general middleware, for example, file system, database, directory, workflow management and security certification et.al through virtualization and integration with physical resources. The abstract services are provided based on physical grid.

(2) Web service layer. In the layer all the grid resources including physical and logical resource are modeled as services. OGSI(Open Grid Services Infrastructures) specification defines grid service and build it on the basis of standard web service technology. OGSI further extends the definition of web service and make use of such web service mechanism as XML and WSDL to provide dynamic, real-time and manageable web service ability for all the grid resources to designate standard connectors, behavior and interaction.

(3) Grid service layer based on OGSA. Web service layer and its OGSI extension provides infrastructure for the upper layer: grid service based on OGSA, which is the core service layer of grid and mainly consists of four kinds of services: service management, service communication, strategy management and security.

(4) Grid application layer. As time goes on, a group of rich service based on grid architecture is developed continuously and new grid application program which uses one or more services based on architecture also appears, which consists the fourth main layer of OGSA architecture.

OGSA conforms to standard web service frame. Web service solves the problem to discover and activate permanent service, but there is a great amount of temporary service in the grid. Therefore, OGSA expands web service and proposed the concept of grid service, so that it can support temporary service cases and dynamically create and delete.

OGSA takes service as the center, which has the following advantages:

In grid, everything is service. Through providing a group of unified core connectors, all the grid services are realized based on the connectors. It is very easy to create hierarchical structured and higher level service, which can cross different abstract levels and be taken on unified way.

Virtualization also makes it possible to map a couple of logical resource to the same physical resource. While combining with service, it is unnecessary to consider specific realization. Based on lower level resources, carry out resource management in virtual organizations. Pass through the virtualization of grid service, can behavior and the service semantic of be general, shine upon the local infrastructure of platform without seam over.

3. Grid application

The discovery net (http://www.discovery-on_the.net/) is a service-oriented frame, which provides a great deal of analysis on scientific data based on workflow or channel technology and adopts Discovery Process Markup Language(DPML) to represent and storage workflow. Discovery net has been applied into such fields as life science, geology disaster modeling et.al.

3.1 genome annotation

The application of genome annotation is not only a kind of work with large amount of data and high computation strength but it also needs the integration of a large number of datasets and tools, which often spread online of course. In addition, it is a kind of coordinated application, in which a lot of scientists who live in different places have to share datasets and analysis results. In supercomputing Conference hold in Baltimore in America in 2002(www.sc-conference.org/sc2002), a kind of prototype of genome annotation has been demonstrated successfully and annotation channel is operating in all kinds of distributed resources. For example, the high-performance resource of London e-science centre (http://www.lesc.ic.ac.uk/), Baltimore's server and databases distributed in all over Europe and America.

3.2 Geology disaster modeling

Make use of images of Landsat-7 ETM+ (http://www.landsat.org/) and basic structure of discovery net, can disorderly movements of earthquake be analyzed. The main characteristics of this application are to analyze the requirements of Landsat image hiding algorithm for a large amount of computation.

Making use of geological hazard model system, remote sensing scientists made an analysis on the Ms8.1 magnitude seismic data which happened in uninhabited region of eastern Kunlun range in China on November 14, 2001. Their conclusions based on the 2D survey moving through this seismic region revealed the illumination mode locating on the left strand displacement of coseismic cycle, which were not researched and in the region between 1.5and 8.1 meter along Kunlun fault.

3.3 The application of SGE(Sun Grid Engine) in Integrated Circuits(IC) design

Synopsys (http://www.synopsys.com) located in California is a software developer of Integrated Circuits(IC) design. The technology of electronic products is developing with unprecedented speed. The integrated circuits which can only contain thousands of transistors previously can contain millions of transistors now and it will reach one billion in the near future. But this kind of increasing complexity of silicon only relies on advanced electronic design automation tools. Without the tools it is impossible to work out so complex products. Under grid environment, the regression test adopting SEG to manage the cluster which is made up of 180 CPU, has to spend 10-12 hours in the past but it just need 2-3 hours now.

3.4 The application of SEG in financial analysis

The BMO financial group (http://www.bmo.com) found in 1817 is one of the biggest providers of financial services in North America. In July 2003, it had about 268 billion dollars of assets and 3400 staff. BMO provides a great deal of retail-banking, healthy management, bank products and solutions. The organization adopted Monte Carlo high strength calculation simulation to carry out risk assessment. In order to accelerate the simulation process, Sun Fire4800 and V880 server built a SEG management cluster and adapted StorEdge3910 server to storage data(Maozhen Li,Mark Baker. 2006). Making use of the cluster to carry out Monte Carlo simulation and other related risk management calculation, the conclusions are drawn and reports are given before the working hours 9:00am of the second day, but this work needs one week in the past.

References

BMO, [Online] Available: http://www.bmo.com.

Discovery Net, [Online] Available: http://www.discovery-on_the.net/.

Du, Zhihui, Chen, Yu & Liu, Peng. (2002). *Grid computing. Beijing:* Tsinghua University Press.

Foster I , Kesselman1 C. (1999). The Grid: Blueprint for a Future Computing Infrastructure[M].USA: Morgan Kaufmann Publishers, 1999.

Foster, I., Kesselman, C., Tuecke, S. (2001). The Anatomy of the Grid: Enabling Scalable Virtual organizations. *International Journal of Supercomputer Applications,* 15(3), 2001.

Foster, I., Kesselman, C., Tuecke, S. (2001). The Anatomy of the Grid: Enabling Scalable Virtual organizations. *International Journal of High Performance computing Applications,* 15(3):200-222, 2001.

I. Foster, C. Kesselman. (2004). The Grid 2: Blueprint for a New Computing Infrastructure, Morgan Kaufmann, 2004.

Landsat, [Online] Available: http://www.landsat.org/.

LeSC, [Online] Available: http://www.lesc.ic.ac.uk/.

Maozhen Li,Mark Baker. (2006). Translated by Wang, Xianglin, Zhang, Shanqing & Wang, Jingli. *The grid core technologies.* Beijing: Tsinghua University Press. 2006.12.

SC2002, [Online] Available: www.sc-conference.org/sc2002.

Synopsys, [Online] Available: http://www.synopsys.com.

Xu, Zhiwei, Feng, Baiming & Li, wei. (2004). *Grid Computing Technology.* Beijing: Electronic Industry Press, 2004:110.

A Rank Based High Resolution Bearing Estimation Method in Passive Arrays

Ali Ranjbaran
School of Electrical and Electronic Engineering, Universiti Sains Malaysia, Engineering Campus
14300 Nibong Tebal, Seberang Perai Selatan, Pulau Pinang, Malaysia
Tel: 60-4-599-5999 ext. 603, Fax: 60-4-594-1023 Email: j.ranjbaran@yahoo.com

Anwar Hasni Abu Hassan
School of Electrical and Electronic Engineering, Universiti Sains Malaysia, Engineering Campus
14300 Nibong Tebal, Seberang Perai Selatan, Pulau Pinang, Malaysia
Tel: 60-4-599-5999 ext. 603, Fax: 60-4-594-1023 Email: anwar@eng.usm.my

Eng Swee Kheng (Corresponding author)
School of Electrical and Electronic Engineering, Universiti Sains Malaysia, Engineering Campus
14300 Nibong Tebal, Seberang Perai Selatan, Pulau Pinang, Malaysia
Tel: 60-4-599-5999 ext. 603, Fax: 60-4-594-1023 Email: khengkent@gmail.com

Abstract

A rank based bearing estimation method of a passive array is proposed in this paper. Adding a random signal to an array data model to increase the rank and changing the location of the signal to reduce the rank, is the main action. To obtain the optimum estimation in noisy environments a criteria function is introduced. The peaks of the function give us the best candidate for location of the main targets. An array of three sensors with two independent targets is simulated to demonstrate the qualification.

Keywords: Correlation, Signal Space, Noise Space, Eigenvalue

1. Introduction

Processing the signals received on an array of sensors to find location of emitters is one of the greatest interesting problems in sonar and radar applications (Kumaresan, R. Trufts, D. W. 1983). A general case considers an arbitrary number and location of sensors and emitters in an arbitrary noise environment with arbitrary mean and covariance. As a real condition in most practical cases, we deal with independent sources and independent noise so that the correlation between emitters and noise and emitters is zero (Huang, Y. D. and Barkat, M. 1991). This property is the basis of many high resolution bearing estimation techniques under assumption of zero mean and independency of noise and emitters (Schmidt, 1979). Our proposed method is concentrated on a half wavelength $M+1$ dimensional array with P independent emitters under the condition of $P \leq M$ and zero mean Gaussian normal noise. We begin our discussion with introducing a data model for an $M+1$ dimensional array and one emitter. After explaining the basic concepts in this area we will present our method.

1.1 The data model

According to the figure-1 the received wavefront on first sensor is x_0 according to the following equation

$$x_0 = \frac{1}{r} a(t - r/v) e^{i\omega(t-r/v)} + n_0 \quad (1)$$

where $a(t)$ is the time varying envelope of the emitter that is attended by $1/r$, r is the distance, v is wave velocity ,ω is working frequency and n_0 is the noise on this sensor(Harabi, F. Changuel, H. and Gharsallah, A. 2007). This signal is received on the second sensor with $\Delta r/v$ sec delay according to the next relation

$$x_1 = \frac{1}{r} a(t - (r + \Delta r)/v) e^{i\omega(t-(r+\Delta r)/v)} + n_1 \quad (2)$$

In this equation $v=\lambda/T$ is the wave velocity where λ and T are the length and period of the wave respectively. After some simplification and considering $d=\lambda/2$ and $\Delta r=d\sin(\theta)$ we have

$$\frac{1}{r} a(t - (r + \Delta r)/v)\, e^{i2\pi/\lambda} \approx c(t) \quad (3)$$

$$x_1 = c(t) e^{i\omega t} e^{i\pi d \sin(\theta)} + n_1 \quad (4)$$

The term $\Delta r/v$ in exponential function creates $\psi = \pi\, d\sin(\theta)$ delay on the sensor signal. Computing the $M+1$ signals of the array we have the following data model

$$x_0 = c(t) e^{i\omega t} + n_0$$
$$x_1 = c(t) e^{i\omega t} e^{i\psi} + n_1$$
$$x_M = c(t) e^{i\omega t} e^{iM\psi} + n_M \quad (5)$$

Now as general model, we arrange the equation to consider P emitters for an array of $M+1$ sensor.

$$x_0 = c_1(t) e^{i\omega t} + c_2(t) e^{i\omega t} + \ldots c_p(t) e^{i\omega t} + n_0$$
$$x_1 = c_1(t) e^{i\omega t} e^{2i\psi 1} + c_2(t) e^{i\omega t} e^{2i\psi 2} + \ldots cp(t) e^{i\omega t} e^{2i\psi p} + n_1$$
$$x_M = c_1(t) e^{i\omega t} e^{Mi\psi 1} + c_2(t) e^{i\omega t} e^{Mi\psi 2} + \ldots c_p(t) e^{i\omega t} e^{Mi\psi p} + n_M \quad (6)$$

We should denote some important problems in the data model that is considered in our method. It is supposed that the location of the targets is constant during the process while the envelope signal is changing with time. This factor limits us to estimate the bearing of low speed targets. Continuing the investigation we consider matrix model of data as follow

$$X = \left(A1(\psi 1) \middle| A2(\psi 2) .... \middle| A_p(\psi_p)\right) \begin{pmatrix} S_1 \\ S_2 \\ S_p \end{pmatrix} + \begin{pmatrix} n_0 \\ n_1 \\ n_M \end{pmatrix} = A_{M\times P}\, S_{Px1} + N_{Mx1} \quad (7)$$

1.2 Basic Concepts

The vector $A_1(\psi_1)$ which is the first column of the incident matrix A, is the incident vector of the first target at angle ψ_1. Each column of matrix A is an incident vector of the related target so this matrix can be interpreted as signal subspace of all the targets that is perpendicular to noise subspace. The rank of matrix A is the number of the independent columns that is equal to the number of independent targets (Nuttall, 1976). If there are two correlated targets in the system one of the columns in matrix A is linear combination of the others so the rank will be decreased consequently. The determinant of the matrix A is zero because the rank is lower than M and this matrix has at least one zero eigenvalue (Donelli, M., S. Caorsi, F. DeNatale, M. Pastorino, and A. Massa, A. 2004). The vector S is the vector of time dependent magnitude of target signals and N is the received noise vector. It should be denoted that this assumption that noise samples are independent of each other is reasonable in most practical applications. Most important is that we do not have A, S and N separately and we can only obtain the X vector in practice. The process to decompose the noise and signal subspaces as the basis of many high resolution algorithms is consisted of two *correlation* and *averaging* steps. So these two steps together are such transformation that distinct the signal and noise subspace from the correlation matrix. The mapping trend begins by taking the K frame of data under the satisfactory sampling rate to compute the K coloration matrices. Averaging then achieves the final correlation matrix with necessary specification that enables us to factorize the matrix to two separated signal and noise subspaces. To show the very interesting property of the process, we first consider the correlation matrix R before the averaging step. Considering the equation (7) the coloration is computed as

$$R = X X^T = (A_{M\times P}\, S_{Px1} + N_{M\times 1})(A_{M\times P}\, S_{P\times 1} + N_{M\times 1})^T \quad (8)$$

After the simplification we have

$$R = ASS^T A^T + ASN^T + NS^T A^T + NN^T \quad (9)$$

The determinant of matrix R is zero so the determinant of all term should be zero. As the conclusion of averaging process, some important changes are happened:

1- SS^T is the correlation matrix of emitters that its entries changes under the averaging process such that the multiplication terms of different targets tends to be zero because they are independent. This event changes its determinant to a non-zero value because the non-diagonal terms go to zero while the diagonal ones remain.

2-SN^T and NS^T are the correlation matrices between noise and signal and all the elements tend to be zero after the averaging process.

3- The interesting change is happened on the noise correlation matrix $\boldsymbol{NN^T}$. The diagonal entries tend to variance of the noise $\boldsymbol{\sigma^2}$, the others go to mean and determinant is non-zero after the averaging step so $\boldsymbol{NN^T}$ is $\boldsymbol{\sigma^2 I}$.

As matrix $\boldsymbol{A}$ is independent of the averaging process, its determinant doesn't change so the determinant of $\boldsymbol{ASS^TA^T}$ is remained zero while $\boldsymbol{NN^T}$ has found a non-zero determinant. The conclusion is that the averaged correlation matrix $\boldsymbol{R_f}$ will have a non-zero determinant. At this condition we obtain

$$\mathrm{Det}(\mathrm{ASS^T A^T}) = \mathrm{Det}(\mathrm{R_f} - \sigma^2 \mathrm{I}) = 0 \tag{10}$$

According to this relation $\boldsymbol{\sigma^2}$ can be interpreted as the eigenvalue of - $\boldsymbol{R_f}$ or $\boldsymbol{\sigma^2}$ is minimum eigenvalue of $\boldsymbol{R_f}$. To find eigenvalues of $\boldsymbol{R_f}$ we have

$$\mathrm{Det}(\lambda \mathrm{I} - \mathrm{R_f}) = 0 \tag{11}$$

where $\boldsymbol{\lambda}$ is eigenvalue of $\boldsymbol{R_f}$. The above relation is equal to

$$\mathrm{Det}((\lambda - \sigma^2 \mathrm{I}) - \mathrm{ASS^T A^T}) = 0 \tag{12}$$

This relation means that eigenvalues of the matrix $\boldsymbol{ASS^TA^T}$ are $\boldsymbol{\lambda - \sigma^2}$ or the eigenvalues of $\boldsymbol{R_f}$ are the eigenvalues of matrix $\boldsymbol{ASS^TA^T}$ plus $\boldsymbol{\sigma^2}$. Therefore for $\boldsymbol{P}$ nonzero eigenvalues of $\boldsymbol{ASS^TA^T}$ as $\boldsymbol{\lambda_p}$, the correlation matrix $\boldsymbol{R_f}$ has $\boldsymbol{\lambda_p + \sigma^2}$ eigenvalues while the $\boldsymbol{Q=M+1-P}$ remained eigenvalues of $\boldsymbol{R_f}$, are $\boldsymbol{\sigma^2}$. The consequent of the above analysis is that the signal subspace can be recovered by $\boldsymbol{P}$ number of $\boldsymbol{\lambda_p + \sigma^2}$ eigenvalues and related eigenvectors while the noise subspace by $\boldsymbol{Q}$ number of $\boldsymbol{\sigma^2}$ eigenvalues and related eigenvectors as the following equation

$$\mathrm{R_f} = \Sigma(\lambda_{\mathrm{pi}} + \sigma^2)\mathrm{V_i V_i^T} + \Sigma \sigma^2 \mathrm{U_j U_j^T} \tag{13}$$

The first term of the equation above recovers the signal subspaces of the correlation matrix $\boldsymbol{R_f}$ in which the eigenvalues are the combination of targets and noise. As we deal with signal to noise relation, under strong noisy condition the eigenvalues that reconstruct signal subspace will be influenced and changed according to the equation (13). The second term that recovers noise subspace and is perpendicular to signal subspace means that the internal product of each vector in the signal subspace with the noise subspace is zero. MUSIC (Multiple Signal Classification) as a high resolution bearing estimation method uses this property to find the location of targets (Schmidt, 1979)(Liggett, 1973). As the incident vectors are perpendicular to the noise subspace this algorithm search to maximize the following cost function

$$J = \left(\begin{pmatrix} 1 e^{i\psi} & e^{ip\psi} \end{pmatrix} \left(\sum U_j U_j^T \right) \begin{pmatrix} 1 \\ e^{-i\psi} \\ e^{-ip\psi} \end{pmatrix} \right)^{-1} \tag{14}$$

The signal vectors that maximize $\boldsymbol{J}$ would be the best candidates for the bearing of the targets.

1.3 Rank of Correlation Matrix

The rank of a matrix is the number of independent columns or rows that can be detected by the number of non-zero eigenvalues under a singular value decomposition process. As practical point of view in the case that signals to noise ratio is weak, computing the rank would be difficult. This difficulty is appeared because the level of noise increases and some of the minimum eigenvalues are places on threshold band of decision. This problem decreases the capability of detecting the matrix rank. In the conditions that the rank plays important roles, using appropriate method is necessary. As in the proposed algorithm in this paper the rank of correlation matrix has the main role, a proper rank detecting method is essential (Saidi, Z. and Bourennane, S. 2007). An adaptive threshold level for decision can decrease the problem by introducing a variable level related to the variance of noise. Independent of the methodology, having reasonable and stable criteria to estimate rank is important. Our idea in this research is to consider a threshold approximately equal to minimum eigenvalue.

2. Methodology

Our proposed method in this article is in the base of the following items:

1- The targets are independent so their correlation is zero

2- The rank of the correlation matrix is equal to the independent targets

The center of concentration of our novel method is that when a target is placed in the direction of another for either independent or correlated condition, the rank of the correlation matrix decreases by one. This property gives the idea of adding an independent target to the data model so that with changing its location, the rank of new correlation matrix reduced by one when it is placed in direction of any targets. Adding an independent

source to the data model to increase the rank of correlation matrix and changing its angle from zero to 180 degree to reduce the rank is the basis for finding the main targets. As the estimation of the rank of the correlation matrix is in the base of computing its eigenvalues, the difficulties of detecting problem are appeared especially when the variance of noise is high. In using this method the following factors are important:

1-Adding new target to the data model should not change the model so the amplitude should not be high.

2- Computing the number of eigenvalues that are approximately equal to minimum

2- Comparison with the original condition should be done under the appropriate criteria

To implement the method we first compute the eigenvalues of the original correlation matrix. Then we add an independent signal to model with proper amplitude and the angle of zero. To detect the rank we change the angle and search to maximize the following function

$$J = \left(\sum(\lambda_{inew} - \lambda_{iold})^2 / \lambda_{1old}\right)^{-1} \quad \text{for i = Q to M} \tag{15}$$

$\boldsymbol{\lambda_{new}}$ and $\boldsymbol{\lambda_{old}}$ are minimum eigenvalues of the new and original correlation matrix respectively. The new minimum eigenvalues $\boldsymbol{\lambda_{new}}$ will be computed for each angle to cover the 180 degree band. The result is a function $\boldsymbol{J}$ that is maximized at the angle of the main targets. The term $\boldsymbol{\lambda_{old}}$ is used to give relative sensibility. The amplitude of the added signal is considered to be about 1/10 of the first diagonal entry of the original correlation matrix to prevent of considerable change in data model. As the added signal should be independent of each target, the best candidate is a random signal. In conclusion we add a noise with variable location to the model and change the location from -90 to 90 to compute $\boldsymbol{J}$. The peak locations of $\boldsymbol{J}$ give us the reduction of rank by one and consequently the location of the targets.

3. Implementation

To implement the algorithm, we first introduce the adding technique. A source at location zero degree means that its related signal is received on array by the same phase so when it is in location $\boldsymbol{\varphi}$, we should add this signal to our data model as follow

$$\begin{aligned} x_{0new} &= x_{0old} + a(t)e^{i\omega t} \\ x_{1new} &= x_{1old} + a(t)e^{i\omega t}\, e^{i\varphi} \\ x_{Mnew} &= x_{Mnew} + a(t)e^{i\omega t}\, e^{iM\varphi} \end{aligned} \tag{16}$$

The added signal is a $\boldsymbol{K}$ sample of a sine wave at working frequency $\boldsymbol{\omega}$. This signal is modulated by a random signal $\boldsymbol{a(t)}$ and shifted by phase $\boldsymbol{\varphi}$. $\boldsymbol{a(t)}$ is a random signal because it should be independent of any arbitrary target to satisfies the translation property as discussed in the data model section. We add this signal with one degree of resolution in a range of -90 to 90 degrees. In each step the new correlation matrix is constructed and decomposed to its subspaces to compute criteria function $\boldsymbol{J}$ as a function of $\boldsymbol{\varphi}$. Reduction of the rank will happen in peak points of $\boldsymbol{J}$ so we can plot $\boldsymbol{J}$ to obtain the result. A data model for an array of three sensors and two targets is simulated to test the method. We locate our target at 21 and 30 degrees as the first test. The conclusion of implementation of the proposed method in 0 db signal to noise ratio is demonstrated in figure-2. The behavior of criteria function is very sharp because the rank is a discrete quantity so it cannot be changed gradually. In the second test according to figure-3, we locate two targets very close at 28 and 30 degrees. The figure clearly shows the capability of the method to detect very near targets in 0 db signal to noise ratio by a passive array of three sensors.

4. Conclusion

A high resolution rank based bearing estimation method in passive array is proposed in this paper. The method works in the base of adding a variable location random signal to the real data model and search to find the locations that reduces rank of the correlation matrix by changing the angle of the added signal. Rank estimation is done by decomposing correlation matrix to its signal and noise subspace and computing minimum eigenvalues of the matrix. A cost function is introduced to show the location of the main targets where it is maximized. An array of three sensors is simulated to show the capability of the method in detecting very near targets in 0 db signal to noise ratio. The graphs demonstrated in the figure-2 and figure-3 clearly show that this technique is enable to distinct two near targets by a simple array. In the first case, there are two targets at 21 and 30 degree respectively. Figure-2 clearly shows that the algorithm has detected two targets sharply. The result of the second case in figure-3 demonstrates that the resolution of the method in three element arrays is approximately 2 degrees in 0 db signals to noise condition. As the resolution can be increased by using more number of elements in an array it can be concluded that this method can achieve more accurate results in a larger array.

References

Liggett, W. S. (1973). Passive sonar: Fitting models to multiple time series, in Signal Processing, J. W. R. Griffiths et al., Eds. New York: Academic Press.

Nuttall, A. (1976). Spectral analysis of a universe process with bad data points, via maximum entropy, and linear predictive techniques. NUSC Tech. Rep. TR 5303, New London, CT.

Schmidt, R. (1983). Multiple emitter location and signal parameter estimation. IEEE Trans. ASSP, 35, pp. 276-280.

Kumaresan, R. Trufts, D. W. (1983). Estimating angles of arrival of multiple plane waves. IEEE Trans. AES, 19, pp. 134-139.

Harabi, F. Changuel, H. and Gharsallah, A.(2007). Direction of arrival estimation method using a 2-L arrays antenna. Progress In Electromagnetics Research, PIER 69, 145{160.

Donelli, M., S. Caorsi, F. DeNatale, M. Pastorino, and A. Massa, A. (2004). Linear antenna synthesis with a hybrid genetic algorithm. Progress In Electromagnetics Research, PIER 49, 1{22.

Huang, Y. D. and Barkat, M. (1991). Near-field multiple source localization by passive sensor array. IEEE Trans. Antennas Propag., vol. 39, no. 7, pp. 968-975, Jul.

Saidi, Z. and Bourennane, S. (2007). Cumulant-based coherent signal subspace method for bearing and range estimation. EURASIP Journal on Advances in Signal Processing, Article ID 84576, 9 pages, doi:10.1155/2007/84576.

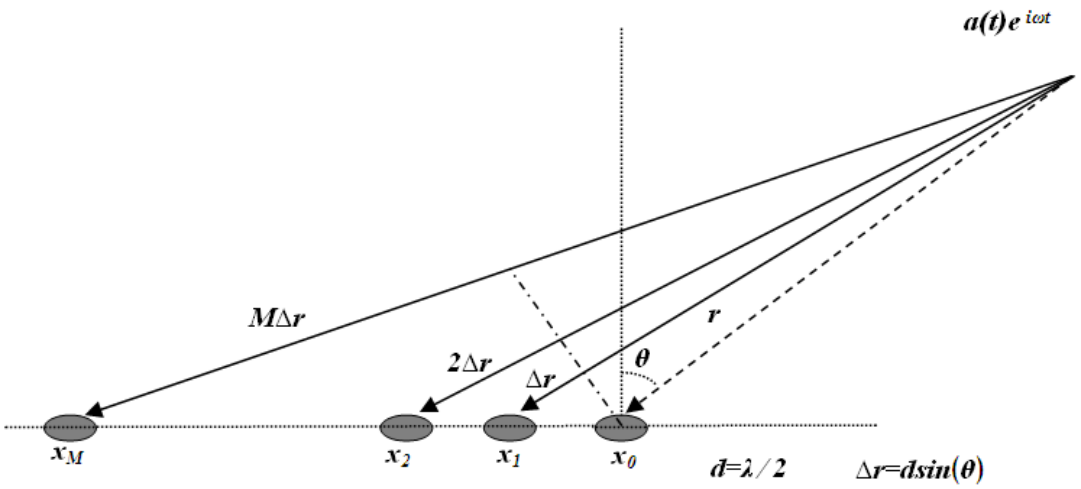

Figure 1. The Passive Array of Sensors

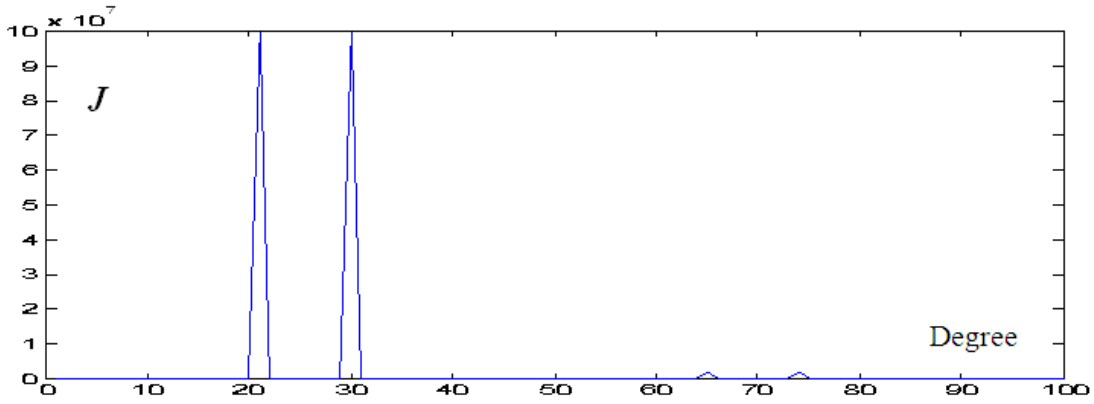

Figure 2. Rank Based Estimation for 21 and 30 Degrees in 0 db Signal to Noise Ratio

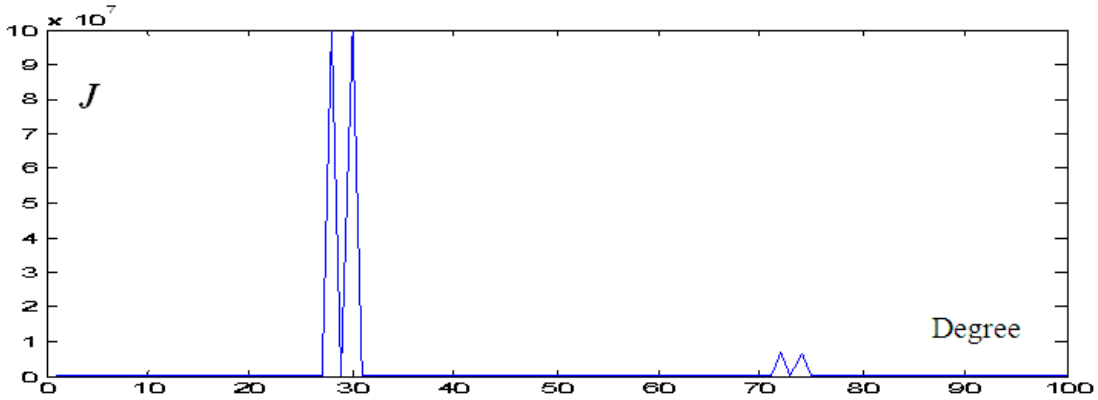

Figure 3. Rank Based Estimation for 28 and 30 degrees in 0 db Signal to noise Ratio

 ISSN 1913-1844 E-ISSN 1913-1852

Structural Characteristics and Genetic Mechanism of Fracture in Shiwu Oilfield

Hu Li & Qirong Qin
Southwest Petroleum University
Chengdu Sichuan 610500, China
E-mail: 349274410@qq.com

Wenhua Tang
Drilling & Pruducing Company of Zhongyuan oilfield
Puyang Henan 457001, China
E-mail: tangwenhua2000@163.com

Mingyuan Tang
Yan Chi producing factory of Huabei Petroleum
Ning Xia 751500, China
E-mail: tmytxl19840120@163.com

Abstract

Based on the core, chip,drilling, Seismic data,etc,Combining the tectonic evolution of shiwu fault, comprehensive study the Charcteristics of Structural, fracture and the genetic mechanism of fracture.after study:on the basis of the reaearch on the Xiaokuan fault and nearby north-south faults,6 secondary structure units are divided.They are: Xiaokuan extrusion and strike-slip zone,Qikeshu syncline belt,Dawujiazi and Xiaowujiazi fault belt,Nanling fault terrace,and Liangjiatun fault terrace.after study on the length and density by Weighting Process, Crack is developed in Shiwu Oilfield;it is affected by five tectonic movements and formed the four periods fracture;extensional directions of these fractures are NE,SN,NW,NNE,NNW,EW, etc.

Keywords: Structural Charcteristics, Fracture, Genetic mechanism, Weighting Process, Shiwu Oilfield

1. Research Area Site

Shiwu Oilfield located at the boundaries of Gongzhuling of Jilin Province, QinJiatun Oilfield is in the east, Siwujiazi Oilfield is in the south and Taipingzhuang Oilfield is in the Northeast. Research area approximately is 100km^2. it is in the tectonic belt of Siwujiazi structure,The conformation is a large-scale broken-nose structure(Liying Yang, Ruilei Li & Jiangtao Zhang. 2005)(Kai Yu, Zhensheng Yang& Baiping Yao. 2000). The tectonic movement of research area is intense and structural features is complicated, it developed a series of fault with NE,NNE,NNW and SN position, Structural form showing the characteristic of North East is high and Southwest is low, Structure fracture growth.

2. Structural Features

2.1 Division of Tectonic Units

Under the control of Xiaokuan fault,Bawu, Daijiatun,Nanling faults present to western-leaning volts and control the local sedimentary of fault period. According to the segmentation of these faults (Haibo Bai. 2002)(Yunsheng Wang& Shitian Wang. 2000)(Danping Yan& Xinwen Wang. 2000),we divided Shiwu Oilfield into the following six tectonic units. Its main characteristics are as follows:

(1) Xiaokuan extrusion and strike-slip zone

It is mainly fault zone as the result of the left-lateral strike-slip of Xiaokuan fault, located on both sides of Xiaokuan fault and face stretching along SW-NE to TaiPingzhuang,nearby TaiPingzhuang, Negative flower structure of Xiaokuan fault is more obvious.in the south of Xiaokuan fault,it has derived a NE reverse slip fault,what is more,it has associated a regulation fault with nearly EW trending, nearly SN,NNW ,NNE en echelon fault and NE abnormal fault. At the same time, it also formed Siwujiazi anticline with NE axial direction,The north side was cut into two north-south,The south side extend to Qikeshu syncline belt.

(2) Qikeshu Syncline Belt

It located between Xiaowujiazi fault belt and Qinjiatun fault belt, and it is a west plunging, north-south direction cocked syncline. Fault subsidence lay showed overlapping In the NE direction, relatively stable, faults developed very simple, and it is easy to form litho stratigraphic reservoir.

(3) Dawujiazi and Xiaowujiazi fault belt, Nanling fault terrace, and Liangjiatun fault terrace

These 4 fault belts are situated at the north of Xiaokuan fault,it is formed from west to east in development, the main foundation of the division:Bawu,Daijiatun,Nanling faults Nearly NS direction ,it is formed earlier. Fault belts had been strike slip displacement last stage of Yingcheng formation and last stage of Denglouku formation most intense period,under the control of Xiaokuan extrusion and strike-slip zone and affected by the sinistral strike slip,it associated with the formation of nearly SN,NNE,NNW faults etc.in the cut plane,it showed negative flower,cabbage-like constructive style.

2.2 Fracture Activities Features

Fracture activities is intense in Shiwu Oilfield,which developed second order fault zone that control structure , developed third order fault zone control traps and block pattern, also developed forth order fault zone, The main fracture characteristics as follows:

Xiaokuan fault: second order fault zone that to the NE overall, Xiaokuan fault acceptted by compression efficiency nearby Xiaowujiazi, it showed positive flower in profile and the thrust is intense, there is a tendency of being thick in Yingcheng formation and overlying formation. It developed a series of en echelon faults within the zone,which become favorable zones of the gas and oil mixed together.Xiaokuan fault take this as the stress release centre,developed negative flower structure in the east and west, especially in the NE of low angle of bedding.Xiaokuan fault control the sedimentary of early SE faulted depression layer,Huoshilin and Shahezi formation east thin with cuneal, amplitude 20-500m, fractured surface dip about 50°, trend SSE, abrupt stratigraphic position T_3-T_5,and it is an important fault which control the tectonic belt that developed at early phase,affected by sinistral strike slip in the end of Yingcheng and Denglouku formation.

Bawu fault:third order fault zone,that is a centripetal fault which near SN trend, the trend of the south near Xiaokuan fault is NWW and the trend of the north is west.the extention of the fault is about 11 km, amplitude 10-180m; abrupt stratigraphic position T_3-T_5, fractured surface form is steeper at the upper portion and gentler in the lower portion,it control the sedimentary of Shahezi and ahove formation,and it is an important fault that control block framework and sedimentary which affected by extensional movement of early fault depression,strike slip motion of lately fault depression and reverse motion of later sunken.

Daijiatun fault: third order fault zone, that is a centripetal fault which near SN trend, the trend of the south is west, the trend of the north is NWW, the extention of the fault is about 11 km, amplitude 10-180m, abrupt stratigraphic position T_3-T_5.it is a a centripetal fault control block framework and local sedimentary which developed in multistage movement.

Nanling fault: third order fault zone, that is a NNE trend centripetal fault, the extention of the fault is about 8 km, abrupt stratigraphic position T_3-T_5.it is a a centripetal fault control block framework and local sedimentary which developed in multistage movement.

3. Development degree and genetic mechanism of Structural fracture

Through the observation and statistics of core crack of the coring Wells in reaserching area(Chuan Guo, Yushuang Zhu& Wenqing Li. 2009)(Xinguo Zhang, Qirong Qin& Jin Huo. 2007), large-scale fracture (> 20cm) accounted for 20%,Medium-scale fracture (2 to 20cm) accounted for more than 70%, Small fracture (0.2 to 2cm) and micro-fracture(<0.2cm) accounted for less than 10%. The main range of crack width is below 1mm, and besides is 1 to 2mm,accounted for more than 20%, other range of width are relatively few. What must point out specially, fractures that range of crack width beyond 5mm also accounted for the greater proportion, so it shows fracture width is relatively big. Density of fracture focused on the range that the density is less than 0.2 strip/m, about accounting for 65% in all fracture-riched sections. Besides, the density of fracture is more than or equal to 0.6 strip/m, accounting for 20% in all fracture-riched sections; and the fracture that density is 0.2 to 0.4 strip/m accounted for 15% in all fracture-riched sections.

As a result of the multiperiodic tectonic action, the tectonic feature of Shiwu Oilfiled accord with the sedimentation development history .According to the feature of regional structural stress field development, field investigation, observation of drill core and the multidisciplinary analysis of log interpretation(Ziliang Liu& Chunxiu Liang. 1999)(Yinli Chen, Yang Gu & Chen Guming. 2008), the author come to the conclusion that the

fractures of research area are mainly generated by several tectonic movement.

Yingcheng tectonic movement is a small-scale tectonic inversion movement in the stage of rift evolution , resulting of the rift basin uplift and denudation in different levels. The tectonic stress field is the compressive stress field which tends the North West - South East. This compressive stress, forming a nearly north-south (10 ° ± 15 °) and the North West to (290 ° ± 15 °) high-angle conjugate shear fractures, NW (330 ° ± 15 °) gash fracture, but also developed in the vicinity of Xiaokuan trending faults (45 ° ± 15 °) which associated with low-angle shear fractures. Nearly north-south (10 ° ± 15 °) fracture development intensity, and NWW (290 ° ± 15 °) fracture development is weak, NE (45 ° ± 15 °) near the crack developed in the comparative fault Xiaokuan intensive, breaking away from the Xiaokuan sparse.

Denglouku formation occurred during the deposition reverses of the tectonic stress. The ectonic stress field in the North West - South East, to the tensile stress field. Cracks in the original development of Shiwu oil field were pulled, sewn into a tension cracks by tensile stress. Meanwhile, earlier pulled after pressure stress field, there are more of the twisted sheets sewn.

Denglouku formation final rift basin tectonic movement led to the depression phase of the transformation stage, the tectonic fault movement is an important form of local structures of the period is also important during the early formation of hydrocarbon reservoirs. It generates the uplift and erosion in the southeast uplift pear rift within the most obvious. Denglouku formaton final stress field is the same with Yingcheng formation, for the North West - South East to the compressive stress, but stress intensity increases. In this stress, the cracks of Yingcheng formation in the board late last movement has been strengthened. Fracture is greater than the end of Yingcheng formation, some cracks develop into north-south fracture strike-slip fault.

Tectonic movement during the late Nenjiang is the most important tectonic rollover movement of Songliao basin. Shiwu oil field were effected by Tan-Lu fault slip and a sinistral transpressional stress field.In this stress field, Xiaokuan fault turned to the left-lateral slip fault and also been pressed, some part of this fault reversed to reversal fault.Early formation of the joint part of the north-southcut open , east-west fracture closure; also formed a NNE (35 ° ± 15 °) and NW (330 ° ± 15 °) of the "X"-type high angle conjugate shear fractures, the tensional fractureformed during the late of yingcheng group and the denglouku group was formed by the late Zhang crack shape as the sheets are cut twisted joints, cracks due to the formation period of this group of late, many cracks were not filled; the Xiaokuan strike-slip fault in the development of a small amount around the fault is also derived seam.

Mingshui tectonic movement is another tectonic rollover movement, mainly impact the middle and western region in the Songliao basin and resulted in regional uplift, folding, erosion, as the important period of the structural formation and shaping in the central depression area and the western slope ,but the tectonic movement did little affection to the southeast uplift area ,so the Mingshui tectonic movement just reworked the Early formation cracks.

Association the structural analysis with structural evolution rule of ShiWu oil field , the author believe that there are four terms of fractures in reaserching area, but the tectonic movement at the late MingShui group only rebuilds the early fractures, not causes new fractures yet (as shown in Table 1).

4. Conclusion

In the basis of the structure interpretation, According to the distribution characteristics and the control of zones of Xiaokuan fault,Bawu fault,Daijiatun fault and Nanling fault, 6 secondary structure units are divided. there are six time of stages of tectonic movement in Shiwu area:intial stage faulted depression, last stage of huoshiling formation, last stage of yingcheng formation, last stage of denglouku formation, last stage of nenjiang formation, last stage of mingshui formation.

Fracture is relatively developed in in Shiwu Oilfield, Width is broader, the length is longer. there are six extensional directions of these fractures are NE,SN,NW,NNE,NNW,EW, etc.

References

Chuan Guo, Yushuang Zhu & Wenqing Li. (2009). Fracture characteristics of Chang 6 reservoir in Pingqiao area of Ansai Oilfield. *Journal of Northwest University(Natural Science Edition)*.

Danping Yan& Xinwen Wang. (2000). Analysis of fold style and It's formation mechanism in the area of boundary among Sichuan,Hubei and Hunan. *Geoscience-journal of graduate school china university of geosciences*.

Haibo Bai. (2002). Research on formation mechanism of earth fissure in Xuzhou coal mining area. *Coal geology*

& exploration.

Hengmao Tong& Daiyong Cao. (2004). Genesis and distribution pattern of fractures in western Qaidam basin. *Oil & Gas Geology.*

Kai Yu, Zhensheng Yang& Baiping Yao. (2000). Structural framwork evolution in ShiWu fault depression and its relation to oil and gas. *Natural gas industr* .

Liying Yang, Ruilei Li & Jiangtao Zhang. (2005). Structural characteristics of Lishu fault in the southeastern uplift area of the Songliao basin. *Progress in Geophysics.*

Xinguo Zhang, Qirong Qin& Jin Huo. (2007). characteristics of the fractures in carboniferous reservoirs, at the zone 9, kramay oil-field. *Journal of Southwest Petroleum University.*

Yinli Chen, Yang Gu&Chen Guming. (2008). Characteristics and stages of fractures in the second member of xujiahe formation in Qiongxi structure, western Sichuan depression. Natural Gas Industry.

Yunsheng Wang& Shitian Wang. (2000). The genetic mechanism analysis of the nappes in the Jianghuan-Heqing region,Yunnan. *Joural of Chengdu university of technology.*

Ziliang Liu& Chunxiu Liang. (1999). Genetic mechanism and distribution direction of structural fracture in southern Songliao basin. *Petroleum exploration and development.*

Table 1. Fracture terms table of Shiwu Oilfield

Term	Period	Stress orientation	fracture orientation and type
1	last stage of yingcheng formation	NW	SN High angle adjoint shear fracture NWW High angle adjoint shear fracture NW Extension fracture NE Low angle accompany shear fracture
2	last stage of denglouku formation	NW	SN NWW NW Extension fracture NE Accompany shear fracture
3	last stage of nenjiangformation	left-lateral strike-slip stress	NE "X" high angle adjoint shear fracture NW "X" high angle adjoint shear fracture SN shear fracture open,NWW hear fracture close
			NW fracture change to tenso shear fracture
4	last stage of mingshui formation	—	—

 ISSN 1913-1844 E-ISSN 1913-1852

The Role of Manganese on Microstructure of High Chromium White Cast Iron

Mohammed Jasim Kadhim
Department of Production Engineering and Metallurgy,
University of Technology, Baghdad, Iraq
Tel: 964-781-731-5836 E-mail: alimohammed1957@yahoo.com

Adnan Naama Abood
Technical College, Baghdad, Iraq
Tel: 964-770-533-4938 E-mail: adnan_naama@yahoo.com

Rabiha Saleh Yaseen
Department of Production Engineering and Metallurgy,
University of Technology, Baghdad, Iraq
Tel: 964-790-132-4978 E-mail: rabihazw@yahoo.com

Abstract

To determine the effect of austenite stabilizer element on the microstructure and behaviour of as–cast high **Cr** white cast iron Fe-21Cr-3Ni-1.7Mo-2.4C, different percentages of Mn (0.4, 0.9, 1.3, 1.7, 2.2 and 2.6 wt%) were added. Detailed investigations were carried out using scanning electron microscopy, energy dispersive spectroscopy analysis (EDS), X-ray diffraction and hardness test. It showed that with increasing Mn addition, the austenite phase **(γ)** of the as-cast alloys refine clearly. The morphology of the austenite phase for all alloys is a mixture of dendrite and plate like. The austenite phase refines clearly with increasing manganese addition. The major carbide phase formed in the as- cast alloys is M_7C_3 with minor carbides of $(Fe,Cr)_{23}C_6$ and Mo_2C. Microstructure analysis showed the presence of small amounts of martensite and delta ferrite in all as-cast alloys. The hardness was decreased continuously with increasing Mn content. This is mainly attributed to the morphology of carbides rather than to small variation in carbides content. It was observed that considerable amounts of Mn were found in the carbides lower than that in the austenite matrix.

Keywords: As-cast white cast iron, Manganese, Austenite phase, EDS, Carbides, Austenite

1. Introduction

High alloyed chromium cast irons were used in applications with extreme demanding requirements such as abrasive, erosion, heat and corrosion resistance (Carpenter, Carpenter and Pearce, 2004; Komarov, Sadovski, Urbanovich and Lifshits, 2002). Also these cast irons were employed with unusual physical properties, such as low thermal expansion or non magnetic properties are desired (Ogi, Yamomoto and MiyaKawat, 2003; Chenje, Simbi and Navara, 2006; Tabrett and Sare, 2000). In the empirical development of alloyed cast irons the first prominent advance was the introduction of the Ni-hard cast iron in which the Ni and Cr are converted the pearlitic matrix to martensitic in the as cast state (Komarov and Sadovski, 2002; Asensio, Pero-Sanz and Verdiga, 2003; Zhou, Nilsson, Anderson and Stahi, 2004). In further modifications, the eutectic carbide was refined somewhat to give improved toughness (Baotong, Jingli and Stefano 2006). The M_7C_3 carbide is the predominant phase which is harder than M_3C present in unalloyed white cast irons and some Ni-hard cast irons, which cause a high abrasion resistance (Bedolla Jacuinde, 2001; Petrovic, Markovic and Pavlovic, 2003; Jun, Cong, Haohuai, Hongshan, Baoluo, Shenji and Sijiu, 2006).

Completely austenitic or completely martensitic matrix structure is desirable for wear resistance. High chromium white cast irons have usually complex mixed iron chromium carbides which are significantly harder than the cementite phase present in unalloyed and even low alloyed cast irons (Kuyucar and Liewiiyn, 2006; Alp, Wazzan and Imaz, 2005). The increase in the carbon content of high-chromium cast irons causes a decrease in the heat resistance and an increase in the rate of cracks propagation (Zhiping, Rulen and Baduo, 2002). On the other hand,

chromium has a negative effect on the resistance of the hypoeutectic alloys to thermo-cycling loads (Bedolla, Correa, Quezada and Maldonado, 2005). Increasing manganese content will cause an increasing in retained austenite at room temperature and a decreasing in hardness. Manganese is soluble in M_7C_3 and M_3C carbides. It provides hardenabiliy increases and prevents pearlite formation.

2. Experimental Procedures

The alloys used were made in a silica lined coreless high frequency induction melting furnace with 45 kg capacity, 1.2 KHz frequency, 150 kW power. The charge materials consisted of pig iron, ferrochromium (Fe-72%Cr), ferromanganese (Fe-75%Mn), ferromolybdenum (Fe-65%Mo) and electrolytic nickel. The molten metal temperature was measured with type-S calibrated thermocouple (Pt-Pt/Re). The pouring temperature was 1450°C. The manganese element added to the molten as ferromanganese, in six series depending on the Mn percentage required. These alloys were poured into sand moulds to obtain square 12 mm×12 mm cross section area and 60 mm length bars. Table 1 lists the chemical composition for the six white cast irons produced. The only varied element is manganese from 0.4 to 2.6 wt%.

Samples for metallographic were prepared using abrasive paper grades 220, 320, 400, 500, 800 and 1000 respectively and then polished with 1 μm diamond paste. The specimens were etched using nital. Quantitative and qualitative determinations of chemical composition of the phases in as cast and heat treated samples were made by using the energy dispersive microanalyses. To aid in the identification of the phases present in the castings, X-ray diffraction was performed. Carbide fraction computing was made to study the effect of manganese content on the carbide fraction for the as cast. Average hardness of the as cast and heat treated specimens measured was using HRC. δ-ferrite content determination for the as cast specimens was also carried out by ferrite Content Meter (FCM).

3. Results and Discussion

High chromium white cast irons are usually produced as hypoeutectic composition, with austenite dendrites, either partially or substantially transformed to martensite and eutectic containing carbides an*d austenite. Figure 1 illustrates the microstructure of the as cast high chromium alloyed cast irons with different amounts of manganese addition. They compose of primarily proeutectic austenite dendrites and eutectic which consists* of eutectic austenite and eutectic carbides (mainly M_7C_3 type). It appears that the solidification of these kinds of alloys starts by austenite dendrites formation, and as the temperature decreases these dendrites grow, till the remaining liquid reaches the eutectic composition. At this stage the eutectic austenite/$(Fe, Cr)_7C_3$ carbide are formed. The austenite phase and $K_2(M_7C_3)$ carbides developed from liquid phase around the primary austenite dendrite which grows and formed as eutectic cells. The dendrites and the dendrites arm spacing differ with increasing manganese content and the regularity of the grains increases positively with manganese content. These structures which improved by the nucleation and growth of the austenite grain size are affected by the manganese content.

XRD analysis showed that there is small amount of martensite appeared as a thin dark-etching layer in the interface between the eutectic phase and primary γ phase. This is because, during eutectic solidification the M_7C_3 carbide which grows along the austenite absorbs carbon from its surrounding and narrow areas at the austenite/carbide interphase become impoverished in carbon. The lack of carbon in these zones of austenite increases the M_s temperature which allows these areas of austenite to transform to martensite during subsequent cooling down. Therefore, it is common to find eutectic M_7C_3 carbides are surrounded by martensite.

Due to the nucleation and growth kinetics of γ phase and M_7C_3 carbides in the eutectic, "rosette" morphology forms as a result of the early formation of a carbide crystal followed by rapid formation of γ around the former (Fig. 1). It appears that the eutectic solidified with a colony structure is consisting of a matrix of fine globular carbides in the central region, string-like or granular. They developed towards the boundary and large massed in the boundary area. At a higher percentage of manganese, the shape of the colony will differ and take another shape as indicated in (Fig. 1) which represents 2.6% Mn-alloy.

The nucleation and growth of the eutectic chromium carbides lead to the depletion of its content in the remaining liquid. This depletion is account for the chromium content of the subsequent and smaller carbide. In addition to eutectic carbides, secondary carbides where precipitated from the austenite matrix during slow cooling. These carbides precipitate due to decrease in C and Cr from the matrix and the destabilized the austenite as confirmed from the energy dispersive spectroscopy (EDS). It transformed to martensite which causes an increase in the bulk hardness. Besides martensite, the secondary carbides play important role in increasing the bulk hardness by their dispersion hardening effect on the matrix.

Presence of molybdenum in the alloys of high chromium white cast irons leads to the formation of Mo_2C carbides. Molybdenum is soluble in M_7C_3 carbide, so most of it partitions to the eutectic M_7C_3 carbide and some dissolve in austenite. It is also possible that small part of Mo also forms M_2C carbide (Mo_2C) due to the presence of carbon in the alloys. This type of carbide is found joined together with M_7C_3 as a lamellar shape (Fig. 2). It demonstrates that Mo_2C recrystalizes in a finely dispersed form as a eutectic in the final stage of solidification.

The shape and the size of eutectic M_7C_3 differ with manganese content. Hexagonal M_7C_3 eutectic carbides type beginning to appear as the manganese content increases especially at 1.3 and 1.7% Mn (Figs. 1 and 2). Also the average size of the carbide phase was increased with increasing manganese content in the alloys. The energy dispersive spectroscopy analysis showed that the manganese percentage in the austenite and carbide increases as its addition increases in the alloys. This leads to increase the retained austenite in the prepared white cast irons. Also, it indicates that the manganese percentage in the austenite is more than its percentage in the carbides. This means that the partition of manganese to the austenite is more than its partition to carbide (Table 2). Manganese affects the austenite dendrites and the austenite dendrite arm spacing. Also the Cr percentage in the carbide phase is more than 50% and its percentage in the γ phase is around 15% except specimen of 2.6%Mn. This is because the analysis is made near the carbide phase. X-Ray diffraction analysis illustrates that the austenite (γ) is the predominant phase in all the prepared high chromium white cast alloys with different manganese additions. Besides γ phase, $(Fe, Cr)_7C_3$ eutectic carbides also exist. Also there is a small amount of martensite and molybdenum rich carbide (Mo_2C) present.

Figure 3 shows that the hardness decreases with increasing manganese content. The hardness does not depend on the carbide fraction only but also on the austenite shape and the percent of manganese content in this grain. The shape of carbides was changed from rosette shape to large plate kind. The δ-ferrite content decreases as the manganese content increases (Fig. 4). This indicates that increasing manganese content reduces the effect of chromium in the content of δ- ferrite; with consideration that δ-ferrite is also affected by casting variables.

4. Conclusion

1) With increasing manganese content, the austenite matrix of the alloys refine considerably.

2) Presence of manganese in high Cr-white cast irons does not affect the tendency of chromium to stabilize the carbides, but increasing in the amount of austenite.

3) There was also found that manganese has a high tendency to change the morphology of carbides formed and decreasing the carbide fraction.

4) All cast alloys contain a small amount of martensite distributes on the interphase between austenite and M_7C_3 carbide.

5) The hardness of alloys decreased continuously with increasing manganese content which attributes mainly to the morphologies of carbides rather than their content.

References

Alp, T., Wazzan, A.A. and Imaz, Y. (2005). Microstructure-properties relationship in cast irons, *The abrasion Journal for Science and Engineering,* 30, 163.

Asensio, A., Pero-Sanz, J.A. and Verdiga, J.I. (2003). Microstructure selection criteria for cast irons with more than 10 wt. % chromium for wear applications, *Materials Characterization,* 49, 83.

Baotong, L., Jingli, L. and Stefano, C. (2006). Corrosion and wear resistance of chrome white irons–A correlation to their composition and microstructure, *Metallurgical and Materials Transaction A,* 37, 3029.

Bedolla, A., Correa, R., Quezada, J.G. and Maldonado, C. (2005). Effect of titanium on the as-Cast microstructure of a 16 % chromium white iron, *Materials Science and Engineering A,* 398, 297.

Bedolla Jacuinde, A. (2001). Microstructure of vanadium, niobium and titanium-alloyed High-chromium white cast irons, *International Journal of Cast Metals Research (UK),* 13, 343.

Carpenter, S.D., Carpenter, D. and Pearce, J.T.H. (2004). XRD and electron microscope study of an as-Cast 26.6 % chromium white iron microstructure, *Materials Chemistry and Physics,* 85, 32.

Chenje, T.W., Simbi, D.J. and Navara, E. (2006). Relationship between microstructure, hardness, impact toughness and wear performance of selected grinding media for mineral ore milling operations, *Materials and Design,* 25, 11.

Jun, W., Cong, L., Haohuai, L., Hongshan, Y., Baoluo, S., Shenji, G. and Sijiu, H. (2006). The precipitation and transformation of secondary carbides in a high chromium cast iron, *Materials Characterization,* 56, 73.

Komarov, K. and Sadovski, V.M. (2002). Thermal stability of high–chromium cast iron, *Metal Science and Heat Treatment,* 44, 32.

Komarov, O.S., Sadovski, V.M., Urbanovich, N.T. and Lifshits, G.F. (2002). Thermal stability of high-chromium cast iron, *Metal Science and Heat Treatment,* 44, 32.

Kuyucar, S. and Liewiiyn, R. (2006). High-chrome white irons incorporating ultra-hard carbide-forming elements for improved wear-resistance, *Transactions-American Foundrymens Society,* 114, 551.

Ogi, K., Yamomoto, K. and MiyaKawat, N. (2003). Alloy design for heat and abrasion resistant high alloy cast iron, *International Journal of Cast Metals Research,* 16, 269.

Petrovic, S.T., Markovic, S. and Pavlovic, Z.A. (2003). The effect of boron on the stereological characteristic of the structural phases present in the structure of the 13 % Cr white iron, *Journal of Materials Science,* 38, 3263.

Tabrett, C.P. and Sare, I.R. (2000). Fracture toughness of high chromium white irons: influence of cast structure, *Journal of Materials science,* 35, 2069.

Zhiping, S., Rulen, Z. and Baduo, S. (2002). TEM study on precipitation and transformation of secondary carbides in 16 Cr-1Mo-1Cu white iron subjected to subcritical treatment, *Materials Characterization,* 55, 403.

Zhou, J.M., Nilsson, A., Anderson, M. and Stahi, J.E. (2004). Machining characteristic of Novel- Abrasion resistance iron, *J. of Materials Processing Technology,* 153-154, 751.

Table 1. Chemical composition of alloyed cast iron studied (wt%)

Specimen No.	*% C*	% Cr	% Mo	% Ni	% Mn	% Si	% S	% P	% Fe
1	2.48	21.76	1.79	3.17	0.4	1.88	0.0026	0.045	rem.
2	2.60	21.52	1.75	3.14	0.9	2.03	0.033	0.049	rem.
3	2.38	21.41	1.80	3.12	1.3	1.91	0.028	0.048	rem.
4	2.37	21.22	1.76	3.13	1.70	1.93	0.023	0.047	rem.
5	2.39	20.63	1.72	2.91	2.20	1.81	0.014	0.015	rem.
6	2.39	20.66	1.73	2.97	2.6	1.79	0.017	0.019	rem.

Table 2. EDS analysis of Mn and Cr in austenite (γ) and carbide phase (wt%)

% Mn in alloy	% Mn in γ	% Mn in carbide	% Cr in γ	% Cr in carbide
0.4	0.76	0.23	14.89	56.81
0.9	1.01	0.52	14.7	57.67
1.3	1.4	1.17	15.45	56.16
1.7	1.81	1.4	15.18	57.78
2.2	2.6	2.14	14.17	51.95
2.6	3.0	2.2	29.17	57.83

 ISSN 1913-1844 E-ISSN 1913-1852

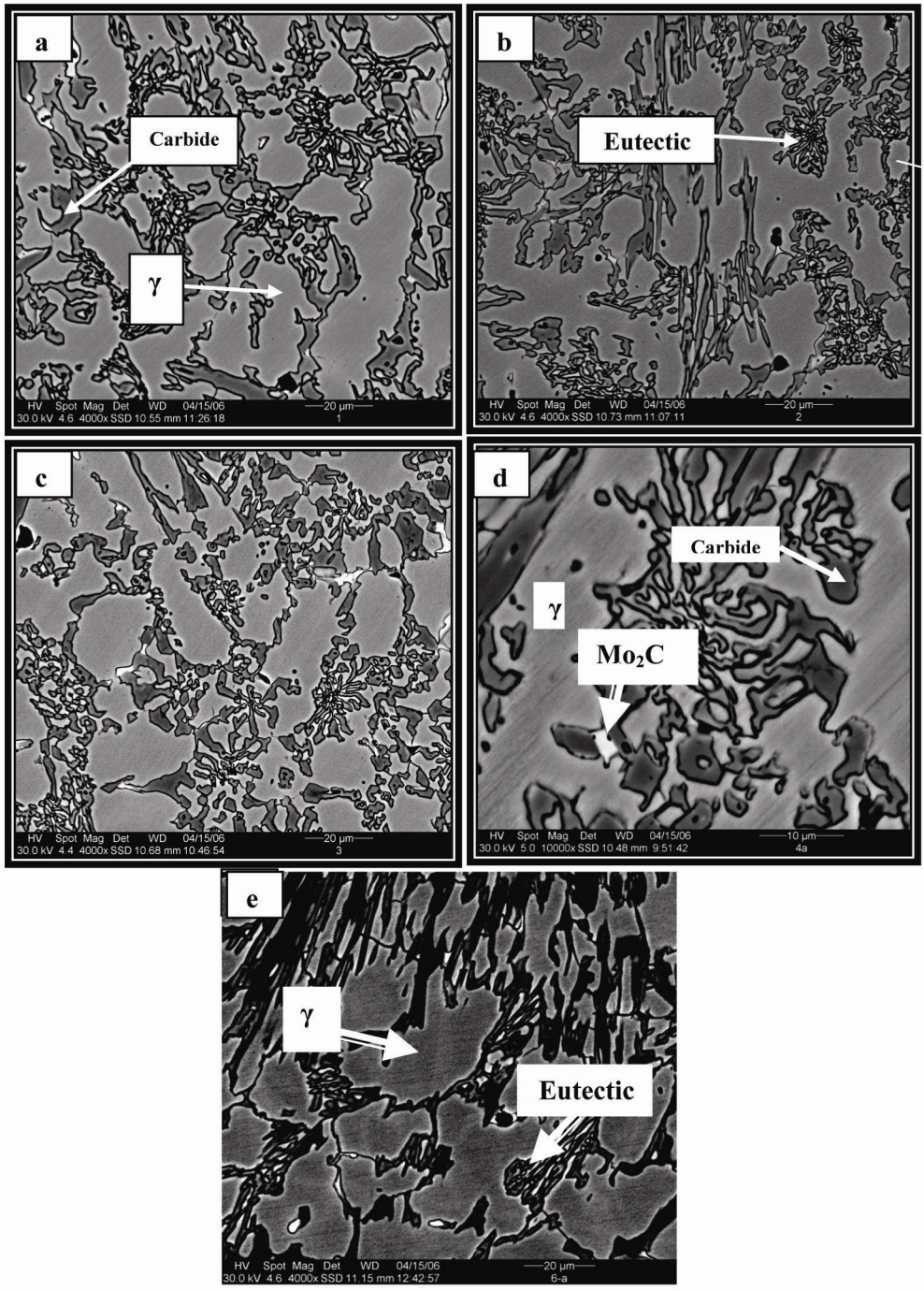

Figure 1. SEM micrographs showing the colony shapes with rosette morphologies of high chromium white cast irons with different percentages of manganese (a) 0.4 wt%, (b) 0.9 wt%, (c) 1.3 wt%, (d) 1.7 wt% and (e) 2.6 wt%.

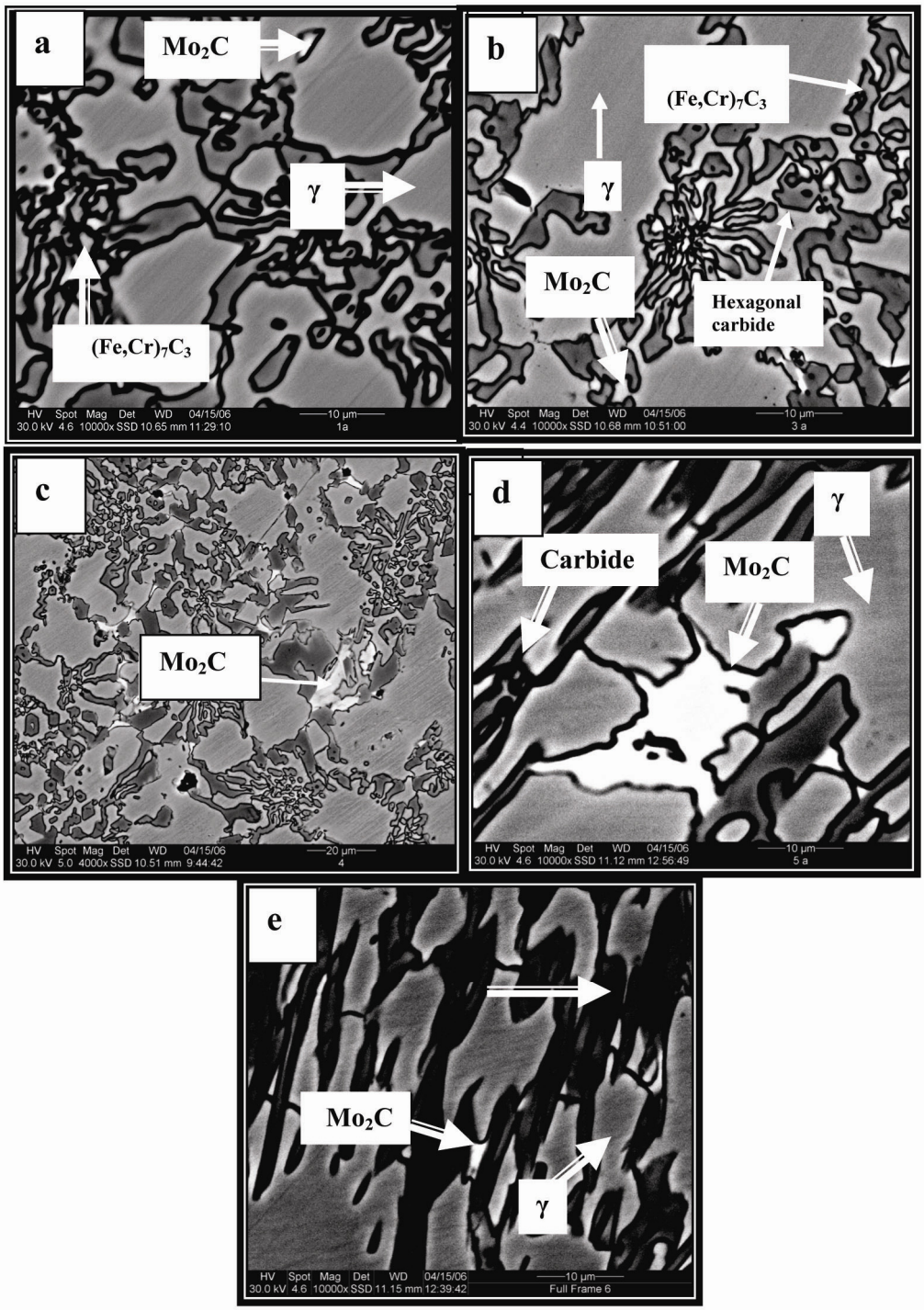

Figure 2. SEM micrographs showing the presence of molybdenum carbide in the high chromium white cast irons at different percentages of manganese (a) 0.4 wt%, (b) 1.3 wt%, (c) 1.7 wt%, (d) 2.2 wt% and (e) 2.6 wt%.

 ISSN 1913-1844 E-ISSN 1913-1852

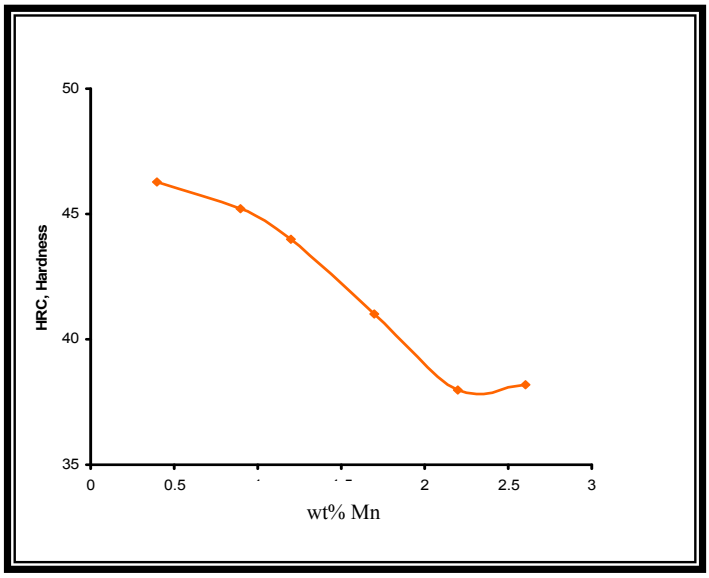

Figure 3. Effect of percentage of manganese on hardness in the as-cast high chromium white cast iron

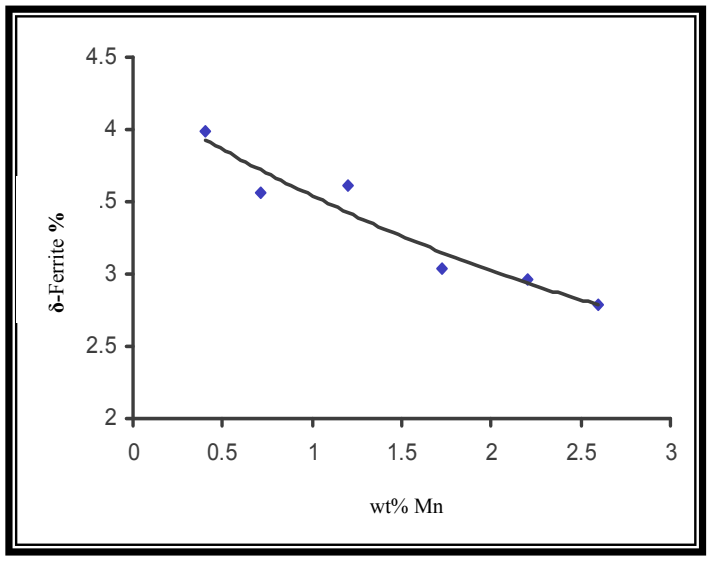

Figure 4. Effect of % Mn on δ –Ferrite in the as-cast high chromium white cast iron

Topological Optimization of Dynamic Characteristics for Orthotropic Material Structure Using Shape Derivative and Augmented Lagrangian Method

Sen Liang

School of Mechanical Engineering, Qingdao Technological University

Shandong Province, Qingdao 266033, China

Tel: 86-532-8507-1299 E-mail: liangsen98@mailst.xjtu.edu.cn

Lei Liang

Department of Mechanical and Electronical Engineering, Baoji University of Arts and Sciences

Shanxi Province, Baoji 721007, China

Tel: 86-917-336-4295 E-mail: lpqdf@yahoo.com.cn

The research is financed by the Natural Science Foundation of Shandong Province, People's Republic of China (Z2007F04)

Abstract

This paper presents a new level set method for topology optimization of dynamic structure of orthotropic materials using the shape derivative analysis and augmented Lagrangian method. The design boundary of the structure is embedded implicitly into the zero level set of a higher dimensional scalar function, which is mathematically represented as a Hamilton-Jacobi partial differential equation (PDE). The design sensitivity of the dynamic structure is obtained by the combination of the level set representation and the shape derivative method. In doing so, the evolution of the design boundary is advanced iteratively in terms of the solutions of the Hamilton-Jacobi PDE using explicit time marching schemes. Some typical numerical examples are applied to demonstrate the validity of the present method.

Keywords: Augmented Lagrangian, Dynamic structure, Topology optimization, Level-set method, Orthotropic material

1. Introduction

Structural optimization, in particular the shape and topology optimization, has been identified as one of the most challenging tasks in structural design. By combining the finite element method with various optimization algorithms, investigation has made a considerable progress in the structural design engineering during the last few decades. The optimization method has been widely received by automotive, aerospace, nuclear and other high-tech industries, which is used to satisfy the design requirements for maximum performance, minimum weight, cost efficiency, and environmental consideration. Various techniques and approaches including ground structure method (Prager 1974, Rozvany 1979, Hagishita and Ohsaki 2009), homogenization method (Bendsøe and Kikuchi 1988), solid isotropic material with penalization (Zhou and Rozvany 1991, Mlejnek 1992, Bendsøe and Sigmund 1999) and level-set method (Wang etc. 2003, Allaire etc. 2004) have been developed. Other methods, such as the current flexible building block method (Kim etc. 2006) , the unit cell approach (Wang 2004), the radial-basis-function (RBF) level-set method (Wang 2006) can be considered nearly as evolutions of the approaches mentioned above, thus they will not be discussed here. The essential idea of all these methods is to transform the design problem into an optimal material distribution problem so that the configuration designed can be measured quantitatively by an objective function. Also, there are some differences among these approaches in their representations and modeling schemes.

It is not easy to design a mechanical structure with the desired natural frequency and mode shape. As for parametric structural optimization problems, many methods were presented for sensitivity analysis of the dynamic structures, such as these reported by Fox and Kapoor 1968, Nelson 1976, Seyranian etc.1994 and Luo etc.2006 etc. For non-parametric structural optimization problems, a technique for topology optimization of

linear elastic continua based on homogenization theory was investigated by Bendsøe & Kikuchi 1988, and it has been applied to topology optimization problems of the dynamic structures by Diaz and Kikuchi 1992 and Tenek and Hagiwara 1994 etc. By employing this technique, the material distribution was formulated with parameters of periodic microstructure. Another few papers explored the nonparametric boundary optimization problems of linear elastic continuum. Based on the gradient method in a Hilbert space, Inzarulfaisham & Azegami 2004 and Meske etc. 2006 proposed a numerical method called the traction method and they applied it to maximum lower-order natural frequencies under a volume constraint. Later, Seonho etc. 2006 developed a topological shape optimization method which was applied to power flow problems at high frequencies and the necessary design gradients were computed by using an efficient adjoint sensitivity analysis method. Allaire and Jouve 2005 applied the level-set method to the shape and topology optimization, and they maximized the first eigenfrequency under the specified weight constraint in the three-dimensional space.

This paper explores the feasibility employing level set method to optimize an orthotropic material structure. The augmented Lagrangian multiplier with inequality constraint is extended into the topology optimization of the design structure. By the combination of the shape derivative, level set and augmented Lagrangian multiplier method, the sensitivity of the maximum lower order natural frequency is investigated theoretically. The optimization boundary of orthotropic material structure is embedded implicitly into the zero level set of a higher dimensional scalar function, which is mathematically represented as a Hamilton-Jacobi type partial differential equation (PDE). The movements of the design boundary are advanced iteratively in terms of the solutions of the Hamilton-Jacobi PDE using explicit time marching schemes. The 2D numerical examples are employed to demonstrate the validity of the current method.

2. Topological optimization theories

In order to obtain the dynamic topological structure of an orthotropic material, the key problem is to develop a formula of the maximum lower order natural frequency. The constructive relationship is the foundation of stress equation and strain equation.

2.1 Constitutive relationship

As we know, the constructive relationship of the orthotropic material under the plane stress state is given as

$$\begin{Bmatrix}\sigma_{11}\\ \sigma_{22}\\ \sigma_{12}\end{Bmatrix}=\begin{bmatrix}Q_{11} & Q_{12} & 0\\ Q_{12} & Q_{22} & 0\\ 0 & 0 & Q_{66}\end{bmatrix}\begin{Bmatrix}\varepsilon_{11}\\ \varepsilon_{22}\\ \varepsilon_{12}\end{Bmatrix} \tag{1}$$

Here Q_{ij} , σ_{ij}, ε_{ij} are the elements of stiffness matrix, stress matrix and strain matrix in the local coordinate system (or the material coordinate system). From the material coordinate system to the global coordinate system，the transformation equation of the elastic parameters is

$$\begin{Bmatrix}Q'_{11}\\ Q'_{22}\\ Q'_{12}\\ Q'_{66}\\ Q'_{16}\\ Q'_{26}\end{Bmatrix}=\begin{bmatrix}m^4 & n^4 & 2m^2n^2 & 4m^2n^2\\ n^4 & m^4 & 2m^2n^2 & 4m^2n^2\\ m^2n^2 & m^2n^2 & m^4+n^4 & -4m^2n^2\\ m^2n^2 & m^2n^2 & -2m^2n^2 & (m^2-n^2)^2\\ m^3n & -mn^3 & mn^3-m^3n & 2(mn^3-m^3n)\\ mn^3 & -m^3n & m^3n-mn^3 & 2(m^3n-mn^3)\end{bmatrix}\begin{Bmatrix}Q_{11}\\ Q_{22}\\ Q_{12}\\ Q_{66}\end{Bmatrix} \tag{2}$$

Here $m=\cos\alpha$, $n=\sin\alpha$ and α is the angle measured from the global coordinate system to the material coordinate system. If the material coordinate system is inconsistent with the global coordinate system, the stress-strain relationship in the global coordinate system can be given as follow

$$\begin{Bmatrix}\sigma_x\\ \sigma_y\\ \sigma_{xy}\end{Bmatrix}=\begin{bmatrix}Q'_{11} & Q'_{12} & Q'_{16}\\ Q'_{21} & Q'_{22} & Q'_{26}\\ Q'_{61} & Q'_{62} & Q'_{66}\end{bmatrix}\begin{Bmatrix}\varepsilon_x\\ \varepsilon_y\\ \varepsilon_{xy}\end{Bmatrix} \tag{3}$$

Here σ_{ij}, ε_{ij} and Q'_{ij} are the elements of stress matrix, strain matrix and stiffness matrix in the global coordinate

system.

Equation (3) is the constructive relationship of 2D orthotropic material. After obtaining the formula of the constructive relationship, the sensitivity of the maximum lower order natural frequency will be derived.

2.2 Augmented Lagrangian method

It is very difficult to obtain a reasonable optimal result with a fixed Lagrangian multiplier in the structural topology optimization. In this paper, the augmented Lagrangian method with slack variables is explored to solve the optimization problem with inequality constraints.

Generally speaking, the augmented Lagrangian method can be classified into equality constraint and inequality constraint problems. In the case of equality constraints, the quadratic penalty function is adopted to penalize constraint violations by squaring the infeasibility (Chen and Shapiro 2006). For the inequality constraint problem, it can be converted into an equality constraint by introducing the slack variables. Let us describe the issue firstly

$$\min_{x} f(x) \qquad \text{subject to } g_j(x) \le 0 \qquad (j = 1,2...m) \tag{4}$$

Here $f(x)$ is objective function, and $g_j(x) \le 0$ are inequality constraints. By defining slack variables r_j, equation (4) can be changed into the following form

$$\min_{x,r} f(x) \qquad \text{subject to } g_j(x) + r_j = 0, \quad r_j \ge 0, \quad (j = 1,2...m) \tag{5}$$

Let's define a new function $g^1{}_j(x) = g_j(x) + r_j = 0$, and the augmented Lagrangian equation with equality constraints at the *k*th iteration can be obtained (Nocedal and Wright 1999).

$$\underset{x.}{\text{Min}} \qquad \mathrm{L}(x, \lambda^k, \eta^k) = \mathrm{f}(x) + \sum_{j=0,1,...,m} \lambda^k{}_j g^1{}_j(x) - \frac{1}{2\eta^k} \sum_{j=0,1,...,m} (g^1{}_j(x))^2 \tag{6}$$

Subject to $r_j \ge 0, \qquad (j = 1,2...m)$

Differentiating equation (6) with respect to r_j, then

$$\frac{\partial L}{\partial r_j} = \lambda^k{}_j - (g_j + r_j)/\eta^k = \mathbf{0} \tag{7}$$

The following equation can be

$$r_j = \lambda^k{}_j \eta^k - g_j \tag{8}$$

Equation (6) is a convex quadratic function with respect to slack variables r_j, so the optimal value of the slack variables is zero. By considering equations (6) and (8), r_j value at *k*th iteration is expressed as follow

$$r_j = \max(-g_j(x) + \eta^k \lambda_j{}^k, 0) \tag{9}$$

Equation (9) solves the problem of slack variables r_j. By substituting r_j into equation (6), the next issue is an optimization problem of equality constraint as follow

$$L(x, \lambda^k, \eta^k) = f(x) + \sum_{\mathbf{j=0,1,...,m}} \lambda^k{}_j g_j(x) - \frac{1}{2\eta^k} \sum_{\mathbf{j=0,1,...,m}} g_j(x)^{\mathbf{2}}, \qquad \text{if } (-g_j(x) + \eta^k \lambda_j{}^k \le 0) \tag{10}$$

$$\text{or } \mathrm{L}(x, \lambda^k, \eta^k) = \mathrm{f}(x) + \sum_{j=0,1,...,m} (\lambda^k{}_j)^2 \eta^k - \frac{1}{2\eta^k} \sum_{j=0,1,...,m} (\eta^k \lambda_j^k)^2 \quad \text{otherwise}$$

Differentiating equation (10) with respect to x, then

$$\frac{\partial L}{\partial x} = \nabla f(x) + \sum_{\mathbf{j=0,1,...,m}} (\lambda_j^k - g_j(x)/\eta^k) \nabla g_j(x), \qquad \text{if } (-g_j(x) + \eta^k \lambda_j{}^k \le 0) \tag{11}$$

$$\text{or } \frac{\partial L}{\partial x} = \nabla f(x) \ ,$$

otherwise

Equation (10) is an augmented Lagrangian equation with equality constraints. We can apply the iteration formula of equality constraints to here, and then we have

$$\lambda_j^{k+1} = \max((\lambda_j^k - g(x_k)/\eta^k, \qquad 0) \tag{12}$$

In this way, the inequality constraint problem can be optimized by the augmented Lagrangian method. For more details, readers can refer to Bertsekas 's book published in 1982. In the next section, this method will be applied to the topological optimization of maximum lower-order nature frequency.

2.3 Maximum lower-order natural frequency

A linear elastic continuum is in an open domain $\Omega \subset R^n$, n=2, 3, with Dirichlet boundary Γ_D as well as Neumann boundary Γ_N, and

$$\Gamma = \partial\Omega = \Gamma_N \cup \Gamma_D$$

The topological optimization structure of maximum lower-order natural frequency with inequality constraints is defined as follow

$$\begin{aligned} &\text{Min} \quad -\Lambda \\ &\text{Subject to} \quad a(u,v) = \Lambda b(u,v) \\ &\int_\Omega d\Omega - M_0 \le 0 \end{aligned} \tag{13}$$

Here $a(u,v) = \int_\Omega Q' e(u) e(v) d\Omega$, $b(u,v) = \int_\Omega \rho uv d\Omega$, $e(u) = (u_{i,j} + u_{j,i})/2$, $u \in U$ and $U = \{u : u \in H^1(\Omega), u = u_0 \text{ on } \Gamma_D\}$. $e(u)$ is strain tensor at any point $u \in \Omega$. Q' =[Q'_{ij}] is the stiffness matrix as shown in equation (3). Utilizing the standard and augmented Lagrangian multiplier methods for equation (13), we have

$$L(u,v,\lambda,\eta) = -\Lambda - a(u,v) + \Lambda b(u,v) + \lambda(\int d\Omega - M_0) - \frac{1}{2\eta}(\int d\Omega - M_0)^2, \text{if} \int d\Omega - M_0 + \eta r \le 0$$

$$\text{or} \quad L(u,v,\lambda,\eta) = -\Lambda - a(u,v) + \Lambda b(u,v) + (\lambda)^2\eta - \frac{\eta\lambda^2}{2} \quad , \quad \text{otherwise} \tag{14}$$

Here *v* stands for both the adjoint variable and Lagrangian multiplier. By solving shape derivative of equation (14) with respect to *t*（Sokolowski etc. 1991）, the following formula, according to equation (11), can be obtained

$$\overline{L} = \int_\Gamma (-Qe(u)e(v) + \Lambda\rho uv + [\lambda - (\int_\Omega d\Omega - M_0)/\eta])V_n d\Gamma, \quad \text{if} \int d\Omega - M_0 + \eta r \le 0$$

$$\text{or} \quad \overline{L} = + \int_\Gamma (-Qe(u)e(v) + \Lambda\rho uv) V_n d\Gamma \quad \text{otherwise} \tag{15}$$

Based on equation (12), the formula to update the Lagrange multiplier is

$$\lambda^{k+1} = \max(\lambda^k - (\int_\Omega d\Omega - M_0)/\eta, \quad 0) \tag{16}$$

As we know, the problem of maximum lower-order natural frequency is a self-adjoint problem（Meske etc. 2006）, so $u = v$. Let us define sensitivity of the objective functional as follows

$$\beta(u) = -Qe(u)e(u) + \Lambda\rho uv \tag{17}$$

The shape derivative of Lagrangian functional can be rewritten as

$$\overline{L} = \int_\Gamma \left\{ \beta + \max[\lambda - (\int_\Omega d\Omega - M_0)/\eta, 0] \right\} V_n d\Gamma \tag{18}$$

Let us take

$$V_n = -\beta - \max\left[\lambda - (\int_\Omega d\Omega - M_0)/\eta, 0 \right] \tag{19}$$

The equation (18) will be changed into

$$\overline{L} = -\int_\Gamma \left\{ \beta + \max[\lambda - (\int_\Omega d\Omega - M_0)/\eta, 0]) \right\}^2 d\Gamma \tag{20}$$

Equation (19) is an evolution speed of the frequency optimization problem. This velocity can make equation (20) not more than zero, so the objective function always decreases until $V_n \equiv 0$. When $V_n \equiv 0$, the shape designed is the optimized result. In next section, level-set method will be investigated in detail.

2.4 Level-set method

After obtained the evolution velocity of the design boundary, the PDE of Hamilton-Jacobi equation (Osher and Sethian 1988) will be introduced in this section.

The level-set method was developed by Osher and Fedkiw 2003 as well as Sethian 1999 to solve the problems such as tracking, computer vision, crack propagation in solid material, image processing, boundary evolution simulating in fluid mechanics etc. The topology optimization can be expressed as a dynamic evolution process of the level-set function varying with pseudo time *t*. The embedded function allows its surface to move up and down on a fixed coordinate system without changing its surface topology structure, and the optimization shape embedded in level-set function can automatically modify the topology structure by boundary merging and breaking. We can track the topological change of the design structure by checking the level-set surface. This process can be completed by solving PDE with the evolution velocity V_n and a set of initial value. The Hamilton-Jacobi PDE is generally solved by using the upwind based on the fixed Eulerian grids. Therefore, in the following paragraph we can employ the level-set method to capture the optimization structure on a fixed mesh.

Let us define a closed subset $\Omega \subseteq R^{\mathrm{d}}(d = 2 \quad or \quad 3)$ as the design domain including the whole admissible shapes. The closed boundary $\Gamma = \partial\Omega \subseteq D$ which is described by zero level-set is Lipschits continuous. We introduce an embedded function $\phi(x(t),t)$ to denote the different parts of the design domain as shown in Fig. 1.

$$\begin{cases} \varphi(x(t),t) > 0 & \forall x \in \Omega \backslash \partial\Omega \\ \varphi(x(t),t) = 0 & \forall x \in \partial\Omega \cap D \\ \varphi(x(t),t) < 0 & \forall x \in D \backslash \Omega \end{cases}$$

In the level-set method, the design boundary is embedded implicitly into the zero level-set of a higher-dimensional level-set surface. The movement of the higher-dimensional embedded function is governed by the Hamilton-Jacobi PDE, the evolution velocity and a set of initial value. The Hamilton-Jacobi equation can be given by differentiating equation $\phi(x(t),t) = 0$ with respect to t

$$\frac{\partial \varphi(x(t),t)}{\partial t} + \mathbf{V}.(\nabla\varphi)^T = 0 \tag{21}$$

Here ∇ is the gradient operator. In the three-dimensional space, let us take

$$\mathbf{V} = V_{\mathbf{n}}\mathbf{S}_{\mathbf{n}} + V_t\mathbf{S}_{\mathbf{t}} \tag{22}$$

Here V_n and V_t are the normal and tangent components of the velocity V, and $\mathrm{S_n}$ & $\mathrm{S_t}$ are unit vectors in the
normal direction and the tangent direction, respectively. Substituting equation (22) into equation (21), we have

$$\varphi_{\mathbf{t}} + V_n(\nabla\varphi)^T.\mathbf{S}_{\mathbf{n}} = 0 \tag{23}$$

Equation (23) demonstrates that only can the normal velocity V_n provide the contribution for the boundary evolution. Furthermore, we simplify the second term of equation (23)

$$(\nabla\varphi)^{\mathbf{T}}\mathbf{S}_{\mathbf{n}} = (\nabla\varphi)^{\mathbf{T}}.\frac{\nabla\varphi}{\|\nabla\varphi\|} = \frac{\|\nabla\varphi\|^2}{\|\nabla\varphi\|} = \|\nabla\varphi\| \tag{24}$$

The Hamilton-Jacobi equation is rewritten as

$$\frac{\partial\varphi}{\partial t} + V_n\|\nabla\varphi\| = 0 \tag{25}$$

$$\phi(x,0) = \phi_0$$

Here $\|\nabla\phi\| = \sqrt{(\nabla\phi)^{\mathrm{T}}.\nabla\phi}$ is a scalar function.

Now, we have velocity V_n to make the objective function decrease. The optimization boundary embedded into the level-set function can automatically be updated in the iteration process. In next section, the optimal

numerical algorithm will be described in detail.

2.5 Optimum numerical algorithms

Once the velocity V_n and Hamilton-Jacobi PDE (21) have been obtained, the finite difference method with respect to t can be obtained

$$\frac{\varphi^{n+1}-\varphi^{n}}{\Delta t}+\mathrm{V}^{n}.(\nabla\varphi^{n})^{T}=0 \tag{26}$$

Here V^{n} is the velocity at time t^n, and ∇ denotes the gradient operator. For the 3D case, the formula can be written as

$$\frac{\varphi^{n+1}-\varphi^{n}}{\Delta t}+\alpha^{n}\varphi_{x}{}^{n}+\beta^{n}\varphi_{y}{}^{n}+\gamma^{n}\varphi_{z}{}^{n}=0 \tag{27}$$

Here $\mathbf{V}=\alpha i+\beta j+\gamma k$, and $\nabla\varphi=\frac{\partial\varphi}{\partial x}i+\frac{\partial\varphi}{\partial y}j+\frac{\partial\varphi}{\partial z}k$. Δt depends on the Courant-Friedreichs-Lewy (CFL) condition. For the 2D case, the CFL condition can be obtained

$$\Delta t\max\{\frac{|\alpha|}{\Delta x}+\frac{|\beta|}{\Delta y}\}=\alpha \tag{28}$$

Here $|\alpha|$ and $|\beta|$ are the absolute values of the evolution velocities in *x* and *y* directions. Δx and Δy are lengths of sides over the entire Cartesian grid. $0<\alpha<1$, the common nearly-optimal value is $\alpha=0.9$. Equation (28) indicates that the numerical waves must be at least as fast as the physical waves. In order to make the level-set function regular, we reinitialize it periodically by solving the following equation

$$\frac{\partial\varphi}{\partial t}+sign(\varphi_0)(|\nabla\varphi|-1)=0 \tag{29}$$

The accurate and robust numerical method was developed by Osher and Fedkiw 2003. To simplify this paper, readers can refer to Osher and Fedkiw's book for more details.

3. Numerical examples

In this section, several topological optimization examples of the orthotropic material are explored by employing the method presented in this paper. The objective function of the optimization problem is the maximum first-order natural frequency. The numerical examples are the cantilever beams of 2D structure whose geometric parameters and boundary conditions are shown in Fig. 2. The material parameters are E_1=135×10^9, E_2=28.8 ×10^9, G_{12}=4.47× 10^9 and ν_{12}=0.33, and mass fraction is no more than 0.4（M_0=0.4）. The initial design structure and initial value of level-set function are shown in Fig.3 and Fig.4, respectively. The length and width of the design domain are 0.1m and 0.05 m, and the thickness is 1 mm. When material directions are 0^0, 30^0, 45^0, 60^0 and 90^0, figures 5, 10, 12, 14, and 16 are some topological optimal results and figures 9, 11, 13, 15 and 17 are the final level-set surface. When material direction is 0^0, Figures 6, 7, 8 are volume, augmented Lagrange multiplier and the first-order natural frequency variable with iteration number, respectively. If the material directions are 0^0 and 90^0, the optimization structures are symmetric. When the material directions are 30^0, 45^0 and 60^0, the optimal results are not symmetric and the result of 30^0 material direction is the most non-symmetrical in the three cases. This result illustrates that the material performance as well as material direction can affect the topological optimal result.

The optimization structures shown in Figures 5, 10, 12, 14, and 16 are basically coinciding with the paper of Allaire and Jouve 2005, which proves our method to be very valid.

4. Conclusions

The feasibility of employing level set method to optimize an orthotropic material structure is explored theoretically. The augmented Lagrangian multiplier with inequality constraints is extended into the topology optimization of the design structure. By the combination of level-set, shape derivative and augmented Lagrangian method, the sensitivity formulae of the topological optimization of dynamic structure is derived. The optimization boundary of the orthotropic material structure is embedded into the zero level-set of a higher-dimensional scalar function. The movements of the boundary are iteratively promoted by the solutions of PDE. The evolution velocity of moving boundary can be controlled by CFL condition and sensitivity. Examples studied are employed to illustrate the validity of the present optimization method. The conclusions indicate this

investigation will provide an important foundation for the advanced development topology optimization of the complex constitutive relationship material.

Acknowledgements

The works was supported by a research granted No. Z2007F04 from the Natural Science Foundation of Shandong Province, People's Republic of China. The authors also show their acknowledgements to the related pioneers' works and to the anonymous reviewers for their valuable comments.

References

Allaire G and Jouve F. (2005). A level-set method for vibration and multiple loads structural optimization. Comput. *Methods Appl. Mech. Eng.* 194:3269–3290.

Allaire G, Jouve F, Toader AM. (2004). Structural optimization using sensitivity analysis and a level-set method, *J. Comp. Phys.* 194:363-393.

Bendsøe MP and Kikuchi N. (1988). Generating optimal topology in structural design using a homogenization method. *Computational Methods in Applied Mechanics and Engineering.* 71:197–224.

Bendsøe MP and Sigmund O. (1999). Material interpolations in topology optimization. *Arch. Appl. Mech.* 69:635–654.

Bertsekas DP. (1982). *Constrained Optimization and Lagrange Multiplier Methods.* Academic Press, New York.

Diaz A and Kikuchi N (1992) Solutions to shape and topology eigenvalue optimization problems using a homegenization method. Int. J. Numer. Methods Eng. 35: 1487–1502.

Fox RL and Kapoor MP. (1968). *Rate of change of eigenvalues and eigenvector.* AAIA J. 6: 2426–2429.

Hagishita T and Ohsaki M. (2009). Topology optimization of trusses by growing ground structure method. *Struct. Multidisc. Optim.* 37:377–393.

Inzarulfaisham AR and Azegami H. (2004). Solution to boundary shape optimization problem of linear elastic continua with prescribed natural vibration mode shapes. *Struct Multidisc Optim.* 27: 210–217.

Jiaqin Chen, Vadim Shapiro, Krishnan Suresh, Igor Tsukanov. (2006). PARAMETRIC AND TOPOLOGICAL CONTROL IN SHAPE OPTIMIZATION. Proceedings of ASME International Design Engineering Technical Conferences and Computers and Information in Engineering Conference, September 10–13, Philadelphia, Pennsylvania, USA.

Kim C, Kota S, Moon Y. (2006). An instant center approach toward the conceptual design of compliant mechanisms. *ASME Journal of Mechanical Design*. 128:542–550.

Luo Z, Yang JZ, Chen LP, etc. (2006). A hybrid fuzzy-goal programming scheme for multi-objective topology optimization of static and dynamic under multiple loading conditions. *Structural and Multidisciplinary Optimization.* 31(1): 26-39.

Meske R, Lauber B, Schnack E. (2006). A new optimality criteria method for shape optimization of natural frequency problems. *Struct Multidisc Optim.* 31:295–310.

Mlejnek HP. (1992). Some exploration of the genesis of structures. In: Bendsøe MP, Mota Soares CA (eds) Topology design of structures. Proceedings of NATO ARW (Sesimbra, Portugal). Kluwer, Dordrecht, pp 287–300.

Nelson RB. (1976). *Simplied calculation of eigenvector derivatives.* AAIA J. 14: 1201–1205.

Nocedal J and Wright JS. (1999). Numerical Optimization. *Science + Business Media Inc.Springer,* New York.

Osher S and Sethian L. (1988). Fronts propagating with curvature dependent speed: Algorithms based on Hamilton-Jacobi formulations, *J. Comput. Phys.* 79: 12–49.

Pederson NL. (2000). Maximization of eigenvalues using topology optimization. *Structural and Multidisciplinary Optimization.* 20: 2-11.

Prager, W. (1974). A note on discretitized Michell structures. *Computer Methods in Applied Mechanics and Engineering.* 3: 249 - 255.

Rozvany, GIN. (1979). Optimal beam layouts: allowance for cost of shear. *Computational Methods in Applied Mechanical Engineering.* 19: 49 - 58.

Sethian JA. (1999). Level-set methods and fast marching methods evolving interfaces in computation geometry, fluid mechanics, computer vision, and materials science. Cambridge University Press, Cambridge, UK.

Seonho Cho, Seung-Hyun Ha, Chan-Young Park. (2006). Topological shape optimization of power flow problems at high frequencies using level set approach. *International Journal of Solids and Structures.* 43: 172–192.

Seyranian AP, Lund E, Olhoff N. (1994). Multiple eigenvalues in structural optimization problems. *Structural and Multidisciplinary Optimization*. 8(4): 207-227.

Sokolowski J and Jean-paul Zolesio. (1991). *Introduction to shape optimization: shape sensitivity analysis.* Berlin, Germany: Springer.

Stanley Osher and Ronald Fedkiw. (2003). *Level-set methods and dynamic implicit surface.* Springer, Berlin, Germany.

Tenek LH and Hagiwara I. (1994). Eigenfrequency maximization of plates by optimization of topology using homegenization and mathematical programming. *JSME Int. J. Ser. C* 37: 667–677.

Wang H. (2004). A Unit Cell Approach for Lightweight Structure and Compliant Mechanism. Ph.d. thesis, Georgia Institute of Technolohy, Atlanda.

Wang M, Wang XM, Guo DM. (2003). A level-set method for structural topology optimization. *Computer Methods in Applied Mechanics and Engineering.* 192: 227–246.

Wang S and Wang M. (2006). Radial basis functions and level-set method for structural topology optimization. *International Journal of Numerical Method for Engineering*. 65: 2060–2090.

Zhou M, Rozvany GIN. (1991). The COC algorithm, Part II: Topological, geometrical and generalized shape optimization. Comp. *Meth. Appl. Mech. Eng.* 89:309-336.

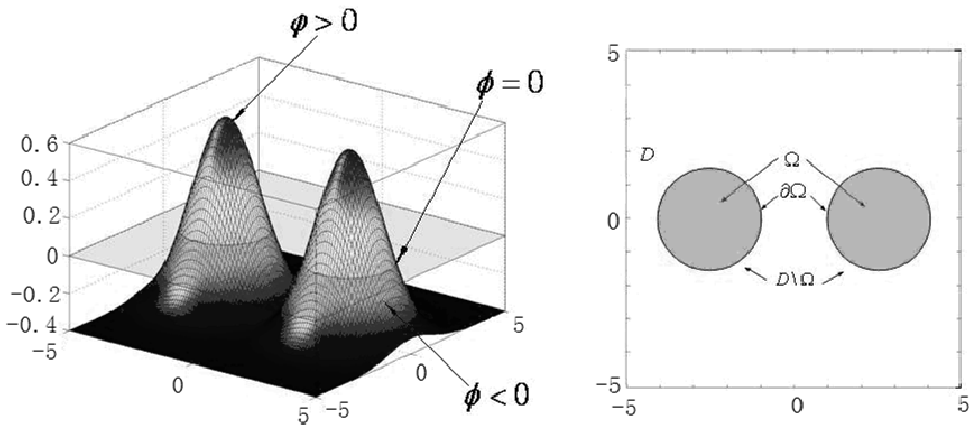

Figure 1. Design domain Ω and level-set embedded function

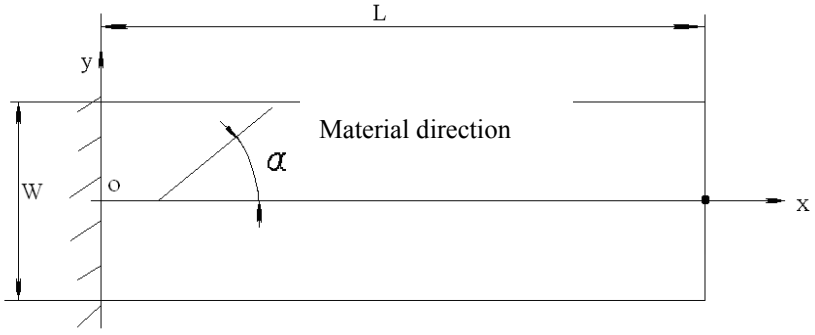

Figure 2. The geometric structure and boundary condition

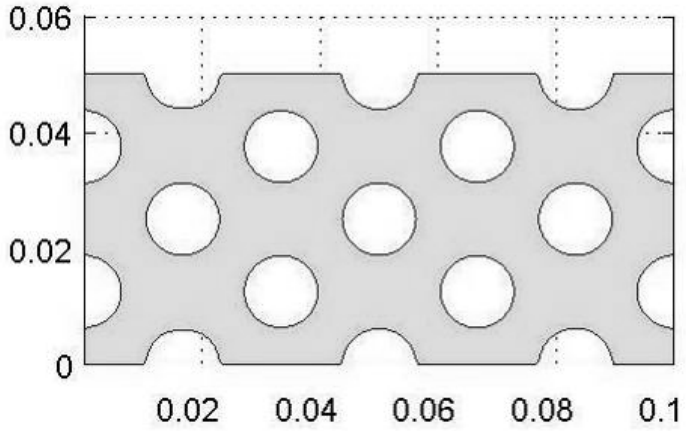

Figure 3. Initial design structure

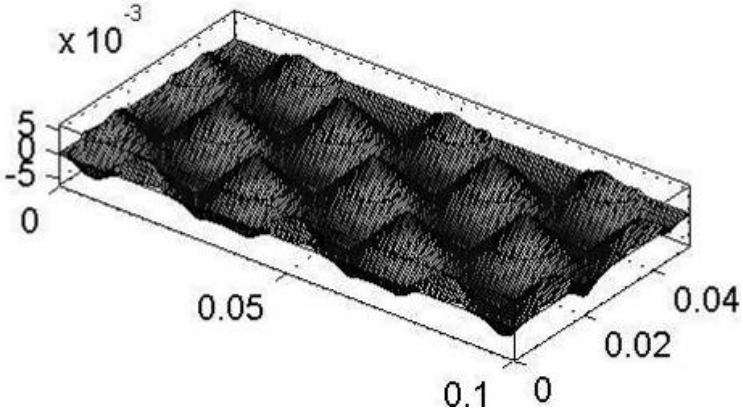

Figure 4. Initial value of level-set function

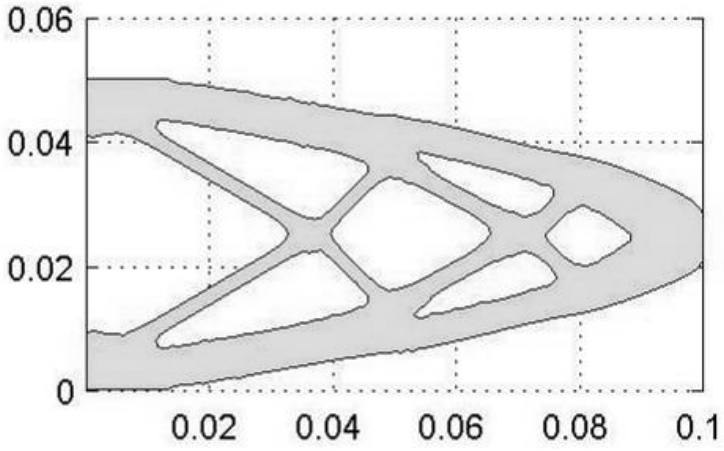

Figure 5. The first-order natural frequency maximization of orthotropic material (0^0)

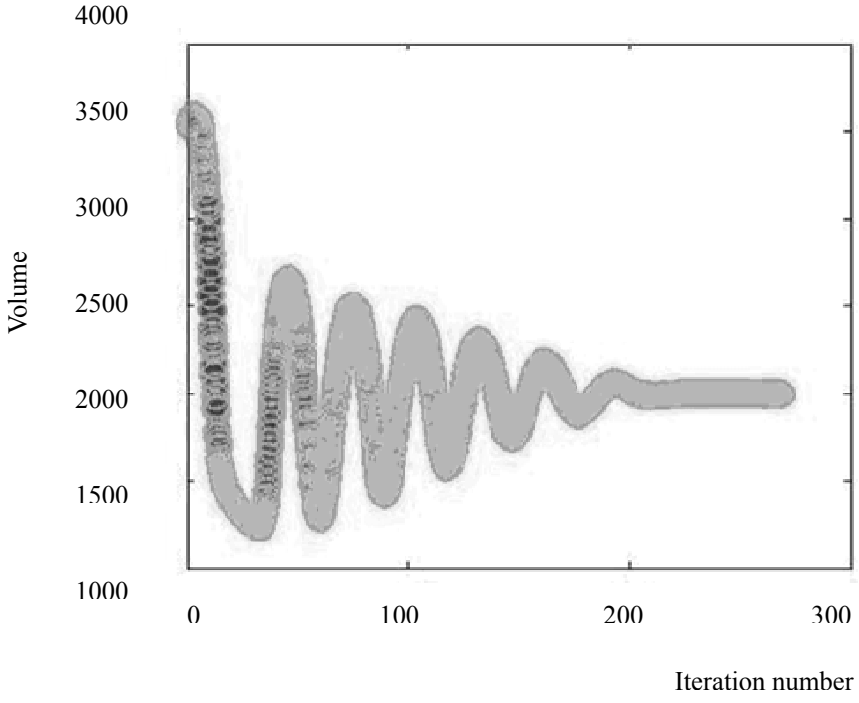

Figure 6. Volume variable with iteration number (0^0)

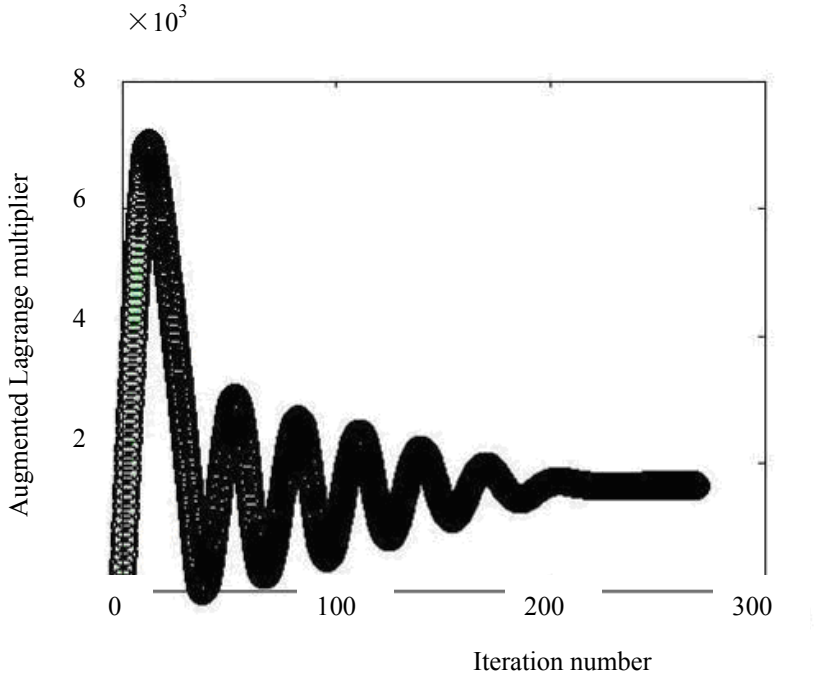

Figure 7. Augmented Lagrange multiplier variable with iteration number (0^0)

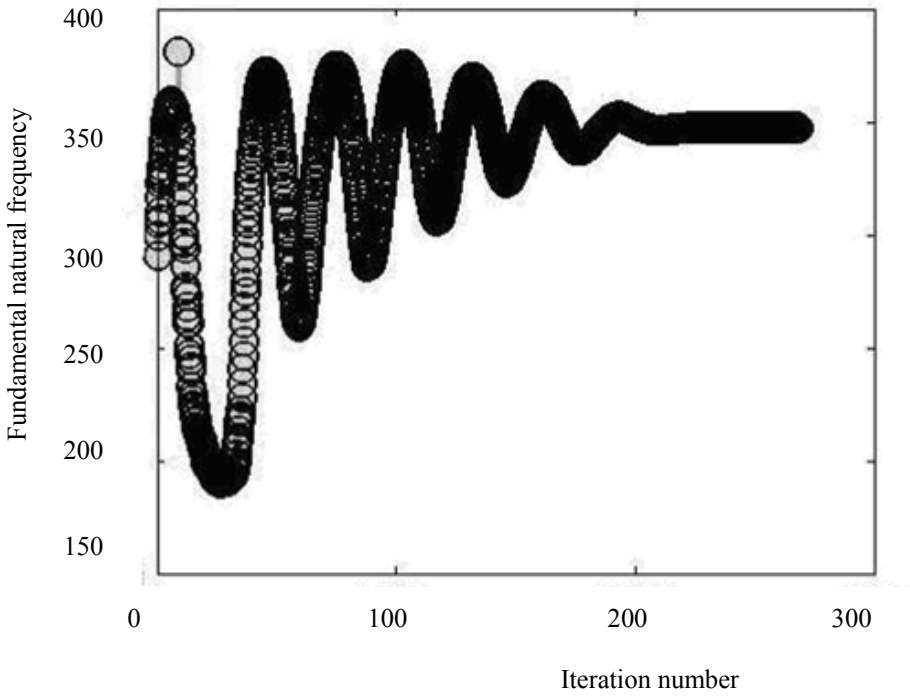

Figure 8. Fundamental natural frequency variable with iteration number (0^0)

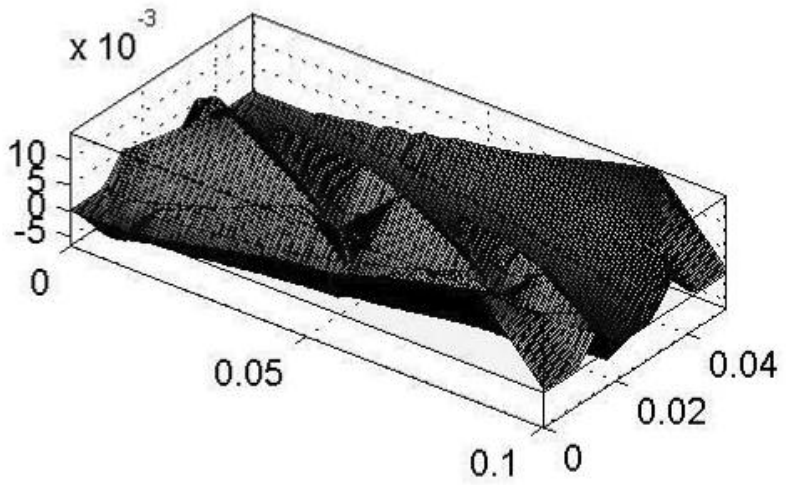

Figure 9. Final level-set surface (0^0)

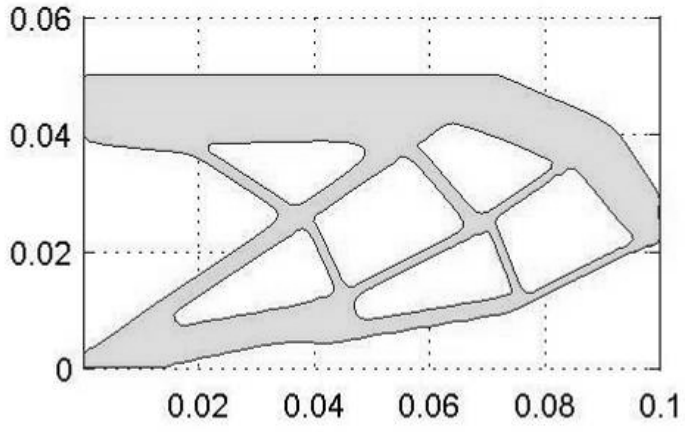

Figure 10. The first-order natural frequency maximization of orthotropic material (30^0)

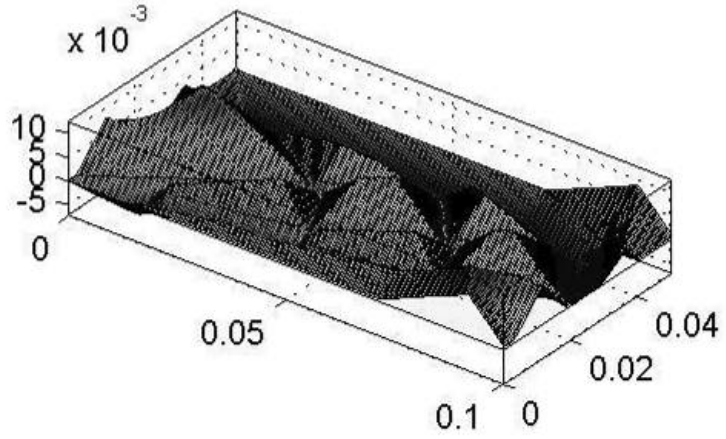

Figure 11. Final level-set surface (30^0)

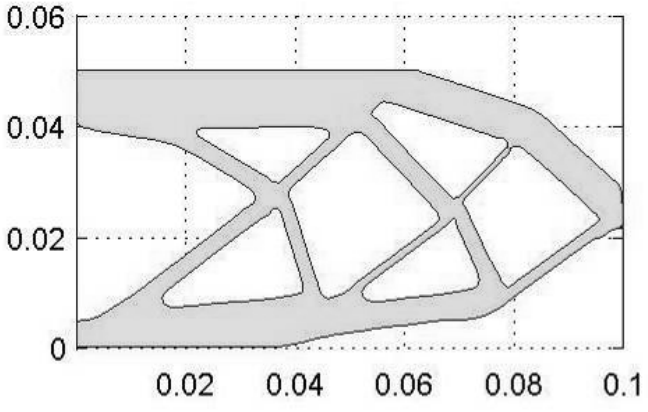

Figure 12. The first-order natural frequency maximization of orthotropic material (45^0)

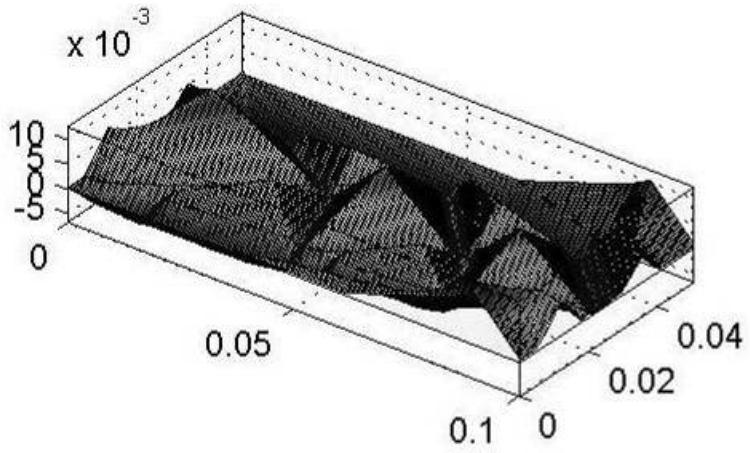

Figure 13. Final level-set surface (45^0)

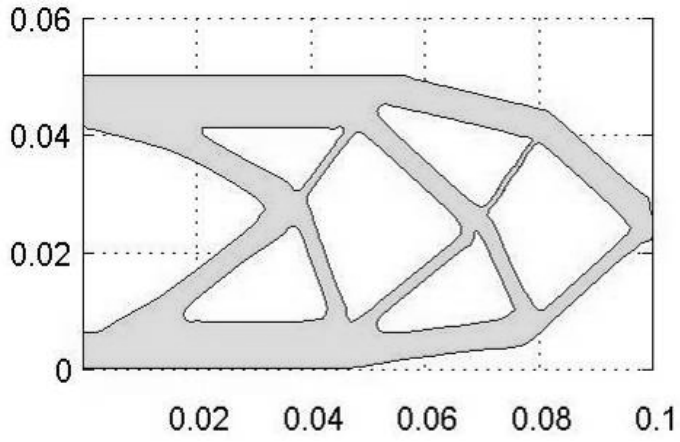

Figure 14. The first-order natural frequency maximization of orthotropic material (60^0)

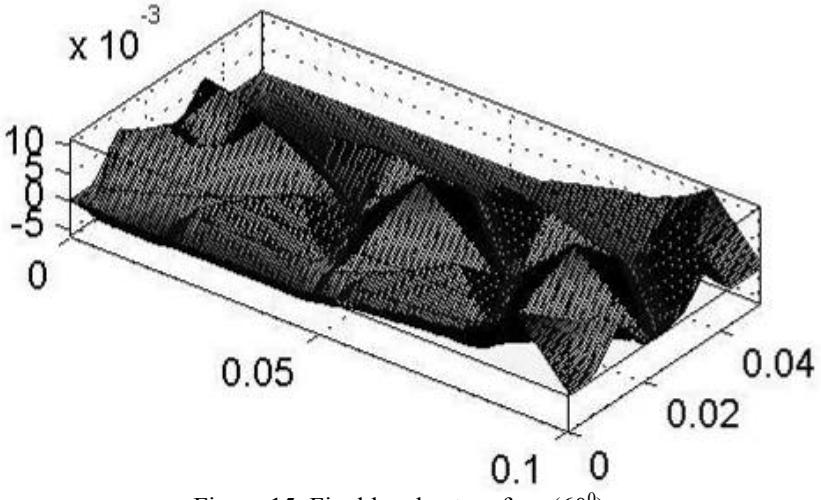

Figure 15. Final level-set surface (60^0)

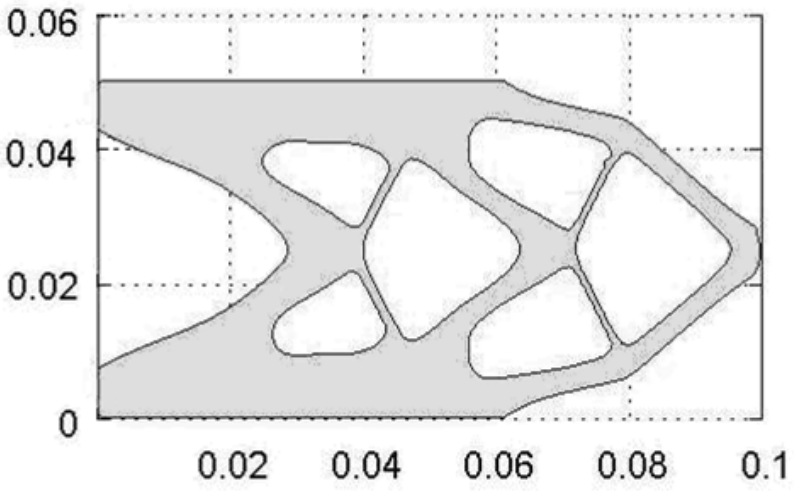

Figure 16. The first-order natural frequency maximization of orthotropic material (90^0)

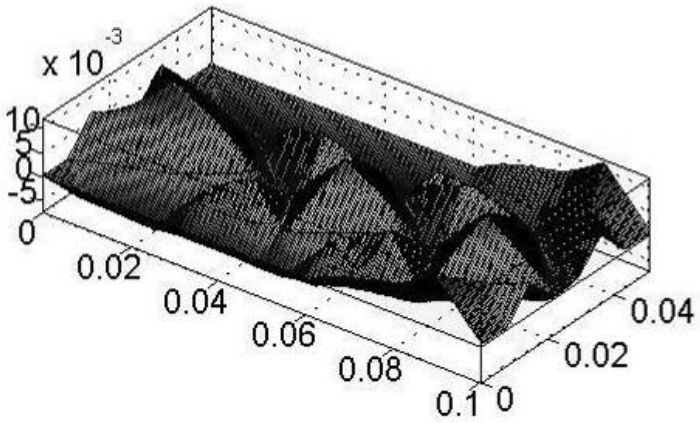

Figure 17. Final level-set surface (90^0)

Effect of Different Treatments on Seed Germination of Honey Locust (*Gleditschia triacanthos*)

Marzieh Babashpour Asl (Corresponding author)
Department of Horticultural Science
Islamic Azad University of Maragheh Branch
PO box 345 Maragheh, East Azarbaijan, Iran
Tel: 91-43-015-052 E-mail: babashpour@iau-maragheh.ac.ir

Raana Sharivivash
Department of Horticultural Science
Islamic Azad University of Maragheh Branch
PO box 345 Maragheh, East Azarbaijan, Iran
Tel: 91-49-209-730 E-mail: raana_sv@yahoo.com

Akram. Rahbari
Department of Horticultural Science
Islamic Azad University of Maragheh Branch
PO box 345 Maragheh, East Azarbaijan, Iran
Tel: 91-41-773-819 E-mail: nasrinrahbary@yahoo.com

Abstract

Honey-locust *(Gleditschia triacanthos)* seeds, like those of many leguminous species, have hard and impermeable coats. Germination is thought to be enhanced when seeds are scarified or soaked in concentrated sulfuric acid or hot water. This experiment was separated into two parts: Scarification methods and stratification investigation. The result from the first experiment showed that acid scarification treatment for 1 hour was the best method for breaking their dormant period. However in the second experiment it was found that the honey locust seeds like those of many leguminous species do not have dormant embryo, because stratification did not affect seed germination and there was no significant difference between stratification treatment and control. It can be concluded that acid scarification without stratification is optimized in breaking honey-locust seed dormancy.

Keywords: Honey-locust, Germination, Stratification, Scarification, Dormancy

1. Introduction

Gleditschia triacanthos (Honey locust) is deciduous tree that is useful for windbreaks, shelterbelts, erosion control, wildlife food, and local wood products (posts and railroad ties) (Blair, 1990). Honeylocust is used for buffer strips along highways or in urban forests, where it can be successfully grown in areas with air pollution, poor drainage, salty soils, and drought (Ertekin & Kirdar, 2010). Honey locust has also become highly valued as an agro-forestry species in other parts of the world (Davies and Macfarlane, 1979; Felker and Bandurski, 1979). This dicot plant is native to the U.S. and has its most active growth period in the spring and summer (Vine, 1960). Honey-locust fruits are flat, indehiscent, often twisted legumes (pods) 15 to 41 cm in length (Blair, 1990). The small flat, brownish seeds, 8 to 12 mm in length, are embedded in a sweet pulp, the feature that attracts livestock and wildlife to the fruits (Vines, 1960). The legumes may have up to 12 seeds. These legume and seed characteristics are the best way to distinguish between species (Brown and Kirkman, 1990). The seeds are close to the same size and contain a thin, flat embryo surrounded by a layer of horny endosperm. The hard seed coats of honey-locust must be treated to make them permeable before germination can occur (Heit, 1942; Liu and *et al,* 1981). Various chemical and mechanical treatments are used to overcome hard or impervious seed coats so that the imbibition of water and exchange of gases necessary for germination can occur. For chemical treatment, seeds can be soaked in concentrated grade H_2SO_4 and for mechanical treatment, for example, dried seeds are

taken and placed in metal container with gravels. The container is vigorously shaken so that the gravels scratch the seed epicarp (Usberti and Martines, 2007). In nature, scarification often occurs by fall seeding. Freezing temperatures or microbial activities modify the seed coat during the winter. Scarification can also occur as seeds pass through the digestive tract of various animals. Scarification can also be forced, rather than waiting for nature to alter the seed coats. Commercial growers scarify seeds by soaking them in concentrated sulfuric acid. Seed coats can also be filed with a metal file, rubbed with sandpaper, nicked with a knife, cracked gently with a hammer to weaken the seed coat or soaked in hot water. Following scarification, the seeds should be dull in appearance, but not deeply pitted or cracked as to damage the embryo. Scarified seeds do not store well and should be planted as soon as possible after treatment (Young, 1992).

Seed collected while they are slightly immature will have thinner seed coats and can often be germinated without any pretreatment. This practice is not recommended, however, because the immature seed coats are not effective barriers against disease. Soaking the seeds in either concentrated sulfuric acid or hot water has been used. Soaking time in acid must be determined for each seed lot because of variation in seed coat hardness due to genetic or developmental differences (Bonner, 1974). This study was designed to test two hypotheses. The first hypothesis was to test whether the germination was inhibited by physical dormancy which could be improved by methods of scarification. The second hypothesis was to test whether the germination was inhibited by physiological dormancy which can be improved by methods of stratification. The objectives of the study were to determine: 1) the effects of scarification and 2) the effects of stratification on germination of honey-locust seeds.

2. Materials and Methods

2.1 Experiment 1

Fully mature fruits of honey-locust (*Gleditschia triacanthos*) were collected from Tabriz in East Azerbaijan province (North West of Iran, Latitude 38° 05′ N, Longitude 46° 17′ E, Altitude 1360 m above sea level) in December. The fruits were air-dried for two days at room temperature, after which seeds separated manually. Uniform (as far as possible) seeds were treated with Captan fungicide. There were five scarification treatments that tested the physical dormancy hypothesis and consisted of three acid treatments, one hot water and a control treatment (untreated seeds). 450 seeds were selected. For acid treatment, 270 seeds were soaked in concentrated sulfuric acid for 1, 2 and 3 hours (90 seeds were used for each treatment). Thereafter, they were washed thoroughly with tap water. For hot water treatment, 90 seeds were placed in 3 to 4 times their volume of water (90°C). Seeds and water are allowed to cool to room temperature. The experiment utilized a Completely Randomized Design (CRC) with two replications. 30 seeds were planted in a tray filled with potting soil/leaf mold growing medium. The seeds were planted at the same time and kept in a growth room with temperature between 20°C -25°C and trays were watered with tap water according to need. Seed germination was recorded daily, the radical emergence (2-5 mm) serving as an index of germination. The germination percentage and germination rate were calculated. Germination rate was calculated according to the formula described by Maguirw (1962) and (Esechie) (1994) as follows:

$$GR=\sum \frac{Si}{Di}$$

S_i = total number of germinated seeds

D_i = number of days per counting

n = counting frequency

Also number of days to 50% germination (T50) and root length (mm) were recorded.

2.2 Experiment 2

Seeds were prepared like experiment 1. There were four treatments in this experiment consisting of two cold stratification treatments and one cold stratification treatment of acid scarified seeds and one control treatment (90 untreated seeds, 30 seeds for each replication). 360 seeds were selected. For cold stratification treatment, 180 non-scarified seeds were kept at 5±1°C for 4 and 10 weeks. For third treatment, 90 seeds were soaked in concentrated sulfuric acid for 2 hours were used. Thereafter, they were kept at 5±1°C for 10 weeks. For stratification, seeds were put into plastic bags filled with vermiculite and watered with tap water according to need.

2.3 Statistical analysis

The data were analyzed using the SAS software and the means were compared with Duncan's Test at p=0.05.

3. Results

3.1 Scarification

The acid scarification treatments significantly ($P<0.05$) increased germination percentage of honey-locust seeds compared to the hot water and control in experiment 1 (Table 1). There were no significant difference between hot water treatment and control (Table 2). Also the acid scarification treatments significantly ($P<0.05$) increased germination rate, number of days to 50% germination (T50) and root length (mm) of honey-locust seeds compared to the hot water and control.

No germination was recorded from seeds in the control for period of the experiment.

The fact that concentrated sulphuric acid for 3 hours gave the highest percentage germination (86.67%) and within the shortest period as compared 1 and 2 hours, indicate that the more rapidly the seed coat is ruptured the faster the rate of germination, however, prolonged Emerson may be injurious to the seeds as the acid may rapture vital parts of the embryo. Sulphuric acid is thought to disrupt the seed coat and expose the lumens of the macrosclereids cells, permitting imbibitions of water (Nikoleave, 1977) which trigger germination. The treatment with sulphuric acid for 1 and 2 hours gave 61.11 % and 78.89% germination, respectively. However there were no significant differences between 3 levels of sulphuric acid.

3.2 Stratification

The stratification and combinational treatment with scarified seeds significantly ($P<0.05$) increased germination percentage of honey-locust seeds compared to control (Table 3). There were no significant differences between combinational treatment and control (Table 4). Also the stratification treatment for 4 weeks significantly ($P<0.05$) increased germination rate (0.0423) and root length (2.39 mm) of honey-locust seed compared to the other treatments. No germination was recorded from seeds in the stratification treatment for 10 weeks. However, 6.67% for germination percentage and 0.0423 and 2.39 for germination rate and root length respectively, are not acceptable numbers for germination of seeds. So, the stratification did not affect germination of honey-locust seeds.

4. Discussion

Seed dormancy is a means to allow seeds to initiate germination when conditions are normally favorable for germination and survival of the seedlings. Dormancy can be regulated by the environment or by the seed itself. The seed dormancy may be due to unfavorable environmental conditions or sometimes, some seeds may not germinate because of some inhibitory factor of the seed itself. Dormancy of seed due to inhibitory factors, are either due to hard seed coat (external) or physical of physiological status of the interior of the seed. Seed dormancy in Honey locust (*Gleditschia triacanthos)* belongs to the first type.

Acid scarification is known to be highly effective in improving germination of species with hard seed coats (Youssef, 2008). The results demonstrate that the most effective method of improving the germination of honey-locust seed proved to be acid scarification. This indicates that the low germination of honey-locust is probably due to physical dormancy which was consistent with the results from previous research done on the legume species *Galactia elliottii* (Muir and Pitman, 1987) and *Medicago sativa subsp.falcata* (Xu and Bou, 2004). Many leguminous seeds have wide dormancy durations induced by the appetence of a hard waterproof coat, but the nature of the hard coat related dormancy is specifically. The blocking of water access into the seed is the most common cause of delay in seed germination (Ballard, 1973; Rolston, 1987; Cavanagh, 1980)

The stratification treatments did not show a consistent response indicating that the low germination of honey-locust was probably not due to physiological dormancy. These results support the findings of previous research on the freezing and thawing of other leguminous seeds which reported that freezing seeds to -20°C had little to no effect on germination (Busse, 1930). However, colder temperatures and longer durations have shown to increase germination in sweet clover (*Melilotus sp.*) and purple-flowered alfalfa (*Medicago sativa*) seeds (Busse, 1930). Further research could be done experimenting with different cold temperatures and durations.

Although hot water treatment had no effect on germination in this study, further experimentation with treatments at different temperatures might produce different results.

5. Conclusions

The best efficiency method for breaking dormancy of *Gleditschia triacanthos* seeds was acid scarification method that soaking in concentrated sulphuric acid for 1 hour.

 ISSN 1913-1844 E-ISSN 1913-1852

References

Ballard, L.A.T. (1973). Physical barriers to germination. *Seed Science and Technology,* 1: 285- 303.

Blair, RM. (1990). *Gleditsia triacanthos* L., honeylocust. In: Burns RM, Honkala BH, tech. coords. Silvics of North America. Volume 2, Hardwoods. Agric. Handbk. 654. Washington, DC: USDA Forest Service: 358B364.

Bonner, F.T., Burton J.D., & Grigsby H.C. (1974). *Gleditsia* L., honeylocust. In: Schopmeyer CS, tech. coord. Seeds of woody plants in the United States. Agric. Handbk. 450. Washington, DC: USDA Forest Service: 431B433.

Brown, C.L., & Kirkman, L.K. (1990). *Trees of Georgia and adjacent states*. Portland, OR: Timber Press. 292 p.

Busse, W. F. (1930). Effect of Low Temperatures on Germination of Impermeable Seeds. *Botanical Gazette* 89(2):169-179.

Cavangh, A.K. (1980). A review of some aspects of the germination of Acacias. Proceedings. of the Royal Society of Victoria, 91: 161-180.

Davies, D.J.G., & Macfarlane, R.P. (1979). Multiple-purpose trees for pastoral farming in New Zealand: with emphasis on tree legumes. *New Zealand Agricultural Science*. 13(4): 177B186 [Forestry Abstracts 42(1): 252; 1981].

Ertekin, M., & Kirdar, E. (2010). Effects of seed coat colour on seed characteristics of honeylocust (*Gleditsia triacanthos*). *Afr. J. Agric. Res.,* 5(17): 2434-2438.

Fredan, M.A.A., & Ali, Y.S.S. (2008).Seed Scarification Requirement in Doum (*Hyphaene thebaica* Mart.). *Sci. J. of King Faisal University (Basic and Applied Sciences)* 9(2): 75-84.

Heit, C.E. (1942). *Acid treatment of honey locust.* Notes For. Invest. 42. Albany: New York Conservation Department. np.

Muir, J. P., & Pitman W.D. (1987). Improving Germination Rate of the Florida Legume *Galactia elliottii*. *Journal of Range Managemen.t* 40(3):452-454.

Nikoleave, M.G. (1977). *Factors controlling seed dormancy pattern.* North Holland publishing Co, Amsterdam, pp. 51-74.

Roleston, M.P. (1978). Water impermeable seed dormancy. *Botanical review,* 44:365-396.

Usberti, R., & Martines, L. (2007). Sulfuric acid scarification effects on *Brachiaria brizantha*, *B. humidicola and Panicum maximum* seed dormancy release. Revista Brasileira de Sementes, 29(2): 143-147.

Vines, R.A. (1960). *Trees, shrubs, and woody vines of the Southwest.* Austin: University of Texas Press. 1104 p.

Xu, L., Boe A., Johnson, P. S., & Kephart, K. (2004). Effects of a Naturalized Population of Yellow-flowered Alfalfa (*Medicago sativa ssp. facata*) on Species Richness and Biomass Production of Native Rangeland. p99-105 *In*: Beef Cattle Research Report, SDSU, Brookings, SD

Young, J. A., & Young, C.G. (1992). *Seeds of Woody Plants in North America*. Revised and enlarged edition. Dioscorides Press, Portland, OR. (This is the most complete and useful book on woody plant seeds and their germination requirements – a "must have" for any woody plant propagation library.)

Youssef, A.M. (2008). Adaptive responses of some desert plants from different ecosystems of Suez road, Egypt. *Res. J. Agric. Biol. Sci.,* 4(5): 595-603.

Table 1. ANOVA for honey locust seed germination (Experiment 1)

Source of variation	d.f.	Means of Squares			
		Germination percentage	Germination rate	T50	Root length(mm)
treatments	4	4653.931*	1.635*	235.767*	286.773*
SD	10	184.469	0.065	0.867	51.442

* = statistically significant at 0.05% probability level.

Table 2. Effect of acid scarification and hot water treatments on different parameters of seed germination of Honey-locust

Treatments → / Parameters ↓	Control	H_2SO_4 (1hour)	H_2SO_4 (2hour)	H_2SO_4 (3hour)	Hot water (90 °C)
Germination percentage	0 [b]	61.11 [a]	78.89 [a]	86.67 [a]	12.22 [b]
Germination rate	0 [b]	1.15 [a]	1.48 [a]	1.63 [a]	0.23 [b]
T50	0 [c]	19.00 [a]	14.33 [ab]	14.00 [b]	0 [c]
Root length(mm)	0 [c]	20.87 [a]	21.20 [a]	18.57 [ab]	5.79 [bc]

In each row or column, means with the similar letter(s) are not significantly different at 5% level of probability using Duncan' Test.

Table 3. ANOVA for honey locust seed germination (Experiment 2)

Source of variation	d.f.	Means of Squares			
		Germination percentage	Germination rate	T50	Root length(mm)
treatments	3	28.06*	0.001*	0	3.03*
SD	8	10.19	0	0	51/442

* = statistically significant at 0.05% probability level.

Table 4. Effect of acid scarification and hot water treatments on different parameters of seed germination of Honey-locust

Treatments → / Parameters ↓	Control	Stratification (4 weeks)	Stratification (10 weeks)	H_2SO_4 (3hour) + Stratification (10 weeks)
Germination percentage	1.11 [ab]	6.67 [a]	0	4.44 [ab]
Germination rate	0.0073 [ab]	0.0423 [a]	0	0.0273 [ab]
T50	0	0	0	0
Root length(mm)	0.71 [ab]	2.39	0	0.95 [ab]

In each row or column, means with the similar letter(s) are not significantly different at 5% level of probability using Duncan' Test.

 ISSN 1913-1844 E-ISSN 1913-1852

Study on Preparation and Application in Flocculants of Modified Lignin

Haiyin Liu
College of Life Science, Changchun Normal University
Changchun, Jilin 130022, China

Xiuyun Yang, Xiaoqiu Liu, Haibo Yao & Yunhui Li (Corresponding author)
School of Chemistry and Environmental Engineering
Changchun University of Science and Technology, Changchun, Jilin 130022, China
E-mail: liyh@cust.edu.cn
Registration Code: Environmental Protection Agency of JiLin (2007-28)

Abstract

The lignin sulfonate was modified with olefins monomer by the method of radiation graft polymerization, by which a new type of natural polymer flocculants can be made. And results of the flocculation and sedimentation are tested in the furfural wastewater treatment process. Furfural wastewater is a complex composition, whose COD is about 20000mg / L, is difficult to be treated by conventional methods. Our results showed that the kind of flocculants can remove 50 percent COD or more from furfural wastewater after aerating and adjusting pH value to 9.

Keywords: Lignin, Irradiation, Flocculants, Furfural wastewater

As a general plant of polymer, lignin is the main material to support plant growth, it constitute the cellulose with cellulose and hemicellulose together. Lignin in plants is the most abundant and most important organic polymer after cellulose. Lignin is non-toxic, source and rich in renewable resources, so it is widely used in industry. Generally, the commercial lignin is the derivative product from paper making by-products. Such as leather, dyestuff, food, architecture, and agricultural industries, it's mainly used as raw materials (such as mulan grain preparation) and additives (such as adhesives, dispersant, chelating agent and emulsifier) (Zhan HuaiYu. 2005).

Lignin, also can use as a flocculent flocculant modified lignin, due to several points such as the sources of the raw materials, inexpensive, non-toxic, easily biodegradable etc, and shows good application prospect. But there are some problems of low molecular weight and average less active absorption points, through the method of cross-linking reaction and condensation reaction, people want to change the spatial configuration and increase and molecular weight. Moreover, people try to introduce flocculation properties of functional and to improve the lignin flocculation properties further (Qiu XueQing, LouHongMing. 1999). Lignin can increase its quality of molecules after grafting in vinyl monomers; it's also a method to improve lignin's flocculation. Qianjun Liu etc(Liu Qianjun, ZhanHuaiYu, Liu mengru & WuHong. 2003). Use potassium sulfate as the initiator and acryl amide monomer to preparate the decoloring agents lignin flocculation. GuiZhen Fang etc(Fang GuiZhen, HeWeiHua & Song ZhanQian. 2003). Synthesize flocculant - lignin salt. B. Phillips (R. B. Phillips, W. Brown & V. Stannett. 1973; R. B. Phillips, W. Brown & V. Stannett. 1972) was studied the irradiation graft copolymerization reaction between styrene and lignin.. These researches contributed to the application of the lignin flocculant.

Base on the past research , this paper use lignosulphonate salt as photo base, join olefins grafted monomer, using irradiation graft polymerization method to preparate natural polymer flocculant lignin. This method is characteristic by the reaction process doesn't need solvent; the reaction process doesn't attract small molecules, so the process of using this kind of flocculant will not cause secondary pollution. We use the flocculant to deal with the furfural wastewater by flocculating sedimentation. Mainly because of COD is about 20000mg/L, pH < 2. According to the characteristics of furfural wastewater, we design the corresponding process. Practice has proved, in appropriate conditions, can achieve very good result flocculation.

1. Experimental

1.1 Raw material and equipment

(1)Llignosulphonate sodium/Beijing; technology Co., LTD. Beijing plant acid, Acetone Beijing chemical plants, Beijing olefin plant monomer.

(2)Furfural wastewater quality

Tan appearance, including a solid aerosol particle

COD 23025 mg/L

pH 4

(3)Rotating evaporator (RE-52AA) Shanghai vibration; the laboratory equipment Co., LTD. Circulating water pump (SHB - multi-purpose type III) trading Co., LTD. Of Zhengzhou wall, 60Co emitter, Chinese academy of sciences, Changchun institute of applied chemistry.

1.2 Flocculant preparation methods

300ml acetic acid was dropped into 500ml flask. drop 150g lignosulphonate sodium into the flask slowly and group by group, of partial, then mix the lignin to be soluble by glass rod. put the flask of lignosulphonate mixed with acetic down for 10 minutes, and then put the filtered solid material into the flask, add appropriate acetone, and the do twice suction filter. We can get purificated yellow lignosulphonate after dry. According to the proportion of purification weigh

of lignosulphonate salt and olefin monomer, grinding, mixing, controlling conditions for radiation graft polymerization reaction which use 60Co as radiant point.

1.3 Furfural wastewater flocculating sedimentation

Taking fresh water samples from furfural, aerating, adding flocculants and auxiliary sorbents according to the design scheme, mixing fastly for1min, stilling for 10min, getting the supernatant and calculating COD as well as COD removal.

1.4 Flocculant surface morphology analysis

We adopt the Nano - I atomic force microscope (type: S - favor - 0000-1) from American Schmidt Co to scan the water.

1.5 Flocculants structure characterization

We adopt the UV - 1240 type uv-vis spectrophotometer from Japanese to do the ultraviolet spectroscopic analysis.

1.6 Furfural COD value method

We adopt HACH COD tester (DR - 2010) from American, the temperature is 150°C, dispelling time is 2h..

2. Results and Discussion

2.1 Flocculant surface morphology analysis

We should make the sample to 0.02 g/L solution and spin coat on the slides about 1500 r/min in room temperature, In order to dry it, we observe the surface morphology in the atomic force microscope. Lignosulphonate salt is a three-dimensional granular structure of organic polymer, there's no organic polymer chain in its molecular structure. We can see from figure 2.1, sodium lignosulphonate is flat, 32.01 nm to devide; the surface properties of modified sodium lignosulphonate is changed. There are some obviously uniform and divide 46.32 nm to rise. This is because of in the modified lignin, the grafted surface by - C - C - composed of amorphous polymer composition of linear low molecular characteristics, main chain molecules, flexibility and good symmetry. When there-dimensional structure lignosulphonate salt on grafting, flexible chain on the surface properties of sodium lignosulphonate produces more changes, grafted long -chain formation obviously uplift and excluded in polarity membrane surface.

2.2 grafted lignin up spectral analysis

Lignin was typical of aromatic compounds. Aromatic compounds have characteristics of ultraviolet absorption, 280 nm will appear a stable absorption peak when there is aromatic substituent in lignin structure. Figure 2.2 shows ultraviolet absorption spectrum lines of lignosulphonate salt and modified lignin sulfonate olefin monomers.

The graph shows that lignin has obvious absorption peaks around 205nm and 280nm of ultraviolet spectrum. The monomer which is grafted to the lignin has been saturation, it lose phenacylmethylene groups to become substituent and there is greater space a resistance. A resistance can make the substituent which conjugate with benzene originally to be rejected out of benzene plane, and resistance also can not make substituent electrons overlap completely with benzene PI system , thus affecting the spectrum. Wave of benzene and the intensity of absorption with wave depend on the planar angle between substituent and benzene. After adjacent bits replace, because of the resistance increases, the factors make Angle reduced, cause absorption electronic overlap with strength successive reduced. Substituent produced blue affect in 280nm. The scope of absorb with strength reduction depends on how long and how much is grafting long chain. Modified sodium lignosulphonate.

2.3 Liquid pH value of furfural COD removal rate

In the Flocculating sedimentation furfural wastewater determination experiment which is in the condition of 8h aeration and different pH value, we can see modified lignin flocculent effect is different and the settlement of COD lower level is not the same. After the aeration the pH of furfural wastewater rise from 4 to approximately 7, and there is a settlement in the solution, then add flocculants and auxiliary sorbents, a large number of floce sedrmation will separate out from solution. From graph 2.3 we can see the biggest decline of COD occurs in the pH-9. Because the condensation reaction occurs under this condition and molecular weight increase ceaselessly

to format the aerosol particles, in addition flocculation agent can play a good role of bridge to prompt to macromolecular flocculating sedimentation.

2.4 Flocculant for COD removal rate of consumption

Taking 250ml fresh furfural liquid; 8h aeration, adjust it to pH - 9. the graph 2.4 shows the change of furfural wastewater COD after adding the Modified lignin natural organic polymer flocculant and auxiliary adsorbent. As we can see from the graph when the amount of flocculants is bigger than 2g, the COD removal rate of furfural wastewater will be more than 50%, if we increase the amount of flocculants; the COD removal rate will reach the highest rate of 60%, the COD removal rate increase. Therefore, in the processing of dealing with furfural wastewater, the advisable dosing quantity of modified lignin flocculants is 8g/L.

3. Conclusion

Irradiation graft copolymerization method is a kind of green chemical processing method. We can get the natural organic polymer flocculants when the modified lignin sulfonates has been processed, the flocculants is cheap price, non-toxic side effects, no secondary pollution and according with environmental protection requirement. the best condition of using This new type of flocculants is : pH-9 of solution, dosage for 8g/L, if it is combined with other technology, the COD removal rate can reach more than 50 percent in the furfural wastewater treatment engineering.

References

Fang GuiZhen, HeWeiHua & Song ZhanQian. (2003). Cation flocculant lignin synthesis of salt and decoloring performance. *Journal of Forest Chemical and Industrial*, 23 (2): 37-42.

Liu Qianjun, ZhanHuaiYu, Liu mengru & WuHong. (2003). Lignin and decoloring agents and flocculation properties of preparation and application. *Hypertension, papermaking, science and technology*, 22(6): 125-128.

Qiu XueQing, LouHongMing. (1999). Wood grain water treatment by namics. *Environmental protection*, 6: 45-47.

R. B. Phillips, W. Brown & V. Stannett. (1972). The graft copolymerization of styrene and lignin. II. Kraft softwood lignin. *Journal of Applied Polymer Science*, 16(1): 1-14.

R. B. Phillips, W. Brown & V. Stannett. (1973). The graft copolymerization of styrene and lignin. III. Chain transfer reactions of lignin and lignin model compounds. *Journal of Applied Polymer Science*, 17(2): 443-451.

Zhan HuaiYu. (2005). *chemistry and physics. Cellulose*. Beijing: science press: 226.

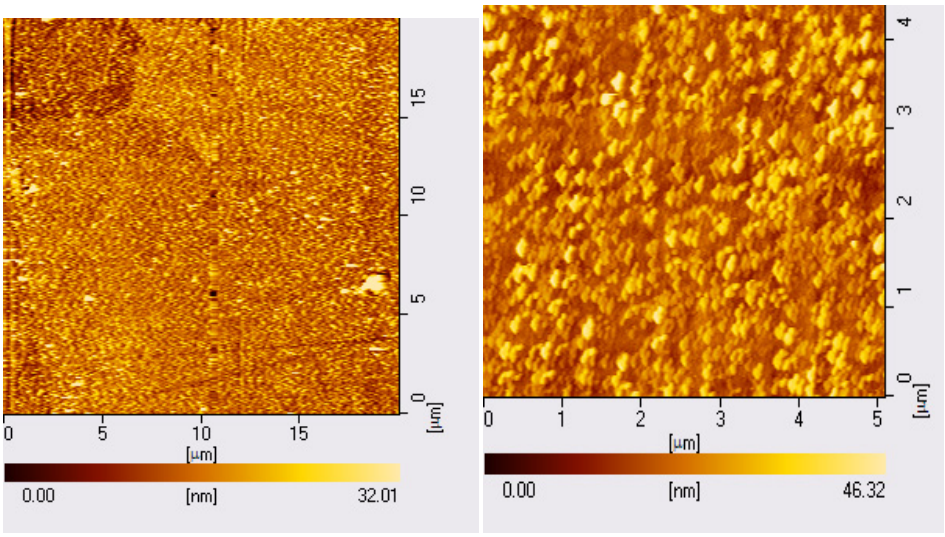

a. Before the modified lignin surface morphology b. Grafted modified lignin surface morphology

Figure 2.1 Modified lignin sulfonate membrane surface morphology

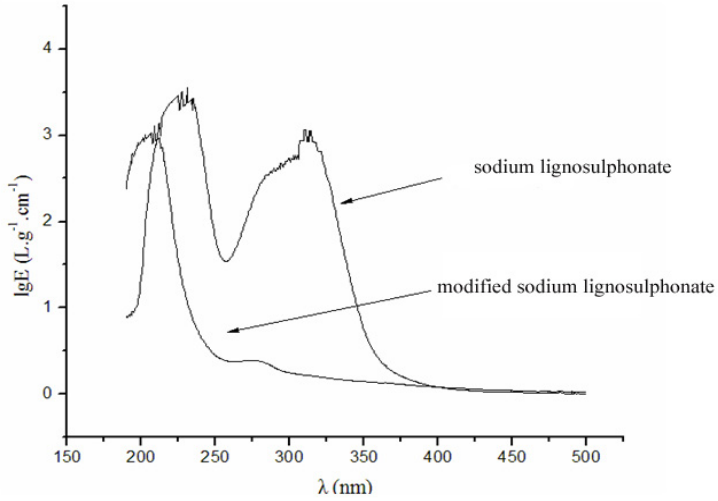

Figure 2.2 Modified lignin sulfonate up spectra

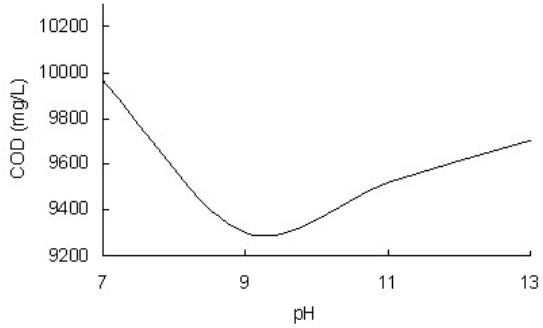

Figure 2.3 of furfural wastewater pH value of COD removal

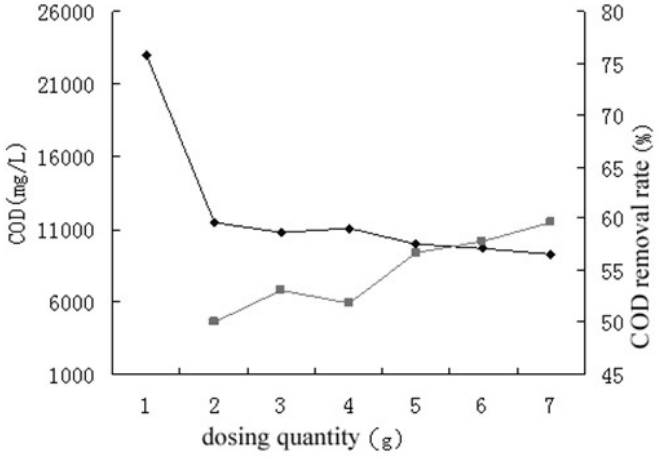

Figure 2.4 modified lignin flocculant dosing quantity of COD removal

Ohmic Processing: Temperature Dependent Electrical Conductivities of Lemon Juice

Hosain Darvishi (Corresponding author)
Department of Mechanical Engineering, Islamic Azad University, Islamshar Branch,Tehran, Iran
Tel: 98-21-4419-4911-4 Fax: 9-21- 4419-6524 E-mail: Hosaindarvishi@yahoo.com

Adel Hosainpour
Department of Farm Machinery Mechanical Engineering, Ilam University, Ilam, Iran
E-mail: A_hosainpour12@yahoo.com

Farzad Nargesi
Department of Farm Machinery Mechanical Engineering, Ilam University, Ilam, Iran
E-mail: Farzad_Nargesi61@yahoo.com

Mohammad Hadi Khoshtaghaza
Department of Farm Machinery Mechanical Engineering, Tarbiat Modares University, Tehran, Iran
E-mail: Khoshtag@gmail.com

Hosain Torang
Department of Mechanical Engineering, Islamic Azad University, Islamshar Branch, Tehran, Iran
E-mail: H_Torang@yahoo.com

Abstract

Development of new technologies for thermal food treatment is still of great industrial and scientific interest. Ohmic heating is one of these new technologies. In this study, lemon juice was heated on a laboratory scale static ohmic at different voltage gradients in the range of 30–55V/cm. The voltage gradient was statistically significant on the ohmic heating rates for lemon juice ($P < 0.05$). Measurements were made from 20 to 74ºC and showed a linear increase in electrical conductivity values with increasing temperature. The ohmic heating system performance coefficients were in the range of 0.54–0.92.

Keywords: Ohmic heating, Electrical conductivity, Lemon juice, Temperature, Performance coefficient

1. Introduction

Ohmic heating is a thermal process in which heat is internally generated by the passage of alternating electrical current (AC) through a body such as a food system that serves as an electrical resistance (Shirsat et al., 2004). The main advantages of ohmic processing are the rapid and relatively uniform heating achieved (Zareifard et al., 2003), ease of process control, High energy efficiency (Ghnimi et al., 2008), lower degradation of vitamin (Vikram et al., 2005), together with the lower capital cost compared to other electro heating methods such as microwave and radio frequency heating (Marra et al., 2009; Kim et al., 1998). Ohmic heating is considered very suitable for thermal processing of particulates in liquid foods because the particulates heated simultaneously at similar or faster rates than the liquid.

The amount of heat generated is directly related to the current induced by the voltage gradient in the field, and the electrical conductivity (Shirsat et al., 2004). Electro-technologies for food processing are cleaner, more environmentally friendly and energy efficient than conventional methods currently in use. In addition, electrical resistance heating can intensify both heat and mass transfer (Kemp and Fryer, 2007). Ohmic heating has been shown to enhance drying rates (Wang and sastry, 2000; Zhong and Lima, 2003) and extraction yields (Wang and Sastry, 2002) in certain fruits and vegetables.

Icier and Ilicali (2005a) reported that the electrical conductivity increased linearly with increasing temperatures for fruit juices orange at voltage gradients ranging from 20 to 60V/cm. Palanippan and Sastry (1991) reported that the electrical conductivity of the orange, carrot and tomato juices increased with temperature and decreased with solids content. Icier et al (2008) similarly found that the electrical conductivity increased as the temperature increased ranging from 0.4 to 0.75S/m for fresh grap juice. Amiali et al. (2006) studied that the electrical conductivity (0.13 to 0.63S/m) increased linearly with increasing temperatures for fruit juices (namely apple, orange, and pineapple juices). The ohmic heating of fruit juice was studied at different voltage gradients (7.5 to 26.25V/cm) by Kong et al. (2008). Results indicated that the voltage gradient significantly influenced the ohmic heating rates. Also, they found that the electrical conductivity changed significantly with temperature.

The aim of this study was to obtain electrical conductivity data for lemon juice during ohmic heating over the sterilization temperatures range. Effects of temperature and voltage gradients on ohmic heating rates of lemon juice were studied. Ohmic heating of lemon juice as a single phase were also mathematically modeled by taking the system performance coefficients into account.

2. Materials and methods

2.1 samples

The fresh lemon fruits used in this study were purchased from a local market in Tehran, Iran and stored at refrigeration conditions (4°C) prior to experiments (not more than 6hr). Fruits were washed with water to remove dirt on the skin; and then the water on the skin surface was drained. For experiment, the fruits were crushed and squeezed. The juice was filtered.

2.2 Ohmic heating system

A schematic diagram of the electrical circuitry is shown in Fig. 1. The experimental device consisted of a power supply, an isolating transformer, a variable transformer, microcomputer and three digital multimeters. The cell employed was constructed from Pyrex. The distance between two electrodes was 0.05m and the diameter of the electrodes was 0.04m, resulting in a total sample volume of 53.8 ml. A K type thermocouple was inserted into the geometric center of the cell. The temperature at the center of the sample was used as the representative value, and was assumed to be spatially uniform because of its small size. The sample was sandwiched between two electrodes in the test cell. End caps, fitted with high grade stainless steel electrodes were held in place using a spring-loaded system which also served to prevent leakages. Temperature, current and voltage applied were monitored with three digital multimeter (ET-2230/2231, Minipa, China) and passed this information to the microcomputer with an RS 232 port at 1secend intervals. This allowed real-time calculation of the total power input to the sample at any given time (Kulshrestha and Sastry, 2006; Shirsat et al., 2004). The ohmic samples were heated at 30, 35, 45 and 55V/cm at 60Hz from 20ºC to final temperature of 70°C.

2.3 Electrical conductivity

Electrical conductivity (S/m) was calculated from voltage and current data using the following equation (Icier et al., 2008):

$$\sigma = LI/VA \quad (1)$$

where σ is electrical conductivity (S/m); I is the current intensity (A), V is the voltage (V), L is the gap between the electrodes (m) and A is the electrode surface area (m^2).

2.4 Mathematical model

The energy given to the system during ohmic processing in unsteady state heat will be equal to the energy required to heat the sample plus the energy loss (Icier and Ilicali, 2005a,b):

$$E_{given} = E_{taken} + E_{loss} \quad (2)$$

$$\sum (VIt) = m\, C_p\, (T_f - T_i) + E_{Loss} \quad (3)$$

where C_p is specific heat capacity (J/kg.K); m is mass of the sample (kg); T_f is final temperature of the sample (ºC); Ti is initial temperature of the sample (ºC); t is time (s) Egiven is the electrical energy given to the system (J); and Eloss is the energy loss (J)

The energy loss term (E_{loss}) is the sum of the heat required to heat up the test cell, the heat loss to the surroundings by natural convection and the electrical energy which has not been converted into heat.

Since low E_{loss} would indicate, a system with a high performance, a system performance coefficient, SPC, was defined as;

 ISSN 1913-1844 E-ISSN 1913-1852

$$SPC = m\ C_p\ (T_f - T_i)/\sum (VIt) \quad (4)$$

The voltage distribution within the sample for the quasi-static can be computed using the following Laplace low:

$$\nabla(\sigma\Delta V) = 0 \quad (5)$$

The average voltage gradient assuming that the voltage only changes in the axial direction can be written as:

$$\nabla V = \Delta V/L \quad (6)$$

To simplify the calculation of balance during heating, the following assumptions were made:

(i) Specific heat capacity of the lemon juice is constant within the range of temperatures considered.

(ii) SPC is constant.

The energy balance becomes:

$$SPC\ (\Delta V^2 \sigma A/L) = m\ Cp\ \partial T/\partial t \quad (7)$$

Eq. (6) was solved by the forward finite difference method numerically. The time step used in the computations was 0.01s. The physical properties used in the computations and the experimental parameters are given in Table 1. A nonlinear analysis of covariance was used to evaluate treatment combination differences. The experiments were replicated three times.

3. Results and discussion

3.1 Effect of temperature and voltage gradient

Results of the nonlinear analysis of covariance are shown in Table 2. The results indicated that that voltage gradient and temperature significantly altered (increased) the electrical conductivity value of lemon juice ($P < 0.05$).

The changes in electrical conductivity of lemon juice with temperature during ohmic heating at four different voltage gradients are given in Fig. 2. As shown in Fig. 2, the electrical conductivity increased as the temperature increased during ohmic heating. The results are similar to those reported by Kemp and Fryer (2007); Icier et al. (2008); Icier and Ilicali (2004 and 2005a, b); Li et al (2004); Zareifard et al (2003) and Tulsiyan et al (2008). Kemp and Fryer (2007); Icier et al. (2008) reported that the increase in the electrical conductivity values with temperature has been explained by reduced drag for the movement. The highest electrical conductivity was observed on 55V/cm, followed by 45, 35 and 30 V/cm. The electrical conductivity at 35 V/cm was slightly higher than that at 30 V/cm. Similar observations were reported for grape juice (Icier et al., 2008), apple and sour cherry juice (Icier and Ilicali, 2004). Between 55 and 75ºC, the electrical conductivity at 40 V/cm was slightly higher than that at 20 or 30 V/cm.

Cristina et al. (1999) reported that the electrical conductivity was dependent on the concentration (°Brix) and the temperature (20-80°C) for lemon juice. The electrical conductivity increases with increasing concentration up to approximately 30°Brix, when it starts to decrease. The decrease in electrical conductivity may be due to the increase in viscosity of the juices with concentration which decreases the mobility of the ions.

Since the experimental electrical conductivity results for the lemon juice samples given in Fig. 2 showed a linear trend with increasing temperature, a linear equation shown in Eq. (8) was used to fit the experimental data. The constants and the linear regression coefficients are given in Table 3.

$$\sigma = B\ T + C \quad (8)$$

where B and C are constant; and T is temperature (ºC). High coefficients of determination ($R^2 > 0.97$) indicate the suitability of the linear model for conductivity variation with temperature.

At high voltage gradients, the current passing through the sample was higher and this increased the heat generation rate. As the voltage gradient increased the heating time of the lemon juice required to reach the prescribed temperature decreased. Other researchers who have found a linear increase in electrical conductivity with increase in temperature include Sarang et al (2008), Tulsiyan et al (2008), Legrand et al. (2007), Icier and Ilicali (2005a,b), Castro et al (2004), Li et al (2004), Zareifard et al (2003) and Fiala et al (2001). The experimental ohmic heating times required to raise the temperatures of the lemon juice from 20 to 74ºC are given in Tables 4. The time required to heat the lemon juice from 20 to 74ºC at 30 V/cm was 1.64, 2.18 and 4 times longer than at 35, 45 and 55 V/cm, respectively. In addition to this, Icier and Ilicali (2004) reported that the decrease in the concentration of the apple and sour-cherry juices from 60% to 20% enhanced the ohmic heating rate of the juices. Icier and Ilicali (2005b) reported similarly that electrical conductivity depended on the drained the viscosity of the heated solution during ohmic heating.

3.2 Performance coefficient

The mathematical model predicted smaller heating rate, which led to higher heating time than the experimental results. The electrical energies given to the system, the heat taken by the fruit juice concentrates, performance coefficients (SPC) and heating times for mathematical model calculated for each voltage gradient experiments are shown in Table 4. For the 30 V/cm voltage gradient SPC was approximately 0.92, which indicated that 8% of the electrical energy given to the system was not used to heat up the test liquid. However, for higher voltage gradients, SPC values were lower and the heat required to heat up the test cell was too small to account for the energy loss term, Eloss. A similar observation was reported by Icier and Ilicali (2004, 2005a) for orange juice, peach puree and apricot puree.

A portion of the electrical energy input was used for physical, chemical and electrochemical changes in the concentrate. It is rather difficult to comment on the exact nature of this loss. In industrial scale production it was concluded that not all of the electrical energy was converted into heat in the lemon juice concentrate. Because a steady state will be obtained as soon the system is heated, so it will be of lesser importance. The stainless steel electrodes caused electrochemical reactions in the food sample that not beneficial (Assiry et al., 2003). They suggested that the titanium coated electrodes using ohmically heating processing, because it could decrease these reactions. Thus, the kind electrodes had different effects during ohmic heating and the amount of energy used for electrochemical reactions.

From the experimental data obtained it is clear that this loss depends on the voltage gradient applied. For low voltage gradients, the conversion of electrical energy into heat was larger. Therefore, the system was performing better. The level of agreement between the predicted and experimental heating times was relatively good when these electrical conductivity models were used.

4. Conclusion

The electrical conductivity increased linearly with increasing of temperature. The electrical conductivity of lemon juice is strongly dependent on temperature. The rate of change of temperature for 55V/cm was higher than each other voltage gradients applied. Ohmic heating times and performance coefficients are dependent on the voltage gradient used. As the voltage gradient increased, time and performance coefficient decreased. This modeling procedure can be used for designing and controlling ohmic heating processes to ensure thermal sterilization and safety of ohmically heated food products.

References

Amiali, M., Ngadi, M., Raghavan, V. G. S., Nguyen, D. H. (2006). Electrical conductivities of liquid egg product and fruit juices exposed to high pulsed electric fields. *International Journal of Food Properties,* 9, 533–540.

Assiry, A., Sastry, S. K., Samaranayake, C. (2003). Degradation kinetics of ascorbic acid during ohmic heating with stainless steel electrodes *Journal of Applied Electrochemistry,* 33(2), 187–196.

Castro, A., Teixeira, J. A., Salengke, S., Sastry, S. K., Vicente, A. A. (2004). Ohmic heating of strawberry products: electrical conductivity measurements and ascorbic acid degradation kinetics. *Innovative Food Science and Emerging Technologies,* 5, 27–36.

Cristina, S. C., Moura, D.R., Vitali, A. D. A. (1999) .A Study of Water Activity and Electrical Conductivity in Fruit Juices: Influence of Temperature and Concentration. Brazil Journal Food Technology, 2, 31-38.

Fiala, A., Wouters, P, C., Bosch, E, D., Creyghton, Y. L. M. (2001). Coupled electrical-fluid model of pulsed electric field treatment in a model food system. *Innovative Food Science & Emerging Technologies,* 2, 229-238

Ghnimi, S., Flach-Malaspina, N., Dresh. M., evaluation of an ohmic heating unit for thermal processing of highly viscous liquids. *Chemical Engineering Research and Design,* 86, 627-632.

Icier, F., Ilicali, C. (2004). Electrical conductivity of apple and sourcherry juice concentrates during ohmic heating. *Journal of Food Process Engineering,* 27(3), 159–180.

Icier, F., Ilicali, C. (2005a). The effects of concentration on electrical conductivity of orange juice concentrates during ohmic heating. *European Food Research and Technology,* 220(3), 406–414.

Icier, F., Ilicali, C. (2005b). Temperature dependent electrical conductivities of fruit purees during ohmic heating. *Food Research International,* 38, 1135–1142.

Icier, F., Yildiz, H., Baysal, T. (2008). Polyphenoloxidase deactivation kinetics during ohmic heating of grape juice. *Journal of Food Engineering,* 85, 410–417.

Kemp, M. R., Fryer, P. J. (2007). Enhancement of diffusion through foods using alternating electric fields. *Innovative Food Science and Emerging Technologies,* 8, 143–153.

Kim, H. J., Choi, Y. M., Yang, A. P. P., Yang, T. C. S., Taub, I. A., Giles, J., Ditusa, C., Chall, S., Zoltai, P. (1996). Microbiological and chemical investigation of ohmic heating of particulate foods using a 5 kW ohmic system, *Journal of Food Processing and Preservation,* 20(1), 41–58.

Kong, Y. Q., Li, D., Wang, L. J., Bhandari, B., Chen, D. X., Mao, Z. H. (2008). Ohmic heating behavior of certain selected liquid food materials. *International journal of food engineering,* 4(3), 1-13.

Kulshrestha, A. S., Sastry, K. S. (2007). Low-frequency dielectric changes in cellular food material from ohmic heating: Effect of end point temperature. *Innovative Food Science and Emerging Technologies,* 7, 257–262.

Legrand, A., Leuliet, J. C., Duquesne, S., Kesteloot, R., Winterton, P., Fillaudeau, L. (2007). Physical, mechanical, thermal and electrical properties of cooked red bean (*Phaseolus vulgaris* L.) for continuous ohmic heating process. *Journal of Food Engineering,* 81, 447–458.

Li, F. D., Li, L. T., Li, Z., Tatsumi, E. (2004). Determination of starch gelatinization temperature by ohmic heating. *Journal of Food Engineering,* 62, 113–120.

Marra, F., Zell, M., Lyng, J. G., Morgan, D. J., Cronin, D. A. (2009). Analysis of heat transfer during ohmic processing of a solid food, *Journal of Food Engineering,* 91, 56–63.

Palaniappan, S., Sastry, S. K. (1991). Electrical conductivity of selected juices: influences of temperature, solids content, applied voltage, and particle size. *Journal of Food Process Engineering,* 14, 247–260.

Sarang, S., Sastry, S. K., Knipe, L. (2008). Electrical conductivity of fruits and meats during ohmic heating. *Journal of Food Engineering,* 87, 351–356.

Shirsat, N., Lyng, J. G., Brunton, N. P., McKenna, B. (2004). Ohmic processing: Electrical conductivities of pork cuts. *Meat Science,* 67, 507–514.

Tulsiyan, P., Sarang, S., Sastry. S. K. (2008). Electrical conductivity of multi component systems during ohmic heating. *International Journal of Food Properties,* 11, 233–241.

Vikram, V. B., Ramesh, M. N., Prapulla, S. G. (2005). Thermal degradation kinetics of nutrients in orange juice heated by electromagnetic and conventional methods. *Journal of Food Engineering,* 69, 31–40.

Wang, W. C., Sastry, S. K. (2000). Effects of thermal and electro thermal pretreatments on hot air drying rate of vegetable tissue. *Journal of Food Process Engineering,* 23, 299–319.

Wang, W. C., Sastry, S. K. (2002). Effects of moderate electrothermal treatments on juice yield from cellular tissue. *Innovative Food Science and Emerging Technologies.* 3 (4), 371–377.

Zareifard, M. R., Ramaswamy, H. S., Trigui, M., Marcotte, M. (2003). Ohmic heating behaviour and electrical conductivity of two-phase food Systems. *Innovative Food Science and Emerging Technologies,* 4, 45–55.

Zhong, T., Lima, M. (2003). The effect of ohmic heating on vacuum drying rate of sweet potato tissue. *Bioresource Technology,* 87, 215–220.

Table 1. The parameters and properties used in model calculations

Property or parameter (unit)	value
Density(kg/m^3)	1071.7
Specific heat (J/kg. K)	3850

Table 2. Nonlinear analysis of covariance table for a completely randomized design with a factorial treatment structure for the lemon juice

Source	Sum of Squares	df	F
Corrected Model	5.81[a]	7	901.2
Intercept	7.63	1	8280
T	1.76	1	19.4
V	0.054	3	5153
T×V	0.129	3	46.8
Error	0.203	220	
Total	100.7	228	
Corrected Total	6.02	227	

[a] $R^2 = 0.970$ (Adjusted $R^2 = 0.965$)

Table 3. The constants and coefficients of liner model of lemon juice during ohmic heating

Voltage gradient (V/cm)	B	C	R^2
55	0.0106	0.2298	0.987
45	0.0058	0.2971	0.967
35	0.01	0.2389	0.999
30	0.0081	0.1994	0.999

Table 4. Experimental data and the model predictions of lemon juice during ohmic heating

V/cm	Q_t(J)	E_g(J)	SPC	T_i	T_f	t_{exp}	t_{adb}	t_T
30	7899	8620	0.92	19.8	73	44	44	44
35	6834	7678	0.90	19.7	73	24	22	30
45	5496	6521	0.84	20	74	18	15	24
55	4518	8382	0.54	20.3	74.7	11	11	13

ISSN 1913-1844 E-ISSN 1913-1852

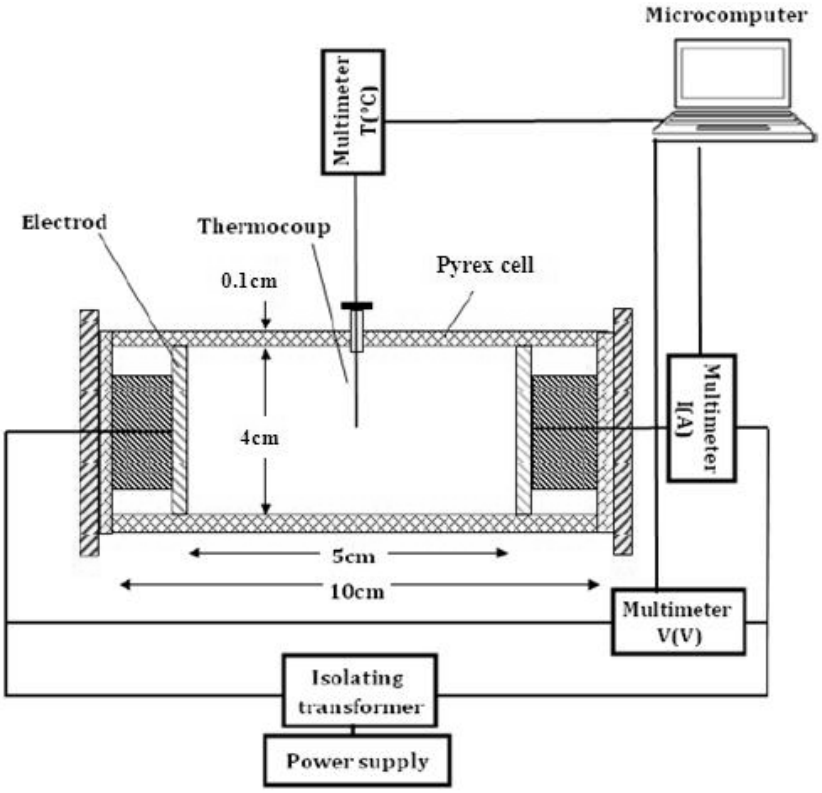

Figure 1. Schematic diagram of the ohmic heating system

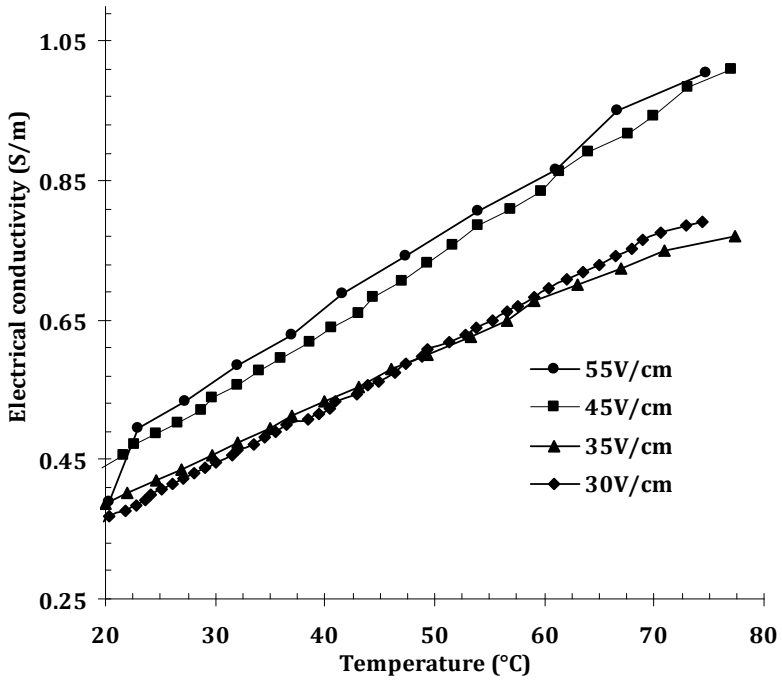

Figure 2. Electrical conductivity changes of lemon juice during ohmic heating at different voltage gradients

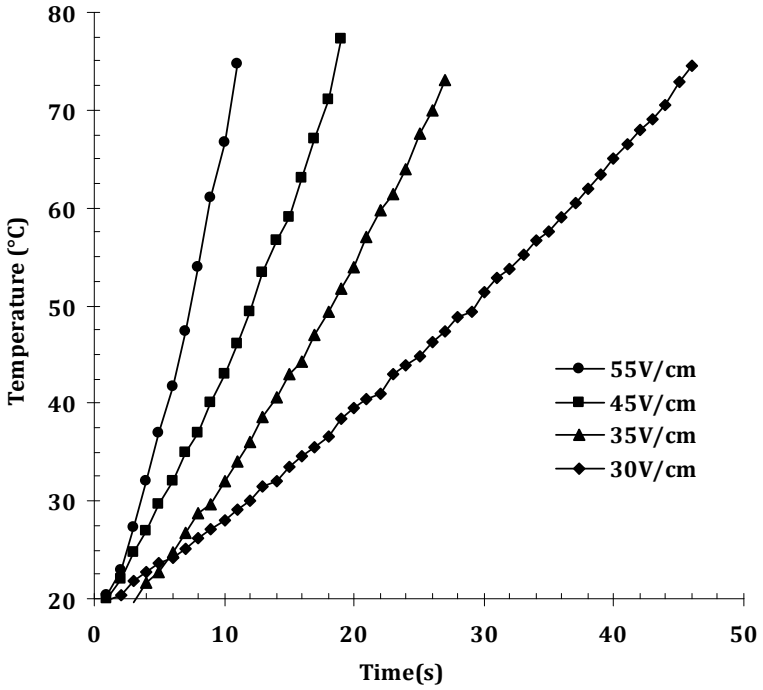

Figure 3. Ohmic heating curves of lemon juices at different voltage gradients

 ISSN 1913-1844 E-ISSN 1913-1852

Design, Synthesis and Antifungal Activity of 3-substituedmethylenethiochroman-4-one Derivatives

Xinghua Zhang
Key Laboratory for Pharmaceutical Quality Control of Hebei Province
College of Pharmaceutical Science, Hebei University, Baoding, Hebei, 071002, China
E-mail: zhangxinghua20061984@126.com

Zhengyue Ma
Key Laboratory for Pharmaceutical Quality Control of Hebei Province
College of Pharmaceutical Science, Hebei University, Baoding, Hebei, 071002, China
Email: mazhengy@126.com

Gengliang Yang (Corresponding author) & Yajun Zheng
Key Laboratory for Pharmaceutical Quality Control of Hebei Province
College of Pharmaceutical Science, Hebei University, Baoding, Hebei, 071002, China

We are grateful for financial support by the National Natural Science Foundation of China (Grant Nos. 20375010, and 20675084), Program for Science and Technology Development of Hebei Province (Grant Nos. 06276479B and 07276407D).

Abstract

Four new 3-substituedmethylenethiochroman-4-one derivatives were prepared from (z)-3-(chloromethylene)thiochroman-4-one. They were characterized by analytical and spectral methods. *In vitro* antifungal activities of these synthesized compounds were evaluated against ten species of fungi, and the results showed that (e)-3-chloromethylene compound exhibited a similar good activity against fungi to (z)-3-chloromethylene compound. (Z)-3-substituedaminomethylene compound also exhibited antifungi activity to some extent.

Keywords: Antifungal activity, Thiochromanones, 3-substituedmethylenethiochroman-4-one

1. Introduction

Over the last three decades there has been a dramatic increase in the incidence of fungal infections. Discovery of new drugs for the treatment of systemic mycoses is a major challenge in infectious disease research.

Thiochromanones had been reported to possess important biological activities(Nakazumi, H., 1984). Nakib T A *et al* reported that thiochromanone derivatives had antifungal activities (Nakib, T. A. 1990). 3-Benzylidene (Qi Ping, 2004), 3-Mannich base (Zhu Quanhong, 2000), 3-bromo (QI Ping, 2003), 2,3,3a,4-tetrahydrothiochromeno[4,3-*c*]pyrazole derivatives (Ma Zhengyue, 2008) and 6*H*-thiochromeno[4,3-*b*]quinoline derivatives (Wang Ge, 2010) had been synthesized and reported to have antifungal activities. In our laboratory, (z)-3-halomethylene of thiochromanone derivatives were synthesized and proved with good antifungal activity (Fang Baoling, 2010; Tian Wei, 2010). To discover new 3-substituedmethylene analogues with good antifungal activity, herein, four new compounds from the (z)-3-(chloromethylene)thiochroman-4-one were designed, synthesized and screened for their antifungal activity. The synthetic route was outlined in the Scheme 1.

2. Experimental

2.1 Chemistry

Substituted benzenethiols (chemically pure) were from SHOUERFU LLC (ZHEJIANG, China). All other materials were commercially available and used as received unless otherwise noted. Mass spectral data were obtained by LC-MSD XCT Trap G2446A (Agilent Technologies, USA). Melting points were determined SGW

X-4 microscopic melting point (Shanghai Precision & Scientific Instrument Co., Ltd, China). IR spectra were recorded in potassium bromide on FTIR-8400S (SHIMADZUCO-RPORATION, Kyoto, Japan). ^{1}H NMR spectra were recorded in $CDCl_3$ on Bruker Avance III 600Hz spectrometer. The chemical shifts are reported as parts per million (δ ppm) from $(CH_3)_4Si$ (TMS) as an internal standard. Elemental analysis was performed on a Carlo Erba-1106 instrument and the results were in acceptable range.

2.2 Preparation of compound (z)-3-(chloromethylene)-6-chlorothiochroman-4-one (3)

Sodium methoxide (20.0 mmol), ethyl formate (10.0 mmol) and toluene (50 mL) were mixtured into a round-bottomed flask (250 mL), then a solution of compound 1 (5.0 mmol) in toluene (20 mL) were dropwise added over 20 min in ice bath. The mixture was stirred for 12 h at the temperature < 10 ^{o}C. The organic phase was extracted twice with water (2×20 mL), the combined aqueous phase was adjusted to about 4 with HCl, maintaining the temperature at < 5 ^{o}C, the solid precipitated was filtered, abundantly washed with water, then air dried. The crude product was recrystallized from 95% (v/v) EtOH to afford the compound 2.

compound 2 (5.0 mmol) and acetyl chloride (7.5 mmol) was dissolved in dichloromethane (40 mL) in a sealed tube, and the mixture was stirred at 50 °C for 2 h. After the the solution was extracted with 0.5 mol/L Na_2CO_3 (2×15 mL), the organic layer was was dried over anhydrous $MgSO_4$ and evaporated in vacuo to give the crude product. The crude product was purified by silica-gel column chromatography (dichloromethane: petroleum ether=1:10 (v/v)) to afford the compound 3 (Tian Wei, 2010; Fang Baoling, 2010), compound 2: yield, 83%; compound 3: yield, 74%.

2.2 Preparation of compound (e)-3-(chloromethylene)-6-chlorothiochroman-4-one (4)

compound 3 (5.0 mmol) was dissolved in methanol (60 mL) in a round bottomed flask (150 mL)irradiating 20 h under 60 W UV lamp, solvent was evaporated in vacuo to give the crude product. The crude product was purified by silica-gel column chromatography (dichloromethane: petroleum ether=1:10(v/v).) to afford the pure compound 4.

2.2.1 (E)-6-Chloro-3-(chloromethylene)thiochroman-4-one (4)

Yellow solid. Yield: 30%; mp: 91-93 °C. UV-vis (MeOH) λ_{max}: 250 nm; ^{1}H NMR (600 MHz, $CDCl_3$) δ ppm: 8.19 (d, J = 1.68 Hz, 1H, Ar-H), 7.39 (dd, J = 8.35, 1.76 Hz, 1H, Ar-H), 7.25 (d, J = 8.43 Hz, 1H, Ar-H), 6.76 (s, 1H, C=CH-),3.87 (s, 2H, SCH_2). IR (KBr): 1670 (C=O), 1593 (C=C) cm^{-1}. MS (APCI): *m/z* 244.9 $[M+H]^+$, 246.9 $[M+2+H]^+$. Anal. Calcd for $C_{10}H_6Cl_2OS$: C, 49.00; H, 2.47; S, 13.08. Found: C, 48.96; H, 2.42; S, 13.12.

2.3 Preparation of compound (Z)-6-Chloro-3-((dimethylamino)methylene)thiochroman-4-one (5)

$NH(CH_3)_2$·HCl (6.0 mmol) and $N(CH_2CH_3)_3$ (15.0 mmol) were dissolved in CH_2Cl_2 (25 mL) and cooled to 0 °C, then a solution of compound 3 (5.0 mmol) in CH_2Cl_2 (5 mL) were added, dropwise, and the mixture was stirred at 0 °C for 2.5 h. After the solution was extracted with water (2×20 mL), the organic layer was dried over anhydrous $MgSO_4$ and evaporated in vacuo to give the crude product. The crude product was recrystallized from 95% (v/v) EtOH to afford the compound **5.**

2.3.1 (Z)-6-Chloro-3-((dimethylamino)methylene)thiochroman-4-one (6)

Yellow solid. Yield: 87%; mp: 123-125 °C. UV-vis (MeOH) λ_{max}: 248 nm; ^{1}H NMR (600 MHz, $CDCl_3$) δ ppm: 8.06 (d, J = 2.35 Hz, 1H, Ar-H), 7.61 (s, 1H, C=CH-), 7.25 (dd, J = 8.33, 2.39 Hz, 1H, Ar-H), 7.19 (d, J = 8.34 Hz, 1H, Ar-H), 4.01 (s, 2H, SCH_2), 3.17 (s, 6H, $C(CH_3)_2$). IR (KBr): 1637 (C=O), 1579 (C=C) cm^{-1}. MS (APCI): *m/z* 253.9 $[M+H]^+$, 255.9 $[M+2+H]^+$. Anal. Calcd for $C_{12}H_{12}ClNOS$: C, 56.80; H, 4.77; N, 5.52; S, 12.64. Found: C, 56.83; H, 4.80; N, 5.47; S, 12.60.

2.4 Preparation of compound 3-(phenylthiomethylene)thiochroman-4-one (6a-6b)

Substituted benzenethiols (6.0 mmol) and NaH (12.5 mmol) were added in dry THF (25 mL) and cooled to 0 °C, then a solution of compound 3 (5.0 mmol) in THF (8 mL) were added, dropwise. After stirring 2 h, added crushed ice slowly to the mixture and removed excess NaH, then added water (60 mL), the solid precipitated was filtered, abundantly washed with water, then air dried. The crude product was purified by silica-gel column chromatography (dichloromethane: petroleum ether = 1:50 (v/v)) to afford the compound 6a and 6b.

2.4.1 (Z)-6-Chloro-3-(p-tolylthiomethylene)thiochroman-4-one (6a)

Green solid. Yield: 34%; mp: 111-113 °C. UV-vis (MeOH) λ_{max}: 254 nm; ^{1}H NMR (600 MHz, $CDCl_3$) δ ppm: 8.07 (d, J = 2.41 Hz, 1H, Ar-H), 7.88 (s, 1H, C=CH-), 7.39 (d, J = 8.06 Hz, 2H, Ar-H), 7.33 (dd, J = 8.43, 2.38 Hz, 1H, Ar-H), 7.25 (d, J = 10.07 Hz, 1H, Ar-H), 7.21 (d, J = 7.94 Hz, 2H, Ar-H), 3.93 (s, 2H, SCH_2), 2.38 (s, 3H, CH_3). IR (KBr): 2923, 2852 (CH_3), 1683 (C=O), 1635 (C=C) cm^{-1}. MS (APCI): *m/z* 333.0 $[M+H]^+$, 335.9

$[M+2+H]^+$. Anal. Calcd for $C_{17}H_{13}ClOS_2$: C, 61.34; H, 3.94; S, 19.27. Found: C, 61.37; H, 3.90; S, 19.31.

2.3.2 (E)-6-Chloro-3-(p-tolylthiomethylene)thiochroman-4-one (6b)

Green solid. Yield: 30%; mp: 104-106 °C. UV-vis (MeOH) λ_{max}: 254 nm; ^{1}H NMR (600 MHz, $CDCl_3$) δ ppm: 8.12 (d, J = 2.41 Hz, 1H, Ar-H), 7.43 (d, J = 8.09 Hz, 2H, Ar-H), 7.35-7.31 (m, 2H, Ar-H), 7.25 (d, J = 8.39 Hz, 1H, C=CH-), 7.21 (d, J = 7.95 Hz, 2H, Ar-H), 3.87 (d, J = 0.75 Hz, 2H, SCH_2), 2.38 (s, 3H, CH_3). IR (KBr): 2921, 1456, 1394(CH_3), 1683 (C=O), 1635 (C=C) cm^{-1}. MS (APCI): m/z 333.0 $[M+H]^+$, 335.9 $[M+2+H]^+$. Anal. Calcd for $C_{17}H_{13}ClOS_2$: C, 61.34; H, 3.94; S, 19.27. Found: C, 61.30; H, 3.90; S, 19.20.

2.5Antifungal Activity in Vitro

In vitro antifungal activities were determined by double dilution method, the Minimum inhibitory concentration (MIC) were determined in accordance with the methods of the National Committee for Clinical Laboratory Standards (Marcelo C. Murguı´a, 2008). *C. parapsilosis*, *C. glabrata*, *C. albicas*, *C. tropicalis*, *C. neoformans*, *C. Krusei*, *E. floccosum*, *M. gypseum*, *A. niger*, *S. schenekn* were used as tested fungi for this study. Fluconazole was used as the reference drugs for positive control. The tested compounds were dissolved in DMSO(1 mL), then the required concentrati- ons (128, 64, 32, 16, 8, 4, 2, 1, 0.5, 0.25, 0.125 μg/mL) were obtained by two fold serial dilution. The fungi were incubated and adjusted to a final concentration of 0.5×10^4-2.5×10^4 CFU/mL. MIC_{100} values were determined by visual observation after 2-7 d of incubation.

3. Results and discussion

3.1 Structure elucidation

The structures of the target compounds synthesized were established by mass spectroscopy, elemental analysis, ^{1}H-NMR spectral data and NOE spectral data. The configuration of compounds 3 and 4 were assigned by their ^{1}H NMR spectra and ^{1}H-^{1}H NOE spectra. For compound 4, NOE correlations were observed from H of -C=CHCl to H of -SCH_2-, but there was no correlation from H of -C=CHCl to H of -SCH_2- on compound 3, as shown in Figure 1. The NOE spectra confirmed the compound 3 was *Z*-configuration and the compound 4 was *E*-configuration (see Figure 2).

During the synthesis of compound 5, only one product was obtained in the reaction. In order to determine its structure, NOE spectra was also studied. The ^{1}H NMR spectrum of compound **5** revealed three singlet signals at δ 3.17, 4.01 and 7.61 characteristic for H of –$N(CH_3)_2$, H of -SCH_2- and H of -C=CHCl, respectively. NOE correlations were observed from H of -C=CHCl to H of -SCH_2-, but there was no correlation from H of -C=CHCl to H of -SCH_2-, as shown in Figure 1. These NOE's confirmed the absolute *E*-configuration of structure 5 (see Figure 2).

During the synthesis of compound 6, there was no selectivity to the compound 6a and 6b, they were generated at the same time. Their structure were also confirmed by ^{1}H NMR spectra and NOE correlations. NOE correlations were observed from H of -C=CHCl to H of -SCH_2- on compound 5b, and there was no correlation from H of -C=CHCl to H of -SCH_2- of compound 5a, as shown in Figure 1. The NOE spectra of compound 5 were also shown in Figure 2.

3.2 Antifungal Activity in vitro

The results of antifungal activities *in vitro* were shown in Table 1. In order to discover new active compound, structure optimization of compound 3 were operated. Compound 4 as *E*-isomers of 3 was prepared, but the result of antifungal activity indicated that there was no apparent difference between 3 and 4. When chloromethylene was replaced with phenylthiomethylene and dimethylaminomethylene respectively, compound 5, 6a, and 6b were synthesized. The tested result showed that dimethylaminomethylene derivative 5 had antigungal activity to some extent. Compound 5 had the best activity when against *C.neoformans*, its MIC was a similar to Fluconazole. However, phenylthiomethylene derivatives 6a and 6b had no antifungal activity against most of the tested fungi. 6a and 6b had the weak bioactive only against *C.neoformans* and *C.Krusei.*

In conclusion, 3-chloromethylene derivatives had good antifungal activity and other substitued 3-methylene derivatives either had lower activity or no acivity. The result should encourage us to design and synthesize more potent antifungal agents. Further biological evaluation of the compounds is in progress.

References

Nakazumi H.,Ueyama T. & Kitao T. (1984). Synthesis and antibacterial of thioflavones and related compounds. *Journal of Heterocyclic Chemisry*, 1, 193-196.

Nakib, T. A., Bezjak, V. & Meegan, M. J. (1990). Synthesis and antifungal activity of some 3-benz-

ylidenechroman-4-ones, 3-benzylidenethiochroman-4-ones and 2-benzylidene-1-tetralones. *European Journal of Medical Chemistry*, 5, 455-462.

QI Ping, JIN Yinghua, GUO Chun & FANG Lin. (2004). Synthesis of 3-benzylthiochromanones and their *in vitro* antifungal activity. *Chinese Journal of New Drugs*. 13, 141-143.

Zhu Quanhong, Fang Lin & Zhang Guoliang. (2000). Synthesis and Antifungal Activities of the Mannich Baes of Thiochromanones Derivatives. *Chinese Journal of Medicinal Chemistry*, (10) 1-3.

Qi Ping, JIN Yinghua, Guo Chun & Fang Lin. (2003). Syntheses and the antifungal activity of 3-bromo-4-thiochrom(an)ones. *Chinese Journal of Medical Chemistry*, 13, 205-207.

Ma Zhengyue, Yang Gengliang, Yan Guoying, Zhu Shiguo & Guan Li. (2008). Synthesis of 2, 3, 3a, 4-tetrahydrothiochromeno[4, 3-*c*]pyrazoles derivatives and their antifungal activity *in vitro*. *Chinese Journal of Medicinal Chemistry*, 18, 170-174.

Wang Ge, Yang Gengliang, Ma Zhengyue, Tian Wei, Fang Baoling & Li Linbo. (2010). Synthseis and antifungal activity of some 6H-thiochromeno[4,3-*b*]quinolines. *International Journal of Chemistry*, 1, 19-25.

Fang Baoling, Ma Zhengyue, Yang Gengliang, Wang Ge, Tian Wei & Li Linbo. (2010). Synthesis and antifungal activity of (z)-3-(bromomethylene)thiochroman-4-ones. *International Journal of Chemistry*, 1, 143-146.

Tian Wei, Ma Zhengyue, Yang Gengliang, Wang Ge, Fang Baoling & Li Linbo. (2010). Synthesis and antifungal activity of (z)-3-chloromethylenethiochroman-4-ones. *Organic Chemistry : An Indian Journal*, 1, 8-12.

Murguı´a, Marcelo C. & Machuca, Laura M. (2008). Synthesis and Properties of Novel Antifungal Gemini Compounds Derived from *N*-Acetyl Diethanolamines. *Journal of Surfactants and Detergent*, 11, 223–230.

Table 1. Antifungal activity of compounds synthesized *in vitro*

Compound	MIC (μg/mL)									
	Cp	Cg	Ca	Ct	Cn	CK	Ef	Mg	An	Ss
3	2	16	4	4	4	32	2	16	>64	4
4	2	32	4	8	4	16	4	16	>64	4
5	32	>64	32	64	4	64	32	64	32	64
6a	>64	>64	>64	>64	4	32	>64	>64	>64	>64
6b	>64	64	>64	>64	8	64	>64	>64	>64	>64
Flu	4	16	0.5	2	4	64	>64	64	>64	>64

Abbreviations: Cp, *C.parapsilosis*; Cg, *C.glabrata*; Ca, *C.albicas*; Ct, *C.tropicalis*; Cn, *C.neoformans*; CK, *C.Krusei*; Ef, *E.floccosum*; Mg, *M.gypseum*; An, *A.niger*; Ss, *S.schenekn*; Flu, Fluconazole.

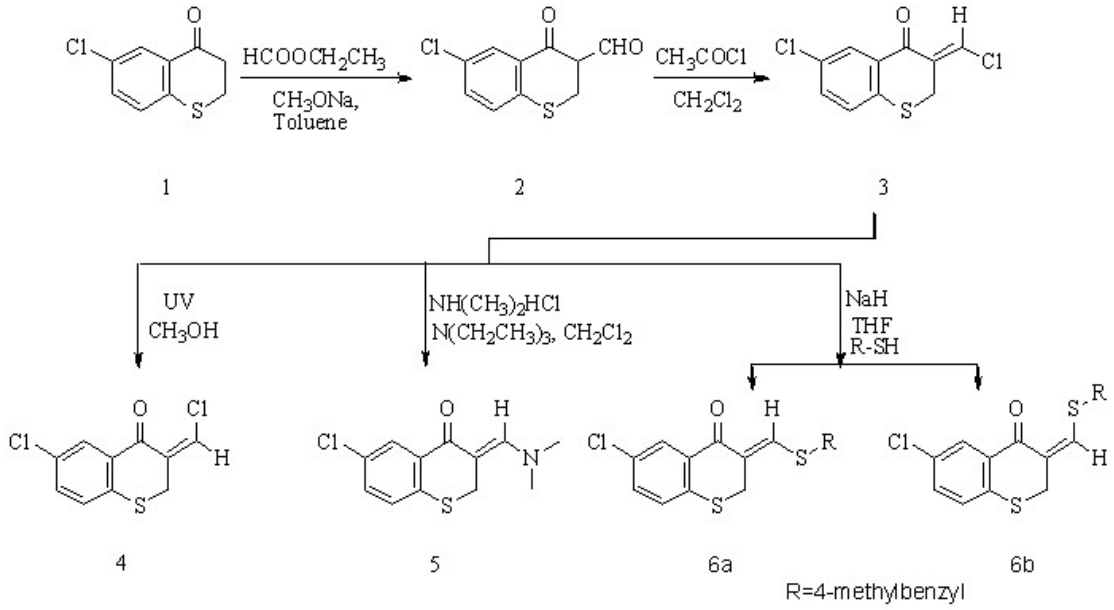

Scheme 1. The synthesis route of target compound

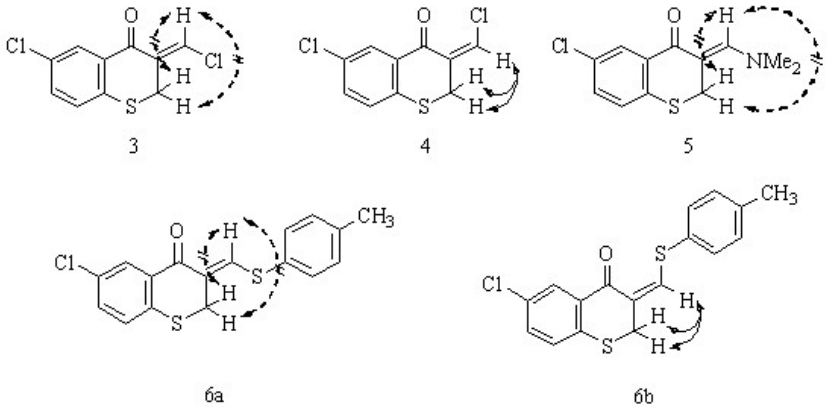

Figure 1. NOE correlations are shown by arrows

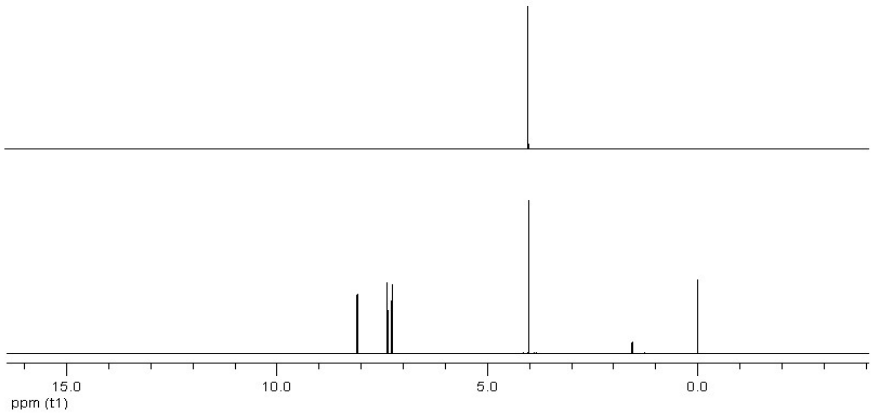

compound 3.

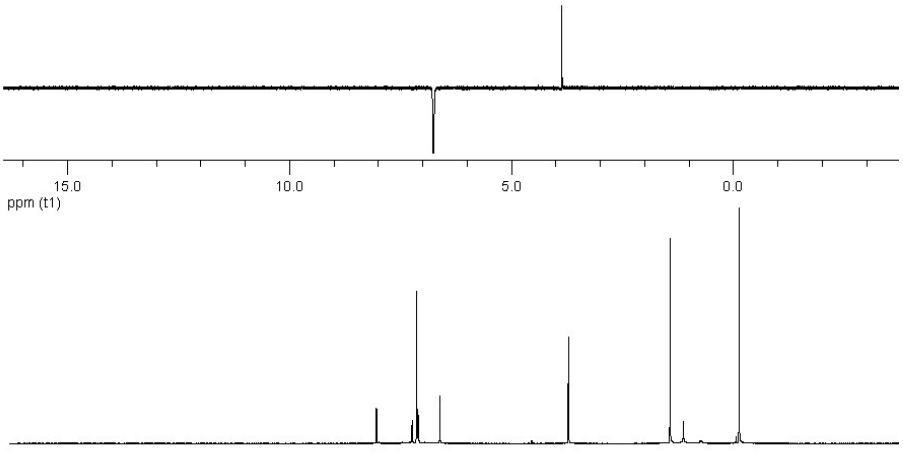

compound 4.

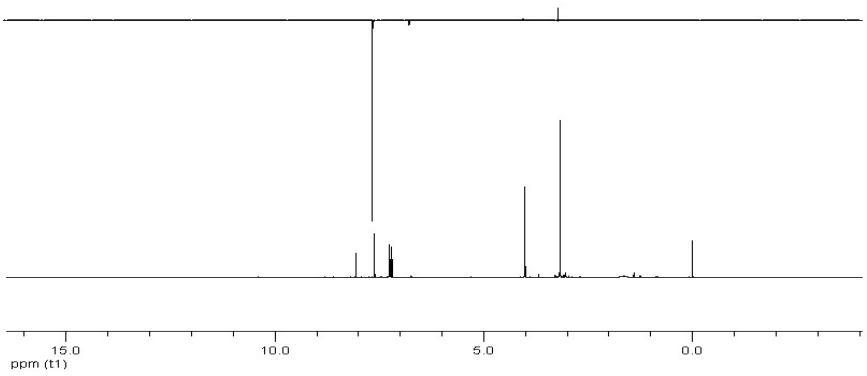

compound 5.

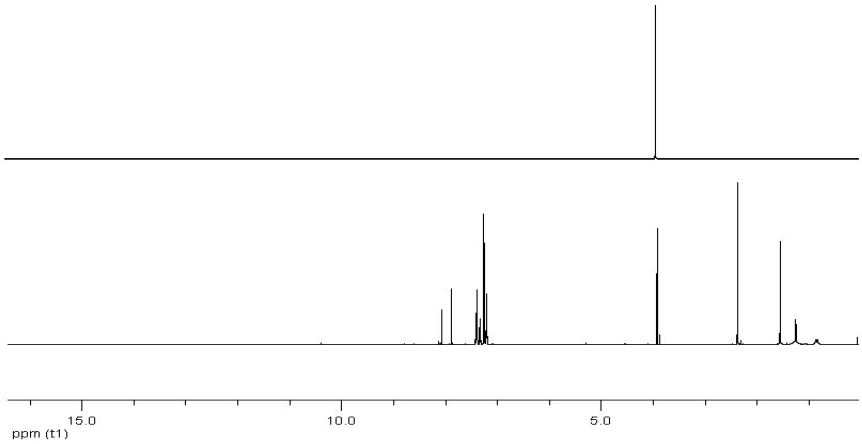

compound 6a.

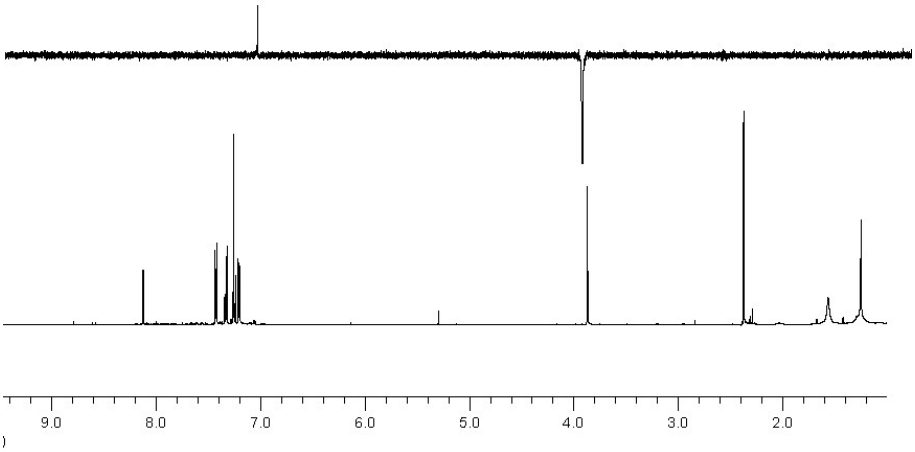

compound 6b.

Figure 2. ^{1}H NMR spectral and NOE spectral of 3a, 4, 5 and 6

Investigation of Carbon Steel Corrosion in Water Base Drilling Mud

Fadhil Sarhan Kadhim

Department of Petroleum Technology, University of Technology, Baghdad, Iraq

Abstract

Carbon steel, the most widely used engineering material, accounts for approximately 85%, of the annual steel production worldwide. Despite its relatively limited corrosion resistance, carbon steel is used in large tonnages in marine applications, nuclear power and fossil fuel power plants, transportation, chemical processing, petroleum production and refining, pipelines, mining, construction and metal-processing equipment. This paper Investigate Carbon steel corrosion in water. The corrosion rate in production and casing pipes in water base drilling mud (packer fluid), different salt concentration (100gm/L , 150 gm/L , 200gm/L) have been used and different temperature (30co , 50 co , 70 co) have been investigated. Weight loss and polarization methods were applied. The results indicate that the corrosion rates decrease with the increasing of salt concentration while the corrosion rates increase with increasing of temperature

Keywords: Carbon Steel, Corrosion, Drilling Mud

1. Introduction

Water base drilling fluids present corrosion problems primarily because they are subject to contamination from corrosion accelerators such as oxygen, carbon dioxide hydrogen sulfide or salts that are always present in varying quantities(B.W Bradley. 1970).

Saturated salt solutions are commonly used both as drilling and as packer fluids. Unsaturated salt solutions are believed to cause more server corrosion than saturated fluids. Increased solubility of acid gases and oxygen in the dilute solution is the basic cause. Inhibitors are commonly recommended for these solutions because corrosion is clearly problem in highly conductive salt environment(H.E BUSH. 1974). In high pressure oil or gas well, the produced fluids flow through a tubing string which is retrievable and positioned in a permanently installed casing .the annulus between the tubing and casing is frequently filled with a drilling fluid to provide weight and to help seal the packer at the bottom of the annulus. The packer fluid may consist of mud formation, emulsion, or a clear packer fluid is less expansive and has some advantages over other fluids.

The evaluation test requires a static system with proper surface - to -volume ratio. Since the required temperature is high and air must be eliminated, a pressurized bomb with a glass liner makes a suitable test vessel. Because a relatively large area is needed, coupons are the simplest and most logical detection technique, although others can be used .the deficiency of the test is that uniform corrosion is measured even though localized pitting is quite often the mode of failure in oil or gas tubing(E.Schasch. 1973). Johnston and Gowan(Jhonston and Cowan. 1964), Simpson(J.P Microbiology on. 1966), Barbee(Barbe, 1966), have contributed information on the cause and effect of contamination in packer fluids. These authors present both laboratory and field data and clearly show that the fluid placed in the annular space of the well requires careful selection if successful and economical completions are to be assured.

The authors (H.E bush, R.D.Barbee and J.P Simpson. 1966) interpretation of drill pipes records from west Texas also indicates that 75 percent of drill pipe loss is due to corrosion. A recent estimate by a large drilling contractor was the drill pipe less amounted to (120 $ a day per rig.). On 75 percent of this corrosion loss, the direct cost of corrosion is seen to be (90 $ a day per rig.).

Of approximately 700.000 producing wells in the United States, 96.000 require some of work over annually. Drilling fluid corrosion, of course dose not cause all of the work over but it is recognized as a significant contributing cause.

2. Experimental

A) Material And Test Solutions

One of the most widely used techniques in drilling fluid corrosion control employs drill string corrosion coupons, supplied by the chemical and petrochemical research center in the ministry of science and technology the coupons was about (3 cm)length and (1cm)width having the following chemical composition

C = 0.042% , P = 0.022% , Si = 0.215% , Mn = 0.797% , S = 0.015% , Cr = 0.205% , Mo = 0.040% , Ni = 0.135% , Cu = 0.202% , Fe = remains

 ISSN 1913-1844 E-ISSN 1913-1852

Water base drilling mud used as a corrosive solution , different salt concentration (100 gm/l ,150 gm/l,200 gm/l) been applied.

B) Procedure

1) Weight Loss Measurement

For weight loss measurement ,the metal samples (3*1cm) were immersed in 300 ml of water base drilling mud at different salt concentration (100 gm/l ,150 gm/l,200 gm/l) , and different temperature (30c° ,50 c° and 70 c°) in a flask in such manner that only (3 cm²) of specimen was exposed in the test solution .

Prior to use the specimen were abraded in sequence tap water by using the following emery paper grades ,220,320,420 and 600 as shown in figure(2) ,washed with tap water followed by distilled water ,dried with clean tissue paper , immersed in ethanol , dried with clean tissues paper ,immersed in ace tone ,and dried with clean tissue paper .

They were then left to dry for on hour over silica gel be for weighted and used the specimens where exposed for a period of 48 hours at different salt concentration and different temperature. After that they where cleaned, washed with running tap water, removing the corrosion product, followed by distilled water dried with clean tissue paper, degreased with acetone dried for on hour over silica get before weighted, then weight loss was determined. Each experiment was cared out twice and the average was taken. Then the corrosion rate calculated by the following equation:

$$C.R = w/(S.A)*t$$

Where ;

C.R=corrosion rate (mg/day.dcm²)

S.A=surface area (dcm²)

T=time (day)

2) Polarization measurement

The four holes were distributed on the cover of container for thermo meter to adjust the required temperature, working electrode reference electro de (saturated calomel Electrode, SCE) and counter electrode. The lugging capillary of electrode was placed (1mm) of working electrode with small amount of KCL (solid) was kept in the solution of SCE as long as the test. A three – electrode system was used in polarization experiment. The working electrode was made of low carbon steel with exposed Area of a bout $3cm^2$. The counter electrode and a saturated calomel electrode (SCE) was the reference electrode, which was connected to the working compartment of the electrochemical cell through a lugging capillary. The test solution was water base drilling mud with different salt concentration(100 gm/l,150gm/l,200gm/l) and temp. (30c).

Before each test, the cell and electrodes were was heel with running tap water, followed by deionizer water, after the corrosion cell parts were joined together, as shown in fig.(3).In the first steep the potential of the specimen (carbon steel) were measured relative to reference electrode and recorded with time.

In the second step the polarization scan began from cathodic to anodic branches. The potential was increased from a value versus SCE below the open – circuit potential (OCP) to a value versus SCE above the (OCP).

3. Results and Discussion

A) Weight loss method

In this technique the average corrosion rate of two runs was equal to the arithmetical average of the two specimens. The effect of salt concentration and temperature was investigated in water-base drilling mud. The results are listed in tables (1,2,3) .The relationship between corrosion rate Vs. salt concentration at different temperature shown in fig.(4).From the relationship between corrosion rate and salt concentration at different temperature and different , it can be seen the corrosion rate decrease with increasing of salt concentration because the ratio of dissolved oxygen decrease with increasing of salt concentration therefore the corrosion rate decrease in agreement with results of Habeeb&Matlub(H.S.Habeeb and F.K.Matlub. 1988),Konsowa&El-Shazly(Konsowa, A.H. and A.A.,Elsevier, 2002)and Kuntiya(Kuntiya,A. and Necolella,C. 2005). From the relationship between corrosion rate and temperature at different salt concentration these finding were in agreement with Habeeb&Matlub(H.S.Habeeb and F.K.Matlub. 1988).

B) Polarization method

The corrosion behavior in water-base drilling mud at different salt concentration at static condition and temperature (30 ±1) were investigated, the results have been shown in fig. (5,6, and 7).

In this mode of measurement the run period was about 90 min. the limiting current being equal to corrosion current in this study, the corrosion current increase with decreasing salt concentration as shown in fig. (8).These finding were in agreement with Habeeb & Matloub (H.S.Habeeb and F.K.Matlub, 1988)&Al-Jendeel (H.A.Al-Jendeel, 2007)

4. Conclusions

The response of carbon steel to water corrosion depends primarily on

1) The corrosion rate increase with increasing the temperature
2) The corrosion rate decrease with increasing the salt concentration

Symbols:

C.R= Corrosion rate

S.A= surface area

t= time

iL= limiting current

i corr.=corrosion current density

References

B.W Bradley. (1970). Cause of brills pipe corrosion. The Petroleum Engineering, December 1970.

Barbe. (1966). Control important in packer fluids: packs. Petroleum equipment march-April, 1966.

E.Schasch. (1973). *Methods for evolution and testing of corrosion inhibitors,* NACE, 1973.

H.A.Al-Jendeel. (2007). Ms.C thesis ,chemical Eng. dept. collage of eng. Baghdad unv.

H.E bush,R.D.Barbee and J.P Simpson. (1966). *Current techniques for combating drill pipe corrosion.* API drilling and production practice pp59-69(1966).

H.E BUSH. (1974). *Controlling corrosion in Petroleum Drilling and in packer fluids.* NACE, 1974.

H.S.Habeeb and F.K.Matlub. (1988). Corrosion investigation of drilling pipe in various concentration of salt mixture with and with out adding mud at different temperature. *Journal of petroleum research,*vol.7,no.1,June 1988.

J.P Microbiology on. (1966). *Corrosivity Drilling and completion fluids.* NACE, Houston section short course, Texas .January, 1966.

Jhonston and Cowan. (1964). Recent Developments in the Microbiology of drilling and completing fluids, *Developments in industrial Microbiology,* volume 6. American institute of Biological sciences, Washington D.C (1964).

Konsowa, A.H. and A.A. (2002). Elsevier, *Desalination,*v.153.

Kuntiya,A. and Necolella,C. (2005). *journal of science technology.*vol.27,no.5.

Table 1. temp 30 cº

Salt concentration	S.A (cm²)	W (gm)	C.R (mdd)
100.000	3	0.0031	123
150.000	3	0.00196	98
200.000	3	0.00184	92

Table 2. temp 50 cº

Salt concentration	S.A (cm²)	W (gm)	C.R (mdd)
100.000	3	0.00256	128
150.000	3	0.0024	120
200.000	3	0.00216	108

Table 3. temp 70 cº

Salt concentration	S.A (cm²)	W (gm)	C.R (mdd)
100.000	3	0.0256	140
150.000	3	0.0024	133
200.000	3	0.0025	125

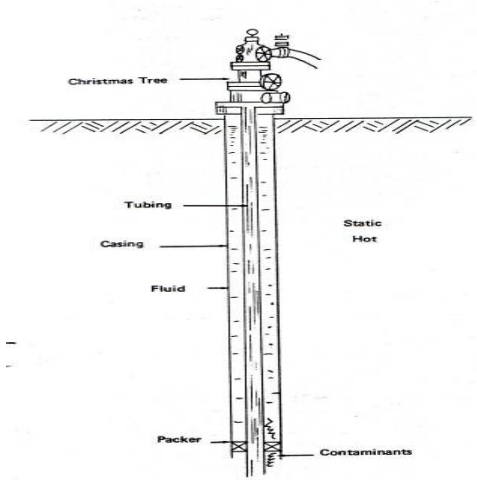

Figure 1. illustrates construction of a well using packer fluid

Figure 2. Experiment Setup

Figure 3. Polarization cell

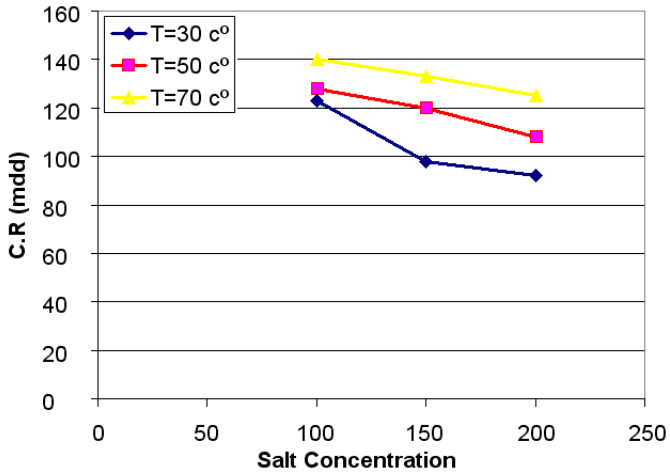

Figure 4. Relation between Corrosion Rate and Salt Con. at diff. temp.

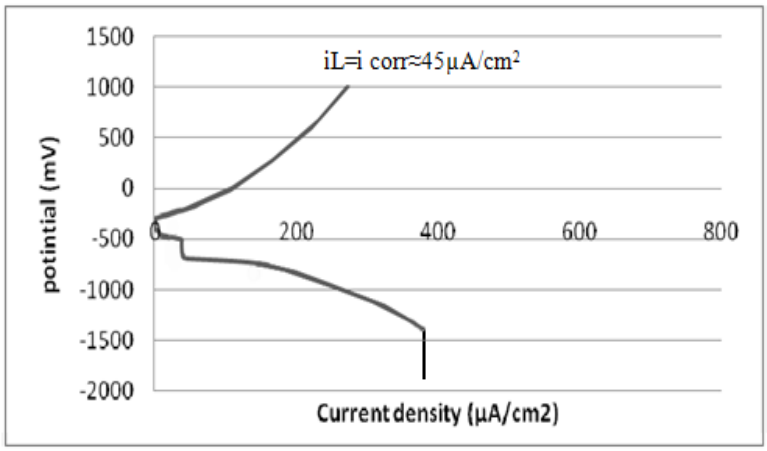

Figure 5. current density vs. potential at salt concentration(100gm/L)

ISSN 1913-1844 E-ISSN 1913-1852

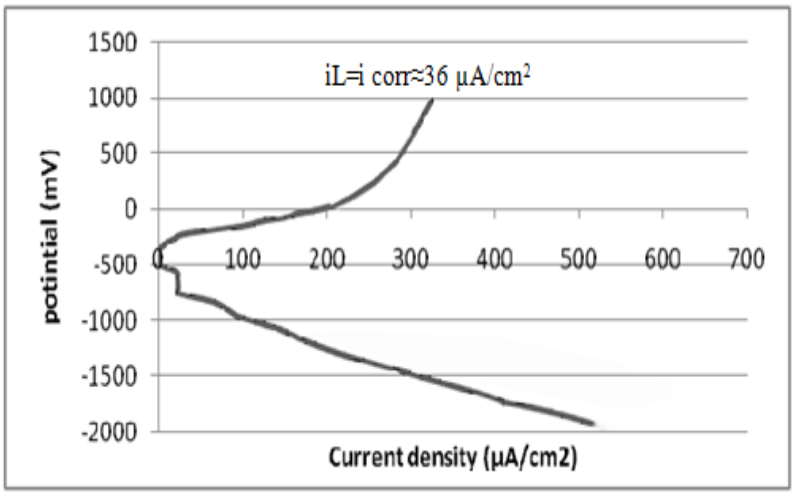

Figure 6. current density vs. potential at salt concentration(150gm/L)

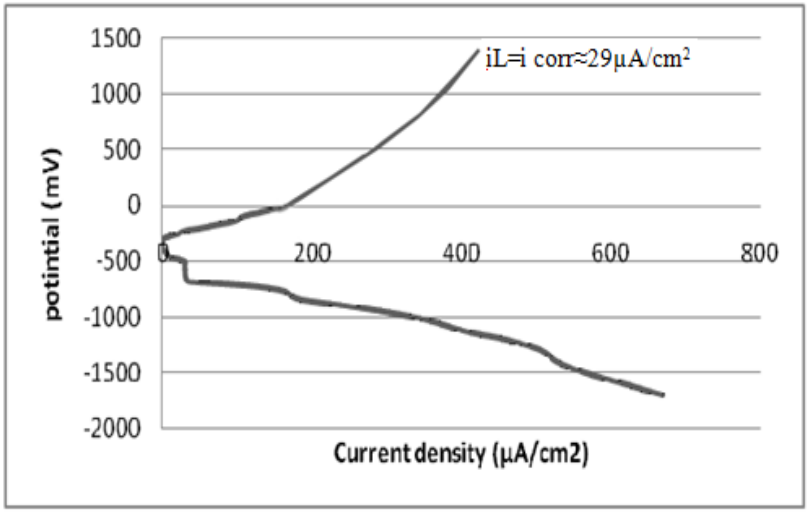

Figure 7. current density vs. potential at salt concentration (200gm/L)

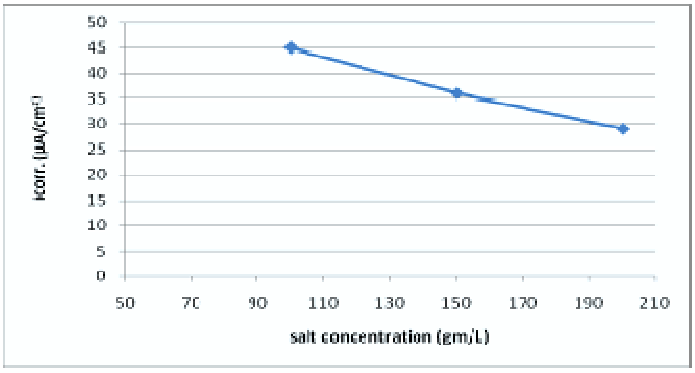

Figure 8. Salt concentration vs. i_{corr} at constant temperature

A Programming of Genetic Algorithm in Matlab7.0

Cheng Guo (Corresponding author)
Department of Mathematics and Physics, XiaMen University of Technology
LiGong Road 600, JiMei Area, XiaMen, FuJian Province 361024, China
E-mail: guocheng@xmut.edu.cn

Xiaoyong Yang
School of Mathematics and Physics, HuaiHai Institute of Technology
Lian yungang, Jiangsu 222005, China
E-mail:163yangxiaoyong@163.com

Abstract

The genetic algorithm is briefly introduced and its complete programming is provided in detail by MATLAB7.0. In addition, the application in optimization of functions and solution of equation is shown through three examples and the method of avoiding local optimization by increasing the value of pm is also discussed.

Keywords: Population, Encoding, Decoding, Cross over, Mutation, Selection

1. Introduction of genetic algorithm

Genetic Algorithm (GA) is a global optimization algorithm derived from evolution and natural selection. Although genetic algorithm cannot always provide optimal solution, it has its own advantages (Liu yong, Kang lishan & Chen yuping. 1997) and is a powerful tool for solving complex problems (Xi yugeng, Chai tianyou & Yun weimin. 1996).

The basic thought of Genetic algorithm:

1) Randomly producing a original population whose number of individuals is a constant N.

2) Producing next generation by crossing over and mutation among individuals.

3) Forming the new population of N individuals from the generation of 2)

4) Producing the next population by repeating the step2) and 3) until obtaining the individual which satisfies conditions.

2. MATLAB programming for genetic algorithm

In order to understand the sense of the MATLAB programming for genetic algorithm, giving the following instances.

Instance one: seeking the maximum of the function $y = f(x_1, x_2, x_3) = 6 - x_1^2 - x_2^2 - x_3^2$.

2.1 individual and population

For instance one, $X = (x_1, x_2, x_3)$ is called individual, and the function $y = f(x_1, x_2, x_3)$ is written as $y = f(X)$, and $f(X)$ is called fitting value of individual X .For example, the fitting value $f(1,1,1) = 3$ for the individual $(1,1,1)$ and lots of individuals form a population, such as, $(1,2,3),(0,0,0),(-1,0,2.4),(0,-0.5,-1.7)$ is a population of four individuals.

In genetic algorithm, the individuals of next population are chosen by the fitting values of individuals, by maintaining the individuals whose fitting values are greater than others. In addition, the fitting values are also as the extermination end condition of genetic algorithm (Liang jiye. 1999). And when the fitting values don't continue to increase, exterminating the programming and the individual with the greatest value is seen as the optimal solution. The number of the generation of populations is another termination condition for genetic algorithm. For example, when after 100 generation of population, terminate the programming and the individual with the greatest fitting value in the last generation is as the optimal solution.

2.2 encoding

In genetic algorithm, coding is expressing the individual by the binary strings of 0s and 1s. In the instance one, every individual has there dimensions, and every dimension is expressed by a 8- bit string of 0s and 1s, so every

individual is expressed as a 24-bit string of 0s and 1s, showing as $\overbrace{01101111}^{x_1}\overbrace{00010101}^{x_2}\overbrace{00110110}^{x_3}$

Programming 1

```
function pop=encoding(popsize,stringlength,dimension)
pop=round(rand(popsize,dimension*stringlength+1));
```

Programming 1 is an encoding function by MATLAB and it randomly produces an encoded original population. Pop in the function encoding is a matrix whose every row indicates an encoded individual and the total number of rows is denoted as popsize. And dimension is the number of dimension of an individual, stringlength is the number of the bits of binary string of encode individual. In the instance one, dimension=3,stringlength=8.In the programming1 ,the last bit of every row record the fitting value of an individual encoded by this row.

2.3 cross-over

Randomly choosing two individuals from pop, and changing the bits of the same section of the two individuals.

Programming 2 for cross-over

```
function new_pop=cross_over(pop,popsize,stringlength,dimension)
match=round(rand(1,popsize)*(popsize-1))+1;
for i=1:popsize
    [child1,child2]=cross_running(pop(i,:),pop(match(i),:),stringlength,dimension);
    new_pop(2*i-1:2*i,:)=[child1;child2];
end
function [child1,child2]=cross_running(parent1,parent2,stringlength,dimension)
cpoint=round((stringlength-1)*rand(1,dimension))+1;
for j=1:dimension
child1((j-1)*stringlength+1:j*stringlength)=[parent1((j-1)*stringlength+1:(j-1)*stringlength+cpoint(j))
parent2((j-1)*stringlength+cpoint(j)+1:j*stringlength)];
child2((j-1)*stringlength+1:j*stringlength)=[parent2((j-1)*stringlength+1:(j-1)*stringlength+cpoint(j))
parent1((j-1)*stringlength+cpoint(j)+1:j*stringlength)];
end
```

Programming 2 includes two functions written by MATLAB which complete the course of mutation by change the part of the binary strings of the chosen individuals.

2.4 mutation

Mutation also simulates biologic evolution mechanism. For the individual to mutate, randomly choose the point to mutate which means the bit of the individual encoded binary string, then change 0 to 1 and change 1 to 0. Pm is the probability of mutation and it is not great in nature and in programming 2, pm=0.05. For every individual, a number of probabilities of mutation are randomly given by the computer. If the giver number is not greater than pm, the individual mutates, otherwise don't mutate.

Programming 3 for mutation

```
function new_pop=mutation(new_pop,stringlength,dimension,pm)
new_popsize=size(new_pop,1);
for i=1:new_popsize
    if rand<pm              mpoint=round(rand(1,dimension)*(stringlength-1))+1;
        for j=1:dimension
            new_pop(i,(j-1)*stringlength+mpoint(j))=1-new_pop(i,(j-1)*stringlength+mpoint(j));
        end
    end
end
```

2.5 decoding

Decoding change the encoding binary strings into decimal number, and then computes fitting values for individuals. Decoding is shown as following through instance one above.

In instance one, each dimension of an individual $X=(x_1,x_2,x_3)$ has a boundary, denoting as $x\_bound=[a_1,b_1,a_2,b_2,a_3,b_3], a_1\le x_1\le b_1, a_2\le x_2\le b_2, a_3\le x_3\le b_3$, an encoded individual : $\overbrace{01101111}^{x_1}\overbrace{00010101}^{x_2}\overbrace{00110110}^{x_3}$.

Encoded binary string for x_1 : 01101111.

Decoded decimal number:

$$\frac{0\times 2^7+1\times 2^6+1\times 2^5+0\times 2^4+1\times 2^3+1\times 2^2+1\times 2^1+1\times 2^0}{2^8-1}\times(b_1-a_1)+a_1$$

Encoded binary string for x_2 : 00010101

Decoded decimal number:

$$\frac{0\times 2^7+0\times 2^6+0\times 2^5+1\times 2^4+0\times 2^3+1\times 2^2+0\times 2^1+1\times 2^0}{2^8-1}\times(b_2-a_2)+a_2$$

Encoded binary string for x_3 : 00110110

Decoded decimal number:

$$\frac{0\times 2^7+0\times 2^6+1\times 2^5+1\times 2^4+0\times 2^3+1\times 2^2+1\times 2^1+0\times 2^0}{2^8-1}\times(b_3-a_3)+a_3$$

Programming 4 for decoding

```
function pop=decoding(pop,stringlength,dimension,x_bound)
popsize=size(pop,1);
temp=2.^(stringlength-1:-1:0)/(2^stringlength-1);
for i=1:dimension
    bound(i)=x_bound(i,2)-x_bound(i,1);
end
for i=1:popsize
    for j=1:dimension
        m(:,j)=pop(i,stringlength*(j-1)+1:stringlength*j);
    end
    x=temp*m;
    x=x.*bound+x_bound(:,1)';
    pop(i,dimension*stringlength+1)=funname(x);
end
```

2.6 selection

Selection is the proceeding through which a new population is formed by choosing the individuals with greater fitting values and eliminating the individuals with smaller fitting values. There are two strategies: the first strategy is that maintaining the individuals with greatest fitting values into the next population; the second strategy is that choosing the individuals to next population by bet ring arithmetic(Zhou ming & Sun shudong. 1999) which guarantee direct ratio between chosen probability and fitting value of the individual. Through selection the fitting values of population is increased constantly and isn't decreased.

Programming 5 for selection

```
function selected=selection(pop,popsize,stringlength,dimension)
popsize_new=size(pop,1);
```

```
r=rand(1,popsize);
fitness=pop(:,dimension*stringlength+1);
fitness=fitness/sum(fitness);
fitness=cumsum(fitness);
for i=1:popsize
    for j=1:popsize_new
        if r(i)<=fitness(j)
            selected(i,:)=pop(j,:);
            break;
        end
    end
end
```

3. Instances

Main programming 6 for solving instances

```
clear;clc;
popsize=10;dimension=3;stringlength=8;x_bound=[-2,3;-2,4;-1,1];pm=0.05;
pop=encoding_guo(popsize,stringlength,dimension);
pop=decoding_guo(pop,stringlength,dimension,x_bound);
[choice_number,choice_k]=max(pop(:,stringlength*dimension+1));
choice=pop(choice_k,:);
for i=1:1000    new_pop=cross_over(pop,popsize,stringlength,dimension);
pop=mutation_guo(new_pop,stringlength,dimension,pm);
pop=decoding_guo(pop,stringlength,dimension,x_bound);
[number,k]=max(pop(:,stringlength*dimension+1));
    if choice_number<number
        choice_number=number;
        choice_k=k;
        choice=pop(choice_k,:);
    end        pop=selection_guo(pop,popsize,stringlength,dimension);
    [number,m]=min(pop(:,stringlength*dimension+1));
    pop(m,:)=choice;
end [value,x]=result_guo(pop,stringlength,dimension,x_bound);
```

Programming 7

```
function [value,x]=result_guo(pop,stringlength,dimension,x_bound)
[value,k]=max(pop(:,stringlength*dimension+1));
temp=2.^(stringlength-1:-1:0)/(2^stringlength-1);
for i=1:dimension
    bound(i)=x_bound(i,2)-x_bound(i,1);
end
for j=1:dimension
    m(:,j)=pop(k,stringlength*(j-1)+1:stringlength*j);
end
x=temp*m;
```

x=x.*bound+x_bound(:,1)'

programming 8

function y=funname(x)

y=6-x(1)^2-x(2)^2-x(3)^2;

For different instances, programmings need to be rewritten. And here is only for instance one.

Instance two: finding the maximum of function $y = f(x_1, x_2, x_3) = 6 - x_1 - x_2 - x_3$,

Running result:
value = 5.9995 x = -0.0159 0 0.0159

This shows that the maximum is 5.9995, and $x_1 = -0.0159, x_2 = 0, x_3 = 0.0159$ after one hundred generations and it closely approaches the real maximum 6 of the function.

Instance three: finding the maximum of function $y = f(x) = \sin(5x) - 2\cos(3x) + 10, x \in [0,10]$, the figure of the function is as the following Figure 1:

Programming for this instance in MATLAB

function y=funname(x)

y=sin(5*x)-2*cos(3*x)+10;

in programming 6, changing the following

popsize=10;dimension=3;stringlength=8;x_bound=[-2,3;-2,4;-1,1];pm=0.05;

as: popsize=10;dimension=1;stringlength=8;x_bound=[0,10];pm=0.5;

running result: value =12.9427 x =5.2941

Through this instance we can validate the power of global optimal seeking and if let pm=0.05, run the programming 6, local optimal solution is found. But increasing pm, let pm=0.5, global optimal solution is obtained. This instance shows that in order to avoid the local optimal solution, pm can be increased. This is the same as biological evolution mechanism: when mutation is fastened, the evolution speed of biological group is increased.

Instance four: Finding $x, x \in [0,10]$ for function $f(x) = \sin(5x) - 2\cos(3x) + 10$, satisfying $f(x) = 11$.

The function in instance 4 is the same as that in instance 3. And by the figure of this function, the value is not only one.

Programming for instance four in MATLAB

function y=funname2(x)

y=-abs(sin(5*x)-2*cos(3*x)+10-11);

in programming 6, changing the following

popsize=10;dimension=3;stringlength=8;x_bound=[-2,3;-2,4;-1,1];pm=0.05;

as: popsize=10;dimension=1;stringlength=8;x_bound=[0,10];pm=0.5;

running result: value =-0.0130 x =1.5686

when x_bound=[0,1], value =-0.0035 x =0.9922; $f(0.9922) = 11.0036$

when x_bound=[1,2], value =-0.0106 x =1.5725; $f(1.5725) = 10.9897$

when x_bound=[2,3], value =-0.0150 x =2.6667; $f(2.6667) = 10.9853$

Through changing x_bound, the nine values satisfying $0 \le x \le 10, f(x) = 11$ are:

0.9922,1.5725,2.6667,3.3098,4.9569,5.6196,7.2745,8.9529,9.5922.

This instance shows that genetic algorithm can also be used to solve equations if the boundaries of the variables are given.

4. Conclusion

MATLAB codes given in literature(Liu guohua, Bao hong & Li wenchao. 2001)(Yin ming, Zhang xinghua & Dai xianzhong. 2000) are incomplete, and somewhere have errors. This article provides the complete original codes in MATLAB which can be directly run through MATLAB7.0. The given instances in this article show that

the genetic algorithm can be applied to find optimal solution and to solve equations and indicate that the genetic algorithm is a powerful global searching tool. In order to avoid local optimal solution, we can increase individual rate of mutation and increase the hereditary generations of population.

References

Liang jiye. (1999). The research of common problems in genetic algorithm application. R*esearch of Computer Application,* 1999 (7): 20-21.

Liu guohua, Bao hong & Li wenchao. (2001). The genetic algorithm programming in MATLAB. *Research of Computer Aapplication,*2001(8):80-82.

Liu yong, Kang lishan & Chen yuping. (1997). *Nonnumerical parallel algorithm(second volumn)—genetic algorithm.* Beijing:science press,1997.

Xi yugeng, Chai tianyou & Yun weimin. (1996). Summarization of genetic algorithm. *Control Theory and Application,* 1996(6):697-708

Yin ming, Zhang xinghua & Dai xianzhong. (2000). The programming of genetic algorithm in MATLAB. *Application of Electronic Technology,* 2000(1):9-11.

Zhou ming & Sun shudong. (1999). *Theory and Application of Genetic Algorithm*. BeiJing: national independence industry press, 1999.

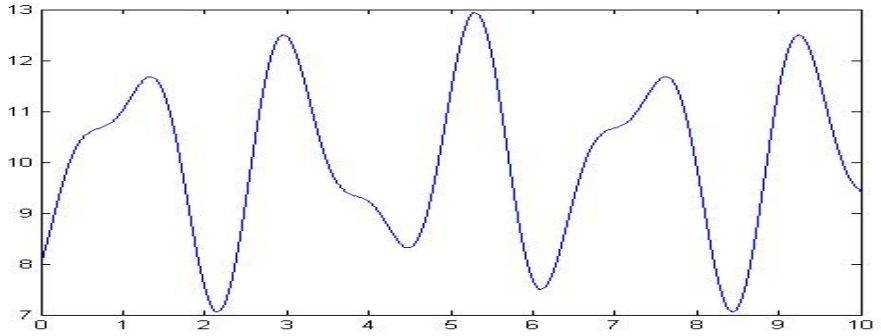

Figure 1. curve for $\sin(5x) - 2\cos(3x) + 10, x \in [0,10]$

Teaching Effect Analysis Based on Function P-sets

Xiuqing Yu

Department of Mathematics Dezhou University, Dezhou253023, China

Tel: 86-139-6923-1258 Email: sddzyxq@163.com

This research was supported by the Natural Science Foundation and the Education Science Foundation of Shandong Province of China (ZR2010AL019), and (2010JZ123) respectively.

Abstract

Function P-sets which is composed of function internal P-set and function outer P-set, is a function set pair and has dynamic and law characteristics. Based on function P-sets, this paper presents the concepts such as data law, $\overline{F}$ - data law, F -data law and bi-data law, and then $\overline{F}$ -data law theorem, F -data law theorem, bi-data law band theorem, data law recovery theorem, bi-data law identification theorem and law identification criterion are proposed. By using these results, teaching effect analysis is obtained and applications on bilingual education are given. Function P-sets is a new method in the research of dynamic data system.

Keywords: Function P-sets, Data law, Teaching effect

1. Introduction

In 2008, Refs.(SHI Kai-quan. 2008)(SHI Kai-quan. 2009) originated P-sets $(X^{\overline{F}}, X^{F})$ by introducing dynamic characteristic into general set X .Refs. (SHI Kai-quan Shi, Li Zhang. 2009)(YU Xiu-qing. 2010) (YU Xiu-qing. 2010) (SHI Kai-quan&Tingcheng Chang. 2005) (SHI Kai-quan &LI Xiu-hong, 2010) discussed application in many fields. In 2010, Refs.(ZHANG Li&CUI Yu-quan. 2010) introduced function into P-sets, and gave concept and structure of function P-sets $(Q^{\overline{F}}, Q^{F})$. Function P-sets are function set pair composed of function internal P-set $Q^{\overline{F}}$ and function outer *P*-set Q^{F} together, they have dynamic and law characteristic. It is also to say: when functions in function set Q are transferred out from Q , Q becomes function internal P-set $Q^{\overline{F}}$, on the other hand ,when functions out of Q are transferred into Q , Q becomes function outer P-set Q^{F} , therefore function P-sets has dynamic characteristic. Moreover because function is law, so it also has law characteristic. Based on above content and features of function P-sets, the concepts of data law, $\overline{F}$ -data law, F -data law and bi-data law are proposed, the bi-data law band theorem, recovery theorem and identification theorem are given, and identification criterion of data law are put forward. Using these results, this paper gives teaching effect analysis modal (TEAM) and discusses application of TEAM on bilingual education in university.

To facilitate the discussion and acceptance of the results, function P-sets and its simple structure are introduced into the following section as theoretical preparation.

2. Function P-sets and its structure

Assumptions: V is a nonempty finite attribute universe, α is a nonempty finite attribute set in V . $\mathsf{T}(x)$ is a nonempty finite function universe of discourse, $Q(x)=\{u(x)_1, u(x)_2, \cdots, u(x)_m\}$ is a finite function sets in $\mathsf{T}(x)$, $u(x)_i, i=1,2,3,...,m$ is a function in $Q(x)$, $F=\{f_1, f_2, ..., f_r\}$ and $\overline{F}=\{\overline{f}_1, \overline{f}_2, ..., \overline{f}_s\}$ are function transfer families, $f \in F$ and $\overline{f} \in \overline{F}$ are function transfer. For expressing briefly and without misunderstanding, $\mathsf{T}(x)$, $Q(x)$ and $[u(x)]$ are denoted by D , Q and $[u]$ respectively.

Given a finite general function set $Q=\{u_1, u_2, \cdots, u_m\} \subset \mathsf{T}$, and $\alpha=\{\alpha_1, \alpha_2, \cdots, \alpha_k\} \subset V$ is the attribute set of Q .

$Q^{\overline{F}}$ is called function internal packet set of Q , called function internal P-set for short, moreover

$$Q^{\overline{F}}=Q-Q^{-}, \tag{1}$$

and Q^{-} is called $\overline{F}$ -function deleted set of Q , moreover

$$Q^{-}=\{u \mid u \in Q, \overline{f}(u)=w \overline{\in} Q, \overline{f} \in \overline{F}\}, \tag{2}$$

if the attribute set α^{F} of $Q^{\overline{F}}$ satisfies

$$\alpha^F = \alpha \bigcup \{|\, \alpha' \mid f(\beta) = \alpha' \in \alpha, f \in F\}, \tag{3}$$

where $\beta \in V, \beta \overline{\in} \alpha$, $f \in F$ turns β into $\alpha' = f(\beta) \in \alpha$.

Q^F is called outer function packet set of X, called outer P-set for short, moreover

$$Q^F = Q \bigcup Q^+, \tag{4}$$

and Q^+ is called F-function supplemented set, moreover

$$Q^+ = \{u' \mid w \in T, w \overline{\in} Q, f(w) = u' \in Q, f \in F\} \tag{5}$$

if the attribute set $\alpha^{\overline{F}}$ of Q^F satisfies

$$\alpha^{\overline{F}} = \alpha - \{\alpha_i \mid \overline{f}(\alpha_i) = \beta_i \overline{\in} \alpha, \overline{f} \in \overline{F}\} \tag{6}$$

where, $\alpha_i \in \alpha$, $\overline{f} \in \overline{F}$ turns α_i into $\overline{f}(\alpha_i) = \beta_i \overline{\in} \alpha$. $\alpha^{\overline{F}} \neq \phi$.

The set pair which is composed of function internal P-set $X^{\overline{F}}$ and function outer P-set X^F is called P-sets (packet sets) generated by the general function set Q, briefly called P-sets, moreover

$$(Q^{\overline{F}}, Q^F) \tag{7}$$

where, the general set Q is called the ground set of $(Q^{\overline{F}}, Q^F)$.

Theorem 2.1 (Dynamic characteristic theorem of function P-sets) Function set Q, its function internal P-set $Q^{\overline{F}}$ and its function outer P-set Q^F satisfies

$$Q^{\overline{F}} \subseteq Q \subseteq Q^F \tag{8}$$

Theorem 2.2 (The relation theorem between P-sets and general set) suppose $F = \{f_1, f_2, \cdots, f_m\}$ and $\overline{F} = \{\overline{f}_1, \overline{f}_2, \cdots, \overline{f}_n\}$ be function transfer families, if $(Q^{\overline{F}}, Q^F)$ is a function P-sets generated by a general function set Q, then

$$(Q^{\overline{F}}, Q^F)_{F=\overline{F}=\phi} = Q \tag{9}$$

In fact, if $F = \phi$, then $\{\alpha' \mid f(\beta) = \alpha' \in \alpha, f \in F\} = \phi$, i.e., $\alpha^F = \alpha$, the equation (1) changes into $Q^{\overline{F}} = Q$ and (2) changes into $Q^- = \{u \mid u \in Q, \overline{f}(u) = w \overline{\in} Q, \overline{f} \in \overline{F}\} = \phi$; if $\overline{F} = \phi$, then $\{\alpha_i \mid \overline{f}(\alpha_i) = \beta_i \overline{\in} \alpha, \overline{f} \in \overline{F}\} = \phi$, i.e., $\alpha^{\overline{F}} = \alpha$, the equation (4) changes into $Q^F = Q$ and (5) changes into $Q^+ = \{u' \mid w \in T, w \overline{\in} Q, f(w) = u' \in Q, f \in F\} = \phi$, then we have (9).

3. Data law and its characteristics

Definition 1 Given finite function set $Q = \{u_1, u_2, u_3, ..., u_m\}, \forall u_i \in Q$ has discrete data distributions, moreover

$$y_i = \left(y_{i1}, y_{i2}, ...y_{ik}, ...y_{in+1}\right) \tag{10}$$

y is called the compound data set of u_i, moreover

$$y = \left(y_1, y_2, ..., y_3, ..., y_{n+1}\right) \tag{11}$$

where, $y_k = \sum_{j=1}^{m} y_{jk}, k = 1, 2, ..., n+1; y_{ik}, y_k \in R^+$, R^+ is nonnegative real number set, $i = 1, 2, ..., m$.

Definition 2 $p(x)$ is called the data law generated by Q, if $p(x)$ is the polynomial function generated by data points

$$(x_1, y_1), (x_2, y_2), ..., (x_{n+1}, y_{n+1}), \tag{12}$$

moreover

$$p(x) = \sum_{j=1}^{n+1} y_j \prod_{\substack{i,j=1 \\ i \neq j}}^{n+1} \frac{x - x_i}{x_j - x_i} = \rho_n x^n + \rho_{n-1} x^{n-1} + ... + \rho_1 x + \rho_0,$$

where (12) is the data points constituted by(11).

Definition 3 Suppose that $Q^{\overline{F}}$ is function internal P-set of Q, $p(x)^{\overline{F}}$ is called internal data law generated by $Q^{\overline{F}}$, briefly called $\overline{F}$-data law, moreover

$$p(x)^{\overline{F}} = a_n x^n + a_{n-1} x^{n-1} + ... + a_1 x_1 + a_0 \tag{13}$$

where $\forall u_i \in Q^{\bar{F}}, u_i$ has discrete data distribution $y_i = (y_{i1}, y_{i2}, ...y_{ik}, ...y_{in+1})$, $i = 1,2,...,card(Q^{\bar{F}})$. *card*=cardinal number. $p(x)^{\bar{F}}$ is generated via formula(10)-(12).

Definition 4 Suppose that Q^F is function outer P-set of Q, $p(x)^F$ is called outer data law generated by Q^F, briefly called F-data law, moreover

$$p(x)^F = b_n x^n + b_{n-1}x^{n-1} + ... + b_1 x_1 + b_0 \tag{14}$$

Where, $\forall u_j \in Q^F, u_j$ has discrete data distribution $y_i = (y_{i1}, y_{i2}, ...y_{ik}, ...y_{in+1})$, $i = 1,\quad 2,...,card(Q^F)$. *card*=cardinal number. $p(x)^F$ is generated via formula(10)-(12).

Definition 5 The data law pair composed of $p(x)^{\bar{F}}$ and $p(x)^F$ is call bi-data law generated by P-sets $(Q^{\bar{F}}, Q^F)$, written as

$$(p(x)^{\bar{F}}, p(x)^F) \tag{15}$$

According to definitions 1-5, the following theorems can be got.

Theorem 3.1 ($\bar{F}$-data law theorem) If $p(x)$ is data law generated by function set Q, then there exists an $\bar{F}$-data law $p(x)^{\bar{F}}$ satisfying

$$p(x)^{\bar{F}} + \nabla p(x)^{\bar{F}} = p(x) \tag{16}$$

where, $\nabla p(x)^{\bar{F}} \geq 0$, $p(x)^{\bar{F}}$ is the data law generated by $Q^{\bar{F}}$.

Proof Assumed that $Q = \{u_1, u_2, \cdots, u_m\}$ is the given finite function set and $y_i = \{y_{i,1}, y_{i,2}, \cdots, y_{i,n+1}\}$ is the data set of $u_i \in Q$. Then there exists data set $y = \{y_1, y_2, \cdots, y_{n+1}\} = \{\sum_{i=1}^{m} y_{i,1}, \sum_{i=1}^{m} y_{i,2}, \cdots, \sum_{i=1}^{m} y_{i,n+1}\}$ with respect to Q. For $Q^{\bar{F}} = \{u_1, u_2, \cdots, u_{m-r}\}$, apparently, there exists $\bar{F}$-data set $y^{\bar{F}} = \{y_1^{\bar{f}}, y_2^{\bar{f}}, \cdots, y_{n+1}^{\bar{f}}\} = \{\sum_{i=1}^{m-r} y_{i,1}, \sum_{i=1}^{m-r} y_{i,2}, \cdots, \sum_{i=1}^{m-r} y_{i,n+1}\}$, namely there is $y_\lambda^{\bar{f}} \in y^{\bar{F}}$. For any $\lambda \in \{1, 2, \cdots, n, n+1\}$, $y_\lambda^{\bar{f}} = \sum_{i=1}^{m-r} y_{i,\lambda} \leq \sum_{i=1}^{m} y_{i,\lambda} = y_\lambda$, then there exists $\nabla\varepsilon_\lambda \in R^+$ satisfying $y_\lambda - \nabla\varepsilon_\lambda = y_\lambda^{\bar{f}}$. By definition 2, formula (16) is got.

Theorem 3.2 (F-data law theorem) If $p(x)$ is data law generated by function set Q, then there exists an F-data law $p(x)^F$ satisfying

$$p(x)^F - \Delta p(x)^F = p(x), \tag{17}$$

where, $\Delta p(x)^F \geq 0$, $p(x)^F$ is the data law generated by Q^F.

Theorem 3.3 (bi-data law band theorem) If $\varphi^{\bar{F}}$ and φ^F are cures generated by $p(x)^{\bar{F}}$ and $p(x)^F$ respectively, then

1. There exists bi-data law band, written as $\mathrm{BAN}\{\varphi^{\bar{F}}, \varphi^F\}$, which takes $\varphi^{\bar{F}}$ as lower boundary and takes φ^F as upper boundary.
2. $p(x)^{\bar{F}}$ and $p(x)^F$ satisfy

$$p(x)^F - p(x)^{\bar{F}} \geq 0 \tag{18}$$

The proof of theorem 3.3 can be easily obtained from formula (1), (4) and (13), so omitted.

Theorem 3.4 (Boundary coincidence theorem) The bi-data law band $\mathrm{BAN}\{\varphi^{\bar{F}}, \varphi^F\}$ satisfies

$$\varphi^{\bar{F}} = \varphi^F \tag{19}$$

if and only if,

$$(Q^{\bar{F}}, Q^F)_{\bar{F}=F=\phi} = Q. \tag{20}$$

In fact, if $\bar{F} = F = \phi$, then the expression (3) turns into $\alpha^F = \alpha$ and the expression (6) turns into $\alpha^{\bar{F}} = \alpha$, thus $Q^{\bar{F}}$ in (1) and Q^F in (4) changes into Q, i.e., $Q^{\bar{F}} = Q^F = Q$. So φ^F is coincident with $\varphi^{\bar{F}}$, i.e., $\varphi^F = \varphi^{\bar{F}} = \varphi$. So the proof of theorem 3.4 is omitted.

Theorem 3.5 (attribute dependence theorem of $\overline{F}$-data law) suppose α_i^F, α_j^F and α_k^F are attribute sets of $Q_i^{\overline{F}}, Q_j^{\overline{F}}$ and $Q_k^{\overline{F}}$ respectively, if they satisfy $\alpha_i^F \subseteq \alpha_j^F \subseteq \alpha_k^F$, then there exists an $\overline{F}$-data law sequence satisfying

$$p(x)_k^{\overline{F}} \le p(x)_j^{\overline{F}} \le p(x)_i^{\overline{F}} \tag{21}$$

where, $p(x)_i^{\overline{F}}, p(x)_j^{\overline{F}}$ and $p(x)_k^{\overline{F}}$ are $\overline{F}$-data laws generated by $Q_i^{\overline{F}}, Q_j^{\overline{F}}$ and $Q_k^{\overline{F}}$ respectively. $Q_i^{\overline{F}}, Q_j^{\overline{F}}$ and $Q_k^{\overline{F}}$ are function internal P-set of function set Q.

Theorem 3.6 (attribute dependence theorem of F-data law) suppose $\alpha_i^{\overline{F}}, \alpha_j^{\overline{F}}$ and $\alpha_k^{\overline{F}}$ are attribute sets of Q_i^F, Q_j^F and Q_k^F respectively, if they satisfy $\alpha_i^{\overline{F}} \subseteq \alpha_j^{\overline{F}} \subseteq \alpha_k^{\overline{F}}$, then there exists an F-data law sequence satisfying

$$p(x)_i^F \le p(x)_j^F \le p(x)_k^F, \tag{22}$$

where, $p(x)_i^F, p(x)_j^F$ and $p(x)_k^F$ are data laws generated by Q_i^F, Q_j^F and Q_k^F respectively. Q_i^F, Q_j^F and Q_k^F are function outer P-set of function set Q.

Theorem 3.7 ($\overline{F}$-data law recovery theorem of bi-data law) Given a bi-data law $(p(x)^{\overline{F}}, p(x)^F)$, if $p(x)^{\overline{F}} = p(x)$, then the

attribute sets α^F and α with respect to $p(x)^{\overline{F}}$ and $p(x)$ respectively satisfy

$$\alpha^F - \{\alpha_i \mid \alpha_i \in \alpha^F, \overline{f}(\alpha_i) = \beta_i \overline{\in} \alpha^F\} = \alpha. \tag{23}$$

Proof Suppose $y = \{y_1, y_2, \cdots, y_{n+1}\}$ and $y^{\overline{F}} = \{y_1^{\overline{f}}, y_2^{\overline{f}}, \cdots, y_{n+1}^{\overline{f}}\}$ are compound data sets of $Q = \{u_1, u_2, \cdots, u_m\}$ and $Q^{\overline{F}} = \{u_1, u_2, \cdots, u_{m-r}\}$ respectively. From the expressions (1)-(3), we know there exist attribute sets α^F and α with respect to $Q^{\overline{F}}$ and Q respectively satisfying $\alpha \subseteq \alpha^F$. Obviously, there exist some attributes α_i in α^F, if they are deleted from it, i.e., $\alpha^F - \{\alpha_i \mid \alpha_i \in \alpha^F, \overline{f}(\alpha_i) = \beta_i \overline{\in} \alpha^F\} = \alpha$, $Q^{\overline{F}}$ is recovered to Q, then $p(x)^{\overline{F}} = p(x)$.

Theorem 3.8 (F-data law recovery theorem of bi-data law) Given a bi-data law $(p(x)^{\overline{F}}, p(x)^F)$, if $p(x)^F = p(x)$, then the

attribute sets $\alpha^{\overline{F}}$ and α with respect to $p(x)^F$ and $p(x)$ respectively satisfy

$$\alpha^{\overline{F}} \bigcup \{\beta_i \mid \beta_i \in V, \beta_i \overline{\in} \alpha^{\overline{F}}, f(\beta_i) = \alpha_i \in \alpha^{\overline{F}}\} = \alpha \tag{24}$$

Its proof is similar to the theorem 3.7, so omitted.

4. Teaching effect analysis

In this section $p(x) = \rho_n x^n + \rho_{n-1} x^{n-1} + \ldots + \rho_1 x + \rho_0$ is data law generated by function set Q, $p(x)^{\overline{F}} = a_n x^n + a_{n-1} x^{n-1} + \ldots + a_1 x_1 + a_0$ $\overline{F}$-data law generated by function internal P-set $Q^{\overline{F}}$ of Q and $p(x)^F = b_n x^n + b_{n-1} x^{n-1} + \ldots + b_1 x_1 + b_0$ F- data law generated by function outer P-set Q^F of Q.

Definition 5 $d^{\overline{F}}$ is called $\overline{F}$-measurement degree, moreover

$$d^{\overline{F}} = \sqrt{\sum_{i=0}^{n} (a_i - p_i)^2} \tag{25}$$

Definition 6 d^F is called F-measurement degree, moreover

$$d^F = \sqrt{\sum_{i=0}^{n} (b_i - p_i)^2} \tag{26}$$

Definition 7 The number pair composed by $d^{\overline{F}}$ and d^F is called bi-measurement degree, denoted as

$$(d^{\overline{F}}, d^F) \tag{27}$$

Theorem 4.1 (Identification theorem of bi-data laws) If $(p(x)_i^{\overline{F}}, p(x)_i^F)$ and $(p(x)_j^{\overline{F}}, p(x)_j^F)$ are bi-data laws generated by $(Q_i^{\overline{F}}, Q_i^F)$ and $(Q_j^{\overline{F}}, Q_j^F)$ of Q respectively, $(d_i^{\overline{F}}, d_i^F)$ and $(d_j^{\overline{F}}, d_j^F)$ are their bi-measurement degree respectively, moreover,

$d_i^{\overline{F}} = d_j^{\overline{F}}, d_i^F = d_j^F$

then the two bi-data law cannot be identified, denoted by

$$\mathrm{UNI}\left((p(x)_i^{\overline{F}}, p(x)_i^F), (p(x)_j^{\overline{F}}, p(x)_j^F)\right) \tag{28}$$

where, UNI is brief expression of unidentification.

Theorem 4.2 If $(p(x)_i^{\overline{F}}, p(x)_i^F)$ and $(p(x)_j^{\overline{F}}, p(x)_j^F)$ are bi-data laws generated by function P-sets $(Q_i^{\overline{F}}, Q_i^F)$ and $(Q_j^{\overline{F}}, Q_j^F)$ of Q respectively, $(d_i^{\overline{F}}, d_i^F)$ and $(d_j^{\overline{F}}, d_j^F)$ are their bi-measurement degree respectively, moreover,

$d_i^{\overline{F}} \geq d_j^{\overline{F}}$

then

$$z(\alpha_i^+) \geq z(\alpha_j^+) \tag{30}$$

Where, $z(\alpha_i^+)$ and $z(\alpha_j^+)$ are important degree of attribute sets α_i^+ and α_j^+ to function set Q respectively, α_i^+ and α_j^+ are supplement attribute sets of α, i.e., $\alpha_i^+ = \{\alpha_i' \mid \beta \in V, \beta \overline{\in} \alpha, f(\beta) = \alpha_i' \in \alpha\}$, $\alpha_j^+ = \{\alpha_j' \mid \beta \in V, \beta \overline{\in} \alpha, f(\beta) = \alpha_j' \in \alpha\}$. α is attribute set of Q.

Theorem 4.3 If $(p(x)_i^{\overline{F}}, p(x)_i^F)$ and $(p(x)_j^{\overline{F}}, p(x)_j^F)$ are bi-data laws generated by function P-sets $(Q_i^{\overline{F}}, Q_i^F)$ and $(Q_j^{\overline{F}}, Q_j^F)$ of Q respectively, $(d_i^{\overline{F}}, d_i^F)$ and $(d_j^{\overline{F}}, d_j^F)$ are their bi-measurement degree respectively, moreover,

$d_i^F \leq d_j^F$

Then

$$z(\alpha_i^-) \geq z(\alpha_j^-) \tag{31}$$

Where, $z(\alpha_i^-)$ and $z(\alpha_j^-)$ express important degree of attribute sets α_i^- and α_j^- to function set Q respectively, α_i^- and α_j^- are deleted attribute sets of α, i.e., $\alpha_i^- = \{\alpha_i \mid \alpha_i \in \alpha, f(\alpha_i) = \beta_i \overline{\in} \alpha\}$ $\alpha_j^- = \{\alpha_j \mid \alpha_j \in \alpha, f(\alpha_j) = \beta_j \overline{\in} \alpha\}$.

Identification criterion of bi-data law

If the attribute sets $(\alpha_i^F, \alpha_i^{\overline{F}})$ of $(p(x)_i^{\overline{F}}, p(x)_i^F)$ and $(p(x)_j^{\overline{F}}, p(x)_j^F)$ satisfy $(\alpha_i^F, \alpha_i^{\overline{F}}) - (\alpha_j^F, \alpha_j^{\overline{F}}) \neq \phi$, then $(p(x)_i^{\overline{F}}, p(x)_i^F)$ and $(p(x)_j^{\overline{F}}, p(x)_j^F)$ can be identified, denoted as

$$\mathrm{IDE}\left((p(x)_i^{\overline{F}}, p(x)_i^F), (p(x)_j^{\overline{F}}, p(x)_j^F)\right) \tag{32}$$

here the expression $(\alpha_i^F, \alpha_i^{\overline{F}}) - (\alpha_j^F, \alpha_j^{\overline{F}}) \neq \phi$ means both $\alpha_i^F - \alpha_j^F \neq \phi$ and $\alpha_i^{\overline{F}} - \alpha_j^{\overline{F}} \neq \phi$. IDE is brief expression of identification.

The following gives teaching effect analysis, for teaching process is similar to function P-sets.

There is teaching effect function set, denoted as $Q = \{u_1, u_2, \cdots, u_m\}$, α is the attribute set of Q, $y_i = \{y_{i1}, y_{i2}, y_{i3}, ..., y_{in+1}\}$ means number value set of $u_i \in Q$, u_i is a discrete function ,which influences teaching effect, $y_{ik} \in R^+$, $k = 1, 2, 3, ..., n+1$, R^+ is the positive real number set, then they form $y = \{y_1, y_2, \cdots, y_{n+1}\} = \{\sum_{i=1}^m y_{i,1}, \sum_{i=1}^m y_{i,2}, \cdots, \sum_{i=1}^m y_{i,n+1}\}$ by formula (11) on interval $[a,b]$. Here $p(x)$ is the teaching effect law on continuous interval $[a,b]$ by formula(13), As a matter of fact, when some unfavorable factors(attribute elements of Q) from teachers , students and other aspects are deleted from α, the class teaching effect expands its scale, that is to say, y expanded into y', then y changed into

$y' = \{y'_1, y'_2, \cdots, y'_{m+r}\} = \{\sum_{i=1}^{m+r} y'_{i,1}, \sum_{i=1}^{m+r} y'_{i,2}, \cdots \sum_{i=1}^{m+r} y'_{i,n+1}\}$; it is easy to get $p(x)^F > p(x)$, $d^F > 0$,and $z(\alpha^-) > 0$. When some unfavorable factors (attribute elements of Q) are transferred into α , the class teaching effect shrinks , that is to say, y shrunk into $y'' = \{y_1, y_2, \cdots, y_{n+1}\}$, $y'' = \{y''_1, y''_2, \cdots, y''_{n+1}\} = \{\sum_{i=1}^{m-\lambda} y''_{i,1}, \sum_{i=1}^{m-\lambda} y''_{i,2}, \cdots, \sum_{i=1}^{m-\lambda} y''_{i,n+1}\}$; it is easy to get $p(x)^{\bar{F}} < p(x)$, $d^{\bar{F}} > 0$,and $z(\alpha^+) > 0$. This fact is very simple and can be accepted by anybody.

In teaching effect analysis system, a effect distribution at a certain period (for example, a term)are generally presented, as a matter of fact, this distribution is a cure $p(x)$ at interval $[a,b]$, here y_k is the teaching effect value at point k , $y_k \in R^+$. The effect distribution is actually a predicted value, it changes along with the factors in many aspects. When there is a good teaching environment, $y_k \in y$ turns into $y'_k = y_k + \Delta\sigma_k$, here $\Delta\sigma_k$ is the added value of effect value y_k at point k , so the cure $p(x)'$ and $p(x)$ satisfy $p(x)' > p(x)$; When there is a bad teaching environment, $y_k \in y$ turns into $y''_k = y_k - \nabla\varepsilon_k$, here $\nabla\varepsilon_k$ is the added value of effect value y_k at point k , so the cure $P(x)''$ and $p(x)$ satisfy $p(x)'' < p(x)$; thus $P(x)''$ and $p(x)'$ form $\mathrm{BAN}\{p(x)'', p(x)'\}$ and $p(x)$ is just in it. This is the real situation of teaching effect analysis system every teacher must meet.

5. Application of bilingual education

Freshmen are divided into three classes according to their entrance grades randomly. No.1 is chosen as compared class. No.2 and No.3 are experiment classes. Advanced mathematics of the three classes are taught by the same teacher. But No1 is taught in native language, No2 mainly in native language including little English professional nouns and little simply sentences, No.3 almost in English only including explaining in Chinese. By using knowledge in section3 and section4, table1 is got.

Table1 four teaching effect compound data of each class in the first term(data has be dealt with.)

Test number	1	2	3	4
y in No.1 (Compared class)	1.22	1.01	0.62	0.61
y^F in No.2	1.52	1.29	1.15	1.09
$y^{\bar{F}}$ in No.3	1.08	0.63	0.21	0.02

According to section 4 and formula(13), the three data law curves of teaching effect are obtained, they are $p_1(x) = -0.597x^3 + 4.855x^2 - 12.098x + 8.92$, $p_2(x) = -1.473x^3 + 11.375x^2 - 24.894x + 17.33$, and $p_3(x) = -0.922x^3 + 7.275x^2 - 17.223x + 12.09$ respectively, moreover $p_3(x) \le p_1(x) \le p_2(x)$. This is fit to real fact. In No.1 students not only met no difficulty, but also had more learning interest than before during learning. In No3 students met more difficulty in understanding what the teacher taught for teacher gave a lesson almost in English, consequently they lose interest to learn and become no self-confidence. This teaching effect analysis shows the necessity of adjusting teaching modal.

6. Discussion

Refs.(ZHANG Li&CUI Yu-quan. 2010) originated the concept and structure of function P-sets. Based on function P-sets, the concept of bi-data law was proposed and the characteristics of bi-data law were discussed in this paper. Bi-data law exists in many kinds of information system, but it does not attract more attention now. In fact, the bi-data law reveals the value characteristics of dynamic information systems. From the discussion and application given in this paper, we can think of that function P-sets is a new theory and a new method in the research of dynamic information system.

References

LIN Hong-kang&LI Yu-ying. (2010). P-sets and its P-separation theorems. *An International Journal Advances in Systems Science and Applications*, 24 -5-251.

SHI Kai-quan &LI Xiu-hong, (2010). Camouflaged information and its on identification and its applications. *An International Journal Advances in Systems Science and Applications*, 208-216.

SHI Kai-quan Shi, Li&Zhang. (2009). Internal P-sets and data outer-recovery. *Journal of Shandong University(Natural Science)*, 8-14.

SHI Kai-quan&Tingcheng Chang. (2005). One direction S-rough sets. *International Journal of Fuzzy Mathematics*, 2005, 13(2):319-334.

SHI Kai-quan. (2008). P-sets. *Journal of Shandong University(Natural Science)*, 77- 84.

SHI Kai-quan. (2009). P-sets and its applications. *Advances in Systems Science and Applications*, 168-178.

YU Xiu-qing. (2010). Dynamic characteristics of P-sets. *Computer Engineering and Applications,* 45-48.

YU Xiu-qing. (2010). Recognition and screening of P-sets. *Journal of Shandong University(Natural Science)*, 94-98.

ZHANG Guan-yu&LI En-zhong. (2010). Information gene and its information knock-out/knock-in. *An International Journal Advances in Systems Science and Applications*, 267-275.

ZHANG Li&CUI Yu-quan. (2010). Outer P-sets and data internal-recovery. *An International Journal Advances in Systems Science and Applications*, 229-236.

Call for Manuscripts

Modern Applied Science is a peer-reviewed journal, published by Canadian Center of Science and Education. The journal publishes research papers in the fields of chemistry, environmental sciences, management and economics, physics, mathematics and statistics, geology, engineering, computer and information sciences, and biology. The journal is published in both printed and online versions. The online version is free access and download.

We are seeking submissions for forthcoming issues. The paper should be written in professional English. The length of 3000-8000 words is preferred. All manuscripts should be prepared in MS-Word format, and submitted online, or sent to: mas@ccsenet.org

Paper Selection and Publication Process

a). Upon receipt of paper submission, the Editor sends an E-mail of confirmation to the corresponding author within 1-3 working days. If you fail to receive this confirmation, your submission/e-mail may be missed. Please contact the Editor in time for that.

b). Peer review. We use single-blind system for peer-review; the reviewers' identities remain anonymous to authors. The paper will be peer-reviewed by three experts; one is an editorial staff and the other two are external reviewers. The review process may take 2-3 weeks.

c). Notification of the result of review by E-mail.

d). The authors revise paper and pay publication fee.

e). After publication, the corresponding author will receive two copies of printed journals, free of charge.

f). E-journal in PDF is available on the journal’s webpage, free of charge for download.

Requirements and Copyrights

Submission of an article implies that the work described has not been published previously (except in the form of an abstract or as part of a published lecture or academic thesis), that it is not under consideration for publication elsewhere, that its publication is approved by all authors and tacitly or explicitly by the responsible authorities where the work was carried out, and that, if accepted, it will not be published elsewhere in the same form, in English or in any other languages, without the written consent of the Publisher. The Editors reserve the right to edit or otherwise alter all contributions, but authors will receive proofs for approval before publication.

Copyrights for articles published in CCSE journals are retained by the authors, with first publication rights granted to the journal. The journal/publisher is not responsible for subsequent uses of the work. It is the author's responsibility to bring an infringement action if so desired by the author.

More Information

E-mail: mas@ccsenet.org

Website: www.ccsenet.org/mas

Paper Submission Guide: www.ccsenet.org/submission

Recruitment for Reviewers: www.ccsenet.org/reviewer.html

The journal is peer-reviewed
The journal is open-access to the full text
The journal is included in:

AMICUS
CABI
CANADIANA
Chemical Abstracts database
DOAJ
EBSCOhost
Excellence in Research Australia (ERA)
Google Scholar
Library and Archives Canada
Open J-Gate
Standard Periodical Directory
Ulrich's
Universe Digital Library
Wanfang Data
Zentralblatt MATH

Modern Applied Science

Bimonthly

Publisher Canadian Center of Science and Education
Address 4915 Bathurst St. Unit 209-309, Toronto, ON. M2R 1X9
Telephone 1-416-642-2606
Fax 1-416-642-2608
E-mail mas@ccsenet.org
Website www.ccsenet.org
Printer Paintsky Printing Inc.
Price CAD.$ 20.00

ISSN 1913-1844